ION SENSING, LIGHT HARVESTING, ENERGY CONVERSION & SELF-ASSEMBLY IN RATIONALLY DESIGNED MOLECULAR CONSTRUCTS

A DISSERTATION SUBMITTED TO
MATERIALS SCIENCE AND NANOTECHNOLOGY PROGRAM
OF THE GRADUATE SCHOOL OF ENGINEERING AND SCIENCE
OF BILKENT UNIVERSITY
IN PARTIAL FULFILLMENT OF THE REQUIREMENTS
FOR THE DEGREE OF
DOCTOR OF PHILOSOPHY

By
ONUR BÜYÜKÇAKIR
July, 2013

I certify that I have read this thesis and that in my opinion it is fully adequate, in scope and in quality, as a thesis of the degree of Doctor of Philosophy.

…….

Prof. Dr. Engin U. Akkaya (Principal Advisor)

I certify that I have read this thesis and that in my opinion it is fully adequate, in scope and in quality, as a thesis of the degree of Doctor of Philosophy.

…….

Assoc. Prof. Dr. Dönüş Tuncel

I certify that I have read this thesis and that in my opinion it is fully adequate, in scope and in quality, as a thesis of the degree of Doctor of Philosophy.

…….

Asst. Prof. Dr. Emrah Özensoy

I certify that I have read this thesis and that in my opinion it is fully adequate, in scope and in quality, as a thesis of the degree of Doctor of Philosophy.

…….

Asst. Prof. Dr. Özgür Altan Bozdemir

I certify that I have read this thesis and that in my opinion it is fully adequate, in scope and in quality, as a thesis of the degree of Doctor of Philosophy.

…….

Asst. Prof. Dr. Serdar Atılgan

Approved for the Institute of Engineering and Science:

…….

Prof. Dr. Levent Onural

Director of the Graduate School

ABSTRACT

ION SENSING, LIGHT HARVESTING, ENERGY CONVERSION & SELF-ASSEMBLY IN RATIONALLY DESIGNED MOLECULAR CONSTRUCTS

Onur Büyükçakır

PhD in Materials Science and Nanotechnology

Supervisor: Prof. Dr. Engin Umut Akkaya

July, 2013

In this thesis, we have constructed rationally designed functional supramolecular systems. In the first chapter, we reported two Bodipy based chemodosimeters to detect fluoride both in solution and in polymethylmethaacraylate (PMMA) matrix. In the second part, we synthesized tetrastyrl-Bodipy derivatives by condensing methyl substituents of 1,3,5,7-tetramethyl-Bodipy dyes with different aromatic aldehydes. The resulting dyes have sharp and intense emission maxima in the near-IR region and they are robust candidates for functional supramolecular systems because of their outstanding properties. In next chapter, we investigated light harvesting properties of these new generation near-IR emissive dyes. In designed light harvesters, a near-IR emissive tetrastyrl-Bodipy dye which was decorated with short wavelength Bodipy fluorophores function as antenna units. In the forth chapter, we reported a Cu(I)-diimine complex as a photosensitizer for dye-sensitized solar cells (DSSC). It was demonstrated that Cu(I) diimine complex with capability of ultrafast electron injection to TiO_2 nanoparticles can be a very good candidate for replacing ruthenium based polypyridyl complexes with a much lower cost. This research potentially can generate significant impact for those working on solar energy conversion and DSSC. In the final chapter, we propose to utilize oscillations in pH to move the two components of pseudorotoxane in relation to each other and this is the first example of a pseudorotaxane in which the mobile component is shuttling autonomously.

Keywords : fluorescence, chemosensors, light harvesting, energy conversion, self assembly, molecular switch, Bodipy

ÖZET

RASYONEL OLARAK DİZAYN EDİLMİŞ MOLEKÜLER YAPILARDA İYON TAYİNİ, IŞIK HASATI, ENERJİ DÖNÜŞÜMÜ VE KENDİLİĞİNDEN BİRARAYA GELME

Onur Büyükçakır
Malzeme Bilimi ve Nanoteknoloji, Doktora
Tez Yoneticisi: Prof. Dr. Engin Umut Akkaya
Temmuz, 2013

Bu tezde rasyonel olarak tasarlanmış fonksiyonel supramoleküler sistemler anlatılmıştır. İlk kısımda, florür iyonunu, hem solüsyonda hem de polimetilmetakrilat (PMMA) ana yapısı içerisinde saptayan iki adet Bodipy bazlı kemodosimetre çalışılmıştır. İkinci kısımda ise 1,3,5,7-tetrametil-bodipy boyalarının metil gruplarının farklı aromatik aldehitler ile kondensasyonu sonucu oluşan tetrasitiril bodipy türevleri anlatılmıştır. Yakın kızıl ötesi bölgede keskin ve yoğun emisyon maksimumuna sahip bu boylar, göze çarpan bu özelliklerinden dolayı fonksiyonel supramoleküler sistemlerin önemli bileşenleri olmuşlardır. Bir sonraki kısımda, yakın kızılötesi emisyona sahip yeni nesil boyaların ışık hasatı özellikleri incelenmiştir. Tasarlanmış ışık hasatı sistemlerinden yakın kızılötesi emisyona sahip tetrasitiril bodipy boyaları, anten birimi olarak çalışmak üzere kısa dalga boyuna sahip Bodipy boyaları ile türevlendirilmiştir. Dördüncü kısımda ise, boya bazlı güneş pilleri (DSSC) için Cu(I)-diimin kompleksinin ışığa duyarlı yapı olarak kullanılması açıklanmıştır. Cu(I)-diimin kompleksinin TiO_2 nanopartiküllerine son derece hızlı elektron transfer yetenekleri ile rutenyum bazlı polipiridil komplekslerin yerini alacak daha ucuz ve etkili alternatif oldukları düşünülmektedir. Son kısımda, pH daki osilasyona bağlı olarak psödorotaksanın iki kısmının birbiri ile uyumlu olarak yer değiştirilmesi gösterilmiş ve hareketli kısmın otonom olarak yer değiştirmesinin literatürdeki ilk örneği verilmiştir.

Anahtar Kelimeler : floresans, kemosensor, ışık hasatı, enerji dönüşümü, kendiliğinden biraraya gelme, moleküler mekik, Bodipy

TO MY PARENTS...

ACKNOWLEDGEMENT

In my doctoral journey, I would like to express my sincere thanks and deepest gratitude to my research supervisor Prof. Engin Umut Akkaya for giving me the opportunity to join his research group and also his guidance, support, patience and continuous encouragement. He was always more than a supervisor for me. It has been a great and wonderful privilege to spend seven years under his supervision. I will never forget his support throughout my life.

I am sincerely grateful to Asst. Prof. Dr. Ali Coşkun, Asst. Prof. Dr. Özgür Altan Bozdemir and Asst. Prof. Dr.Serdar Atılgan for sharing their experience with me, their endless help and support. They always serve a wonderful role model to me as a junior member of academic circle.

I would like to express my gratitude to the thesis committee members Assoc. Prof. Dr. Dönüş Tuncel and Asst. Prof. Dr. Emrah Özensoy for their guidance and help.

I would like to thank to TUBITAK (The Scientific and Technological Research Council of Turkey) for giving me the opportunity of abroad scholarship programmed (PhD Visiting Support). I also want to thank Sir Prof. Dr. Fraser Stoddart for giving me the opportunity to join his dynamic and marvelous research group. Moreover, my special thanks go to Prof. Dr. Jean Pierre Sauvage and Prof. Dr. Lin X. Chen for their wonderful collaboration.

I am sincerly thankful to my close friends Ruslan Guliyev, F. Tuba Yaşar, Fazlı Sözmen, Yusuf Çakmak, Tuğba Özdemir Kütük, Sündüs Erbaş Çakmak, Safacan Kölemen, Tuğçe Durgut, İlker Kütük, and Yiğit Altay for their support, understanding and friendship. They are very precious for me.

My special thanks go to all the present and past members of Akkaya Laboratory, Dr. Deniz Yılmaz, Dr. Gökhan Barın, Dr. Murat Işık, Bora Bilgiç, Nisa Yeşilgül, Bilal

Kılıç, İlke Şimşek, Taha Bilal Uyar, Ahmet Atılgan, Hale Atılgan, Ahmet Bekdemir, Ziya Köstereli, Muhammed Büyüktemiz, Tuğrul Nalbantoğlu, Sencer Selçuk, Hande Boyacı and others for providing a great research atmosphere. I also want to thank all UNAM family for their support and help.

My special thanks to go to my family my mother, father, sister, my uncle Adnan Bölükoğlu, my aunts Neşe Bölükoğlu & Perihan Bölükoğlu and my cousins Pınar & İlkim for their love and support throughout my life. Actually, there is no way to thank them and I am grateful for their invaluable care.

I would express my thanks to my love and wife Hüsniye Büyükçakır for everything. She has my heart and no words can express my appreciation and feelings to her. Maybe I can just say to her ``thanks`` from the bottom of my heart.

LIST OF ABBREVIATIONS

AcOH	**:**	Acetic Acid
Bodipy	**:**	Boradiazaindacene
$CHCl_3$	**:**	Chloroform
DDQ	**:**	Dichlorodicyanoquinone
DMF	**:**	Dimethylformamide
DSSC	**:**	Dye Sensitized Solar Cell
EPR	:	Electron Paramagnetic Resonance
Et_3N	**:**	Triethylamine
FRET	**:**	Förster Resonance Energy Transfer
GFP	**:**	Green Fluorescent Protein
HOMO	**:**	Highest Occupied Molecular Orbital
ICT	**:**	Internal Charge Transfer
IFE	**:**	Inner Filter Effect
LUMO	**:**	Lowest Unoccupied Molecular Orbital
MALDI	**:**	Matrix-Assisted Laser Desorption/Ionization
MS	**:**	Mass Spectroscopy
NMR	**:**	Nuclear Magnetic Resonance
PCT	**:**	Photoinduced Charge Transfer
PET	**:**	Photoinduced Electron Transfer
PMMA	**:**	Poly(methyl methacrylate)
RET	**:**	Resonance Energy Transfer
TA	**:**	Optical Transient Absorption
TFA	**:**	Trifluoroacetic Acid

THF	**:**	Tetrahydrofuran
TLC	**:**	Thin Layer Chromotography
TOF	**:**	Time of Flight
XANES	**:**	X-ray Absorption Near Edge Structure
XTA	**:**	X-ray Transient Absorption

TABLE OF CONTENTS

LIST OF FIGURES

LIST OF TABLES

CHAPTER 1

1. INTRODUCTION

Almost forty-six years ago, Charles Pedersen published a very important paper describing the formation of cyclic polyethers[1]. He called these cyclic compounds as crown ethers. These molecules showed outstanding properties by exhibiting an affinity towards different alkali metals. Moreover, they can selectively bind alkali metals depending on the size of their cavity. Then, Jean-Marie Lehn designed the bicylic form of crown ethers namely cryptands which have better selectivity. Donald J. Cram described the immobile host molecules that construct strong complexes with superior selectivity. These discoveries laid the foundation of new horizon of chemistry. Donald J. Cram describes this new field of chemistry as host/guest chemistry[2]. Then, Jean-Marie Lehn called as supramolecular chemistry[3].

The molecular chemistry investigates the properties of molecular species. On the other hand, supramolecular chemistry focuses on the organized architectures of molecular entities constructed from the binding of two or more chemical compounds by intermolecular forces. These features promote the supramolecular chemistry beyond the molecule.

Supramolecular chemistry relies on two major concepts host-guest chemistry and self-assembly. The host molecule accommodates a specific guest molecule by means of molecular recognition principle. Self-assembly, on the other hand, investigates the construction of defined non-covalent architectures from specific molecular species. The intermolecular interactions play a crucial role both in host-guest chemistry and self-assembly. The other key concept is the molecular recognition which serves selectivity for reactions. Supramolecular chemistry works with key and lock principle which was defined in 1984 by Emil Fischer. The host and guest molecules must be complement to each other. In other words, there is only one key for one lock.

In biological life, chemical species have not a meaning alone in terms of functionality. However, these molecules work in a synchrony and construct complex entities to accomplish a biological process. With same analogy, the molecular species shows higher complexity than simple molecules that are organized by intermolecular interactions in supramolecular chemistry. These features of supramolecular chemistry can be utilized to mimic the biological process with using the bottom-up approach. By using the same approach, one can be designed new complex structures with micro or macro entities having novel functions. The roots of these investigations lie not only in chemistry but also the other fields of science. This is a clear proof of interdisciplinary character of supramolecular chemistry.

Supramolecular chemistry benefits from organic chemistry to synthesize molecular constructions, from coordination chemistry to form metal ion-ligand complexes, from physical chemistry to analyze theoretical and experimental studies of interactions, from biochemistry to explore biological processes, from material science to grasp mechanical features of solids. This high interdisciplinary opens wide range of perspectives towards the developments of new functional supramolecular systems. These versatility and richness is the most important force which drives supramolecular chemistry. There is no doubt that this emerging field of chemistry has attracted great attention from all creative and imaginative world scientists and it has fueled numerous applications and developments in many areas. Therefore, there is a strong demand for the development of new functional systems in this field. For this purpose, on this fertile ground, we have harvested rationally designed molecular constructions to feed today`s science and technology.

In the first chapter, we have developed two different fluorescent molecular sensors for the detection of highly toxic and lethal fluoride anion. These reactions based molecular sensors, namely chemodosimeter, served selective and sensitive sensing both in solution and in polymethylmethaacraylate (PMMA) matrix. These chemodosimeters signal fluoride concentration in a way fluorometric or ratiometric according to position of sily-ptotected phenolic functionality on Bodipy core.

In the second chapter, we have reported new near-IR emissive tetrastyrl-Bodipy dyes. These dyes have been sythetized by condensing the methyl groups of 1,3,5,7-Tetramethyl-Bodipy derivatives with different aromatic aldehyde and also we constituted a mini library for tetrastry dyes having a wide span and tunable emission wavelenght by changing the Bodipy core and aldehyde substituent. This revolution is a strong proof of the richness of the Bodipy fluorophore. These new generation tetrastryl-Bodipy dyes are likely to be used in variety of functional supramolecular constructions as a building block. The next chapter is about the application of these near-IR emissive tetrastryl-Bodipy dyes in light harvesting system. Tetrastryl dyes were embedded to the core part of the light harvesting dendrimers in which short wavelength Bodipy dyes act as an antenna.

One of the main concerns of today's science and technology is to explore new alternative energy sources. Solar cells are the strongest candidates in these alternatives. Although dye sensitized solar cells (DSSCs) are mostly investigated type of solar cells because of their low cost and simplicity, the price to performance ratio is still high. Therefore, there is great interest to manufacture new DSSC solar cell prototypes. Although ruthenium polypridyl complex based DSSC systems shows high light-to-electron energy conversion efficiency, there is a still a cost problem because of low abundance of ruthenium in the world. Therefore, the replacement of ruthenium with cheaper alternative plays a crucial role for the future of DSSC. Cu-diimine complexes are good alternative for the ruthenium complexes. In this study (Chapter 4), it was proved that Cu(I) diimine complexes with capability of ultrafast electron injection to TiO_2 nanoparticles could be a very good candidate for replacing Ru(II) polypridiyl complexes at a much lower cost. This work potentially will generate significant impact for those working on solar energy conversion and DSSC.

Molecular motor proteins are important part of life and locate at the center of biological process. These natural motors are very complex systems. Therefore, mimicking these complex systems in nanometer scale opens new perspective for scientists. Artificial molecular machine based on rotaxane and catenane architectures have been studied extensively in recent years. However, there are very limited

numbers of autonomous molecular machine published in literature. We offer a fresh new approach in initiating and controlling molecular shuttling. Oscillations reactions intrigued chemist for a long time, in this study, we propose to utilize oscillations in pH to move the two components of a pseudorotaxane in relation to each other. In a well behaved oscillatory system, the shuttling could be sustained as long as the oscillations continue. This is the first demonstration of a molecular shuttle system in which the "mobile" component is moving from one station to the other in a truly autonomous fashion. The coupling of pH oscillation to the shuttling process is clear, during which free energy of the oscillatory reactions is exploited. This kind of chemical coupling of an energetically favorable reaction (or set of reactions with complex kinetics) to molecular motion is reminiscent of many biological analogs and therefore highly exciting.

CHAPTER 2

2. BACKGROUND

2.1. Fluorescence

Fluorescence technology plays a crucial role in most of the field of today`s science such as biotechnology, molecular biology, material science, analytical and environmental chemistry. Especially, fluorescence technology shows a remarkable growth in medicine. Fluorescence bio-imaging is now an indispensable tool for clinical diagnostic and genetic analysis. Fluorescence spectroscopy or imaging provides information in a wide range from single-molecule detection to tissue imaging and recent developments in fluorescence technology increases its sensitivity while decreasing the cost and complexity in measurement techniques. These advances are also enhancing the scientists` capability of gaining deeper understanding of the complex chemical or biological systems.

2.1.1. Principles and Characteristics of Fluorescence

When a molecule is excited by means of light, it returns to ground state in several pathways.[4,5] These possible pathways are shown in Figure 1. Fluorescence can be explained as one of the radiative pathway which is the emission of photons without change in spin multiplicity.[6] The other radiative pathway is called phosphorescence which requires a change in spin multiplicity. Sometimes de-excitation process proceeds as the nonradiative pathway in which the exited molecule returns to the ground state without emission of photon. These pathways are called internal conversion. On the other hand, the excited molecule can be exposed to intramolecular processes such as charge transfer, conformational change etc. Besides intramolecular processes, intermolecular interactions (energy transfer, electron, proton transfer, excimer formation, exciplex formation so on) also compete with the fluorescence.[7]

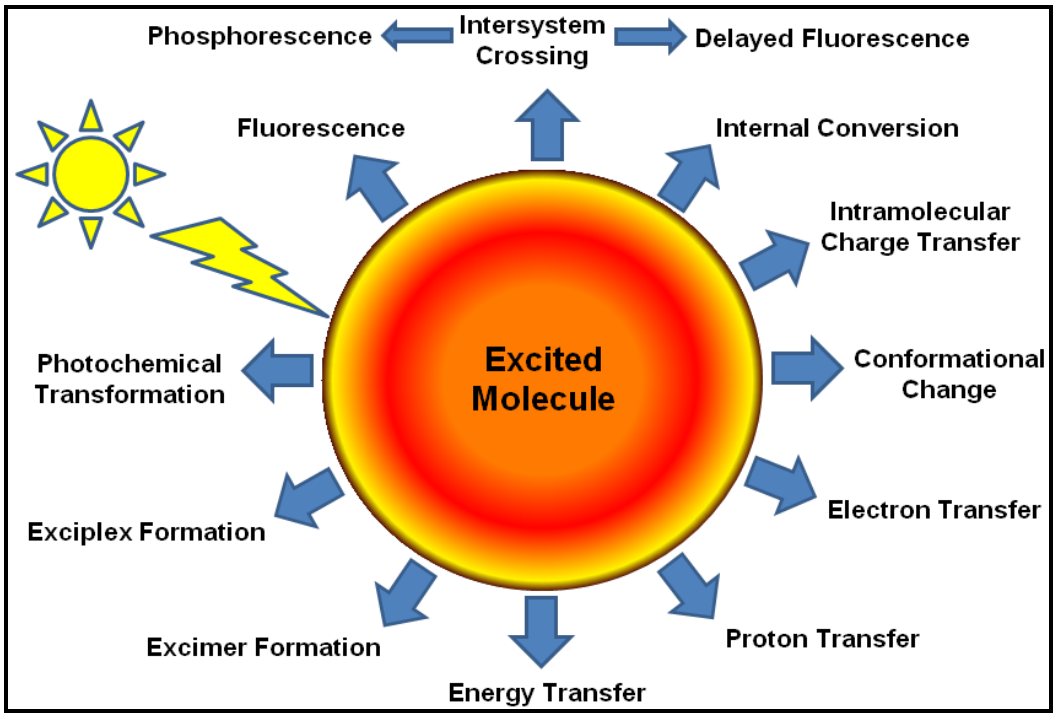

Figure 1. Possible de-excitation process after excitation of a molecule

The characteristics of fluorescence can be affected from the microenvironment of the excited molecule located. The changes in characteristics of fluorescence get able scientist to spatial and temporal information. Not only the chemical parameters but also physical parameters characterize a microenvironment. These parameters (polarity, hydrogen bonds, pH, temperature, electric potential, pressure, viscosity, ions, quenchers, ions, etc.) affect the emission of fluorescence.

The most efficient way to visualize the processes involved in excitation and de-excitation of a fluorescent molecule is the Perrin-Jablonski diagram.[8] These diagrams show the processes starting from the photon absorption and represent all possible de-excitation pathways: fluorescence, phospherence, internal conversion, intersystem crossing, triplet-triplet transition, so on. A typical example of Jablonski diagram is shown in Figure 2. The singlet electronic states are symbolized as S_0, S_1, S_2.....S_n. While S_0 indicates the ground state, S_1, S_2.....S_n symbols denote the other electronic states. The triplet states are depicted by T_1, T_2.....T_n. Vibrational levels are located between electronic states and denoted as 0, 1, 2,.... in order of increasing energy. The

electronic transitions between any states are shown as vertical lines in Jablonski diagram. Since according to Frank-Condon principles[9,10], the transitions between states take place much faster than the nuclear displacement or motions. The time level of transition is about ~10^{-15} s; on the other hand, the nuclear motions are at ~10^{-14} s time level.

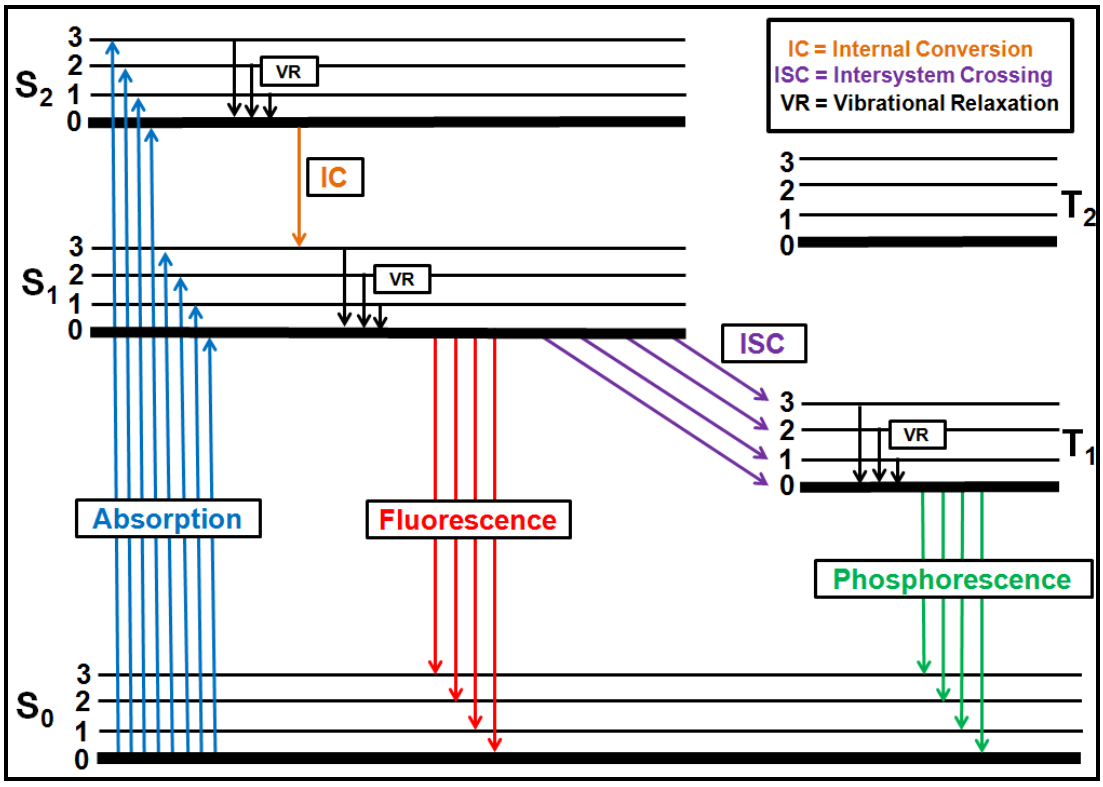

Figure 2. The Perrin-Jablonski diagram

A molecule stays on one of the possible vibrational levels of one of its excitated states after the absorption of the light. Normally, de-exciation process takes longer time (10^{-14} to several seconds) when it compares with the absorption (10^{-15}) process. Molecular luminescence is also very slow process taking about 10^{-10} to few seconds. On the other hand, the molecule reaches the thermal equilibrium by losing the vibrational energy which takes much shorter time about 10^{-14} to 10^{-12} seconds when it is compared with molecular luminescence process. Therefore, after the absorption of the light, the excited molecule settles one of the vibrational levels of excited singlet states (S_1 or S_2) and immediately the molecule relaxes to the lowest vibrational level

of the electronically excited state by just vibrating in a frequency which matches with characteristic of excited state. The forms of energies are infrared quanta or just kinetic energy such as a collision with other molecules. This process is called vibrational relaxation and it takes about 10^{-12} or 10^{-14} seconds.

After the excited molecule relaxes to the lowest vibrational level of higher electronically excited state (S_2) via vibrational relaxation, the population of higher vibrational level of lower excited state (S_1) will take place. This process is called internal conversion and occurs within 10^{-12} seconds. The energy difference between upper and lower electronic states play an important role in the competition of internal conversion and fluorescence. Generally, the energy gap between excited states is closer to each other when it is compared with the energy interval between the lower excited states and ground state. Therefore, the internal conversion is more favorable in excited states. On the other hand, apart from a few exceptions, the fluorescence generally occurs from the lowest vibrational level of lowest excited state (S_1).

In most cases, the upper triplet state takes a position between the lower excited singlet state and ground state. Therefore, in some cases, the triplet state can be populated by the excited singlet state, although this process includes a spin angular momentum change which is forbidden. This non-radiative transition from excited singlet state to triplet state is called intersystem crossing. As indicated above, this process occurs between states with different multiplicity that is principally forbidden, however the large spin-orbit coupling make it possible. Hence, the heavy atoms such as I, Br, etc. which increase the spin-orbit coupling enhance the possibility of intersystem crossing process. The average lifetime of intersystem crossing is about 10^{-8} seconds. It is very slow process when it compares with the lifetimes of vibrational relaxation or internal conversion.

As defined and mentioned, the fluorescence can be explained as the emission of photons without any change in multiplicity from an excited molecule. Actually, the emission of photon is very fast process (10^{-15} seconds) as absorption process. However, the emission generally occurs from the lowest excited state (S_1) to ground

state and the population of photons at the lowest vibrational level of lowest excited state (S_1) takes times about 10^{-10} to 10^{-7} seconds. The time changes according to excited molecules nature and the other process taking places before emission such as internal conversion, vibrational relaxation or intersystem crossing.

In most cases, the emission maximum has longer wavelength than absorption. It means that the energy of the fluorescence less than the excitation or absorption energy. This energy or wavelength difference is called Stokes Shift. One of the reason of this energy loses is the fast decay time to lowest vibrational level of S_1. Furthermore, typically an excited molecule shows a de-excitation to higher vibrational levels of ground state (S_0). The microenvironment of excited molecule can also affects the stokes shift character. For instance, a fluorescent molecule has a has higher dipole moment in the excited state when compared with the ground state. Therefore, any increase in the solvent polarity cause to an increase in the stokes shift. There are also others parameters which plays an important role in the stoke shift phenomena such as excited-state reactions, temperature, complex formation, energy transfer etc.

The other characteristics of fluorescence are to show only one emission band, although the absorption spectrum may have several absorption band. Actually, this phenomena is one of the proof of the case which is the emission just occurs from the lowest excited state. It is known that vibrational relaxation and internal conversion from the higher excited states to lower excited states is very fast. This radiationless deactivation occurs before the emission and populates the lowest excited state. As a result of this, the fluorescence only originates from the lowest excited state and we only observe one band in the fluorescence.

The internal conversion and vibrational relaxation compete with the fluorescence. Thus, not all excited molecules cannot return the ground state via fluorescence. The fraction of excited molecules which shows fluorescence is called fluorescence quantum yield (Φ_F). The quantum yield is calculated by means of relative rate constants; namely, emission of fluorescence ($k_{r(F)}$), internal conversion (k_{ic}),

intersystem crossing (k_{isc}), emission of phosphorescence ($k_{r(P)}$), and overall non-radiative deactivation ($k_{nr} = k_{ic} + k_{isc}$). The fluorescence quantum yield can be formulated as;

$$\mathbf{\Phi_F = k_r / k_r + k_{nr}}$$

This equation does not include the other deactivation parameters resulting from the intermolecular interactions because of giving the concept in a straightforward way. However, these rate constants can be added to denominator part of the equation since these factors compete with emission of fluorescence. The fluorescence quantum yield close the unity when the possibility of non-radiative deactivation decreases. Conventionally, the fluorescence quantum yield has been calculated by comparing the molecule absorption spectra area and emission intensity with a reference compound.

The average time which the molecule spends in the excited state before returning to ground state is called excited state lifetime. The fluorescence life time can be formulated as;

$$\mathbf{\tau = 1 / k_r + k_{nr}}$$

It is important to realize that the lifetime is an average value. It means that excited molecules can emit fluorescence before or after the lifetime. Therefore, an exponential decay is observed in fluorescence lifetime measurements.

In theory, if the depopulation of excited states occurs only with the radiative process such as fluorescence, the calculated lifetime is defined as natural lifetime or radiative lifetime and denoted as τ_n or τ_r.

$$\mathbf{\tau_n = 1 / k_r}$$

2.2. Fluorescent Dyes

Fluorescent dyes are widely used in today`s science because of their versatility, sensitivity and distinctive capabilities. Fluorescent dyes are indispensable tools for many applications which are widely used in medicine, biology, and chemistry and material science. The usage of fluorescent dyes as a reporter in the design of a fluorescent indicator offers several advantages especially for biological sciences. Fluorescent probes, for instance, enable real time monitoring of ions, neutral molecules or biological markers in vitro and vivo analysis.[11]

All fluorescent dyes have specific excitation and emission wavelength ranging from ultraviolet through the near-IR region. As indicated earlier section, the emission wavelength does not exactly overlap with the excitation wavelength due to the energy loss before emission of photons. That energy loss leads to a wavelength difference between excitation and emission spectra. This wavelength difference is called Stokes shift which is also a distinctive characteristic for fluorescent dyes. It must be noted that the stoke shift of a particular dye is highly dependent on the environment. For instance, a dye molecule can have different stoke shift values in different solvents.

The other important parameter for fluorescent dyes is brightness. Two parameters should be taken into account in the determination of brightness of a dye, namely extinction coefficient and fluorescence quantum yield. The extinction coefficient can be defined as the quantity of absorbed light at a specific wavelength and concentration. The unit of extinction coefficient is M^{-1} cm^{-1}. The fluorescence quantum yield is the ratio of number of emitted photons to the number of absorbed photons. Moreover, the quantum yield also depends on nature of dye and environment.

Fluorescent dyes can be classified into three categories[12]:

- Biological fluorophores
- Quantum dots

- Organic dyes

2.2.1. Biological Fluorophores

Some biological compounds are naturally fluorescent. These biological compounds are generally fluorescent proteins. There is a large number of fluorescent proteins existing in nature but the most important member of these fluorescent proteins family is the green fluorescent proteins (GFP). The first GFP was extracted from the jellyfish Aequorea victoria and its properties was firstly studied by Osamu Shimomura in 1962.[13] However, the usage of GFP as gene expression reporter is the revolution on GFP research which was firstly demonstrated by Martin Chalfie and co-workers.[14] Roger Tsien is another important name for the GFP. Tsien and coworkers studied on the chemistry of GFP and synthesized new GFP derivatives having different spectral properties.[15] These new GFP derivatives show higher brightness, photostability, and variable emission wavelength (red emissive GFP variants).

GFP and derivatives are widely used to visualize the process taking place in the living cells such as gene expression[16], protein-protein interactions[17], intracellular transport[18], cell division[19], chromosome replication[20] and so on. The development in fluorescence technology broadens the application area of GFP fluorophores. However, there are some limitations of GFP fluorophores because of its nature. The expression of fluorescein proteins takes too much time. Furthermore, the over expression of GFP leads to some misfunctionality in cell operation and also toxicity.

2.2.2. Quantum Dots

Quantum dots are nanometer scale sized semicondoctors. The size of quantum dots can change between 2 nm to 50 nm. Quantum dots are fluorogenic nanocrystals whose optical and physical properties are basically different than traditional fluorescent organic dyes. Quantum dots show outstanding photophysical characteristics such as high fluorescent quantum yield, strong photostability, broad

absorption cross-section, norrow emission band and high chemical stability. The other important characters of quantum dots are size-unable absorption and emission spectra. The wavelength of emitted light shifts to red as the size of quantum dots increases. Due to synthesis methodology, the size of quantum dots can be tightly and easily controlled. These prominent properties of quantum dots have been attracting great attention in the scientific community and these flurorophore nanocrystals have been used in variety of applications since the discovery of quantum dots by Russian physicist Alexai Ekimov in 1980[21]. They have been widely used as sensing tool in the detection of ions, organic molecules and biomolecules.[2223] In recent years, their biological applications have been highly promoted by improving their biocompatibility. While they have been working as a biosensor in vitro, they have been used as a targeting or imaging tool in vivo studies.[24]

2.2.3. Organic Dyes

Fluorescence techniques are emerging as an essential tool for the modern technology and todays` science such as medicine, biotechnology, environmental chemistry, pharmacy and nanotechnology. Undoubtedly, fluorescent organic dyes play a crucial role in the usage of these fluorescent techniques. Fluorescent organic dyes have evoked great interest due to their versatilty, low cost, easily adjustable photophysical and chemical properties. There is a large number of fluorescent dyes reported in the literature[25],[26]. These dyes can be categorized according to their chemical structure (Figure 3).

Although the decoration of the dye with substituent leads to some small changes on photophysical features, derivatives from same family show similar characteristics. Each dye family show unique features. For example, xanthene dyes can be subdivided into two groups' fluorones and fluorenes. The most important and well-known dyes of this family are fluorescein (from the group of fluorones) and rhodamonine (from the group of fluorenes) derivatives. Fluorescein dyes have been widely used in biological applications. These dyes have serve great water solubility and high quantum yield. On the other hand, fluorescein dyes are highly pH sensitive

and they are easily photobleached. Usage of these dyes in quantitative analysis cause to some difficulties due to lacking of sensitivity resulted from photobleaching. However, scientists spend remarkable effort to design new fluorescein derivatives with improved features. Furthermore, there are lots of rationally designed fluorescein derivatives commercialized to label amino acids, proteins and peptides. The fluorescein isothiocyanates is one of the most popular commercially available labeling probes (Figure 4).

Figure 3. Categorization of organic dyes according to their chemical structure

The other member of Xanthene class of dyes is the rhodamine. These dyes have strong excitation coefficient in the visible region and also high quantum yields. Any substitution on the skeleton of the dye can leads to a drastic photophysical change. Therefore, rhodamine derivatives have a large span of absorption and emission wavelength. Most of rhodamine derivatives, like fluorescein dyes, have been commercialized and these dyes have been used in bioanalysis as a probe; like Rhodamine 800, Texas Red, Rhodamine 6G or Rhodamine B (Figure 4).

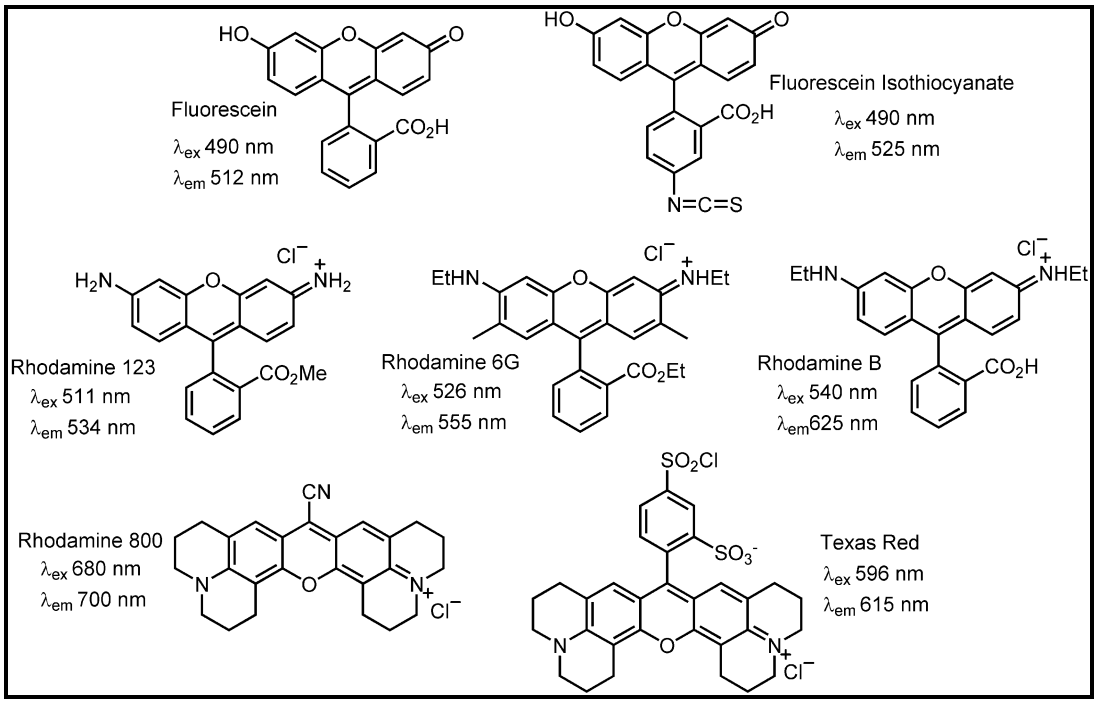

Figure 4. Some commercialized fluorescein and rhodamine derivatives with their absorption and emission wavelength maxima

Cyanine dyes have been used in many technical and biological applications. Most of them have long wavelength absorption and emission maxima (between 600 to 900 nm). Tetrapyrole family includes two important dyes porphyrin and phtoloccyanne. As indicated above, all dye families have specific features and all families has been growing so fast. Thus, it is very difficult to analyze all organic dyes and also this is not the scope of this thesis.

There is also a great number of trademark dyes. These trademark dye families are commercially available and these dyes have been decorated with suitable recognition sites to bind a specific analyte via covalently or non-covalently. Trademark dyes serve both some advantageous and disadvantageous. Therefore, before choosing the dye for a specific application, their properties should be taken into consideration carefully. Some of trademark dyes were demonstrated in Figure 5 with their absorption and florescence maxima.

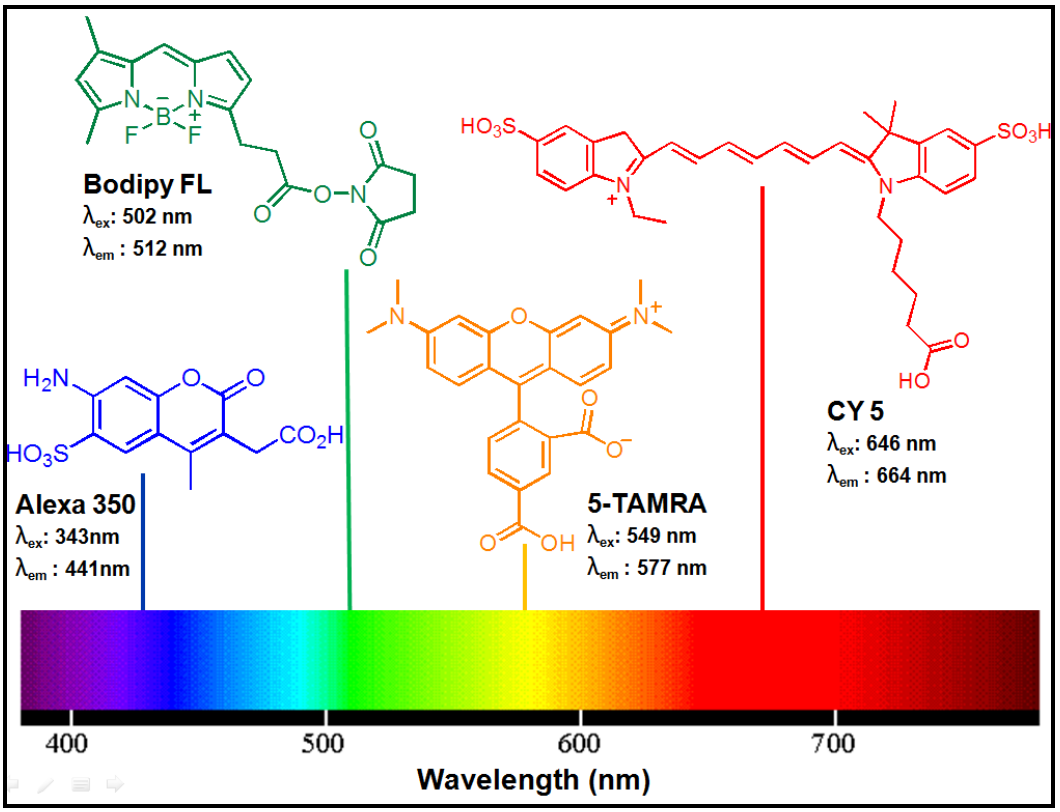

Figure 5. Some example of trademark dyes in the visible region

2.3. Fluorescent Molecular Sensors

The chemical sensor was defined as ``a receptor that interacts with an analyte producing a detectable change in a signal``.[27] Use of fluorophores as a signaling unit has drawn great attention among chemists. The fluorescent molecular sensors have been widely used as an analytical tool in medicine, chemistry, biology,

environmental and material science to detect cations, anions and neutral molecules.[28,29] There is a great interest in the field of fluorescent molecular sensing to design new chemosensors with improved sensitivity, selectivity, response time and targeting capabilities.[30,31]

The fluorescent molecular sensors are composed of two main parts, namely signaling and recognition unit. The fluorophore is the signaling unit and the receptor works as a recognition unit. In most cases, the receptor unit covalently attached to a fluorophere unit via a spacer, or not. The design and nature of the receptor unit determines selectivity and sensitivity to a specific analyte. The recognition of an analyte by the receptor unit can be followed by the changes in the photophysical characteristic of a fluorophore. The signaling features of fluorophores directly relate with the photophysical character of fluorophore and also the design of chemosensor. The most common fluorescent molecular sensors can be grouped into three classes.[4,32] In the first group, the fluorophore acts not only as a signaling unit but also receptor unit as well. The complexation of an analyte could cause either enhancement or quenching of the fluorescence signal of fluorophore. This type of chemosensors mostly have been used to monitor the pH changes (Figure 6).

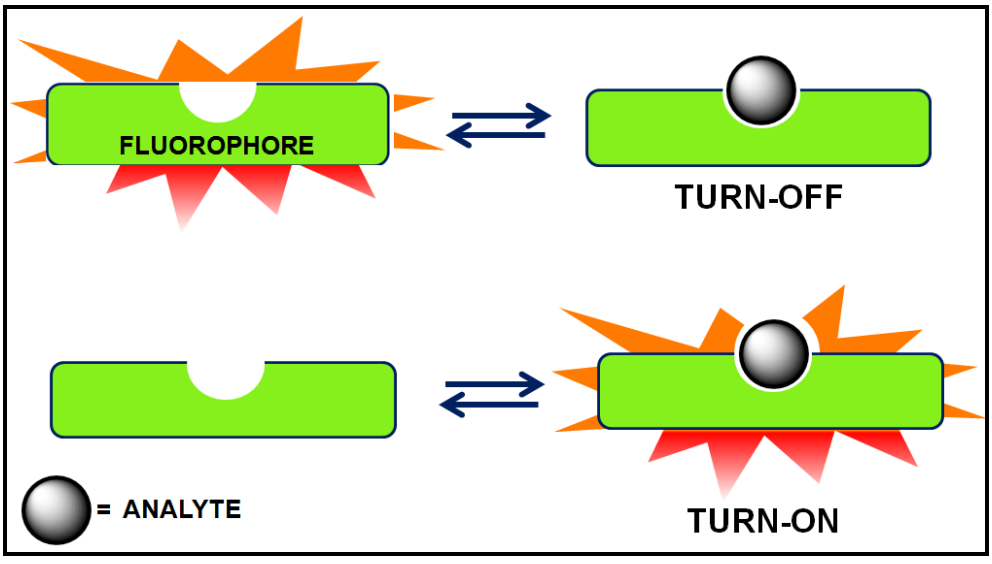

Figure 6. Fluoresccent molecular sensor with complexing fluorophore type

The most common fluorescent molecular sensor type consists of a fluorophore and an analyte selective receptor unit both of which are connected to each other covalently. These chemosensors can be constructed as fluorophore-spacer-receptor or integrated fluorescent molecular sensors (Figure 7). For the integrated fluorescent chemosensor, a fluorophore and a receptor unit are linked to each other covalently by maintaining the conjugation between each other, i.e. the fluorophore and the receptor unit can get involved in the same π-system. On the other hand, the fluorophore and the receptor unit are attached covalently via a spacer unit. These types of probes can be in the form of turn-on (chelation or complexation enhancement of fluorescence) or turn-off (chelation or complextion quenching of fluorescence).

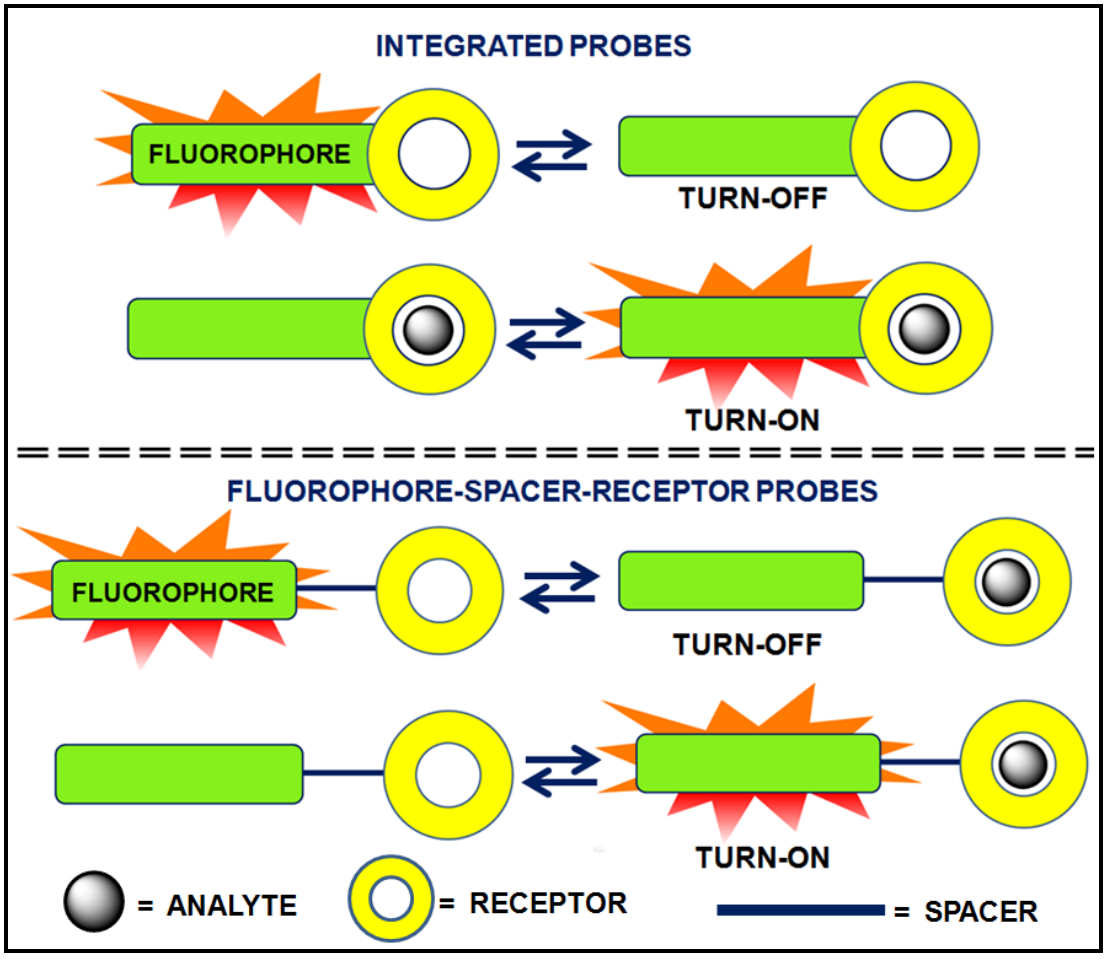

Figure 7. Fluoresccent molecular sensor in which fluorophore part linked to a receptor via direct integration or spacer

Another widely used molecular fluorescent sensor family is named chemodosimeter.[33] This type of sensors has a different working mechanism. The receptor unit selectively gives a reaction with the analyte. The reaction leads to some changes in the photophysical character of the fluorophore. Therefore, the reaction can be followed by fluorescence spectroscopy. The kinetics of the reaction is determined by the environmental conditions (concentration of analyte, temperature, etc) and the nature of the reaction between analyte and receptor. These types of sensors are generally irreversible whereas the other chemosensors are reversible.

The determination of the state of the molecular fluorescent sensor turns on or off base on a few principles. Fluorescent chemical sensors switch between turn on- and off states according to principles, namely photoinduced energy transfer (PET), photoinduced charge transfer (PCT), energy transfer and excimer formation.

2.3.1. Photoinduced Electron Transfer (PET)

PET is one of the principle which is commonly exploited in supromolecular recognition by fluorescent molecular sensors.[32] Most of PET based chemosensors are designed with fluorophore-spacer-receptor type molecular sensor format.[34,35] This design also shows up the supramolecular nature of this fluorescent signaling strategy since each component works distinctively for a necessary function. A fluorophore unit is responsible for monitoring photophysical alterations. The responsibility of a receptor unit is to satisfy a selective recognizition for a specific analyte. On the other hand, the receptor and the fluorphore moieties hold together in a way separate to each other by a spacer unit.

PET can be simply defined as a fluorescent signaling system which relies on enhancement or quenching of emission. The switchability of designed PET based chemosensors can be guest-induced turn on (off-on) or turn-off (on-off) fluorescence. The working mechanism of PET in a turn on (off-on) type signaling system was schematically shown in Figure 8. The receptor unit plays the role of an electron donor (e.g. amino group) and the fluorophore is an acceptor. The excitation of the

fluorophore leads to a promotion of an electron from the highest occupied molecular orbital (HOMO) to the lowest unoccupied molecular orbital (LUMO). Normally, fluorescence can be observed if this excited electron gets back to HOMO from the LUMO via releasing its excess energy as a light. However, if the fully occupied HOMO level of the donor group (it is the receptor unit in this system) exist between the HOMO and LUMO level of fluorophore, a photoinduced electron transfer occurs from HOMO of the donor to the HOMO of the acceptor unit (the fluorophore). These electron transfer cause to a quenching of emission intensity and weak fluorescent is observed. However, the binding of an analyte to the receptor unit, where the donor moiety (donor atom i.e. amino nitrogen) is present, leads to a decrease in the energy level of HOMO of receptor and the electron transfer cannot take place from donor-to acceptor unit (fluorophore). This results with an enhancement in fluorescence.

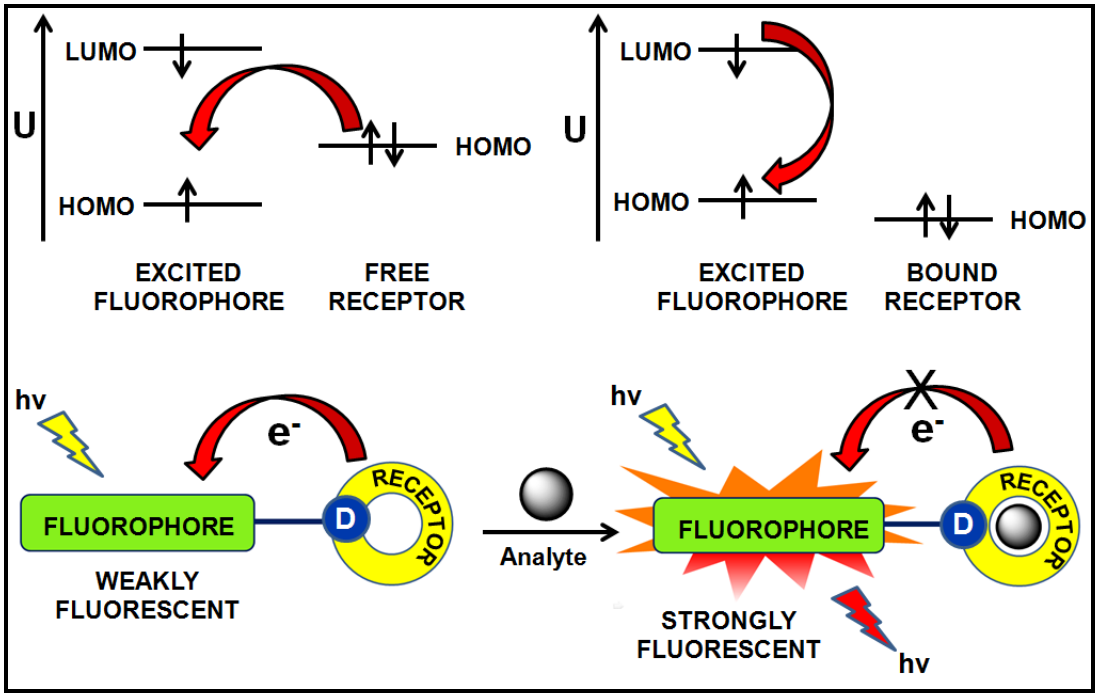

Figure 8. Principles of cation sensing in fluorescent molecular sensors with PET mechanism

Most of fluorescent molecular sensor works with PET principle, especially off-on type fluorescent signaling event have been widely used in the detection of cations, anions and neutral molecules. As depicted in Figure 9, the first PET sensor is (**1**) and

it was synthesized by de Silva et.al. in 1986.[36] The fluorophore part consists of an anthracene skeleton and the azo-crown ether constitutes the receptor moiety. The binding of K^+ in methanol solution cause about 47 fold fluorescence quantum yield increase for the chemosensor (**1**) (quantum yileds ; before addition of K^+ = 0.003 to after the addition of K^+ = 0.14). The compound (**2**) can detect soft metal ions like Zn^{2+} with its polyazamacrocycle based receptor site.[37] The addition of Zn^{2+} cations to the solution of (**2**) blocks the PET process and 14-fold fluorescent quantum yield increase is observed. On the other hand, the compound (**3**) is a BODIPY based visible range chemosensor for the detection of an organic molecule saxitoxin.[38] It shows high binding affinity to saxitoxin and 100% fluorescence enhancement.

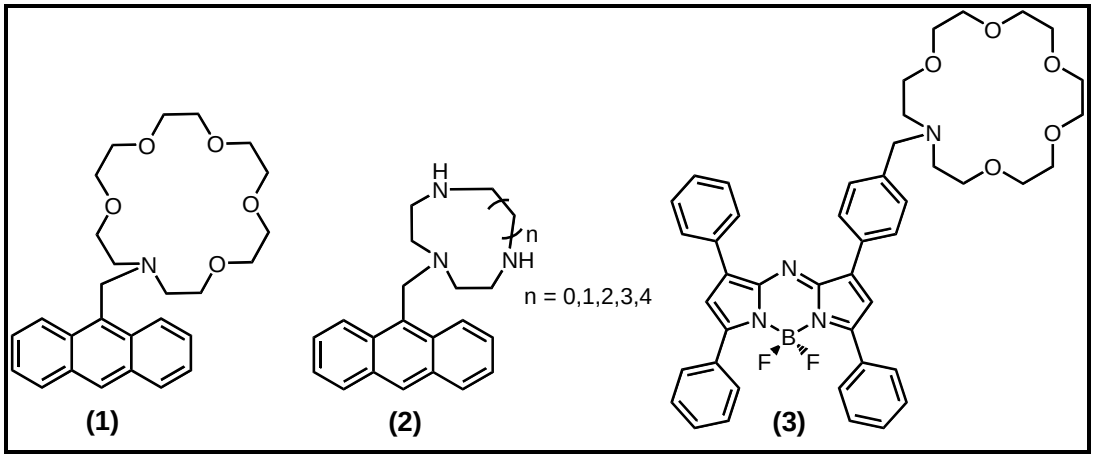

Figure 9. Some fluorescent molecular sensor works with PET principle

The recognition moiety can be cyrptands, podands, calixarenes or chelatings. (**4**)[39] and (**5**)[40] are cryptand based molecular sensors to detect K^+ (Figure 10). Although the protonation of the nitrogen atoms at acidic pH decrease the chemosensor sensitivity, it was successfully used for detecting the potassium level in blood. On the other hand, the pH sensitivity was overcome by using benzannelated cryptand in the design of the compound (**5**). The nitrogen atoms of aromatic atoms have lower pK_a range than aliphatic amines.

Podand based chemosensors (**6**)[41] and (**7**)[42] was designed to detect the Zn^{2+} cation (Figure 10). Polyamine chains construct the receptor site of (**6**). However, these

chains cannot serve a selective and sensitive binding site. The compound (**6**) is very pH sensitive and it gives a response not only to Zn^{2+} but also Cu^{2+} cation. On the other hand, (**7**) contains dipicolyamine moiety which provides a selective Zn^{2+} detection in physiological conditions. It exhibits an increase in florescence quantum yield from 0.39 to 0.87 in the presence of Zn^{2+} in solution. This chemosensor was also used in living cells.

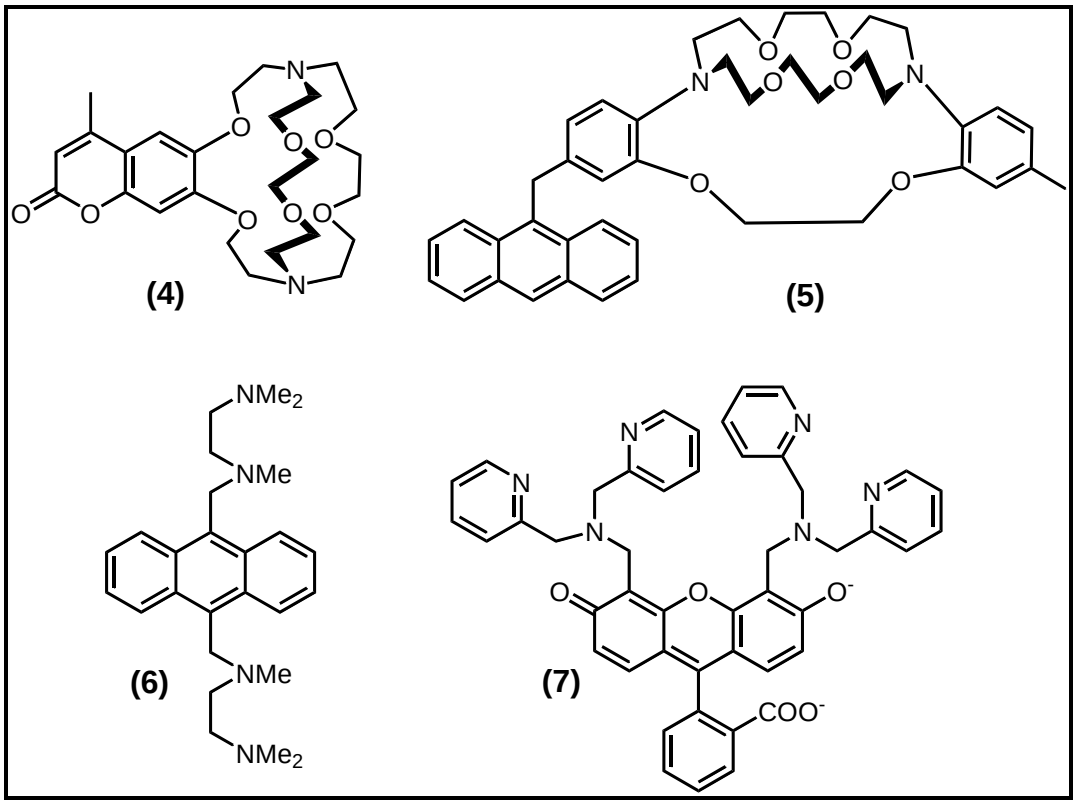

Figure 10. Some fluorescent molecular sensor works with PET principle based on cyrptands, podands, or chelatings

In the previous case, the fluorophore units act as an acceptor unit whereas the receptor moiety as donor and the electron transfer occurs from the receptor to fluorophore unit. However, there is another possibility in which the direction of electron transfer is from the flurophorophore (acceptor) to receptor (donor). This type of PET process is called oxidative-PET and it is used to design turn-off (on-off) type fluorescent molecular sensors. Figure 11 represents the working mechanism of oxidative-PET in which the binding of analyte to receptor quenches the emission intensity of fluorophore. In this case, HOMO and LUMO levels of the receptor is

lowered by binding of an analyte and this permits an electron transfer from the LUMO level of excited flurophore to LUMO level of receptor.

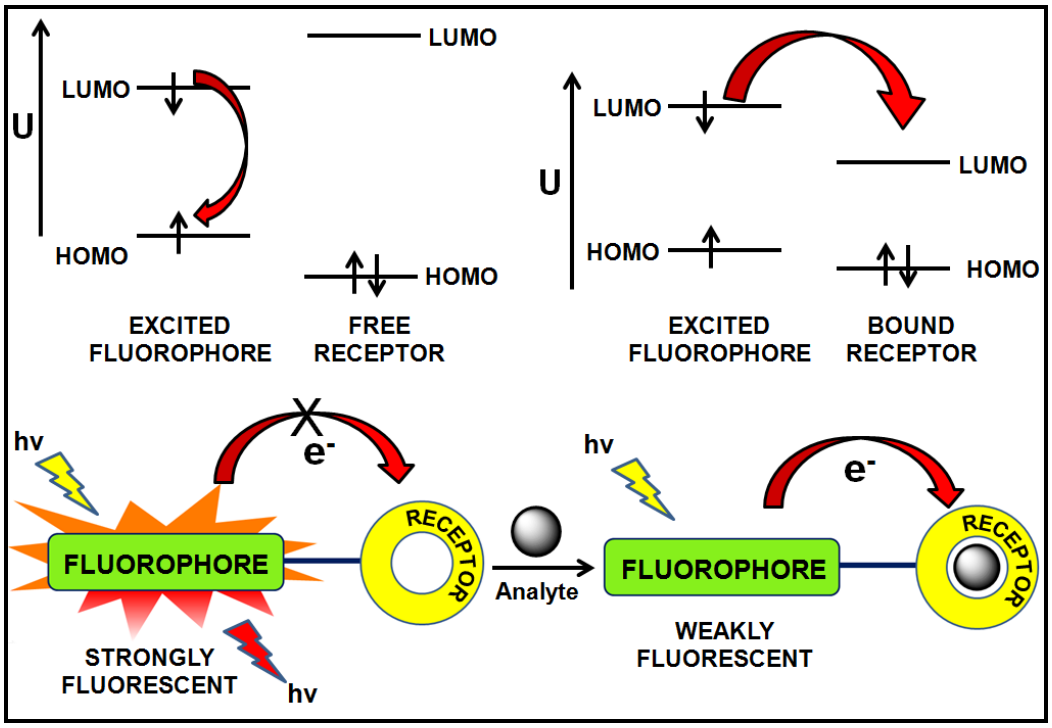

Figure 11. Principles of cation sensing in fluorescent molecular sensors with oxidative-PET mechanism

Akkaya research group was designed a BODIPY based fluorescent molecular sensor (**8**) which is an example for oxidative PET (Figure 12).[43] The compound (**8**) has a high fluorescent quantum yield and strong emission intensity at green region of visible range before the addition of zinc cation. However, after the binding of Zn^{2+} cation to the bipyridine unit, fluorescence was significantly diminished because of oxidative PET process. Therefore, the binding of Zn^{2+} cation was monitored with quenching of emission.

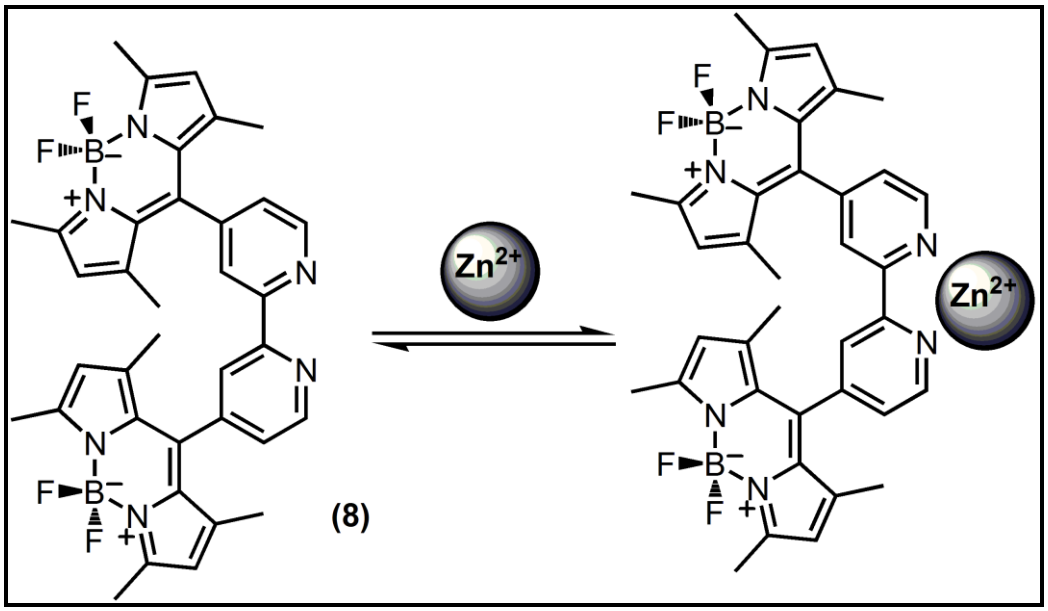

Figure 12. An example of Zn^{2+} chemosensor working with oxidative PET mechanism

2.3.2. Photoinduced Charge Transfer

The integrated type probes in which the fluorophore is directly attached to the receptor have been used in the case of PCT systems. In contrast with probes including a spacer, the orbitals of conjugative linked fluorophore and receptor moieties overlap and each component gets involved in their π-systems. Therefore, one terminal tends to be a electron donor and the other is electron withdrawing. The excitation of system leads to a donor-acceptor intramolecular charge transfer from donor site to the acceptor site in fluorophore unit. As a result of this excited-state charge transfer, the elecron donor site becomes strongly positively charged and it creates a significant dipole. Therefore, any change in the dipole moment cause to a stokes shift according to the microenvironment of the fluorophore. It is very easy to predict that the binding of an analyte to acceptor or donor site changes the dipole. This change results with substantially alterations in photophysical features of the fluorophore.

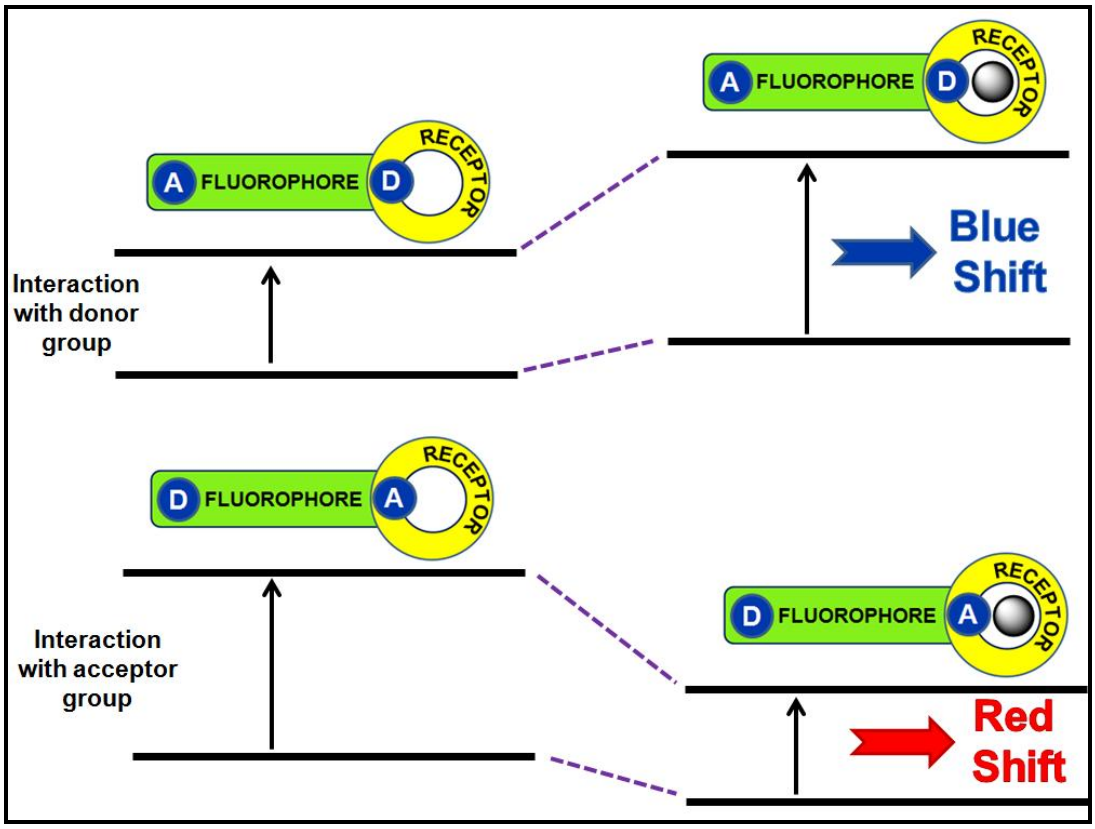

Figure 13. PCT mechanism in cation chemosensors with an electron withdrawing and electron donating receptors

When a receptor containing an electron donating (like amino group) interacts with a cation, the electron donating capability of receptor decreases. As a result of this reduction, the conjugation and polarization of system diminish and as expected a blue shift is observed in the absorption spectrum of fluorophore with a decrease in molar absorption coefficient. On the other hand, if a receptor unit contains an electron acceptor group (like carbonyl moiety), the electron withdrawing character of this group is enhanced by the addition of cation. This enhancement also provides an extra stabilization for the system and this result with a red-shift in the absorption spectrum. The molar absorption coefficient of system is also increases. Principally, emission spectrum also shows a shift parallel to absorption spectrum. The fluorescence quantum yields and life time of systems is also affected.

The shifts can also be described in terms of charge-dipole interaction. The resonance form of the ground state looks like the excited state. Therefore, the donor group such as amino group is positively charged in the excited state. The interacion of amino group and the cation destabilize the excited state. Thus destabilizization leads to an increase in the energy gap between ground state (S_0) and the excited state (S_1) energy levels. This increase in the energy levels cause a decrease in the wavelength and a blue shift is observed. When a receptor unit having an acceptor moiety such as a carbonyl group, it is negatively polarized in the excited state. Therefore, the interaction of cation with carbonyl group stabilize the negative charge. As a result of this, the excited state is more stabilized than ground state and the energy gap decreases between S_0 and S_1.This reduction leads to a red shift both absorption and emission spectra.

The efficient usage of the PCT mechanism in fluorescent molecular sensing is well demonstrated by many examples in the literature. Our group was published an ICT based two chemosensors.[44] One of them was functionalized with aniline groups (**9**) which are electron donating moiety and the other was substituted with an electron withdrawing pyridine group (**10**) working as receptor unit (Figure 14). The interactions of these receptors with proton lead to opposite spectral shift. The proton bound electron donating receptor showed a blue shift. On the other hand, the pyridine (electron accepting moiety) exploited a red shift.

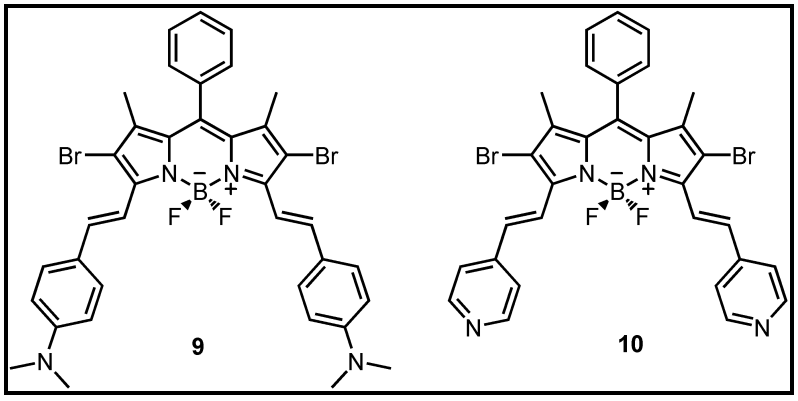

Figure 14. PCT donor and acceptor characteristics

2.3.3. Fluorescent Molecular Sensors for Cation &Anion Recognition

There is a strong demand for fluorescent molecular sensors for many fields of science including chemistry, environmental chemistry, biochemistry and biology. The detection of metal ions and anions participate in lots of biological and environmental process. For example, zinc ion (Zn^{2+}) takes a role in brain functions and recent studies proved that Zn^{2+} is an important factor in Alzheimer`s disease.[45] On the other hand, cyanide anion (CN^-) is an extremely toxic because of its capability to inhibit the enzyme cytochrome oxidase and the allowable cyanide concentration in drinking water must not exceed 1.9μM. Therefore, it is a very difficult and important issue to detect CN^- in this low concentration. As a result of this, there is a great interest to develop rationally designed sensitive and selective fluorescent sensors to detect cation and anions. There are numerous critical reviews published in recent years.[46,47,48,49] In this thesis, some representative examples have been exemplified and briefly discussed.

One of the most common recognition unit for sensing Zn^{2+} is di-2-picolyamine (DPA) based ligands which show high affinity towards Zn^{2+}. The attachment of DPA to the proper fluorophores provides an effective detection. **11**, **12** and **13** are some representative examples for this type of chemosensing (Figure 15). **11** and **12** gave rapid response to Zn^{2+} concentration selectively and sensitively.[50] Moreover, the decoration of sensors with sulfonic acid moiety provides water solubility. The other sensor **13** is a classical PET type chemosensor.[51] The binding of Zn^{2+} to DPA site cause about a twenty fold incresase in fluorescence quantum yield. According to Job`s plot, there is a one to one binding between ligand site and Zn^{2+}.

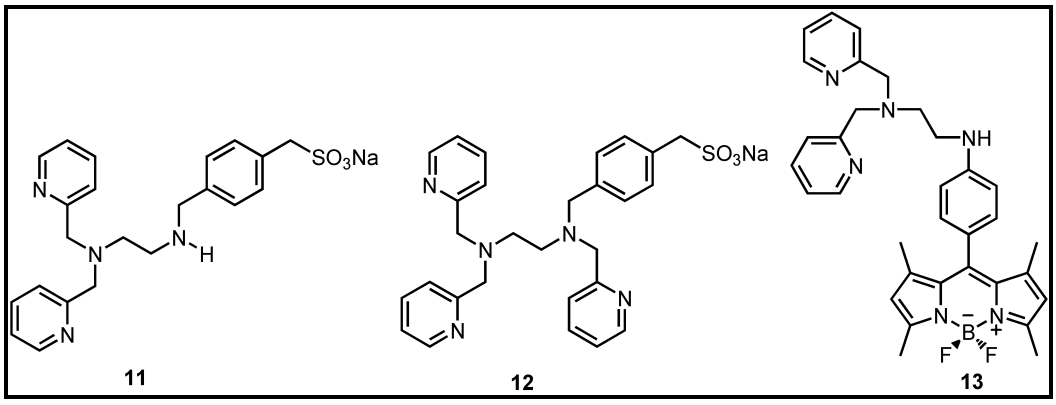

Figure 15. Structures of DPA based chemosensors to sense Zn^{2+}

Our research group was published a paper in 2010 about the usage of chemosensors in molecular logic gate application. The molecule **14** (Figure 16) is a three-input logic gate which responds Ca^{2+}, Zn^{2+} and Hg^{2+} selectively and sensitively.[52] The harder Ca^{2+} showed affinity to azacrown ether which is attached to meso position of Bodipy dye. The binding of Ca^{2+} inhibited the PET process and fluorescence was recovered. On the other hand, Zn^{2+} and Hg^{2+} interacted with DPA and thiocrownether based receptor moieties, respectively. These interaction led to a moderate blue-shift both in fluorescence and absorption spectra.

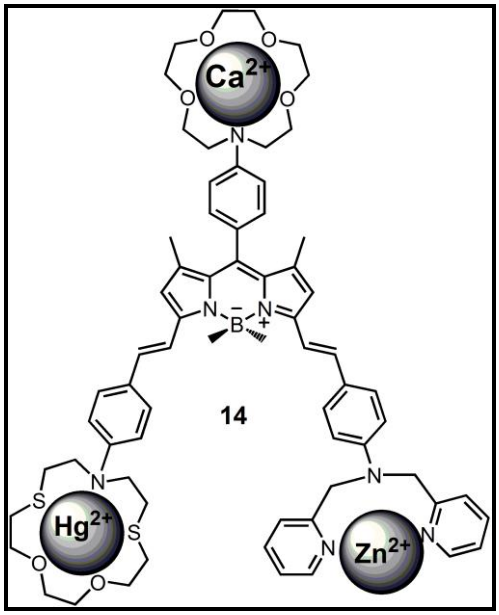

Figure 16. Three recognition sites in one Bodipy based chemosensor

15 is an example of a reaction based detection of fluoride anion F^- (Figure 17).[53] This chemodosimeter exploited high sensitivity and selectivity to F^- with a very rapid reaction response time. In the presence of F^-, a remarkable blue-shift was observed both in absorption and emission in THF solution. **16** was designed from our research group to detect CN^-.[54] This fluorometric and colorimetric chemodosimeter is very selective to CN^-. Furthermore, by doping **16** into polymethylmethaacrylate (PMMA), it was used to detect CN^- in solid matrices. Although most chemodosimeters are not reversible, it is possible to regain the chemesensor by adding trifluoroacetic acid (TFA) (Figure 17).

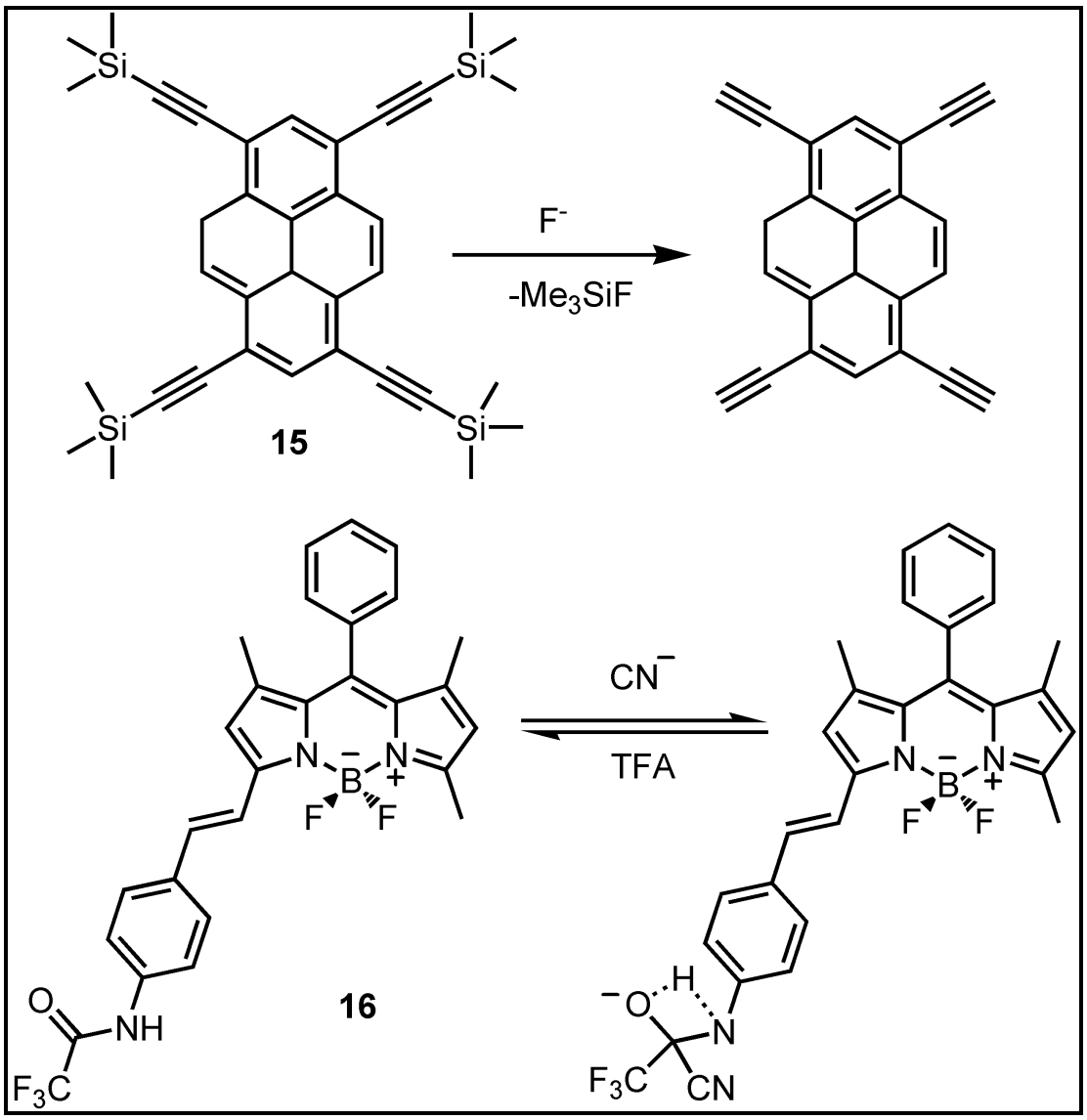

Figure 17. Reaction based sensing of F^- and CN^- anions by using chemososimeters

2.4. Energy Transfer

From its discovery, resonance energy transfer (RET) have been effectively used in many biological and chemical systems.[55,56,57] Especially, RET plays a crucial role in biomedical research and drug discovery.[58] As indicated early parts, although there are numbers of fluorescent organic dyes, their undesirable characteristic properties limit their usage. For instance, most of organic dyes have small stokes shifts. This narrow wavelength interval between absorption and emission leads to some limitation in sensing via self-quenching and excitation back scattering effects.

The fluorescence detection based on enhancement of emission intensity at a specific wavelength without any significant shift also have lots of disadvantageous since the emission wavelength can easily be influenced by any factors such as environmental changes (temperature, pH, pressure, polarity, etc.) and the localization of the fluorophores. On the other hand, the ratiometric measurements, in which fluorescence intensities can be simultaneously monitored at two wavelengths, can solve these problems to some extent. The PCT principle can be used to get these ratiometric fluorescent probes. However, these probes still do not have sufficient stokes shifts to provide efficient detection of an analyte. At this point, multichromophore systems with energy donor-acceptor architectures can be utilized to solve these problems with their large stoke shifts for efficient detection and imaging. These energy transfer systems enable scientist to follow the emission intensities from two different wavelength channels at the same time.

Resonance energy transfer (RET) mechanism can be simply described as energy transfer between two chromophores and if the chromospheres are fluorescent then it is called fluorescent resonance energy transfer (Figure 18). There are some parameters to accomplish an effective energy transfer. First of all, the donor should have high quantum yield. The other important parameter is that the emission donor should overlap with the acceptor absorption. Furthermore, the distances between the donor and the acceptor is also important and should be less than 10 nm.

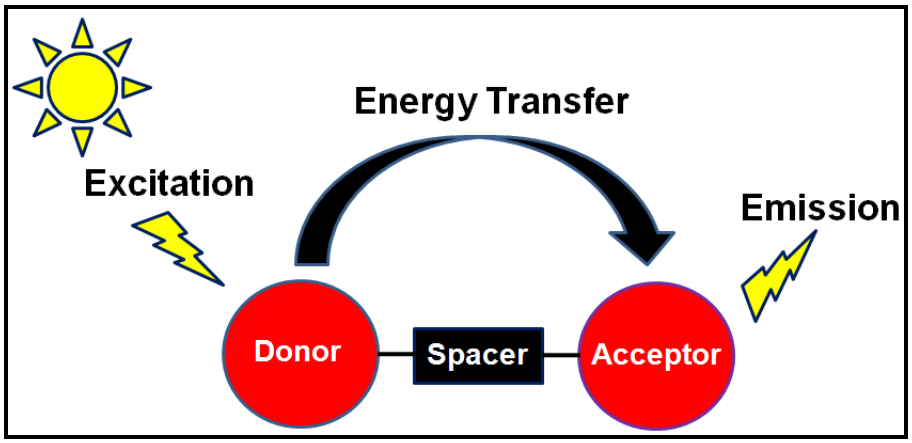

Figure 18. Schematic representation of fluorescence resonance energy transfer

In most of fluorescent RET systems; energy transfer occurs through space in which fluorophores are linked to each other with a non-conjugated spacer. As seen in Figure 19, the chromophores are attached with a spacer like aliphatic structures. Through space energy transfer is described by means of Forster mechanism and mostly named as Forster resonance energy transfer. There are several parameters that play key role in this mechanism and the details are mentioned in next section.

There are also some energy transfer systems in which the donor is linked to an acceptor via electronically conjugated spacer (Figure 19). This type of energy transfer systems are called as through-bond energy transfer. Although the chromophores can transfer energy via several pathways in these systems, dexter energy transfer mechanism is widely used to explain whole process.

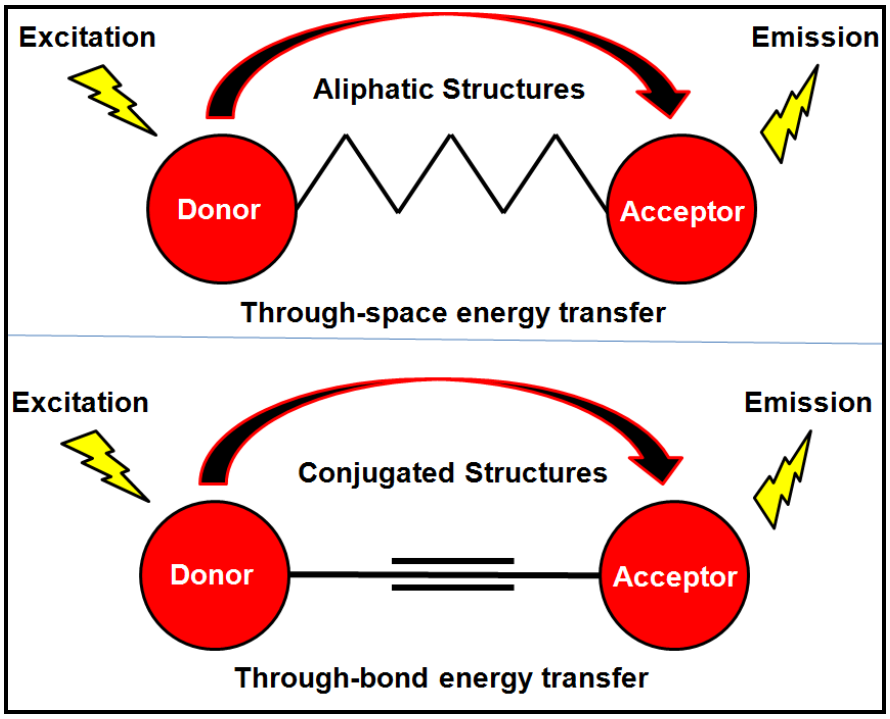

Figure 19. Schematic representation of through-space and through-bond energy transfer systems

2.4.1. Forster Type Energy Transfer

The energy transfer occurring over long distance (from 1 A^o to 100 A^o) from a donor chromophore to an acceptor chromophore is called Forster resonance energy transfer (FRET). It was fist defined in 1948 by Forster.[59] However, it must be noted that Forster resonance energy transfer (FRET) is also referred as fluorescence resonance energy transfer. Actually, FRET is a radiationless energy transfer process in which the electronically excited donor molecule transfers energy to an acceptor molecule through dipole-dipole coupling. Then, the energetically excited acceptor molecule (fluorophore) releasing its energy via fluorescence. The Jablonski diagram summarizes the FRET process (Figure 20). As depicted in Figure 20, the donor chromophore is excited by absorption of light and simultaneously energy transfer takes place from excited donor to acceptor chromophere via the dipolar coupling between donor choromophore emission and acceptor chromophore excitation dipole moments.

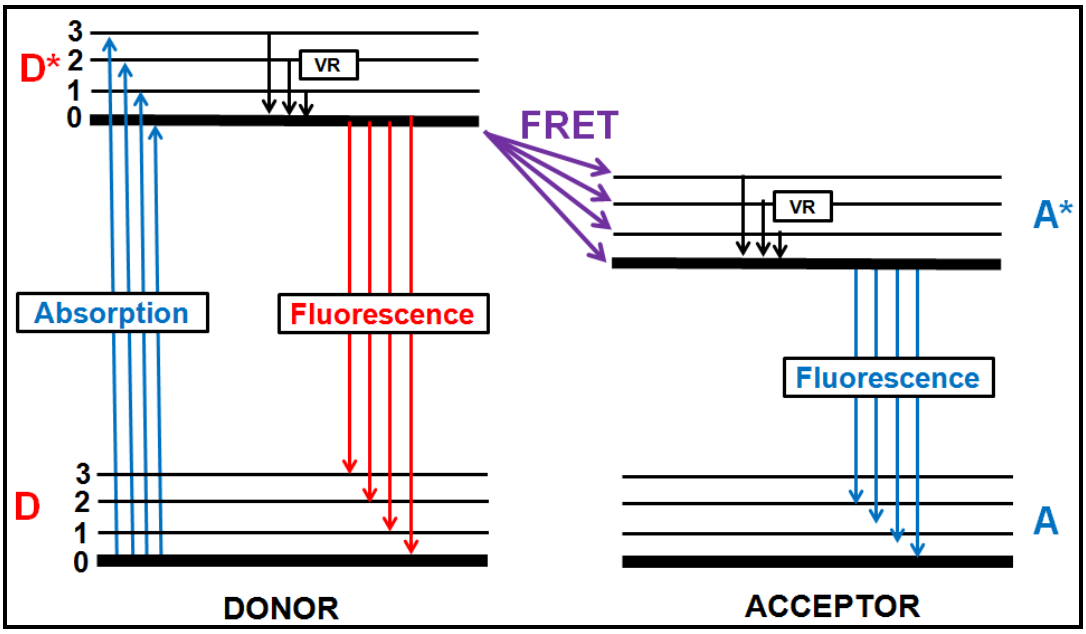

Figure 20. The Jablonski diagram summarizes the FRET process

Efficiency of FRET (E_{FRET}) depends on the distance between the donor and the acceptor according to following reaction:

$$E_{FRET} = R_0^6 / (R_0^6 + R^6)$$

The R_0 is the Forster radius and it is sometimes called critical distance. The critical distance can be calculated by equation:

$$R_0 = [8.79 \times 10^{-5} (\kappa^2 \eta^{-4} QJ(\lambda))]^{1/6} A^0$$

where κ is the angle between the two chromophore dipole moments. η represents refractive index of medium and the spectral overlap integral is denoted as J(λ). It is represented by the equation where F_D is the normalized donor fluorescence:

$$J(\lambda) = [\int F_D(\lambda) \mathcal{E}_A(\lambda) \lambda^4 d\lambda] / \int F_D(\lambda) d\lambda \ \ mol^{-1} cm^{-1} nm^4$$

The efficiency of energy transfer can also be determined by following the fluorescence intensity of donor or life time of donor chromophore.

$$\mathbf{E_{FRET} = 1 - (I_{DA} / I_D) \text{ and } E_{FRET} = 1 - (\tau_{DA} / \tau_D)}$$

I_{DA} = Fluorescence intensity of donor chromophore in the presence of acceptor chromophore

I_D = Fluorescence of donor chromophore in the absence of acceptor chromophore

τ_{DA} = Fluorescence lifetime of donor chromophore in the presence of acceptor chromophore

τ_D = Fluorescence lifetime of donor chromophore in the absence of acceptor chromophore

There are several parameters that affect the E_{FRET}. For example, the emission spectrum of donor should overlap with the absorption spectrum of acceptor. The distance (R) between the donor chromophore and the acceptor choromophore is very critical which should be in the range of between 1 to 10 nm. As equated in above, E_{FRET} is proportional with R and it affects the efficiency with the sixth power. The emission dipole moment of donor and the acceptor absorption dipole moment should be in suitable orientation. Also, their separation vector should also lie down in appropriate orientation.

Our group was designed an energy transfer system based on a dendrimer skeleton (Figure 21). This dendritic light harvester (**17)** consists of bodipy and perlenediimides dyes as donor and acceptor, respectively.[60] The donor units were attached to the acceptor moiety via click chemistry. It is a very important and first example of efficient energy transfer system based on bodipy-perlenediimides dyes in a dendritic architecture. Highly fluorescent Bodipy dyes quenched because of energy transfer. The quantum yields of Bodipy dyes decreases to 0.01. According to experimental data, the energy transfer efficiency was calculated as 99%.

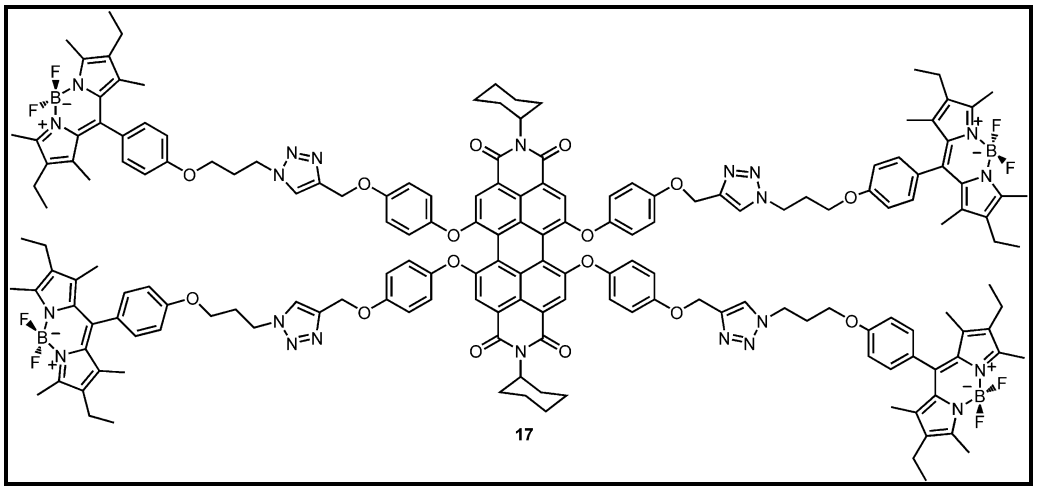

Figure 21. The structure of dendritic light harvester consists of bodipy and perlenediimides

The another example is a demonstration of an energy transfer system in which an UV emissive coumarin transfers its energy to an near-IR emissive perlenediimide dye (**18)**.[61] As seen in Figure 22, two coumarin dyes was excited at 345 nm and their emission totaly quenched because of energy transfer. The efficiency of energy transfer is 99%.

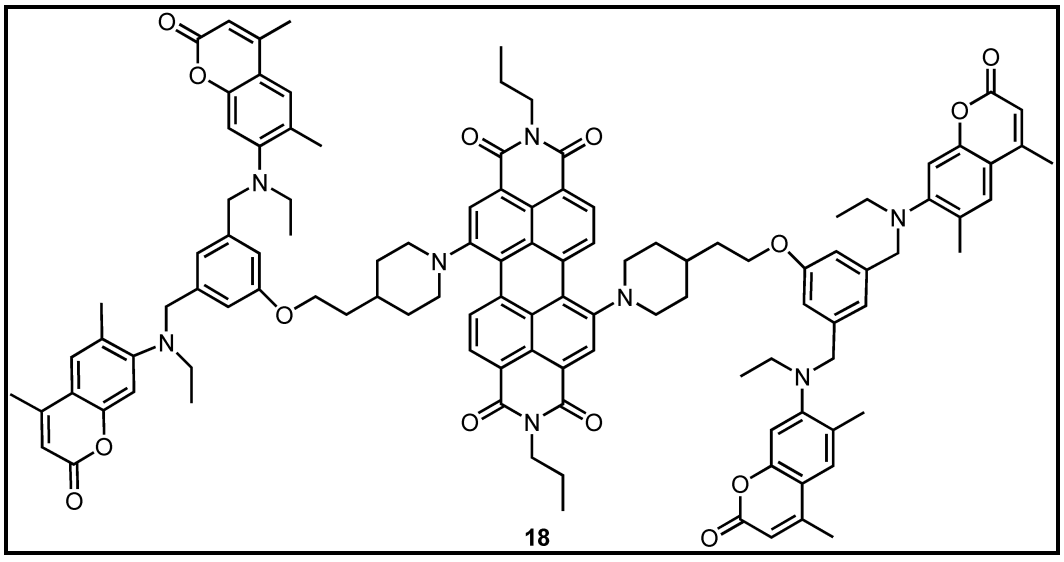

Figure 22. The structure of dendritic light harvester consists of coumarin and perlenediimides

2.4.2. Dexter Type Energy Transfer

There is no restriction, which is the overlapping between the emission wavelength of donor fluorophore and the absorption wavelength of acceptor, for an efficient energy transfer in through-bond energy transfer systems. Through-bond energy transfer mechanism is defined by dexter model and most of through-bond energy transfer is called dexter type energy transfer. In this type of energy transfer systems, the donor and the acceptor unit attached together via conjugative spacers. Although there is no requirement for spectrum overlap, there must be an orbital interaction between donor and acceptor via direct or bridge spacers. Because of orbital interaction requirement, dexter type energy transfer occurs in short range ($<10A^0$). The rate of energy transfer depends on the distance between the donor and the acceptor.[62]

$$\mathbf{k_{Dexter} = KJe^{(-2R_{DA} / L)}}$$

where **K** denotes orbital interaction, the overlap integral between donor emission and acceptor absorbance is depicted as J. **L** is the Van der Waals radii and $\mathbf{R_{DA}}$ is the donor acceptor separation.

One example of through bond energy transfer systems (**19**) were constructed as attaching the rhodamine dye with a coumarin dye conjugatively via using a proper spacer which inhibits the planarity between the donor and the acceptor and enable the through bond energy transfer.[63] These systems behave like an energy transfer cassettes instead of single molecules and they have been working as pH probe (Figure 23). Furthermore, the pH alteriations leads to a change both excitation and emission wavelengths of the acceptor (rhodamine derivative) which plays a key role in the efficiency of energy transfer. The compounds **19a-d** were excited about from 372 nm in phosphate buffer/MeOH (3:2) and an intense emission was gathered from 582 nm which is characteristic rhodamine emission. The energy transfer efficiency was 99%. On the other hand, **19e** showed a large blue-shift with a remarkable change in emission intensity by changing the pH of the environment.

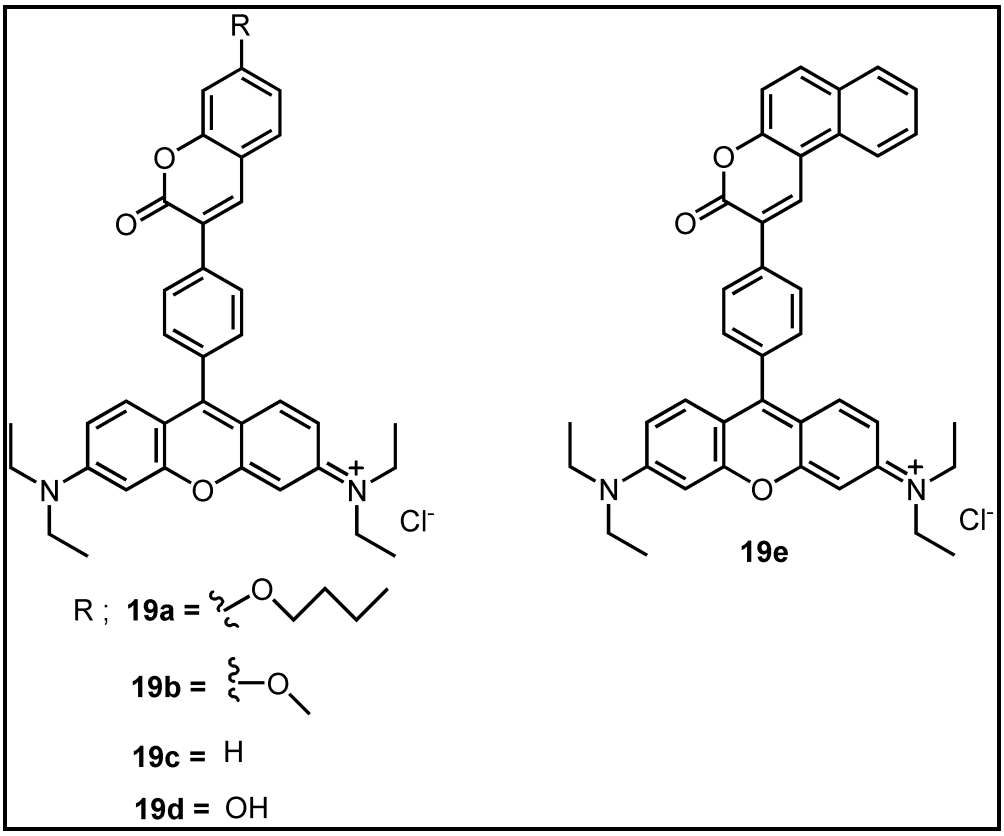

Figure 23. The structures of pH indicators working with Dexter type energy transfer principle

Burgess et al. was designed two energy transfer system which clearly demonstrated the through bond energy transfer system.[64] These two examples clearly shows the importance of orientation between the donor and the acceptor fluorophore on energy transfer efficiency (Figure 24). It must be indicated that the compond **20** is not energy transfer cassette since it is a fully conjugated system. This system has a red shifted broad absorbance. On the other hand, the compound **21** has a twist at the linkage point between bodipy and anthracene unit. This twisted structure facilitates the through bond energy transfer ad makes **21** an efficient energy transfer cassette.

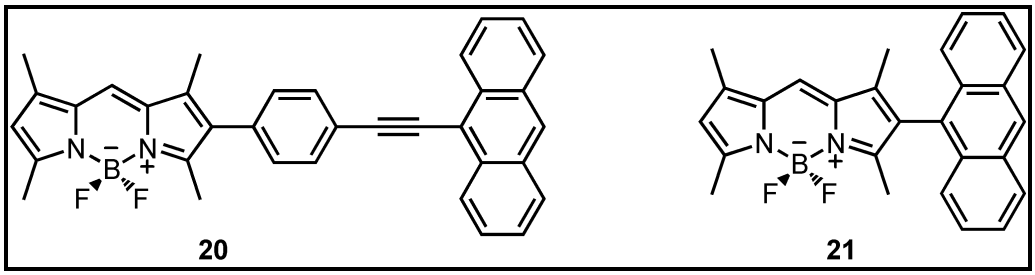

Figure 24. Bodipy based through bond energy transfer systems

2.4.3. Light Harvesting Systems

The science world has turned towards to explore new alternative energy sources to supply exponentially increasing energy need. In this era, some concepts became popular and they have been investigated extensively. One of them is artificial photosynthesis systems. These systems have been designed to harvest the solar energy (sun light) and then convert it to chemical or elecrochemical energy forms. This energy conversion plays a key role to solve energy-thirsty of modern world. Therefore, there is strong demand to design rationally construct light harvesting systems. Many light harvesting systems have been reported in literature.[65,66] However, some remarkable and representative examples will be discussed in this section.

One of light harvesting system has been designed from our research group.[67] We reported a dendritic light harvesting system (**22**) in which eight Bodipy dyes located at periphery and perlenediimide dye centered at the core. The system could efficiently collected the visible light with its large absorption cross section and effectively funnel this harvested energy to the core unit. The calculated energy transfer rate is 6.77×10^9 s^{-1} and the energy transfer efficiency is 95.7%.

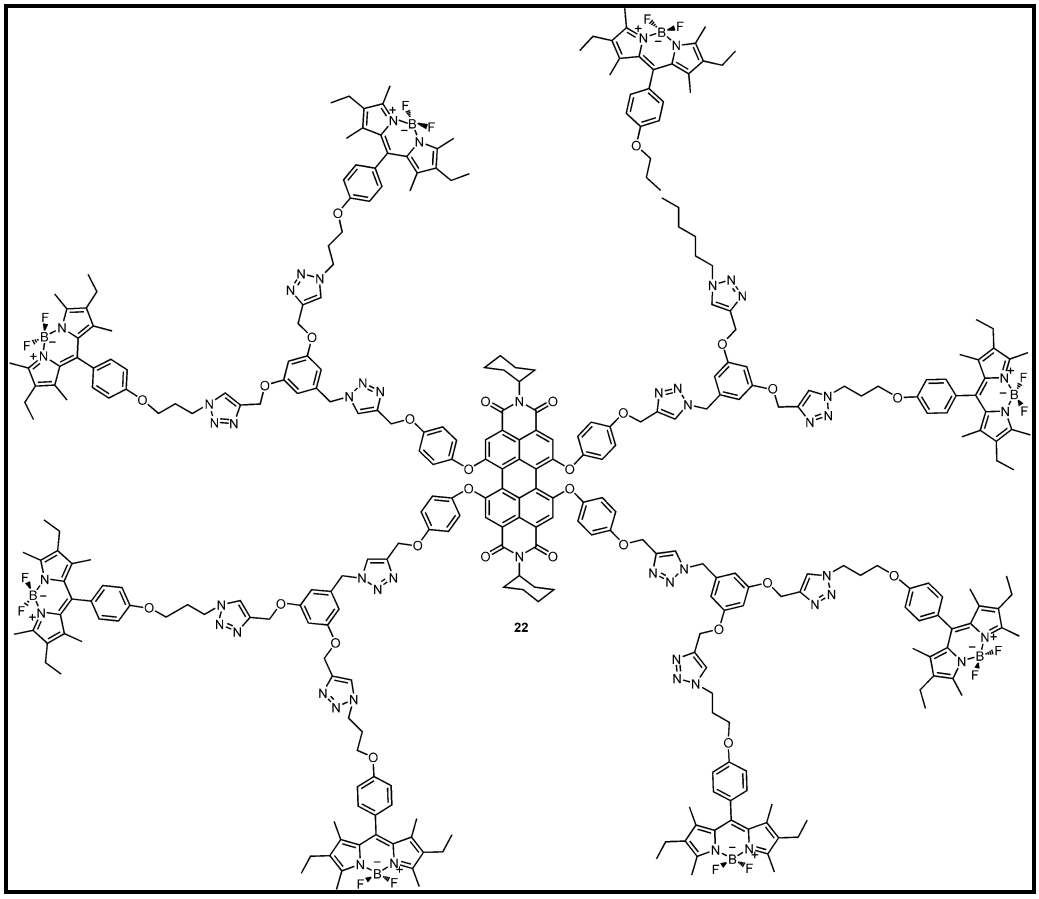

Figure 25. Structure of dendritic light harvesting system **22**

It is possible to synthesize a multi component cluster by attaching each fluoregenic part in a controllable way. Compound **23** is an example at this type of light harvesting system (Figure 26).[68] The acceptor unit is a krypto-Bodipy which has emission maxima at 540 nm. Multi-chromophoric donor parts were attached to acceptor unit by replacing the fluorine atom located at the boron center. This light harvesting system can absorb the light from 200 to 550 nm. The ethynylfluorene is responsible for the absorption of light below 300 nm. On the other hand, pyrene dye collected the region between 280 and 420 nm while 1,4-diethynylphenyl group absorb the light from 320 to 490 nm.

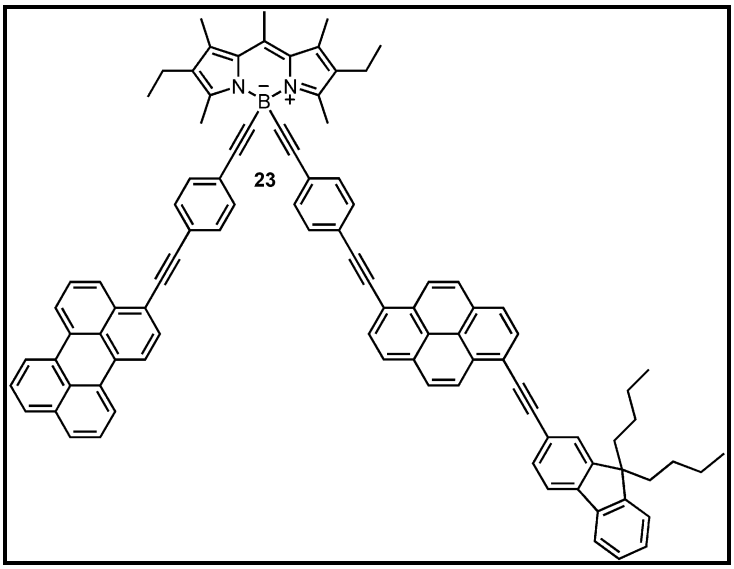

Figure 26. Structure of multi chromophoric light harvesting system **23**

2.5. Energy Conversion

Energy is a key factor of life and exiting in all areas. Because of its nature, energy cannot be destroyed and also cannot be created. Therefore, the energy just transforms from one form to another. There are various forms of energy such as chemical, kinetic, thermal, electrical, potential, or radiation. The transformation between energy forms can only just take place by means of energy conversion systems. Hence, energy conversion systems play an indispensable role in the generation and utilization of energy. It must be noted that generation or utilization of energy always refers to convert one energy form into another form.

Although the energy consumption have been increasing dramatically, the fossil based energy sources shows much faster depletion. Therefore, there is strong demand for the development of renewable and alternative energy sources and strategies for energy conversion systems into electrical or rotational or propulsive mechanical power to meet the energy need. When it's renewable and environment friendly features are considered, the solar energy conversion is the most promising strategy to solve energy problem.

There are lots of solar energy conversion systems converting solar energy into thermal energy or electricity. However, the production electricity from the solar

energy has attracted great attention in science world. There are two ways for generating electricity. The first one is to capture solar energy as thermal energy such as heat than transforming this heat into electricity by means of power plants or classical engines. The second and popular way is direct conversion of solar energy into electricity by using solar cells. In the next section, one of the most studied solar cell type, DSSC, will be covered briefly.

2.5.1. Dye Sensitized Solar Cell (DSSC)

As indicted above, solar cells are more promising energy conversion systems using the sun light as an energy source. Most of commercial solar cells are silicon based. Although they have moderate efficiencies (15%)[69], their production`s techniques are so difficult and this difficulty leads to high cost which inhibits the wide usage. On the other hand, DSSC have gained popularity after its discovery in 1991 by Michael Gratzel.[70] It can be a strong candidate for the replacement of silicon based solar cells because of their high solar light-to-electricity conversion efficiency, easy fabrication techniques and their lower cost. In spite of their lower cost, DSSCs still show lower over-all efficiency. Therefore, these systems must be intensively investigated to satisfy optimum price to performance ratio.

The DSSC is composed of two electrodes that are a photo-anode and a photoinert counter electrode (working as cathode). There is a redox mediator (liquid electrolyte) between these two electrodes like a sandwich. Five materials are used to construct DSSC. These materials are; 1) a fluorine doped tin oxide (FTO) glass substrate that is also identified as conductive and transparent oxide (CTO); 2) a photosensitizer (dye senitizer); 3) a nanocrystalline titanium oxide (TiO_2) thin film working as a semiconductor; 4) a platinum coated glass substrate as a counter electrode; 5) an electrolyte (also called as redox mediator) (Figure 27).

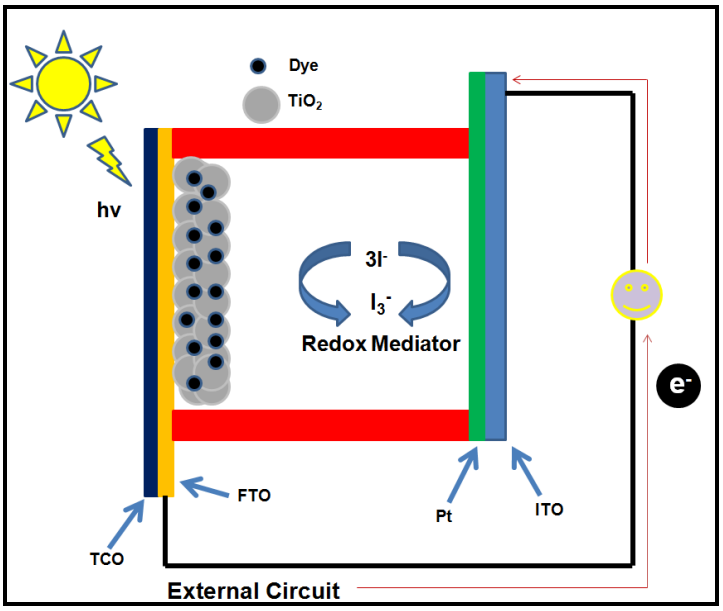

Figure 27. Schematic representation of the construction of DSSCs

There is a great effort to improve the efficiency of DSSC by developing the constitutional parts of systems. However, when we consider the operational principle of DSSC, which was discussed in-depth in latest reviews[71,72], the photosensitizer (dye) is the most critical part of the system. As a result of it, almost all of the research for the development of DSSC has been focused on designing more efficient photosensitizers. There are some important characteristics which a photosensitizer should have them. First of all, a photosensitizer should broad absorption spectrum which covers not only visible region but also near-IR region. Secondly, a photosensitizer should have functional groups such as -COOH, SO_3H, H_2PO_3 to bind semiconductor surface. Thirdly, to satisfy an efficient electron transfer, the excited level of the photosensitizer should have a higher energy than the conduction band of semiconductor. The other parameter is to provide a back electron transfer from electrolyte to the photosensitizer, the oxidized state level of the photosensitizer should have more positive value than the redox level of electrolyte. Then, dye molecules should not be aggregate onto semiconductor surface. Finally, the photostability of the photosensitizer should be high. Generally, photosensitizers can be grouped into two main class which are metal complex based and metal free organic dyes.

2.5.2. Metal complex Based Photosensitizers

Metal complex based photosensitizer can be classified into two groups, namely ruthenium based complexes and other metal complexes. Both of them have similar structure skeleton based on metal ligand complexation in which a metal ion is wrapped up with ancillary ligands having at least one anchoring functionality to bind semiconductor surface. In these photosensitizers, metal to ligand charge transfer (MLCT) process is responsible for light absorption which is mostly in the visible region. Therefore, central metal ion plays a leading role in the properties of photosensitizer. Ligands also affect the photophysical characteristics of photosensitizer. It is possible to improve the efficiency of photosensitizer by tuning ligands with different substituent.

- **Ruthenium based complexes**

Ruthenium based metal complexes are the most widely used photosensitizers in DSSC applications because of its compatible photovoltaic properties such as a broad absorption spectrum, favorable ground and excited state levels, electrochemical and photostability, and appreciable long excited-state lifetime. Some of complexes show highest solar cell efficiency more than 10%. The influence of ruthenium complexes on DSSC was reviewed recently in the literature[3,73].

Gratzel and co workers were designed various ruthenium-bipyridyl complexes in 1993.[74] However, one of them, the cis-(SCN)2-bis(2,2`-bipyridiyl-4,4`-dicarboxylate) ruthenium(II) (**24**) which is called as N3, shows outstanding features broad and wide span (up to 800nm) light absorption spectrum, long excited state lifetime, and strong adsorption capability onto semiconductor surface by means of four carboxylic groups. The conversion efficiency of N3 for solar energy-to-electricity is 10% which is the first obtained result in this range. Moreover, its incident photon-to-current efficiency (ICPE) in the visible region is about 80%. Right after, same research group was synthesized a ruthenium based dye tri-thiocyanato-4,4`,4``-tricarboxy-2,2`:6`,2`-terpyridineruthenium(II) (**25**), which is known as black dye.[75] It is called as black dye because of its wide and strong

absoption capability which makes the color of dye black. It has similar high efficiencies with appreciable photostability up to 50 million cycles which equals to 10 years sun light exposure in Switzerland (Figure 28).

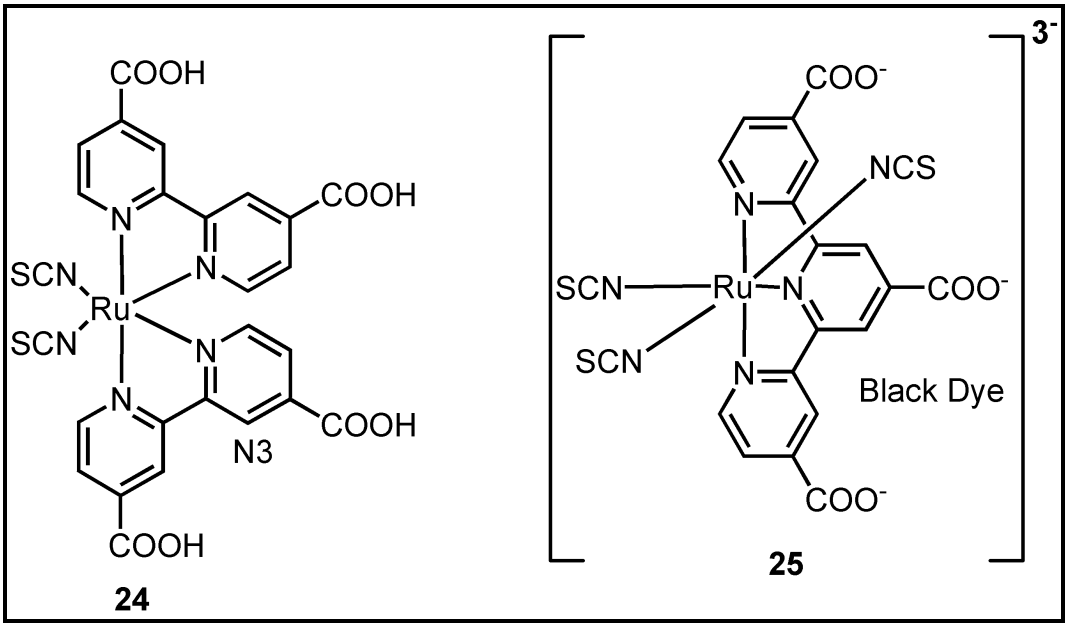

Figure 28. Structure of Ru-polypyridyl complexes for DSSCs

Wang and co-workers designed some heteroleptic ruthenium based polypyridiyl photosensitizers which have high molar excitation coefficient. The ancillary ligand units of complexes were decorated with electron-donating groups such as alkyl thiophene **26**[76] and alkyl thieno[3,2-b]thiophene **27**[77] (Figure 29). 11% efficiency was obtained by using the dye X in an acetonitrile based electrolyte. Moreover, it was discovered that titannium oxide film thickness can be reduced by using this type of photosensitizer having high extinction coefficient. The decreased thickness leads to an increase in efficiency. The photosensitizer Y has also a high molar extinction coefficient and it has been demonstrated that under 1.5 global sunlight it has 10.53% conversion efficiency in DSSC.

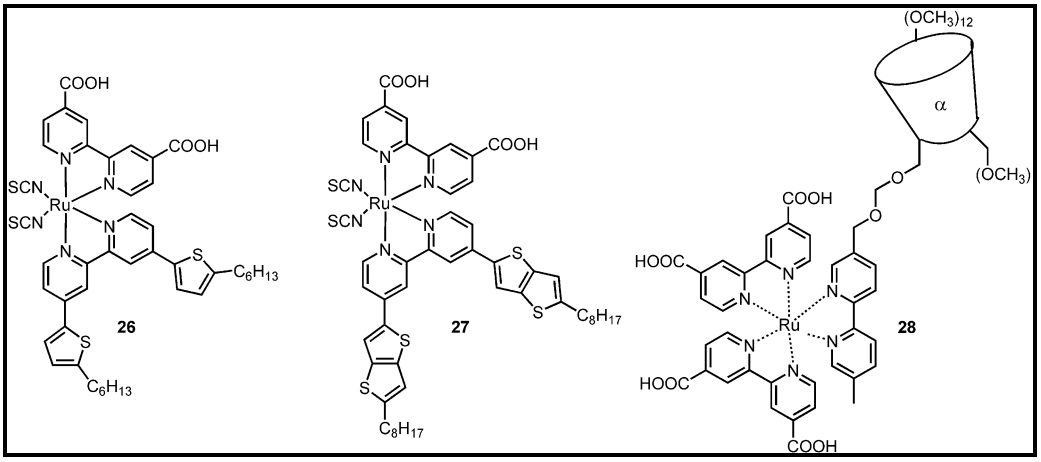

Figure 29. Chemical structure of Ru-based photosensitizers for DSSCs

The photosensitizer **28** is very interesting example which serves an efficient photosensitizer/redox couple interaction and dye regeneration (Figure 29).[78] The comparison between of photosensitizers with and without cyclodextrin (CD) functionality showed that the cyclodextrin substitutions leads an enhancement in short-circuit photocurrent density and open circuit voltage. The difference stems from the iodide-triiodide electrolyte (redox couple) having an affinity to CD. The binding of the redox couple to CD cavity makes easier dye regeneration.

- **Other metal based complexes**

Ruthenium is rare earth metal. The low abundance of ruthenium cause to high cost for DSSC and this inhibits the large scale production. Therefore, there are lots of effort to design DSSC having other metal complexes working as photosensitizer.

Platinum [Pt (II)] diimine dithiolate based square planar complexes have been widely studied. Any functional subsitution on diimine or dithiolate groups leads to dramatic change in electronic and photopyhsical features of orbitals (LUMO and HOMO). One of the efficient Pt based photosensitizer **29**[79] showed a moderate efficiency (3%) under 1.5 G solar light (Figure 30). On the other hand, Osmium [Os(II)] based photosensitizers can be considered as a good replacement for ruthenium centered photosensitizer. They have an extended and strong MLCT band region. For example, by using the dye **30**[80], it is possible to take an photon conversion spectrum up to far

near-IR region (up to 1100 nm) and it exploited great photovoltaic efficiency in DSSC applications (Figure 30). Fe(II) complexes are also strong candidates for DSSC applications (Figure 30). After the adsorption of complex **31** onto TiO_2 films, the illumination with power of 75mW/cm^2 resulted with an open circuit photovoltage of -360 mA and a short cicuit photocurrent up to 75μA/cm^2 (Figure 30). The ICPE efficiency is about 10-11% which is so low when compared with ruthenium complexes.[81]

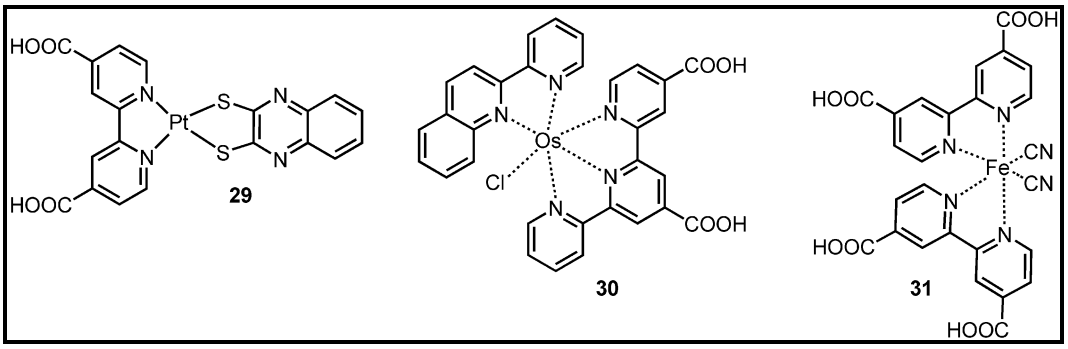

Figure 30. Structures of Pt(II), Os(II) and Fe(II) based complexes for DSSCs

Cu(I) complexes are the most promising alternative to replace ruthenium based photosensitizers since they exploits similar photophysical characteristics as ruthenium complexes. Their low cost also serves a great opportunity for manufacturing. However, there has been very limited research published in the literature. Some examples were depicted in Figure 31. The complex **32** yielded a photocurrent about 4 mA cm^{-2} and the ICPE value is 30%.[82] **33** and **34** were reported by Gratzel and co-workers.[83] The complex **34** has higher molar excitation coefficient than the complex **33** because of its extended conjugation. The solar conversion efficiency of **34** in DSSC with liquid electrolyte is 2.3%.

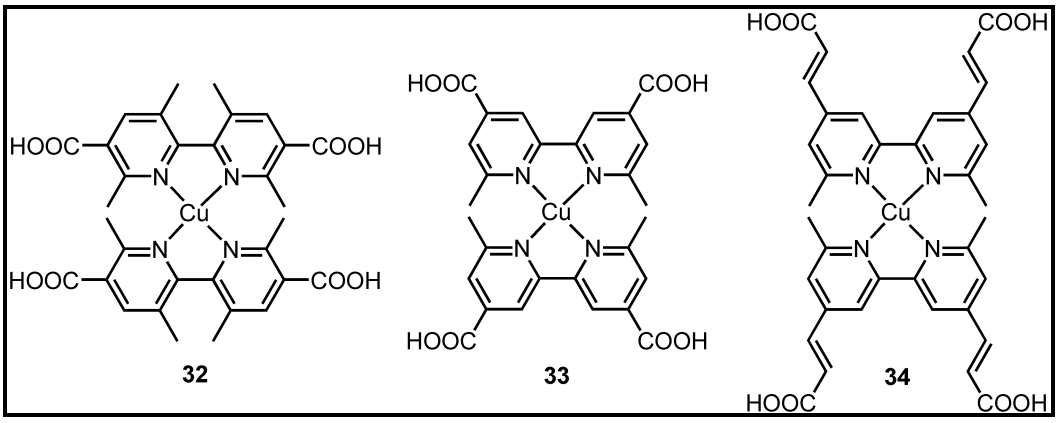

Figure 31. Structures of Cu(I) based complexes

2.5.3. Organic dyes (Metal free photosensitizers)

Organic dyes are considered as a great alternative to ruthenium complexes because of their superior features. There are numerous example of organic based photosensitizers reported. These versatility stems from their easier synthesis and design methodology. Besides their high molar excitation coefficient, the other advantageous of organic dyes is their low cost and environment friendly character.

Some examples of organic photosensitizers were depicted in Figure 32. The dye **35**[84] was called as the original coumarin sensitizer. In spite of its great performance in electron injection process, it yielded very low energy conversion efficiency. On the other hand, the vinylene functionalized dye **36** has higher molar excitation with its red shifted absorption spectrum. However, vinyl groups triggered the aggregation of dyes The cyano carboxy unit provides a binding side onto TiO_2 surface. The conversion efficiency of it is about 6% under AM 1.5 G.[85]

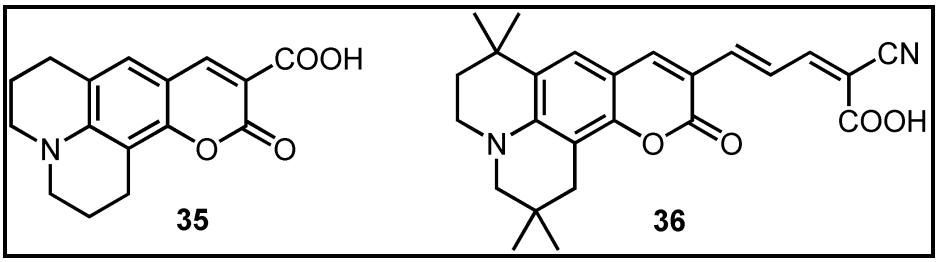

Figure 32. Representative examples for organic dyes based photosensitzers

Mullen research group has been designed a boutique library of organic dyes based on spacers.[86] The dye **37** is one of them (Figure 33). Although the highest ICPE value was observed 73%, it showed moderate solar conversion efficiency in liquid DSSC about 2.3%. In general, organic dyes cannot produce high power conversion efficiencies in DSSC systems but their versatility and richness motivate the scientists to design novel dyes with higher solar conversion capabilities.

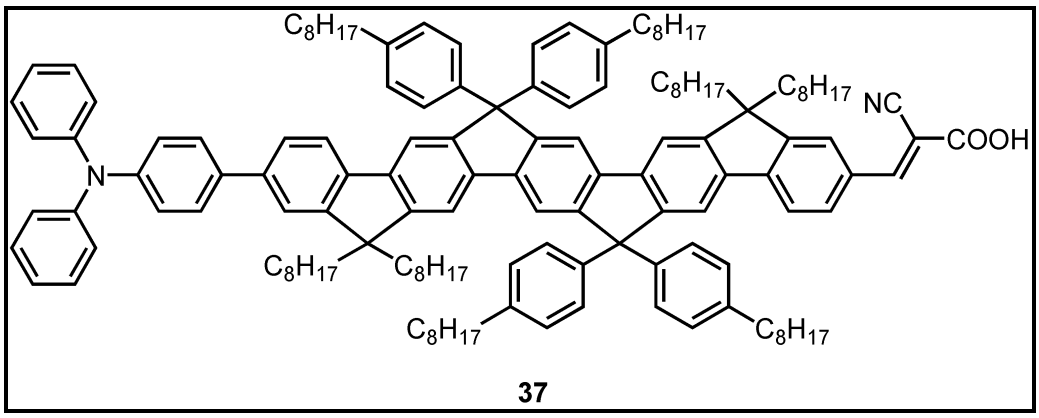

Figure 33. Structure of organic dye **37** for DSSCs application

2.6. Bodipy Dyes

Although many fluorescent dyes have been reported in recent years, after its discovery[87], Bodipy has attracted great attention and increased its popularity dramatically over the past thirty decades.[88,89] Its high fluorescent quantum yield, high molar absorption coefficient, narrower emission bandwidth, high thermal stability, high photostability, great solubility, low triplet state formation and ease of functionalization from various positions make BODIPY fluorophore favorable over the other commercial fluorescent dyes. As a result of its superior properties, Bodipy dyes serve multidisciplinary applicability and they have been effectively used not only in chemistry field but also in biochemistry, physical chemistry, and supramolecular chemistry.

2.6.1. The Numbering System of BODIPY Skeleton

The numbering system of Bodipy dye is different from its precursor namely dipyrrin. However, meso, α, and β terms point out same pasitions for both structures. The numbering system of Bodipy and dipyrrin was schematically depicted in Figure 34.

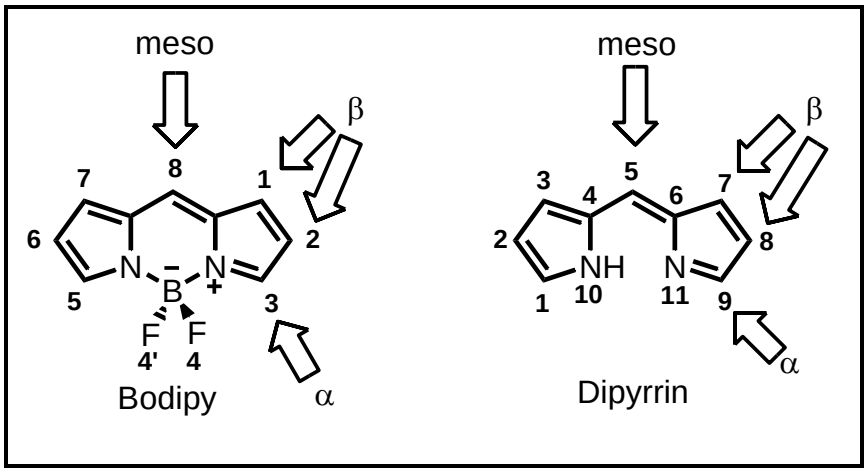

Figure 34. Numbering systems of BODIPY core and dipyrromethene

2.6.2. The Functionalization of BODIPY Skeleton

The versatility of Bodipy originates from its richness in functionality. Today, all positions of Bodipy dyes have been decorated with different substituents. Each positions gives different reaction according to its electronic and chemical properties. For example, electrophilic aromatic substitution reaction can be valid for 2 and 6 positions. The treatment of Bodipy core with chlorosulphonic acid yielded a water soluble Bodipy derivative **38** (Figure 35).[90]

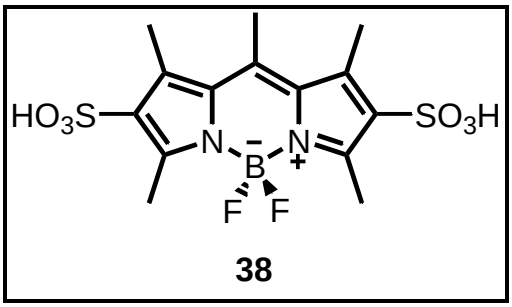

Figure 35. Chlorosulfonic acid substituted water soluble BODIPY Derivative

Moreover, 2 and 6 positions can give reaction with other electrophiles such as iodine or bromine. It can be possible di-bromo **39**[91] and di-iodo **40**[92] substituted Bodipy derivatives (Figure 36). Both bromination and iodonation cause a remarkable amount red shift in the absorption and emission spectra. Furthermore, these modifications leads to a dramatic decrease in the fluorescence quantum yield of Bodipy core by heavy atom effect which increases the rate of intersystem crossing. Therefore, especially di-iodo substituted Bodipy derivatives can be used a photodynamic therapy reagent because of their high singlet oxygen generation capabilities.

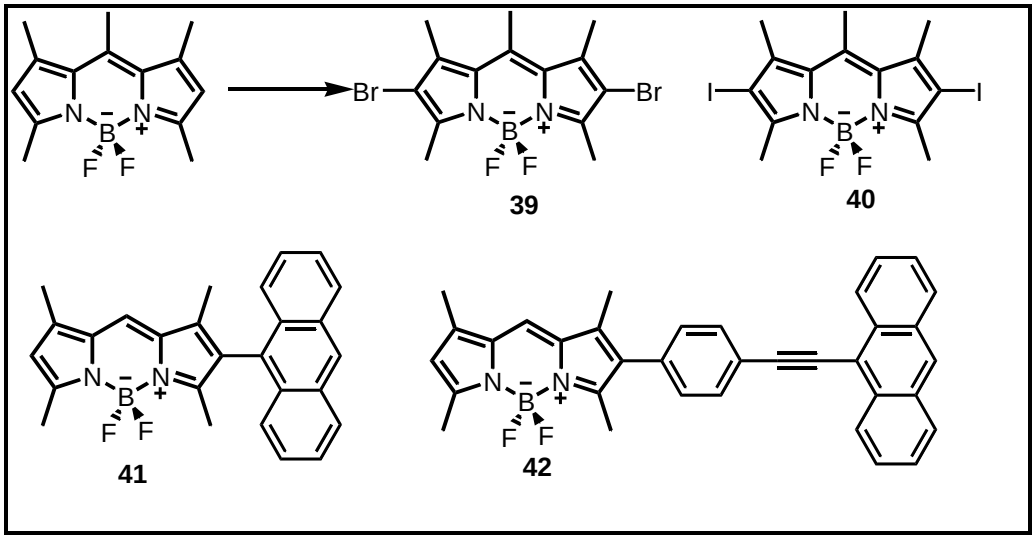

Figure 36. Synthesis iodo and bromo functionalized Bodipy dyes and anthrecene grafted Bodipy cores

By means of palladium assisted Suzuki and Sonogashira coupling reactions, mono or di substituted derivatives can be extended with acetylene functional organic modalities. **41** and **42** are two molecules prepared by using these coupling reactions (Figure 36).[93] After these modifications, an appreciable amount of red shift can be observed.

Fluoride atoms attached to boron unit of Bodipy core can undergo a displacement reaction. This functionilazation methodology is widely used to construct energy transfer systems and it does not cause any change in emission or absorption maxima.

Fluoride units gave a replacement reaction with aryl (**43**)[94], ethynyl (**44**)[95] and ethynylaryl (**45**)[96] groups by Zieessel research group as seen in Figure 37.

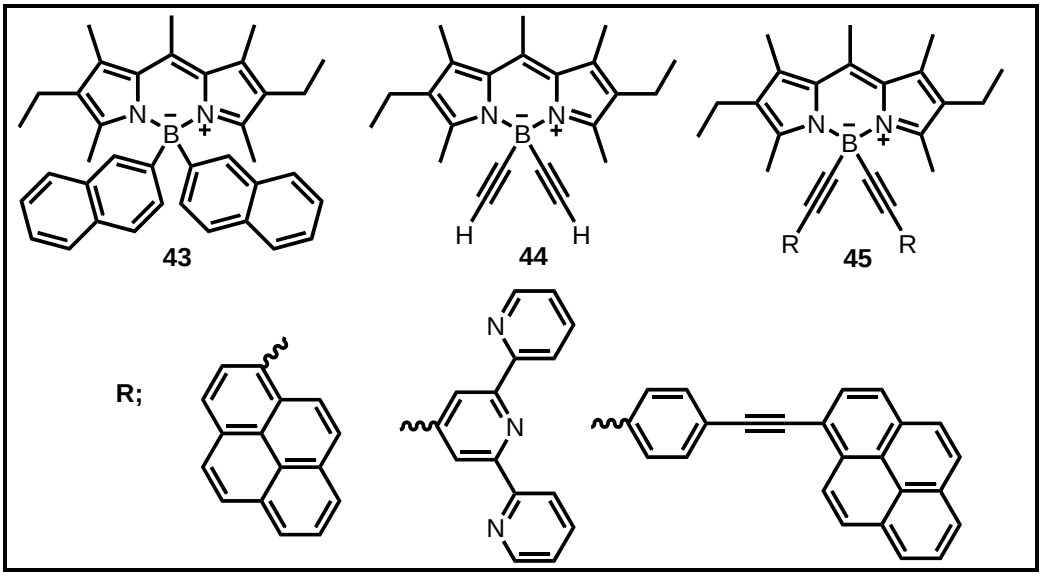

Figure 37. Modification of Boron center of BODIPY skeleton

If the Bodipy core consists of methyl groups at 3 and 5 positions, these methyl substituents can undergo Knovonagel type condensation reaction with different aromatic aldehydes. This stryly modification serves an easy and efficient way to fabricate new long wavelength fluorophores without any significant loss in fluorescence quantum yield. Our group was discovered that methyl groups located at 1 and 7 positions can also undergo condensation reaction with aromatic aldehydes. This discovery is a breakthrough for the preparation of near-IR emissive Bodipy dyes. As depicted in Figure 38, it is possible to synthesize mono **46**, di **47**, tri **48** and tetrastryl **49** functionalized Bodipy derivatives.[97] This methodology provides an easy tunability in emission wavelength maxima.

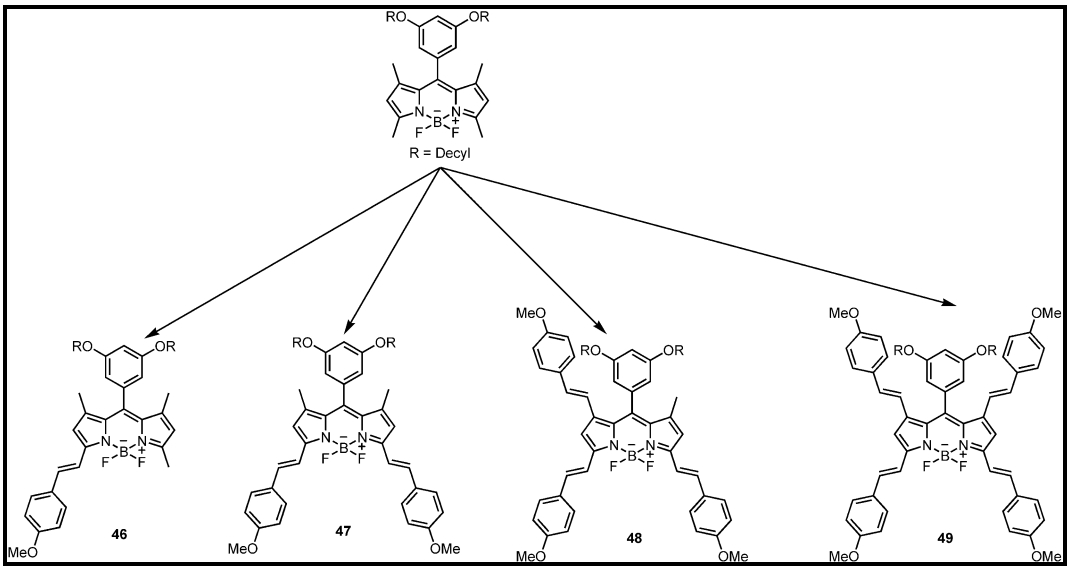

Figure 38. Knovanagel type condensation reactions from 1,3,5 and 7-positions of Bodipy cores

3 and 5 positions allow the nucleophilic substitution reaction if these positions host good leaving groups such as chloride. Alkoxy **50**, thioalkoxide **51** or amino **52** functionalities can be used as a nucleophile to replace chlorine atoms (Figure 39).[98,99,100] As a result of this substitution reaction, the photophysical characteristic of Bodily core remarkably changes.

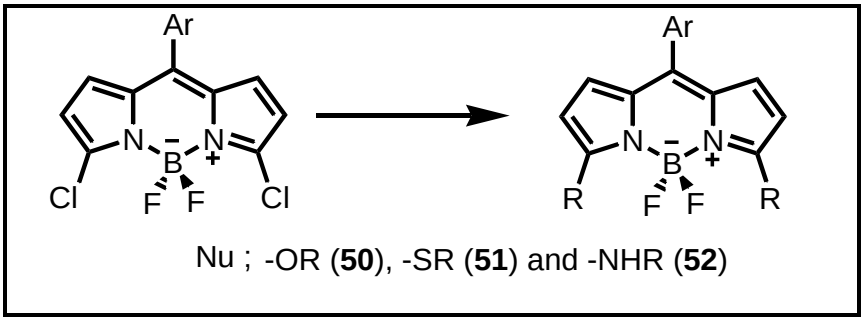

Figure 39. Nucleophilic substitution reactions at 3 and 5 positions of Bodipy core

2.7. Self-Assembly

One of the most important concept of supramolecular chemistry is self-assembly. Self-assembly can be defined as the spontaneous clustering of molecular building

blocks to construct complex superstructures. As it is known, the root of most biological processes and systems extend to self assembly. Therefore, self-assembly plays a crucial role not only in the understanding of biological proceses but also provides innovatiave visions to construct new molecular architetures. It is possible to construct more complex systems consiting of small building blocks by using self-assembly. Normally, it is so difficult or inaccesible to form such a complicated sytems by using traditional covalent bond chemistry. There is a great interst towards the self-assembly due to its programmabiliy. When the nature of self-assembly is considered, the programmability enables the construction of superstructures from small components automatically.

Self assembly have been used in many applicacitions of supramolecular chemistry. However, to cover all these topics is not the scope of this thesis. Therefore, I will focus on the the artificial molecular machine and one novel molecular machine will be presented in seventh chapter.

2.7.1. The Artificial Molecular Machine

The artificial molecular machines can be defined as the assembly of a variable number of molecular structures constructed to provide a function through the mechanical motion of its segments which takes place with external stimuli. One of its important segments is the motor part which can convert energy into mechanical work. These movements mostly arise as nuclear arrangements in their components. These motions and rearrangements has been followed by using various and advanced techniques. When it is considered that the recent advances and developments in chemistry world especially in supramolecular field provides a better understanding in for biological molecular machine system and this enlightenment makes possible to design novel artificial molecular machines which can mimic the biological predecessors. The transfer of machine concept into molecular level as artificial molecular machines has attracted great attention from science world and recent efforts play a indispensable role in the development of nanoscience and nanotechnology.

The first molecular concept wad defined about 50 years ago by Feynman who proposed the miniaturized machinery concept and laid the foundation of today's research goal on artificial molecular machine which is the fabrication of nanorobots.[101] These nanorobots can undertake intelligence missions and functions. There have been reported numerous example of artificial molecular machines in the literature and many review articles were published to demonstrate these prototypes.[102,103,104] However, most of them have been based on rotaxane or catenane like systems.

A catenane is a chemical compound which consists of mechanically interlocked two or more rings. This interlocking does not contain any chemical interaction between rings. On the other hand, a rotaxane has a linear molecule that is threaded through a ring and with the ends of the thread capped with bulky substituent, namely stopper, which inhibits the dethtreading of the ring from the thread or axle. A pseudorotaxane, on the other hand, is a rotaxane like structure without stoppers (Figure 40).

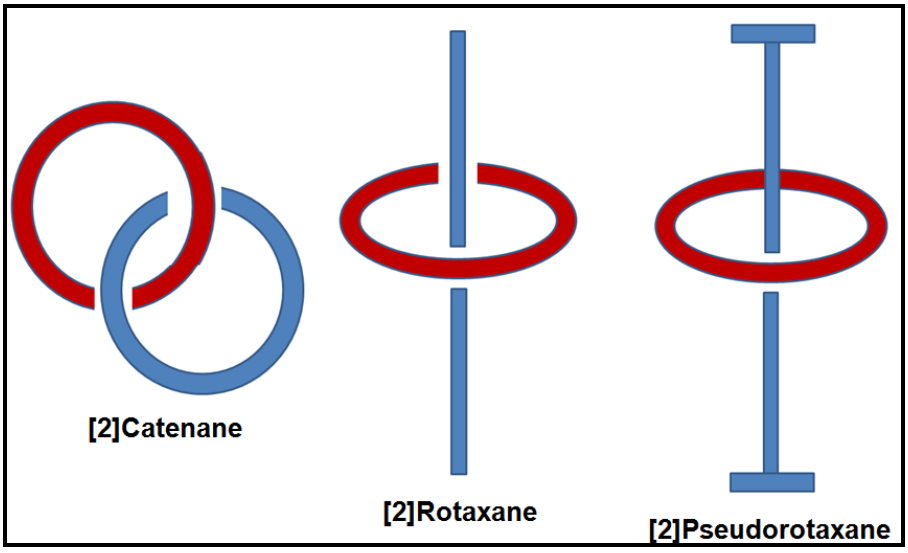

Figure 40. Cartoon representation of [2]catenane, [2]rotaxane and [2]pseudorotaxane

There are lots of artificial molecular machines prototypes consisting of rotoxane or catenane structures have been reported. Molecular shuttle is one of these prototypes.

Molecular shuttles can be controllable. These stimuli responsive shuttles can be relied on chemical, electrochemical, photochemical stimulation. The compound **53** is a chemically driven molecular shuttle[105] consisting of dumbbell component containing ammonium functionality and a bipyridinium part that can form a hydrogen bonding and charge transfer interactions, respectively, with the ring unit having an electron donating character which is a crown ether, dibenzo-24-crown-8. The anthracene unit worked as a stopper. There is a strong N^+ - H ...O hydrogen bonding interaction between the ring component and ammonium moiety. This interaction is much stronger than charge transfer interaction establishing between ring unit and bipyridinium component. Thus, the deprotonation of ammonium moiety by increasing pH leads to a displacement for the ring component to bipyridinium unit from ammonium moiety. This displacement took place in a ratio of nearly 100%. This displacement of shuttle system schematically is depicted in Figure 41.

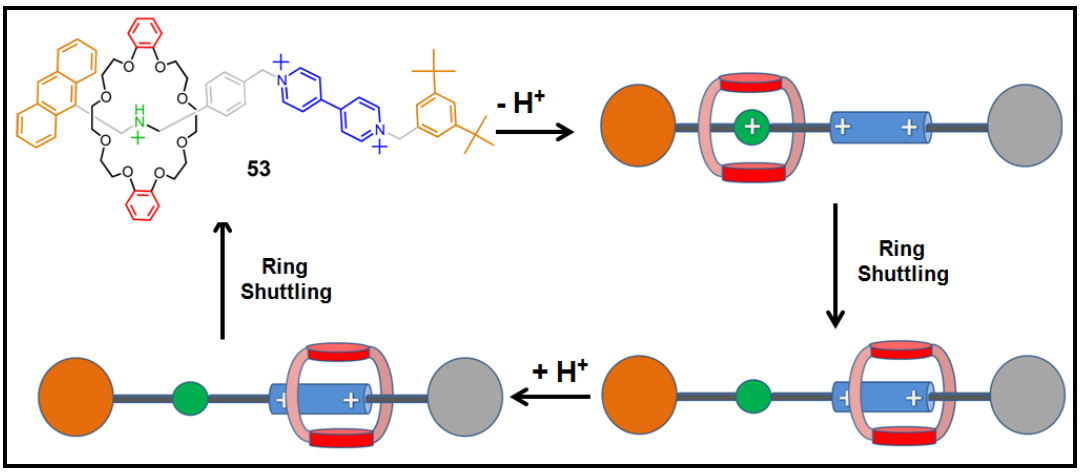

Figure 41. The representation of chemical structure of **53** and operation of the molecular shuttle in solution

2.7.2. Autonomous Molecular Machines

Although numerous example of artificial molecular machine have been designed, there is very limited number of autonomous molecular machine have been reported. The rotaxane **54** is a prototype of a autonomous light driven molecular shuttle.[106] Before the description of operational principles of shuttle, it must be noted that the

ring component encircled the A_1 station since this station is much better electron acceptor than A_2 station. The activation of ruthenium(II) polypyridine complex (P) by light leads to deactivation in station A_1 and the displacement of the ring was observed from A_1 to A_2. Then, a back electron transfer occurs from A_1 to oxidized P unit and A_1 station regains its electron acceptor power. Again, the ring component was relocated at the station A_1.

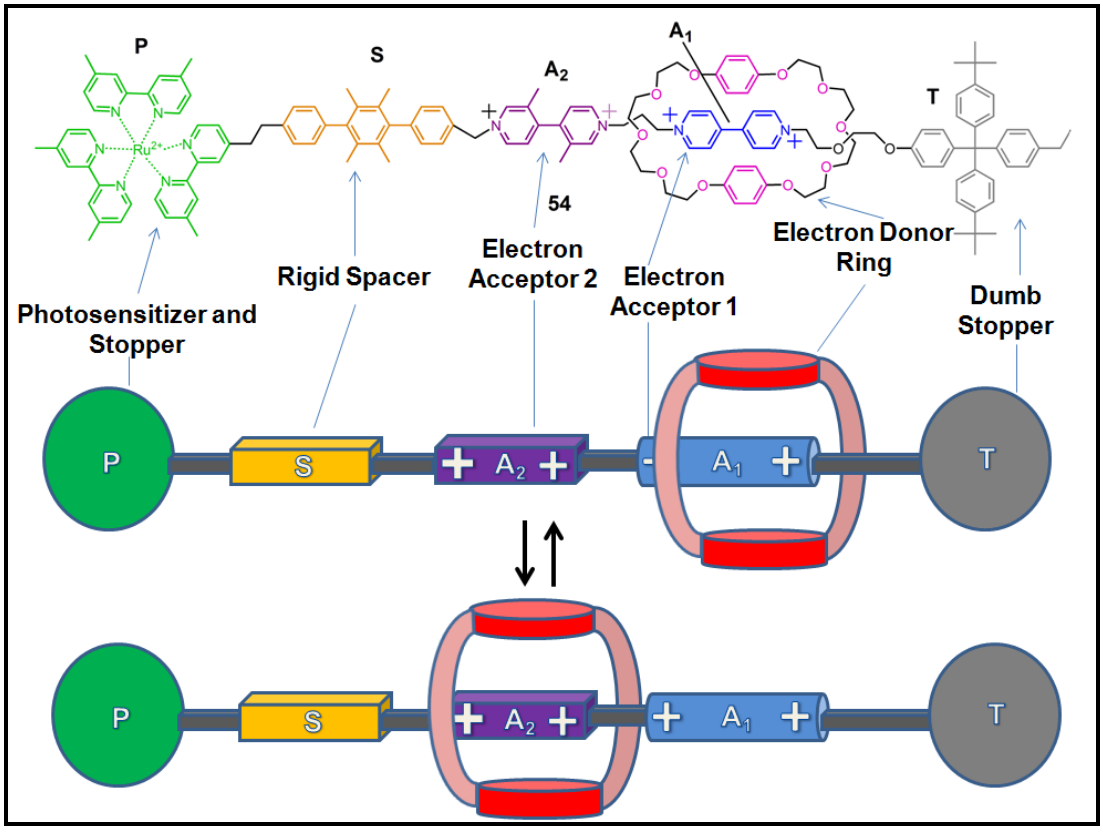

Figure 42. Chemical structure and cartoon representation of autonomous molecular shuttle **54**

CHAPTER 3

3. Reaction-based Sensing of Fluoride Ions

This work is partially described in the following publication:

Bozdemir, O.A.; Sozmen, F.; **Buyukcakir, O**.; Guliyev, R.; Cakmak, Y.; Akkaya, E.U. *Org. Lett*. **2010**, *12*, 1400-1403.

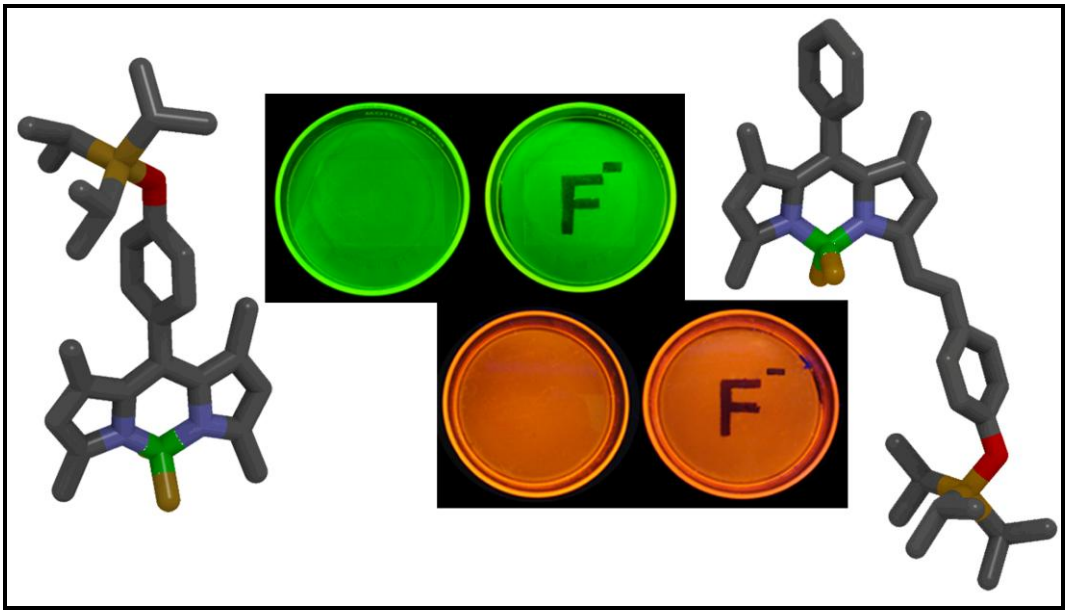

3.1. Objective

In recent decades, the detection of fluoride anion has attracted great attention because of its importance in many biological and chemical processes. Moreover, fluoride can be found in various processes ranging from technological entities to medical treatment modalities. For example, fluoride works as a tooth decay inhibitor in toothpaste and nerve gases consists of appreciable amount fluoride. In spite of its wide usage, fluoride is very toxic and lethal at high concentration. Therefore, the detection of fluoride concentration is highly important and there is a great interest to design new sensitive and selective fluoride sensors. In this sense, we designed two Bodipy based chemososimeters to detect fluoride both in solution and in polymethylmethaacraylate (PMMA) matrix. The detection mechanism is based on the removal of triisoproplysily (TIPS) group from TIPS-protected phenoxy substituent in presence of fluoride. The deprotection of TIPS groups cause to formation of a strongly electron donating nascent phenolate group on Bodipy chromophore. PET or Internal charge transfer (ICT) is triggered depending on the location of this strong electron donating moiety on Bodipy core.

3.2. Introduction

Anion detection is one of the challenging issue.[107,108] This difficulty stems from anions large variations in size, shape, charge distribution and strong solvation in polar and/or H-bond donor solvents. Not only while continuous monitoring but also during real time imaging of anionic species require reversible chemosensors, for some anions, a reaction based sensor,[109] a "chemical dosimeter" would be equally useful. For practical applications, it can easily envisioned a "dipstick" for selected anions such as cyanide or fluoride considering how and where it could be relevant to measure the concentrations of these ions. Fluoride is an easy target for sensing[110,111] , since it is a strong base in organic solvents. Furthermore, as many different types of fluorescence signals can be produced by the changes in acid-base equilibria and *via* strong hydrogen bonding interactions in non-competitive media. However, it must be noted that fluoride sensing or signaling has proved to be very difficult in aqueous

solution, and there are few molecular systems which can reversibly sense fluoride anions in aqueous systems[112] and each system suffers certain complications such as, requirement for large fluoride concentrations, such as the requirement for signal generation, or dependence on ternary systems with complex equilibria. Reaction based sensors, while irreversible in nature, can be coerced to work in aqueous solution. There are only a few reactions taking place in aqueous system which involves fluoride anions.

3.3. Result and Discussion

Most reaction based sensors for fluoride anion exploit the extraordinary affinity of fluoride to silicon. Considering this particular affinity and literature examples[113] for fluoride sensing based on removal of silyl protective groups on alcohols or phenols, **55** and **56** were designed as potential fluoride responsive molecules. Earlier studies in Akkaya group,[114] and in others,[115] has demonstrated that a phenoxy substituent at the meso (8) position of the Bodipy core is a very strong PET donor. The spectral signature of PET is quenching of fluorescence without any significant changes in the emission wavelength.[116] So, using probe compound **55**, fluoride anions should be signaled by a decrease in the emission intensity as a consequence of the removal of the TIPS (triisopropylsilyl) protective group. In aprotic organic solvents, the immediate product of deprotection is a phenolate anion, which as stated previously, will quench the emission *via* PET.

In the second design, we made use of a Knoevenagel type of a reaction of Bodipy methyl groups (methyl groups at 3 and 5 were previously shown to be reactive in Knoevenagel condensation with aldehydes; very recently, we demonstrated that methyl groups at the 1 and 7 positions can also react under similar, (but somewhat forcing conditions) to place a styryl linked, TIPS-protected phenol moiety. Here, the expectation is that the deprotection reaction facilitated by fluoride anions, will generate strong ICT donor phenoxide ion in full conjugation to Bodipy dye, which would raise the HOMO level, reduce the energy gap for S_0-S_1 transition, and thus

result in a large red shift in the major peak in absorbance. In most instances, such large red shifts result in a decrease in the emission intensity.

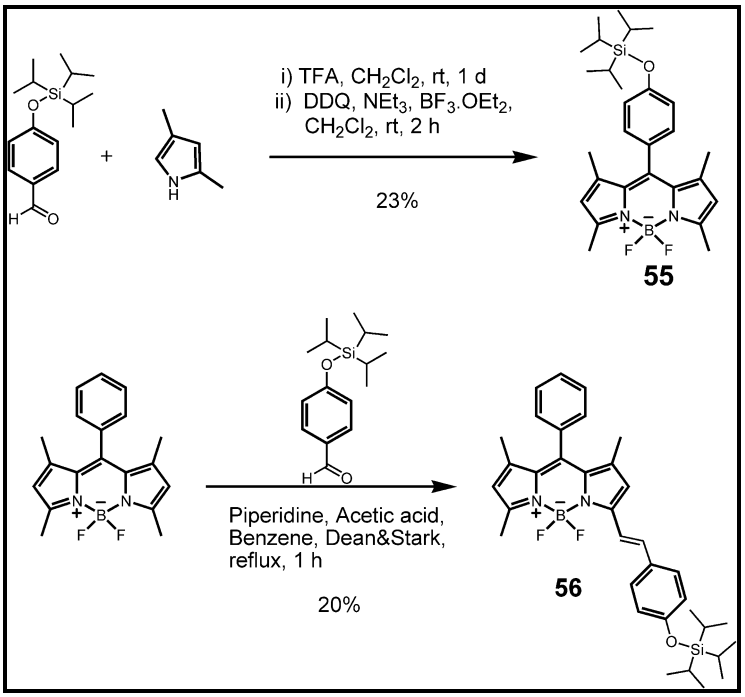

Figure 43. Synthesis of compounds **55** and **56**.

With these expectations, target molecules **55** and **56**.were synthesized The syntheses are shown in Figure 43. TIPS-protected hydroxybenzaldehyde is the key reagent which is easily obtained from commercially available materials (see Experimental Details). Target **55** was obtained following a routine Bodipy formation procedure in a reasonable yield. The second fluoride probe **56**, was obtained by condensation reaction of the aldehyde with a known Bodipy derivative, 1,3,5,7-tetramethyl-8-phenyl-Bodipy.

The absorbance spectra of the compounds **55** and **56** show peaks at 498 nm and 560 nm, respectively. For compound **55**, the addition of fluoride ions in form of a tetrabutylammonium salt results in minimal changes to the absorption spectrum (10 nm blue shift, Figure 44). The most remarkable change is in the emission spectrum,

because the emission at 506 nm is quenched by a factor of 20 in the presence of 0.5 mM fluoride ions (Figure 45).

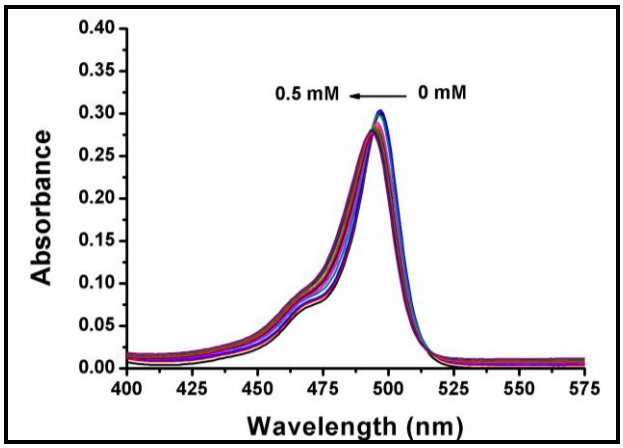

Figure 44. Absorbance spectra of compound **55**+F^- in acetonitrile in the presence of increasing F^- concentrations (0, 0.025, 0.05, 0.075, 0.1, 0.125 0.15, 0.2, 0.25, 0.375, 0.5 mM). Probe concentration is 5.0 x 10^{-6} M.

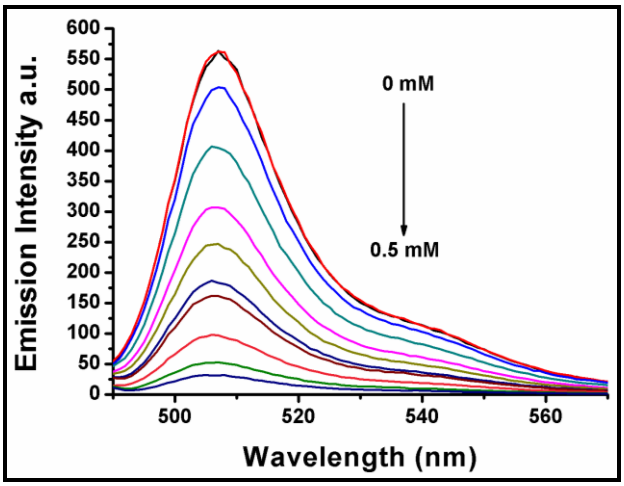

Figure 45. Emission spectra of compound **55**+F^- in acetonitrile in the presence of increasing F^- concentrations (0, 0.025, 0.05, 0.075, 0.1, 0.125 0.15, 0.2, 0.25, 0.375, 0.5 mM). Probe concentration is 5.0 x 10^{-6} M. Excitation wavelength is 480 nm.

In accordance with the design expectations, probe **56** shows a large bathochromic shift on exposure to fluoride ions. The absorption peak (Figure 46) at 560 nm gradually decreases and a new peak at 682 nm emerges. The transition has an

identifiable isosbestic point at 581 nm suggesting the existence of two chromophores related by a chemical transformation. A bathochromic shift of 120 nm looks quite spectacular in solution, which corresponds to a color change from purple to green.

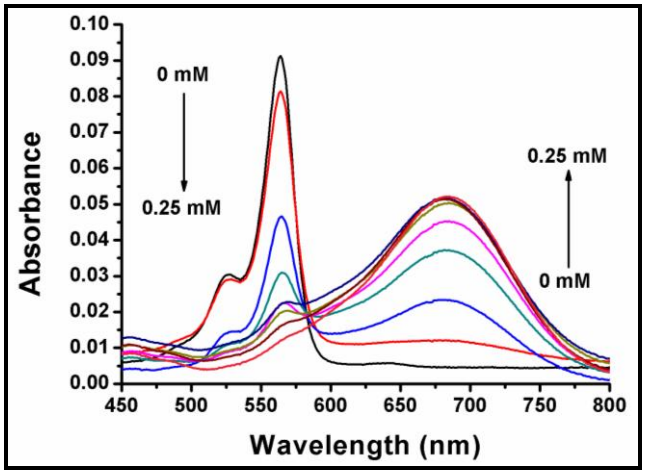

Figure 46. Absorbance spectra of compound **56**+F^- in the presence of increasing F^- concentrations after 5 min. (0, 0.025, 0.05, 0.075, 0.1, 0.125 0.15, 0.2, 0.25 mM). Probe concentration is 5.0 x 10^{-6} M.

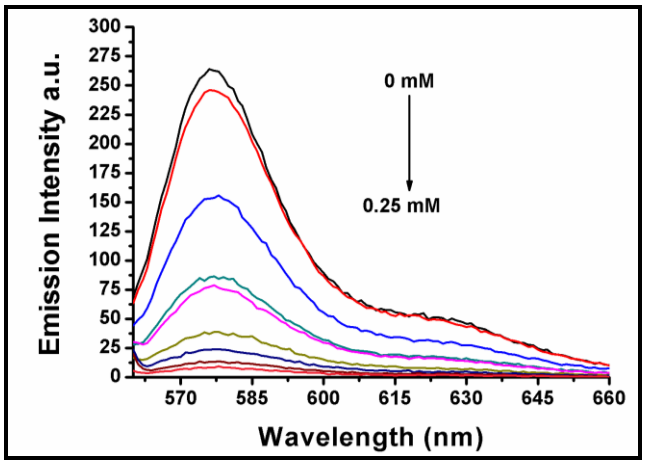

Figure 47. Emission spectra of compound **56**+F^- in acetonitrile in the presence of increasing F^- concentrations after 5 min. (0, 0.025, 0.05, 0.075, 0.1, 0.125 0.15, 0.2, 0.25 mM). Probe concentration is 5.0 x 10^{-6} M. Excitation wavelength is 550 nm.

The emission spectrum (Figure 47) on the other hand, shows the presence of one emissive species, and it is the probe compound **56**. Deprotection leads to the

formation of non-emissive phenolate. These reactions, as expected are highly selective fluoride. Comparative studies of the effects of a series of anions are shown in Figure 48 for compounds **55** and **56** in the form of bar graphs. In addition, the insets are the digital photographs of acetonitrile solutions under indicated conditions. The fluoride selectivity is impressive for both of the probe compounds.

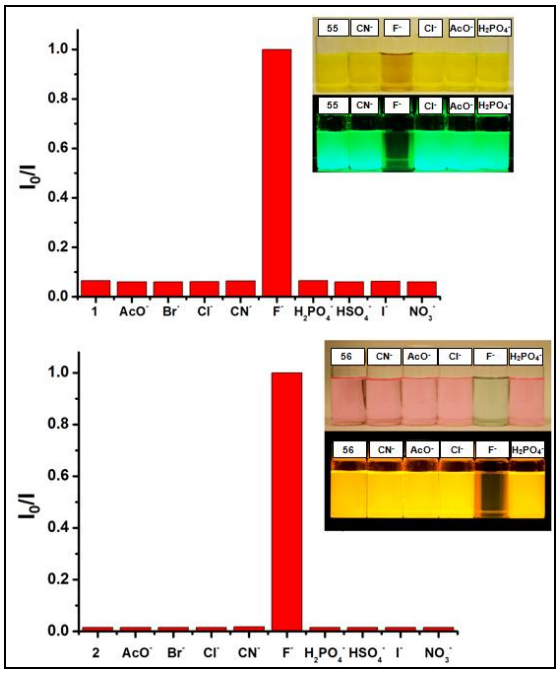

Figure 48. Normalized emission ratios ("probe + anions" to free probe). Normalization was done by setting the maximal value to 1. The probe was excited at 490 nm and the emission data at 507 nm were collected. The insets show the appearance of solutions of under ambient light (top) under a hand-held UV-lamp (360 nm). Probe concentrations were 5 x 10^{-6} M, and the anions were added at 0.5 mM (**55**) or 0.25 mM (**56**) concentrations, all in acetonitrile. Top: data for probe **55**, bottom probe **56**.

The deprotection reaction is very fast for compound **55**. Essentially, the reaction seems to reach an equilibrium during the time that is needed for mixing of the fluoride solution and taking the measurement at all concentrations. Naturally, the position of the equilibrium is different at each fluoride concentration, allowing quantification of a concentration dependent response. In compound **56** however, the deprotection is slower. To accommodate for the time dependence, we allowed 5 minutes of equilibriation period following the addition of fluoride before we obtained

absorption and emission spectra. A time course of deprotection as assessed by spectrophotometry is available in the Figure 49. A pseudo-first order rate constant can be calculated relatively easy; at 0.25 mM F^- concentration and 5 x 10^{-6} M probe concentration (probe **56)** the rate constant was determined to 2.3 x 10^{-2} s^{-1} at 25 ^oC in acetonitrile (Figure 50).

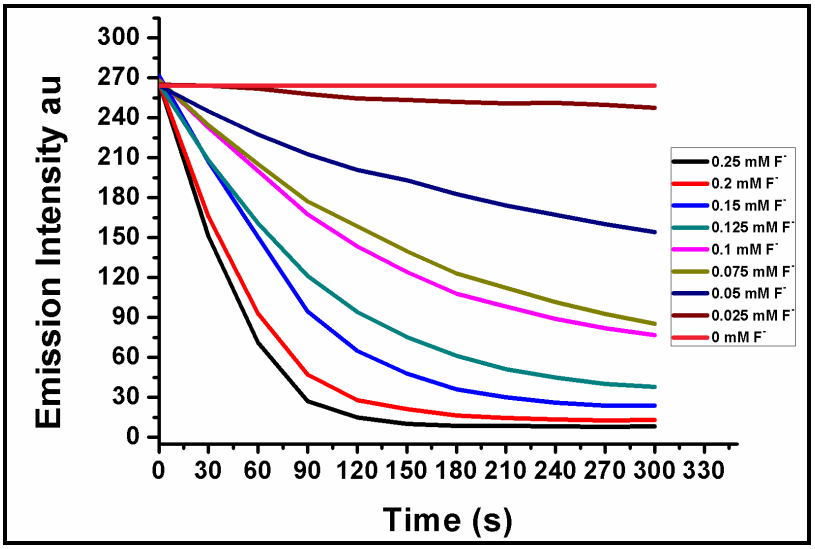

Figure 49. A time of course deprotection reaction for compound **56** using different concentrations of tetrabutylammonium fluoride in acetonitrile followed by emission change at 576 nm. The concentration of the probe compound is 5 x 10^{-6} M.

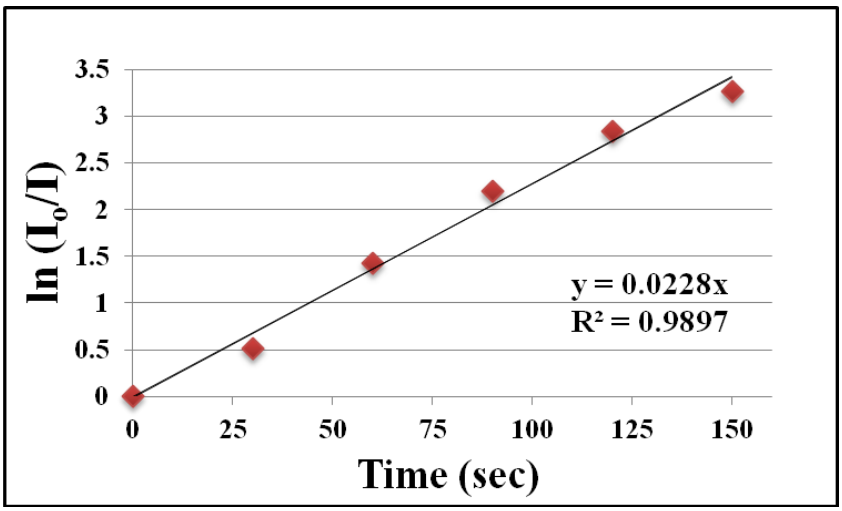

Figure 50. Plot of $\ln(I_0/I)$ versus time (sec) for the emission wavelength at 576 nm associated with the phenolate anion species formed on addition of 0.25 mM tetrabutylammonium fluoride to the solution of compound **56** in acetonitrile.

Thus, ion sensing in a polar organic solvent was demonstrated. Since the silyl group is unreactive in neutral aqueous solutions, (pOH=7), the silyl-deprotection based chemodosimetry concept is fully transferable to aqueous solutions with minor modifications to improve water solubility. However, much larger concentrations of fluoride would be required to overcome inactivation by strong hydrogen bond donor H_2O. Instead of creating the illusion of relevance by swamping the cells with ions, at concentrations orders of magnitude higher than any realistic situation could account for, for the creation of ion responsive polymer films was opted. In order to emphasize practical potential of these probe compounds, we prepared PMMA (polymethylmethacrylate) films impregnated (0.5 mg of probe compounds and 500 mg PMMA) with the probe compounds **55** and **56**. The probes in the polymer matrix responded to tetrabutylammonium fluoride solution as expected.

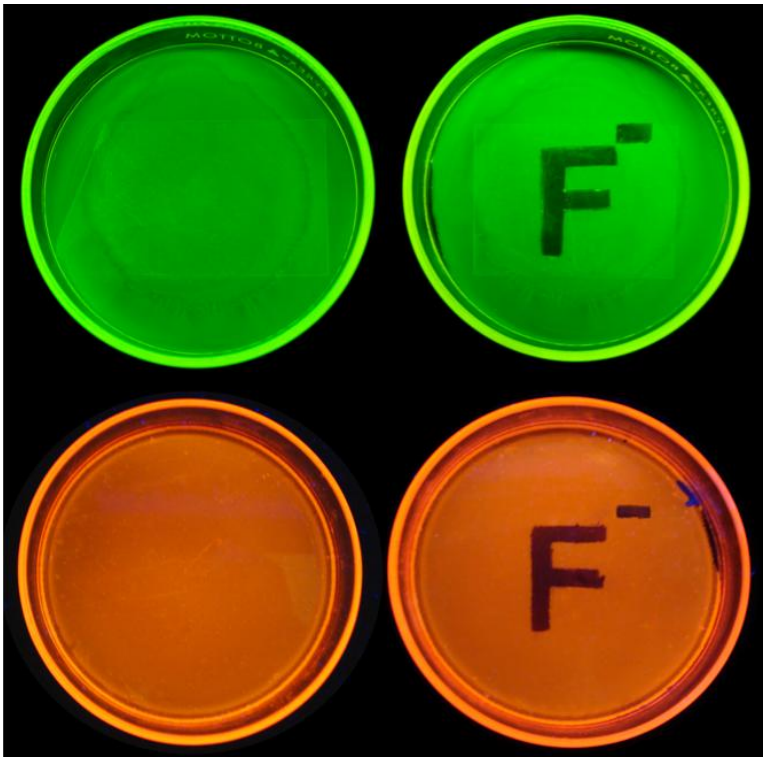

Figure 51. Digital photographs PMMA polymer sheets doped with chemosensor **55** (top) and **56** (bottom) under UV irradiation. Fluoride solution in aqueous acetonitrile (% 20 pH 10.0 buffer in acetonitrile) was applied using an appropriate mask (right). UV irradiation was achieved using a hand-held UV lamp at 360 nm.

Figure 51 shows the appearance of the fluoride exposed polymer films in the ambient light conditions and under UV illumination at 360 nm. Quenching of the emission is clear on the fluoride exposed regions in both cases, and for the polymer film containing fluoride probe **56,** color is visibly changed. The polymer films are stable under ambient light and temperature over weeks, with no discernible change in color or in response. The dyes do not wash off from the films as well Figure 52. Both compounds respond apparently much faster in the polymer matrix (instantaneously) than in solutions and do not wash off the aqueous solutions. This simple demonstration shows the viability of polymer-strip design for fluoride monitoring in environmental samples.

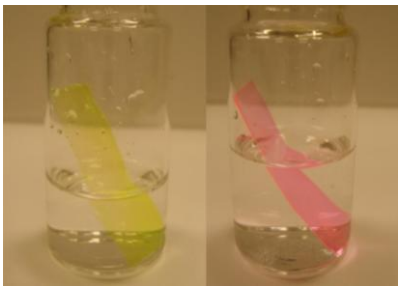

Figure 52. The dye doped PMMA films do not show any color changes when stirred in water for extended periods of time (up to 1 week). The dyes do not wash off.

3.4. Experimental Details

3.4.1. General Methods

^{1}H NMR and ^{13}C NMR spectra were recorded on Bruker DPX-400 (operating at 400 MHz for ^{1}H NMR and 100 MHz for ^{13}C NMR) in $CDCl_3$ with tetramethylsilane as internal standard. All spectra were recorded at 25^{o}C and coupling constants (*J* values) are given in Hz. Chemical shifts are given in parts per million (ppm). All the ^{13}C spectra were recorded with simultaneous decoupling of proton nuclei. Absorption spectra were performed by using a Varian Cary-100 spectrophotometer. Fluorescence measurements were conducted on a Varian Eclipse spectrofluometer. Reactions were monitored by thin layer chromatography using Merck TLC Silica gel 60 F_{254}. Silica gel column chromatography was performed over Merck Silica gel 60

(particle size: 0.040-0.063 mm, 230-400 mesh ASTM). All other reagents and solvents were purchased from Aldrich and used without further purification. 4-triisopropylsilyloxybenzaldehyde[117], and 4,4-difluoro-8-phenyl-1,3,5,7-tetramethyl-4-bora-3a,4a-diaza-*s*-indacene[118] were synthesized according to literature.

3.4.2. Synthesis

Synthesis of Compound (55)

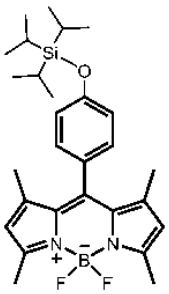

To a 1.0 L round-bottomed flask containing 400 mL argon-degassed CH_2Cl_2 were added 2,4-dimethyl pyrrole (4.4 mmol, 0.4 g), 4-triisopropylsilyloxybenzaldehyde (1.98 mmol, 0.6 g) and one drop of trifluoroacetic acid. The solution was stirred under N_2 at room temperature for 1d. After addition of a solution of DDQ (1.98 mmol, 0.45 g) in 100 mL of CH_2Cl_2 to the reaction mixture, stirring was continued for 30 min. 6 mL of Et_3N and 5 mL of $BF_3.OEt_2$ were successively added and after 30 min, the reaction mixture was washed with water (3 x 300 mL) and dried over anhydrous Na_2SO_4. The solvent was evaporated and the residue was purified by silica gel column chromatography using $CHCl_3$: Methanol (97 : 5) as the eluant. Orange solid (0.25 g, 23%). ^{1}H NMR (400 MHz, $CDCl_3$): δ_H 7.11 (2H, d, *J* = 8.2 Hz, ArH), 7.01 (2H, t, *J* = 8.2 Hz, ArH), 5.97 (2H, s, ArH), 2.54 (6H, s, C*H*$_3$), 1.45 (6H, s, C*H*$_3$), 1.28 (3H, septet, *J* = 3.5 Hz, C*H*), 1.15 (10H, s, C*H*$_3$), 1.12 (8H, s, C*H*$_3$); ^{13}C NMR (100 MHz, $CDCl_3$): δ_C 156.9, 155.2, 143.1, 142.0, 131.8, 130.3, 129.2, 127.6, 121.1, 17.9, 14.6, 14.5, 12.6 ppm. MS (TOF- ESI): m/z: : Calcd: 497.2971 $[M+H]^+$, Found: 497.2983 $[M+H]^+$, Δ=2.4 ppm.

Synthesis of Compound (56)

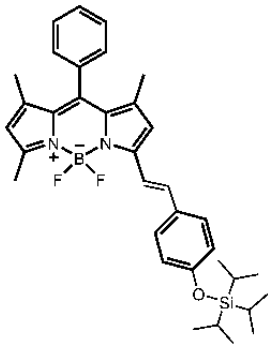

In a 100 mL round-bottomed flask equipped with a Dean-Stark trap and a reflux condenser were added 40 mL of benzene, 4,4-difluoro-8-phenyl-1,3,5,7-tetramethyl-4-bora-3a,4a-diaza-*s*-indacene (0.15 mmol, 80 mg), 4-(1,4-dioxa-7,13-dithia-10-azacyclopentadecan-10-yl)benzaldehyde (0.15 mmol, 54 mg), acetic acid (0.2 mL), and piperidine (0.2 mL).

The reaction mixture was stirred at reflux temperature and concentrated nearly to dryness. Progress of the reaction was monitored by TLC (1:1 Hexanes : Acetone). When all the starting material had been consumed, water (100 mL) was added and mixture was extracted into $CHCl_3$. The organic layer was dried on Na_2SO_4 and evaporated. Column chromatographic separation (silica gel, 1:1 Hexanes : Acetone) of the residue yielded the desired product as a dark blue solid. (25 mg, 20%). ^{1}H NMR (400 MHz, $CDCl_3$): δ_H 7.55 (1H, d, *J* = 16.3 Hz, C*H*), 7.50-7.46 (5H, m: ArH), 7.33-7.29 (2H, m: ArH), 7.19 (1H, d, *J* = 16.3 Hz, C*H*), 6.87 (2H, t, *J* = 8.6 Hz, ArH), 6.58 (1H, s, ArH), 5.99 (1H, s, ArH), 2.58 (6H, s, CH_3), 1.44 (3H, s, CH_3), 1.39 (3H, s, CH_3), 1.27 (3H, septet, *J* = 3.9 Hz, C*H*), 1.13 (10H, s, CH_3), 1.19 (8H, s, CH_3); ^{13}C NMR (100 MHz, $CDCl_3$): δ_C 157.2, 154.6, 153.5, 142.6, 142.2, 139.9, 136.2, 135.2, 130.8, 129.6, 129.0, 128.9, 128.8, 128.2, 121.0, 120.2, 117.5, 117.1, 29.7, 17.9, 14.6, 14.3, 12.7 ppm. MS (TOF- ESI): m/z: : Calcd: 585.3284 $[M+H]^+$, Found: 585.3286 $[M+H]^+$, Δ=0.34 ppm.

3.5. Conclusion

In conclusion, in this work, we were able to demonstrate that the designs based on selective chemical reactions, especially when parameters which influence triggering of certain photophysical processes are incorporated, can be quite successful. In the probes, or dosimetric reagents reported above, this has been achieved for PET and ICT. Thus, it is clear that depending on the exact requirements for a particular application, either an emission change or visible color change can reproducibly be produced. It was easily proposed that other rationally designed reaction based probes, with built-in triggers for photophysical and even photochemical processes will appear in due course.

CHAPTER 4

4. Convenient Synthesis of Near IR Emitting Tetrastyryl-Bodipy Dyes

This work is partially described in the following publication:

Buyukcakir, O.; Bozdemir, O.A.; Erbas, S.; Kolemen S.; Akkaya, E.U. *Org. Lett*. **2009**, *11*, 4644-4647.

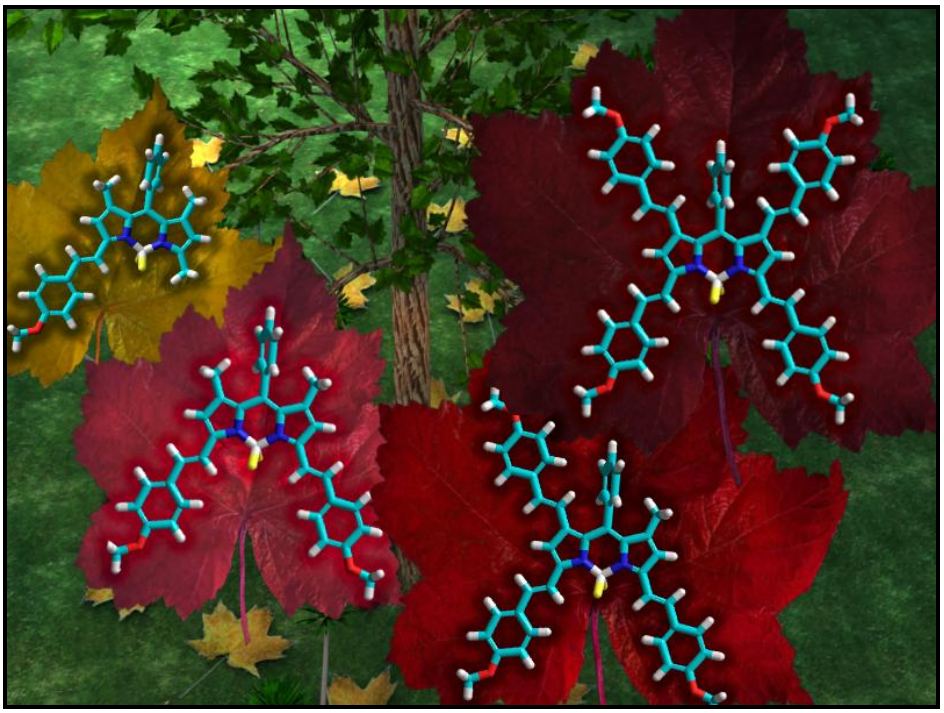

4.1. Objective

1,3,5,7-Tetramethyl-Bodipy derivatives undergo Knoevenagel type condensations with aromatic aldehydes to ultimately yield tetrastyryl-Bodipy derivatives. The resulting dyes absorb and emit strongly in the near IR. As the versatility of the Bodipy dyes are fully appreciated, these new tetrastyryl dyes are likely to be featured in a variety of functional supramolecular systems.

4.2. Introduction

For more than three decades after their initial synthesis,[119] Bodipy dyes were known only as bright fluorescent dyes for use in cellular imaging as supplied by a few commercial sources. However, especially within the last five years there has been a Bodipy renaissance of sorts.[88,89] This is in large part sparked by the new tactics[120] in the functionalization of the Bodipy core, which led to the synthesis of longer wavelength absorbing/emitting fluorescent dyes,[121] energy transfer cassettes,[122] light harvesters,[123] sensitizers for solar cells[124] and photodynamic therapy,[125] non-linear optical materials,[126] mesogenic materials,[127] supramolecular polymers,[128] fluorescent chemosensors[129] and molecular logic systems[130]. This remarkable versatility of Bodipy dyes, easily comparable to structurally related porphyrins, prompted Ziessel to label Bodipy as "porphyrin's little sister".[88]

The parent Bodipy unit has a major absorption peak (S_0-S_1 transition) near 500 nm, however incorporation of aromatic rings,[131] extension of π-conjugation,[132] and aza-substitution at the meso (8) position,[133] push this peak into the red end of the visible spectrum. All of these approaches are adaptable in certain applications, nevertheless mono and distyryl modifications seem to offer greater degree of versatility as judged by the recent interest,[134] apart from our group. This clearly stems from the following facts: i) Knoevenagel reaction of the 3 and 5-methyls are in most cases high yielding; ii) the reaction conditions tolerate the use of a variety of aldehydes with different stereoelectronic characteristics; and, iii) strong charge donor substituents are likely to

yield switchable fluorescent molecules with internal charge transfer characteristics useful as chemosensors and molecular logic gates.

4.3. Result and Discussion

While considering the possibility of further functionalization of the Bodipy core, we carried out a Mulliken-charge analysis on the core carbon atoms of tetramethyl-Bodipy. The electron density of the carbon atoms vary in the following order: 2,6 >> 1,7 > 3,5. The results suggested that the methyl groups in positions 1 and 7 could be almost as acidic as 3,5-methyls. ^{1}H-NMR spectra should provide additional support for this argument, however, the correlation between acidity and the chemical shifts is problematic due to magnetic anisotropy effects. In the 8-phenyl substituted Bodipy dyes, 1,7-methyls are in the shielding zone of the phenyl substituents and experience a shielding by approximately 0.7 ppm. The situation is more revealing in the tetramethyl and pentamethyl derivatives lacking the phenyl substituent (Figure 53). The chemical shifts for two sets of methyl protons (3,5 and 1,7) resonate closely especially in the pentamethyl derivative, which could be interpreted as a sign of increased acidity. Encouraged by these observations, we looked for likely conditions to extend Knoevenagel condensation to other methyl substituents on the Bodipy core. The earlier experience with the distyryl was directed us to start with Bodipy dyes with electron-withdrawing substituents, as they clearly enhance the acidity of the methyl substituents on the Bodipy core.

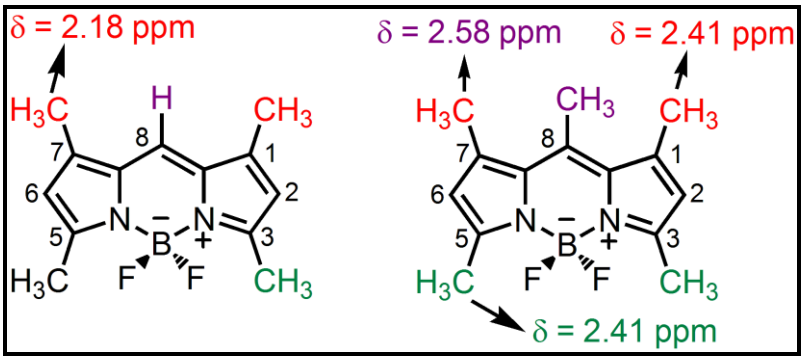

Figure 53. 1,3,5,7-tetramethyl- and 1,3,5,7,8-pentamethyl-Bodipy derivatives; numbering and relevant ^{1}H NMR chemical shifts in $CDCl_3$

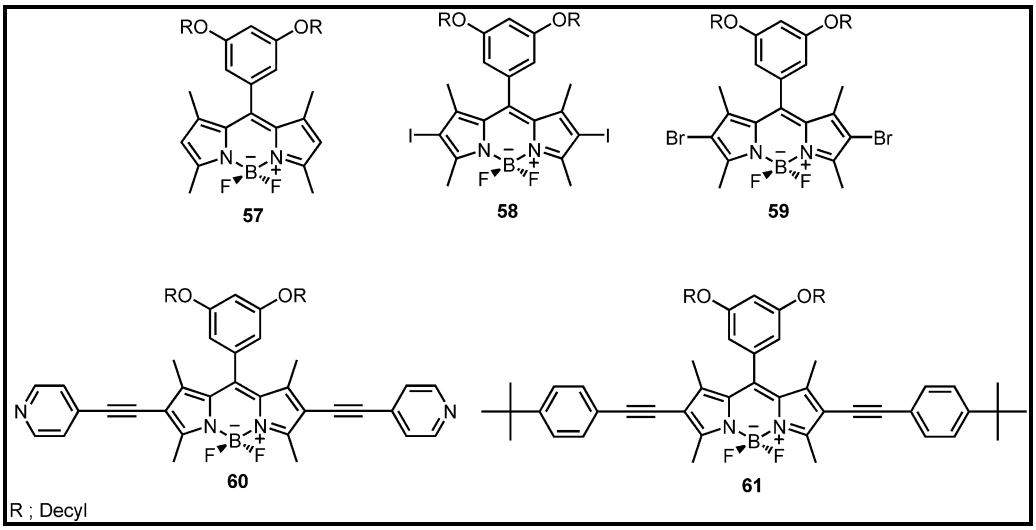

Figure 54. The chemical structure of precursors of tetrastryl Bodipy dyes

The precursor Bodipy dyes **57**, **58** and **59** have been synthesized according to literature and the synthesis procedures of the dyes **60** and **61** were explained briefly in experimental details section (Figure 54). As indicated before, the electron withdrawing decoration on Bodipy skeleton leads to an increase in the methy substituents located at the positions of 3 and 5. Thus, the first dye we chose for quadruple Knoevenagel reaction was a Bodipy derivative carried pyridinyl-ethynyl substituents on the 2,6-positions (Figure 55, Y=4-pyridinylethynyl), and the aromatic aldehyde was *p*-anisaldehyde (X =OCH_3). The reactions conditions were set just like that which was used for mono- and di-styryl functionalizations. The selected aldehyde and Bodipy were dissolved in benzene. We used acetic acid and piperidine in catalytic amount. The dean-stark trap was used to remove the water from reaction media. The progress of the reaction was easily followed by thin layer chromatography. And in a few hours under reflux, a compound what it was considered as a tetrastyryl derivative was the only major product by tlc analysis. A similar reaction with a Bodipy derivative which has 4-*t*-butylphenylethynyl substituents on the 2,6 positions, reacted similarly, requiring slightly longer time under reflux for full conversion.

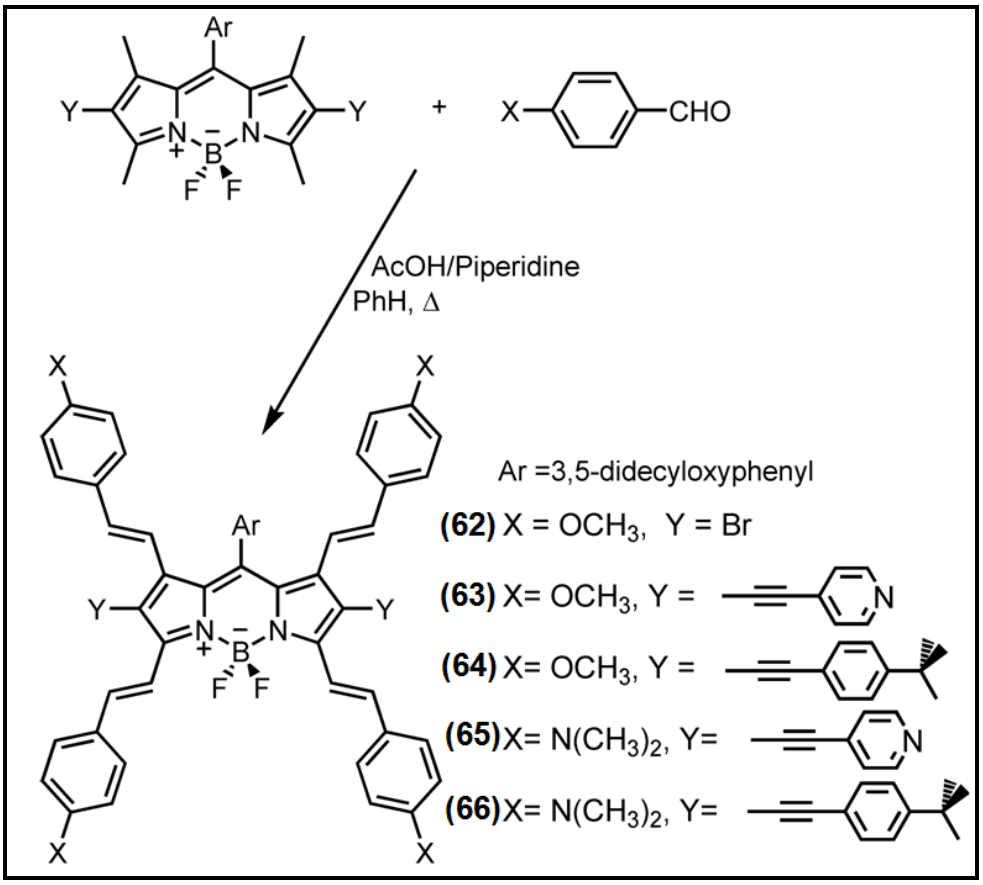

Figure 55. Quadruple Knoevenagel reaction and the structure of products **62-66**

The ^{1}H NMR spectra of the compounds were highly revealing. Knoevenagel reaction introduced the styryl group exclusively in a *trans* configuration. In distyryl compounds, this is easily by the existence of two pairs of protons with chemical shift difference of approximately 1 ppm, and with large coupling constants (> 16 Hz). In the tetrastyryl compounds, there are two additional pairs of protons showing peaks around 7.7 and 6.1 ppm. Figure 56 shows the aromatic regions of the ^{1}H NMR spectra of the tetrastyryl-bodipy **66** and the intermediate distyryl-bodipy **67**. The integration ratios and the upfield shift of one pair of ethylenic protons are exactly as should be expected.

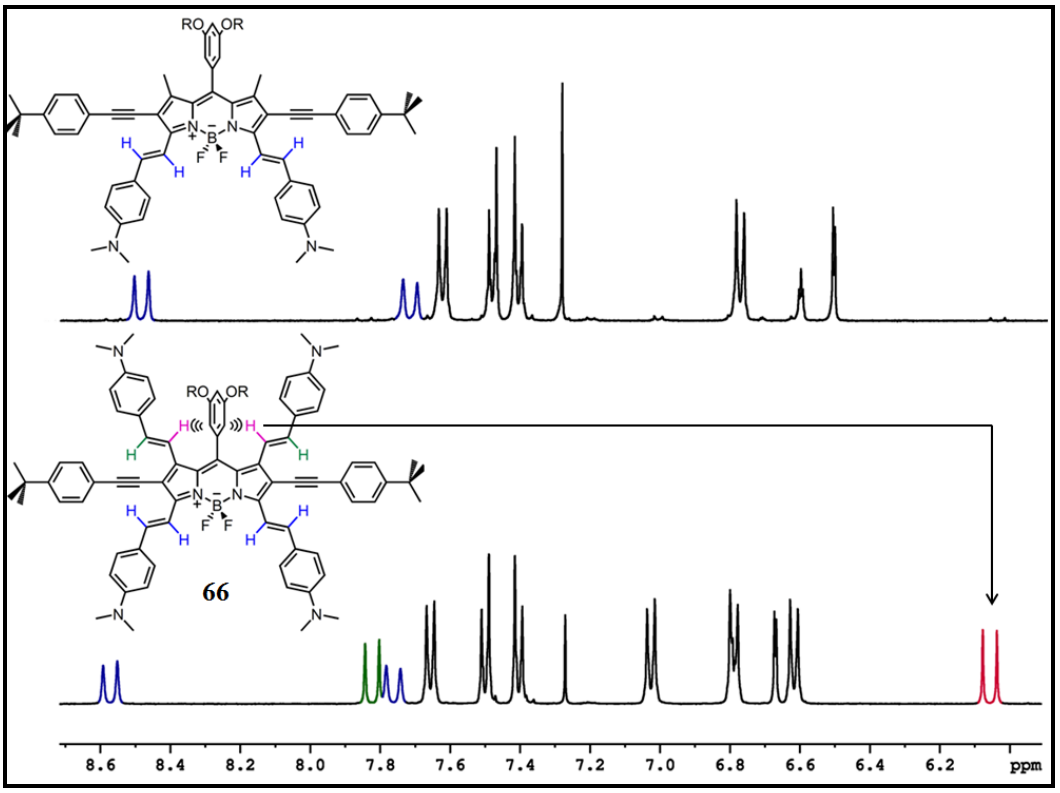

Figure 56. Structures and partial 1H NMR spectra of the distyryl **67** (top) and the tetrastyryl-Bodipy **66** (bottom). Significant upfield shift of one pair (colour coded in red) of trans-vicinally coupled protons due to their protrusion towards the meso-phenyl ring is obvious. It is a signature feature for 8-phenyl substituted tetrastyryl-Bodipy's. The other pair (green) is not affected.

In order gain an insight into the scope of the reaction, the reaction with a bromo-substituents and with no substituents on the 2,6-positions were tried. The 2,6-dibromo derivative reacted as efficiently as the ethynyl substituted derivatives to yield the tetrastyryl compound. 2,6-H Bodipy derivative (**57**) however, as expected, reacted slowly, but this allowed to be consideres as a remarkable feat. By simply stopping the reaction at different times, it is possible to isolate mono, di, tri and the tetrastyryl derivatives as the major products (Figure 57). This fact alone, should give a hint to the versatility of this reaction.

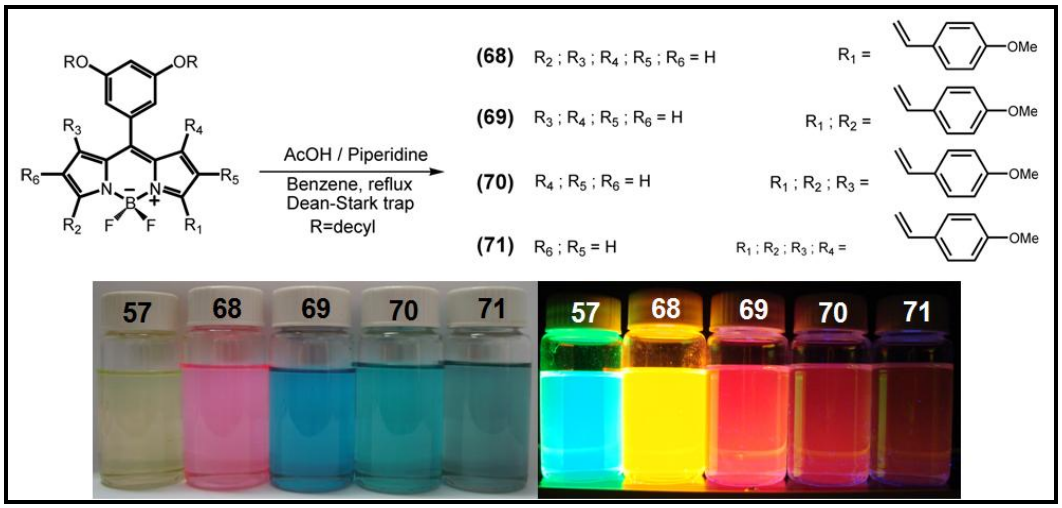

Figure 57. One pot synthesis of four different styryl-Bodipy dyes. The reactions can be stopped at appropriate times to maximize the yield for a particular derivative. The inset picture shows the colors under ambient light (top half) and when excited using a hand-held UV lamp at 360 nm(bottom half).

Figure 58 shows the absorption and the emission spectra of this series of Bodipy dyes (**57 & 68-71**). It is also interesting to note that first methyls to react are exclusively 3,5-methyls, tri and tetra-substituted products are obtained only when the concentration of all the reactants are increased by the removal of most of the solvent. Thus, by simple condensation reactions, the absorption peak of a Bodipy dye **57** can be pushed stepwise from 498 nm to 572, 645, 665 and 689 nm. Next, we wanted to demonstrate that the reaction is not limited to *p*-anisaldehyde. Condensation with *p*-N,N-dimethylamino-benzaldehyde also proceeds smoothly.

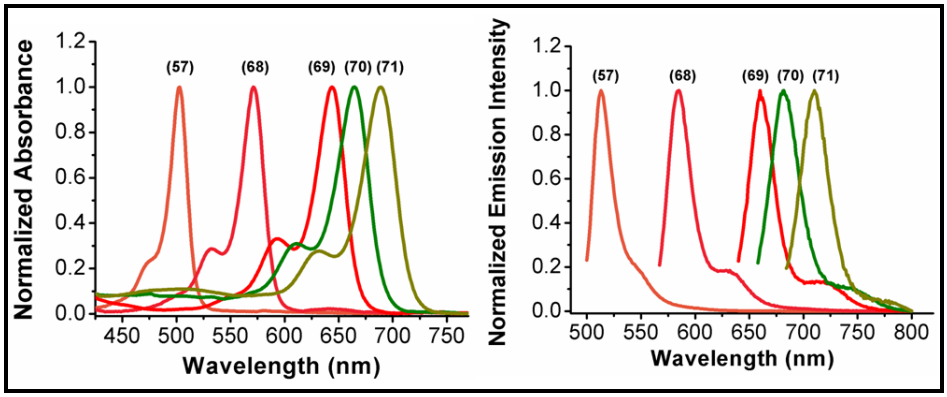

Figure 58. Absorption and emission spectra of compounds **57 & 68-71**

The spectroscopic data for the new tetrastyryl-bodipy dyes are presented in Table 1. The tetrastyryl dyes **65** and **66** are *bona fide* near IR dyes, absorbing maximally around 800 nm and emitting maximally around 835 nm in chloroform. The peaks are also relatively sharp as judged by the less than 50 nm full-width at half-maximum values. The dyes have very large extinction coefficients rivalling those of typical cyanine dyes. Their quantum yields were also found to be moderate to high, except for dimethylaminostyryl dye **66**. The strong charge transfer and highly polar excited states in **65** and **66** tend to decrease the emission quantum yield, so this is not unexpected.

Table 1. Spectral data for tetrastyryl-Bodipy dyes and selected intermediate dyes isolated from the Knoevenagel reaction media.

Compound[a]	λ_{abs} (nm)	λ_{em} (nm)	Φ_f[b]	ε_{max}[c]
62	700	727	0.12	48,800
63	721	747	0.42	88,200
64	732	756	0.23	173,900
65	802	837	0.13	141,500
66	797	835	0.05	144,700
68	572	585	0.92	58,900
69	645	660	0.37	116,400
70	665	682	0.35	96,900
71	689	710	0.34	127,900

[a] Data acquired in $CHCl_3$ in dilute solutions. [b] relative quantum yields. [c] unit: $cm^{-1}M^{-1}$.

4.4. Experimental Details

4.4.1. General Methods

^1H NMR and ^{13}C NMR spectra were recorded on Bruker DPX-400 (operating at 400 MHz for ^1H NMR and 100 MHz for ^{13}C NMR) in $CDCl_3$ with tetramethylsilane as internal standard. All spectra were recorded at 25^oC and coupling constants (*J values*) are given in Hz. Chemical shifts are given in parts per million (ppm). Absorption spectra were performed by using a Varian Cary-100 spectrophotometer. Fluorescence measurements were conducted on a Varian Eclipse spectrofluometer.

Mass spectra were recorded at the Sh University of Sheffield, Mass Spectrometry Service Laboratory, Shieffield, U.K. Reactions were monitored by thin layer chromatography using Merck TLC Silica gel 60 F_{254}. Silica gel column chromatography was performed over Merck Silica gel 60 (particle size: 0.040-0.063 mm, 230-400 mesh ASTM). Compunds **57**, **58**, and **59** were synthesized according to literature.[128] Anhydrous tetrahydrofuran was obtained by refluxing over sodium/benzophenone prior to use. All other reagents and solvents were purchased from Aldrich and used without further purification.

4.4.2. Synthesis

Compound 60

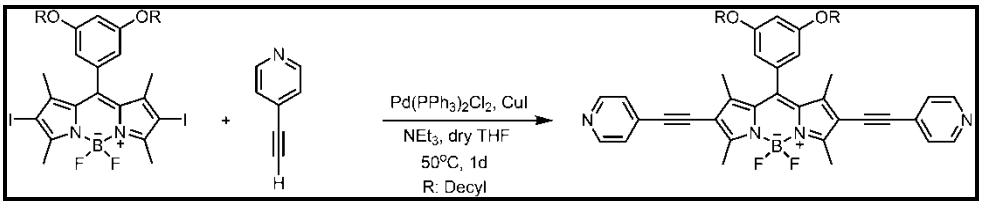

In a 50 mL Schlenk tube were added **58** (0.360 mmol, 320 mg), 4-ethynylpyridine (1.08 mmol, 151 mg), $(PPh_3)_2PdCl_2$ (0.044 mmol, 31.2 mg), CuI (0.059 mmol, 11.3 mg). 15 mL of freshly distilled THF and 7 mL of diisopropylamine were added and resulting suspension was excessively deaerated by bubbling with Argon at 50°C for 40 min. After degassing, the reaction mixture was stirred at 50°C for 1d. Solvents were removed at reduced pressure and the residue was washed with water (100 mL) and extracted into $CHCl_3$. The organic layer was removed and separation by column chromatography on silica gel using ethyl acetate as the eluant yielded the desired product as a violet solid. (227 mg, 75%). ^{1}H NMR (400 MHz, $CDCl_3$): δ = 8.58 (4H, d; *J* = 6.1 Hz, Ar*H*), 7.29 (4H, d; *J* = 6.0 Hz, Ar*H*), 6.60 (1H, t; *J* = 2.2 Hz, Ar*H*), 6.43 (2H, d; *J* = 2.2 Hz, Ar*H*), 3.96 (4H, t; *J* = 6.6 Hz, OCH_2), 2.75 (6H, s; CH_3), 1.85-1.75 (4H, m; CH_2), 1.72 (6H, s; CH_3), 1.50-1.40 (4H, m; CH_2), 1.40-1.20 (24H, m; CH_2), 0.85 (6H, t; *J* = 6.8 Hz, CH_3); ^{13}C NMR (100 MHz, $CDCl_3$): δ = 161.5, 158.0, 149.8, 135.4, 132.1, 132.0, 131.9, 131.8, 131.4, 128.5, 128.4, 126.0, 125.1, 105.9, 103.2, 94.0, 86.5, 68.5, 34.8, 31.9, 29.5, 29.3, 29.1, 26.0, 22.7, 14.1, 13.4. MS (TOF- ESI): m/z: : Calcd: 839.5247 $[M+H]^+$, Found: 839.5223 $[M+H]^+$.

Compound 61

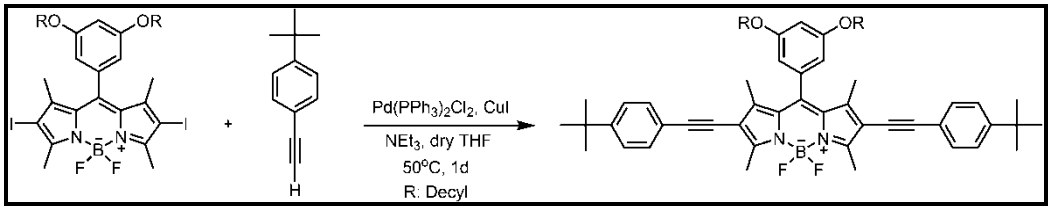

In a 50 mL Schlenk tube were added **58** (0.470 mmol, 420 mg), 4-*t*-butyl-ethynylbenzene (1.50 mmol, 238 mg), $(PPh_3)_2PdCl_2$ (0.044 mmol, 39.6 mg), CuI (0.074 mmol, 14.3 mg). 15 mL of freshly distilled THF and 7 mL of diisopropylamine were added and resulting suspension was excessively deaerated by bubbling with Argon at 50°C for 40 min. After degassing, the reaction mixture was stirred at 50°C for 1d. Solvents were removed at reduced pressure and the residue was washed with water (100 mL) and extracted into $CHCl_3$. The organic layer was removed and separation by column chromatography on silica gel using 1:1 $CHCl_3$: Hexanes as the eluant yielded the desired product as a violet solid. (347 mg, 80%). ^{1}H NMR (400 MHz, $CDCl_3$): δ = 7.52 (4H, d; *J* = 8.2 Hz, Ar*H*), 7.32 (4H, d; *J* = 8.2 Hz, Ar*H*), 6.56 (1H, t; *J* = 2.2 Hz, Ar*H*), 6.42 (2H, d; *J* = 2.2 Hz, Ar*H*), 3.95 (4H, t; *J* = 6.6 Hz, OCH_2), 2.72 (6H, s; CH_3), 1.83-1.73 (4H, m; CH_2), 1.70 (6H, s; CH_3), 1.50-1.40 (4H, m; CH_2), 1.40-1.30 (24H, m; CH_2), 1.25 (18H s; CH_3), 0.90 (6H, t; *J* = 6.9 Hz, CH_3); ^{13}C NMR (100 MHz, $CDCl_3$): δ = 161.3, 158.0, 151.4, 143.5, 142.0, 135.9, 131.1, 125.3, 120.4, 116.5, 108.1, 102.6, 96.5, 80.9, 68.5, 34.8, 31.9, 31.2, 29.6, 29.5, 29.4, 29.3, 29.1, 26.0, 22.9, 14.1, 13.7, 13.2. MS (TOF- ESI): m/z: : Calcd: 949.6594 $[M]^+$, Found: 949.6591 $[M]^+$.

Compound 62

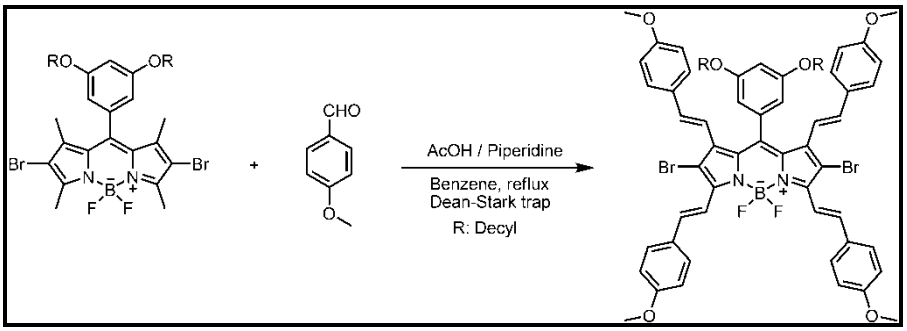

Compound **59** (0.19 mmol, 150 mg) and 4-methoxy benzaldehyde (1.33 mmol, 181 mg) were added to a 100 mL round-bottomed flask containing 50 mL benzene and to this solution was added piperidine (0.4 mL) and acetic acid (0.4 mL). The mixture was heated under reflux by using a Dean Stark trap and reaction was monitored by TLC 3:1 $CHCl_3$: Hexanes. When all the starting material had been consumed, the mixture was cooled to room temperature and solvent was evaporated. Water (100 mL) added to the residue and the product was extracted into the chloroform (3 x 100 mL). Organic phase dried over Na_2SO_4, evaporated and residue was purified by silica gel column chromatography using 3:1 $CHCl_3$: Hexanes as the eluant. Deep green waxy solid (70 mg, 29%). ^{1}H NMR (400 MHz, $CDCl_3$): δ = 8.15 (2H, d; *J* = 16.5 Hz, C*H*), 7.70-7.60 (6H, m; 2H: C*H*, and 4H: Ar*H*), 7.05 (2H, d; *J* = 16.5 Hz, C*H*), 7.02-6.92 (8H, m; Ar*H*), 6.78 (4H, d; *J* = 8.8 Hz, Ar*H*), 6.49 (3H, s; Ar*H*), 5.88 (2H, d; *J* = 16.5 Hz, C*H*), 3.89 (6H, s; OCH_3), 3.82 (6H, s; OCH_3), 3.67 (4H, t; *J* = 6.6 Hz, OCH_2), 1.60-1.50 (4H, m; CH_2), 1.35-1.15 (32H, m; CH_2), 0.87 (6H, t; *J* = 6.9 Hz, CH_3); ^{13}C NMR (100 MHz, $CDCl_3$): δ = 161.4, 160.8, 159.8, 149.5, 139.2, 136.0, 134.8, 129.8, 129.3, 128.0, 118.3, 116.1, 114.3, 113.8, 108.1, 103.3, 68.5, 55.4, 55.3, 31.9, 29.6, 29.4, 29.3, 29.0, 25.9, 22.9, 14.1. MS (TOF- ESI): m/z: : Calcd: 1264.4523 $[M]^+$, Found: 989.5676 $[M+Na]^+$.

Compound 63

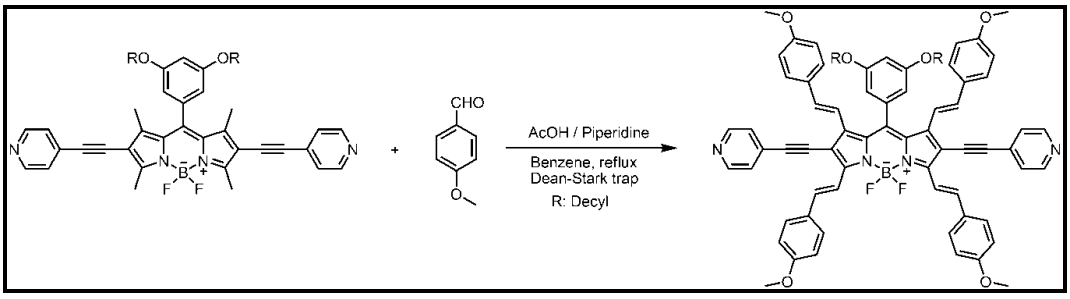

Compound **60** (0.12 mmol, 100 mg) and 4-methoxy benzaldehyde (0.84 mmol, 114 mg) were added to a 100 mL round-bottomed flask containing 50 mL benzene and to this solution was added piperidine (0.4 mL) and acetic acid (0.4 mL). The mixture was heated under reflux by using a Dean Stark trap and reaction was monitored by TLC 5:95 MeOH : $CHCl_3$. When all the starting material had been consumed, the mixture was cooled to room temperature and solvent was evaporated. Water (100

mL) added to the residue and the product was extracted into the chloroform (3 x 100 mL). Organic phase dried over Na_2SO_4, evaporated and residue was purified by silica gel column chromatography using 3:97 MeOH : $CHCl_3$ as the eluant. Deep green waxy solid (31 mg, 33%). ^{1}H NMR (400 MHz, $CDCl_3$): δ = 8.62 (4H, d; *J* = 6.1 Hz, Ar*H*), 8.42 (2H, d; *J* = 16.4 Hz, C*H*), 7.78 (2H, d; *J* = 16.5 Hz, C*H*), 7.67 (4H, d, *J* = 8.8 Hz, Ar*H*), 7.60 (2H, d; *J* = 16.2 Hz, C*H*), 7.32 (4H, d; *J* = 6.0 Hz, Ar*H*), 7.05-6.95 (8H, m; Ar*H*), 6.85 (4H, d; *J* = 8.8 Hz, Ar*H*), 6.75 (1H, t; *J* = 2.2 Hz, Ar*H*), 6.65 (2H, d; *J* = 2.2 Hz, Ar*H*), 6.07 (2H, d; *J* = 16.2 Hz, C*H*), 3.90 (6H, s; OCH_3), 3.86-3.80 (10H, m; 4H: OCH_2, 6H: OCH_3), 1.70-1.50 (4H, m; CH_2), 1.40-1.20 (32H, m; CH_2), 0.85 (6H, t; *J* = 6.9 Hz, CH_3); ^{13}C NMR (100 MHz, $CDCl_3$): δ = 161.6, 161.0, 160.1, 150.0, 142.2, 139.6, 134.7, 131.8, 129.8, 129.6, 129.4, 128.1, 124.5, 118.8, 114.5, 114.1, 108.1, 103.4, 95.0, 91.3, 68.7, 55.4, 55.3, 34.9, 31.9, 29.8, 29.7, 29.5, 29.3, 29.0, 25.9, 22.7, 14.1. MS (TOF- ESI): m/z: : Calcd: 1311.6921 $[M+H]^+$, Found: 1311.6903 $[M+H]^+$.

Compound 64

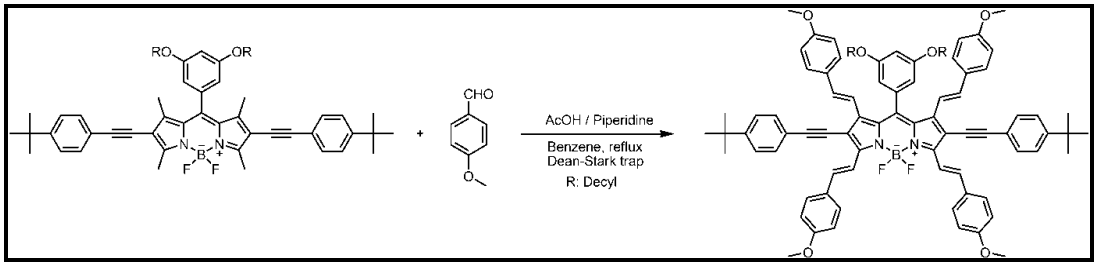

Compound **61** (0.10 mmol, 100 mg) and 4-methoxy benzaldehyde (0.70 mmol, 96 mg) were added to a 100 mL round-bottomed flask containing 50 mL benzene and to this solution was added piperidine (0.4 mL) and acetic acid (0.4 mL). The mixture was heated under reflux by using a Dean Stark trap and reaction was monitored by TLC 2:1 $CHCl_3$: Hexanes. When all the starting material had been consumed, the mixture was cooled to room temperature and solvent was evaporated. Water (100 mL) added to the residue and the product was extracted into the chloroform (3 x 100 mL). Organic phase dried over Na_2SO_4, evaporated and residue was purified by silica gel column chromatography using 2:1 $CHCl_3$: Hexanes as the eluant. Deep green waxy solid (45 mg, 32%). ^{1}H NMR (400 MHz, $CDCl_3$): δ = 8.55 (2H, d; *J* = 16.4

Hz, C*H*), 7.80 (2H, d; *J* = 16.3 Hz, C*H*), 7.78 (2H, d; *J* = 16.2 Hz, C*H*), 7.68 (4H, d; *J* = 8.8 Hz, Ar*H*), 7.47 (4H, d; *J* = 8.1 Hz, Ar*H*), 7.40 (4H, d; *J* = 8.5 Hz, Ar*H*), 7.07 (4H, d; *J* = 8.8 Hz, Ar*H*), 7.02 (4H, d; *J* = 8.8 Hz, Ar*H*), 6.82 (4H, d; *J* = 8.7 Hz, Ar*H*), 6.73 (1H, t; *J* = 2.2 Hz, Ar*H*), 6.63 (2H, d; *J* = 2.2 Hz, Ar*H*), 6.07 (2H, d; *J* = 16.2 Hz, C*H*), 3.90 (6H, s; OCH_3), 3.88-3.80 (10H, m; 4H: OCH_2, 6H: OCH_3), 1.65-1.55 (4H, m; CH_2), 1.37 (18H, s; CH_3), 1.30-1.15 (32H, m; CH_2), 0.90 (6H, t; *J* = 6.9 Hz, CH_3); ^{13}C NMR (100 MHz, $CDCl_3$): δ = 161.5, 160.7, 159.8, 153.4, 151.6, 142.2, 138.9, 136.7, 133.9, 132.8, 130.5, 130.3, 130.0, 129.3, 128.1, 125.7, 120.8, 119.3, 117.0, 114.4, 113.9, 108.3, 103.4, 98.7, 85.8, 68.6, 55.4, 55.3, 34.9, 31.9, 31.2, 29.3, 29.0, 25.9, 22.7, 14.1. MS (TOF- ESI): m/z: : Calcd: 1420.6190 $[M]^+$, Found: 989.5676 $[M+Na]^+$.

Compound 65

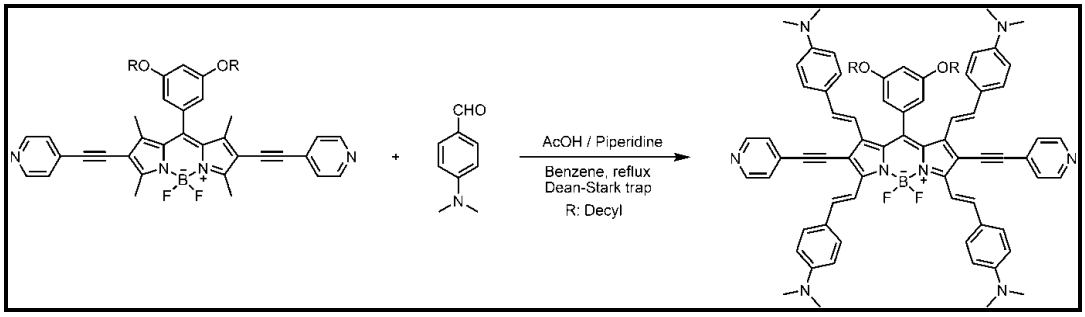

Compound **60** (0.12 mmol, 100 mg) and 4-dimethylamino benzaldehyde (0.84 mmol, 125 mg) were added to a 100 mL round-bottomed flask containing 50 mL benzene and to this solution was added piperidine (0.4 mL) and acetic acid (0.4 mL). The mixture was heated under reflux by using a Dean Stark trap and reaction was monitored by TLC ($CHCl_3$). When all the starting material had been consumed, the mixture was cooled to room temperature and solvent was evaporated. Water (100 mL) added to the residue and the product was extracted into the chloroform (3 x 100 mL). Organic phase dried over Na_2SO_4, evaporated and residue was purified by silica gel column chromatography using 5:95 MeOH : $CHCl_3$ as the eluant. Deep green waxy solid (78 mg, 48%). ^{1}H NMR (400 MHz, $CDCl_3$): δ = 8.62 (4H, s; Ar*H*), 8.42 (2H, d; *J* = 16.4 Hz, C*H*), 7.73 (2H, d; *J* = 16.2 Hz, C*H*), 7.68 (2H, d; *J* = 16.3 Hz, C*H*), 7.62 (4H, d, *J* = 8.8 Hz, Ar*H*), 7.35 (4H, d; *J* = 5.8 Hz, Ar*H*), 7.00 (8H, d; *J* = 8.8 Hz, Ar*H*), 6.85-6.75 (5H, m; Ar*H*), 6.68-6.58 (6H, m; Ar*H*), 6.03 (2H, d; *J* = 16.1

Hz, C*H*), 3.85 (4H, t; *J* = 6.5 Hz, OCH_2), 3.10 (6H, s; NCH_3), 3.02 (6H, s; NCH_3), 1.67-1.57 (4H, m; CH_2), 1.35-1.15 (28H, m; CH_2), 0.85 (6H, t; *J* = 6.8 Hz, CH_3); ^{13}C NMR (100 MHz, $CDCl_3$): δ = 161.5, 154.0, 151.3, 150.5, 149.8, 143.6, 139.8, 136.9, 135.7, 135.0, 132.8, 132.2, 129.4, 128.2, 125.6, 125.2 124.5, 117.0, 114.3, 112.2, 111.0, 108.3, 106.1, 103.6, 95.0, 92.7, 40.3, 40.2, 31.9, 29.6, 29.4, 29.3, 29.0, 25.9, 22.7, 14.1. MS (TOF- ESI): m/z: : Calcd: 1362.8109 $[M]^+$, Found: 989.5676 $[M+Na]^+$.

Compound 66

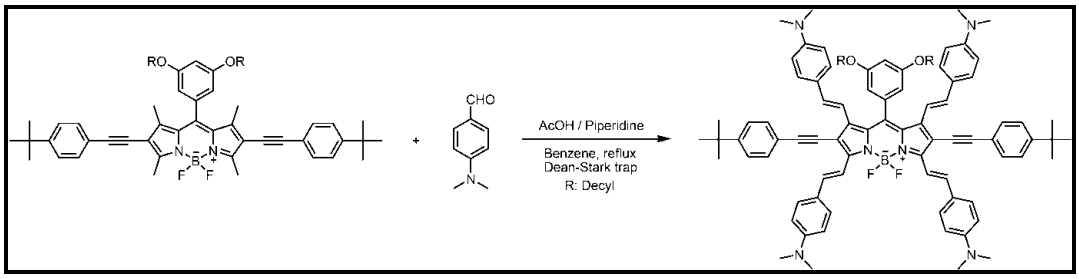

Compound **61** (0.10 mmol, 100 mg) and 4-dimethylamino benzaldehyde (0.70 mmol, 105 mg) were added to a 100 mL round-bottomed flask containing 50 mL benzene and to this solution was added piperidine (0.4 mL) and acetic acid (0.4 mL). The mixture was heated under reflux by using a Dean Stark trap and reaction was monitored by TLC ($CHCl_3$). When all the starting material had been consumed, the mixture was cooled to room temperature and solvent was evaporated. Water (100 mL) added to the residue and the product was extracted into the chloroform (3 x 100 mL). Organic phase dried over Na_2SO_4, evaporated and residue was purified by silica gel column chromatography using $CHCl_3$ as the eluant. Deep green waxy solid (78 mg, 50%). ^{1}H NMR (400 MHz, $CDCl_3$): δ = 8.58 (2H, d; *J* = 16.2 Hz, C*H*), 7.82 (2H, d; *J* = 16.1 Hz, C*H*), 7.78 (2H, d; *J* = 16.2 Hz, C*H*), 7.67 (4H, d; *J* = 8.8 Hz, Ar*H*), 7.50 (4H, d; *J* = 8.4 Hz, Ar*H*), 7.41 (4H, d; *J* = 8.4 Hz, Ar*H*), 7.03 (4H, d; *J* = 8.8 Hz, Ar*H*), 6.82-6.78 (5H, m; Ar*H*), 6.67 (2H, d; *J* = 2.2 Hz, Ar*H*), 6.63 (4H, d; *J* = 8.8 Hz, Ar*H*), 6.05 (2H, d; *J* = 16.2 Hz, C*H*), 3.88 (4H, t; *J* = 6.6 Hz OCH_2), 3.09 (6H, s; NCH_3), 3.02 (6H, s; NCH_3), 1.70-1.60 (4H, m; CH_2), 1.35 (18H, s; CH_3), 1.40-1.15 (32H, m; CH_2), 0.88 (6H, t; *J* = 6.9 Hz, CH_3); ^{13}C NMR (100 MHz, $CDCl_3$): δ = 161.4, 154.0, 151.1, 150.3, 142.1, 139.2, 137.4, 134.2, 130.4, 129.3,

128.1, 126.2, 125.8, 121.2, 117.5, 117.0, 114.9, 112.2, 112.1, 108.4, 103.7, 98.2, 86.8, 68.7, 40.4, 40.3, 31.9, 31.2, 29.7, 29.6, 29.0, 25.9, 22.7, 14.1. MS (TOF- ESI): m/z: : Calcd: 1472.9456 $[M+Na]^+$, Found: 989.5676 $[M+Na]^+$.

Compound 67

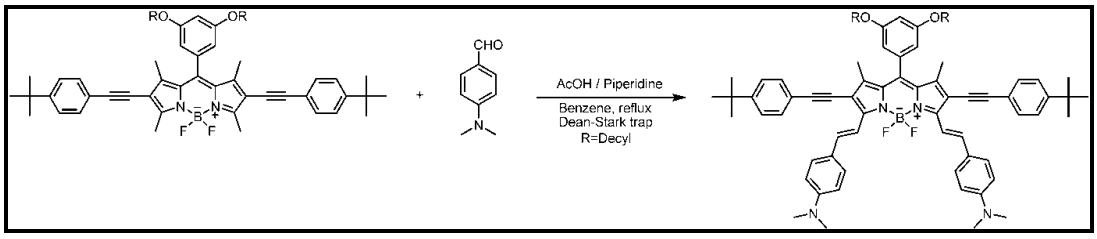

Compound **61** (0.05 mmol, 50 mg) and 4-dimethylamino benzaldehyde (0.15 mmol, 22.5 mg) were added to a 50 mL round-bottomed flask containing 30 mL benzene and to this solution was added piperidine (0.2 mL) and acetic acid (0.2 mL). The mixture was heated under reflux by using a Dean Stark trap and reaction was monitored by TLC ($CHCl_3$). When all the starting material had been consumed, the mixture was cooled to room temperature and solvent was evaporated. Water (100 mL) added to the residue and the product was extracted into the chloroform (3 x 100 mL). Organic phase dried over Na_2SO_4, evaporated and residue was purified by silica gel column chromatography using $CHCl_3$ as the eluant. Green waxy solid (21 mg, 35%). ^{1}H NMR (400 MHz, $CDCl_3$): δ = 8.48 (2H, d; *J* = 16.1 Hz, C*H*), 7.70 (2H, d; *J* = 16.1 Hz, C*H*), 7.62 (4H, d; *J* = 8.8 Hz, Ar*H*), 7.48 (4H, d; *J* = 8.4 Hz, Ar*H*), 7.40 (4H, d; *J* = 8.3 Hz, Ar*H*), 6.76 (4H, d; *J* = 8.8 Hz, Ar*H*), 6.58 (1H, t; *J* = 2.1 Hz, Ar*H*), 6.49 (2H, d; *J* = 2.2 Hz, Ar*H*), 3.95 (4H, t; *J* = 6.6 Hz OCH_2), 3.07 (6H, s; NCH_3), 1.75-1.65 (10H, m; 4H CH_2 : 6H CH_3), 1.50-1.40 (4H, m; CH_2), 1.35 (24H, s; CH_3), 1.30-1.20 (24H, m; CH_2), 0.88 (6H, t; *J* = 6.8 Hz, CH_3); ^{13}C NMR (100 MHz, $CDCl_3$): δ = 161.1, 151.3, 151.1, 139.3, 130.8, 129.4, 125.6, 125.5, 120.8, 112.1, 107.0, 103.7, 97.9, 83.8, 68.4, 40.3, 31.9, 29.6, 29.5, 29.4, 29.3, 29.2, 26.0, 22.7, 14.1. 13.1. MS (TOF- ESI): m/z: : Calcd: 1211.5020 $[M+Na]^+$, Found: 989.5676 $[M+Na]^+$.

Compound 68

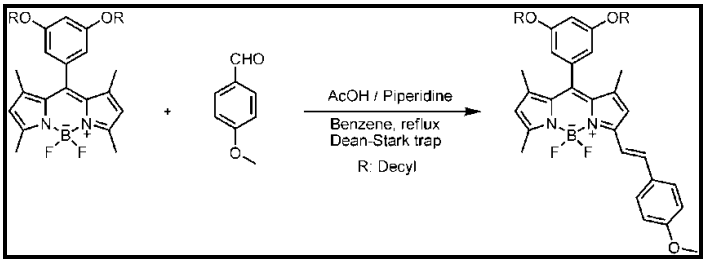

Compound **57** (0.16 mmol, 100 mg) and 4-methoxy benzaldehyde (0.16 mmol, 22 mg) were added to a 100 mL round-bottomed flask containing 50 mL benzene and to this solution was added piperidine (0.2 mL) and acetic acid (0.2 mL). The mixture was heated under reflux by using a Dean Stark trap and reaction was monitored by TLC 1:1 $CHCl_3$: Hexanes. When all the starting material had been consumed, the mixture was cooled to room temperature and solvent was evaporated. Water (100 mL) added to the residue and the product was extracted into the chloroform (3 x 100 mL). Organic phase dried over Na_2SO_4, evaporated and residue was purified by silica gel column chromatography using 1:1 $CHCl_3$: Hexanes as the eluant. Purple waxy solid (40 mg, 33%). ^{1}H NMR (400 MHz, $CDCl_3$): δ = 7.57 (1H, d; *J* = 16.0 Hz, C*H*), 7.55 (2H, d; *J* = 8.8 Hz, Ar*H*), 7.21 (1H, d; *J* = 16.2 Hz, C*H*), 6.92 (2H, d; *J* = 8.8 Hz, Ar*H*), 6.60 (1H, s; Ar*H*), 6.55 (1H, t; *J* = 2.2 Hz, Ar*H*), 6.45 (2H, d; *J* = 2.2 Hz, Ar*H*), 6.00 (1H, s; Ar*H*), 3.97 (4H, t; *J* = 6.6 Hz, OCH_2), 3.85 (3H, s; OCH_3), 2.60 (3H, s; CH_3), 1.83-1.74 (4H, m; CH_2), 1.62 (3H, s; CH_3), 1.57 (3H, s; CH_3), 1.47-1.40 (4H, m; CH_2), 1.40-1.20 (28H, br s; CH_2), 0.90 (6H, t; *J* = 6.9 Hz, CH_3); ^{13}C NMR (100 MHz, $CDCl_3$): δ = 161.0, 160.4, 153.2, 142.7, 137.0, 136.0, 130.0, 129.0, 121.1, 117.1, 114.2, 106.7, 102.0, 68.4, 55.4, 31.9, 29.7, 29.5, 29.4, 29.3, 29.1, 26.0, 22.7, 14.5, 14.2, 14.1. MS (TOF- ESI): m/z: : Calcd: 754.5056 $[M]^+$, Found: 754.5068 $[M]^+$.

Compound 69

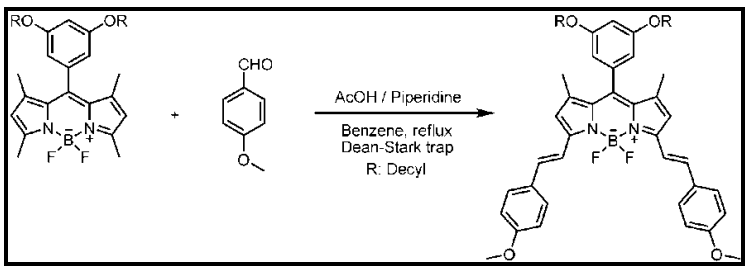

Compound **57** (0.16 mmol, 100 mg) and 4-methoxy benzaldehyde (0.32 mmol, 44 mg) were added to a 100 mL round-bottomed flask containing 50 mL benzene and to this solution was added piperidine (0.4 mL) and acetic acid (0.4 mL). The mixture was heated under reflux by using a Dean Stark trap and reaction was monitored by TLC 1:1 $CHCl_3$: Hexanes. When all the starting material had been consumed, the mixture was cooled to room temperature and solvent was evaporated. Water (100 mL) added to the residue and the product was extracted into the chloroform (3 x 100 mL). Organic phase dried over Na_2SO_4, evaporated and residue was purified by silica gel column chromatography using 1:1 $CHCl_3$: Hexanes as the eluant. Purple waxy solid (77 mg, 55%). ^{1}H NMR (400 MHz, $CDCl_3$): δ = 7.62 (2H, d; *J* = 16.0 Hz, C*H*), 7.58 (4H, d; *J* = 8.7 Hz, Ar*H*), 7.22 (2H, d; *J* = 16.2 Hz, C*H*), 6.94 (4H, d; *J* = 8.6 Hz, Ar*H*), 6.62 (2H, s; Ar*H*), 6.55 (1H, t; *J* = 1.9 Hz, Ar*H*), 6.47 (2H, d; *J* = 2.2 Hz, Ar*H*), 3.95 (4H, t; *J* = 6.6 Hz, OCH_2), 3.87 (6H, s; OCH_3), 1.84-1.75 (4H, m; CH_2), 1.62 (6H, s; CH_3), 1.50-1.40 (4H, m; CH_2), 1.40-1.20 (28H, br s; CH_2), 0.90 (6H, t; *J* = 6.9 Hz, CH_3); ^{13}C NMR (100 MHz, $CDCl_3$): δ = 161.0, 160.4, 152.4, 142.0, 136.7, 135.6, 129.6, 129.0, 117.3, 114.2, 108.9, 102.3, 68.4, 55.4, 31.9, 29.6, 29.5, 29.4, 29.3, 29.2, 25.7, 22.7, 14.5, 14.2, 14.1. MS (TOF- ESI): m/z: : Calcd: 872.5475 $[M]^+$, Found: 872.5435 $[M]^+$.

Compound 70

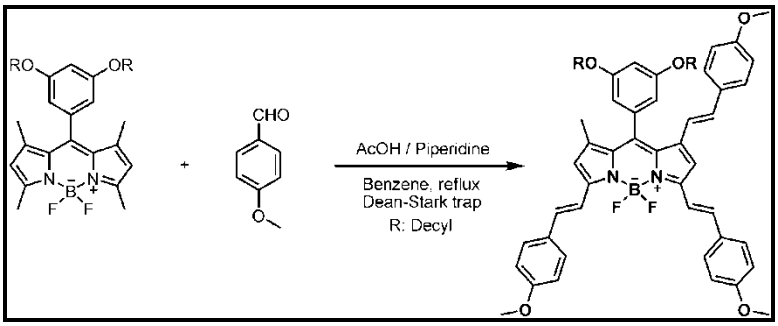

Compound **57** (0.16 mmol, 100 mg) and 4-methoxy benzaldehyde (0.48 mmol, 66 mg) were added to a 100 mL round-bottomed flask containing 50 mL benzene and to this solution was added piperidine (0.4 mL) and acetic acid (0.4 mL). The mixture was heated under reflux by using a Dean Stark trap and reaction was monitored by TLC 1:1:1 CH_2Cl_2 : Hexanes : Toluene. When all the starting material had been

consumed, the mixture was cooled to room temperature and solvent was evaporated. Water (100 mL) added to the residue and the product was extracted into the chloroform (3 x 100 mL). Organic phase dried over Na_2SO_4, evaporated and residue was purified by silica gel column chromatography using 1:1:1 CH_2Cl_2 : Hexanes : Toluene as the eluant. Purple waxy solid (15 mg, 9.5%). ^{1}H NMR (400 MHz, $CDCl_3$): δ = 7.69-7.59 (6H, m; 2H: C*H*, and 4H: Ar*H*), 7.32 (1H, d; *J* = 17.7 Hz, C*H*), 7.27 (1H, d; *J* = 16.7 Hz, C*H*), 7.04 (1H, s; Ar*H*), 7.01 (2H, d; *J* = 8.7 Hz, Ar*H*), 6.96 (4H, d; *J* = 8.8 Hz, Ar*H*), 6.85 (1H, d; *J* = 16.1 Hz, C*H*), 6.79 (2H d; *J* = 8.8 Hz, Ar*H*), 6.69 (1H, s; Ar*H*), 6.68 (1H, t; *J* = 2.3 Hz, Ar*H*), 6.57 (2H, d; *J* = 2.2 Hz, Ar*H*), 5.85 (1H, d; *J* = 16.1 Hz, C*H*), 3.93 (4H, t; *J* = 6.6 Hz, OCH_2), 3.87 (6H, s; OCH_3), 3.81 (3H, s; OCH_3), 1.75-1.64 (7H, m; 3H: CH_3, 4H: CH_2), 1.40-1.20 (30H, m; CH_2), 0.90 (6H, t; *J* = 6.9 Hz, CH_3); ^{13}C NMR (100 MHz, $CDCl_3$): δ = 161.1, 160.3, 159.5, 152.4, 142.7, 137.5, 136.8, 131.0, 130.2, 129.2, 128.9, 127.8, 119.8, 118.1, 117.3, 114.2, 113.9, 107.7, 102.8, 68.5, 55.4, 31.9, 29.5, 29.3, 29.2, 29.1, 25.9, 22.7, 14.5, 14.2, 14.1. MS (TOF- ESI): m/z: : Calcd: 990.5894 $[M]^+$, Found: 990.5902 $[M]^+$.

Compound 71

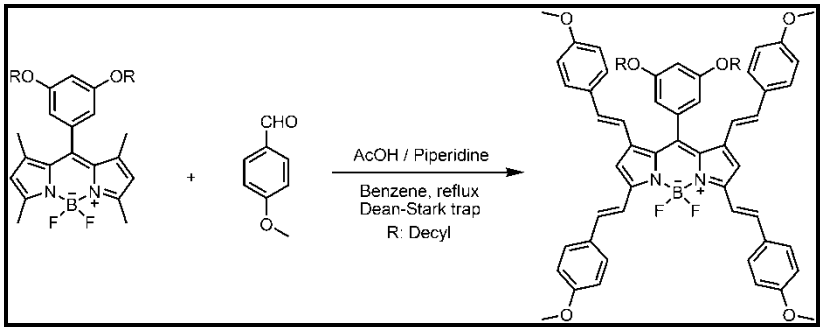

Compound **57** (0.16 mmol, 100 mg) and 4-methoxy benzaldehyde (1.12 mmol, 154 mg) were added to a 100 mL round-bottomed flask containing 50 mL benzene and to this solution was added piperidine (0.4 mL) and acetic acid (0.4 mL). The mixture was heated under reflux by using a Dean Stark trap and reaction was monitored by TLC 1:1:1 CH_2Cl_2 : Hexanes : Toluene. When all the starting material had been consumed, the mixture was cooled to room temperature and solvent was evaporated. Water (100 mL) added to the residue and the product was extracted into the

chloroform (3 x 100 mL). Organic phase dried over Na_2SO_4, evaporated and residue was purified by silica gel column chromatography using 1:1:1 CH_2Cl_2 : Hexanes : Toluene as the eluant. Purple waxy solid (20 mg, 11%). ^{1}H NMR (400 MHz, $CDCl_3$): δ = 7.67 (2H, d; *J* = 16.5 Hz, C*H*), 7.63 (4H, d; *J* = 8.8 Hz, Ar*H*), 7.35 (2H, d; *J* = 16.3 Hz, C*H*), 7.08 (2H, s; Ar*H*), 7.04 (4H, d; *J* = 8.7 Hz, Ar*H*), 6.97 (4H, d; *J* = 8.8 Hz, Ar*H*), 6.87 (2H, d; *J* = 16.0 Hz, C*H*), 6.82 (4H d; *J* = 8.8 Hz, Ar*H*), 6.78 (1H, t; *J* = 2.3 Hz, Ar*H*), 6.65 (2H, d; *J* = 2.3 Hz, Ar*H*), 5.96 (1H, d; *J* = 16.1 Hz, C*H*), 3.95-3.87 (10H, m; 4H: OCH_2, 6H: OCH_3), 3.82 (6H, s; OCH_3), 1.70-1.60 (4H, m; CH_2), 1.40-1.20 (32H, m; CH_2), 0.87 (6H, t; *J* = 7.0 Hz, CH_3); ^{13}C NMR (100 MHz, $CDCl_3$): δ = 161.2, 160.5, 159.6, 153.5, 142.0, 136.8, 135.9, 131.1, 130.0, 129.6, 129.1, 127.9, 119.8, 117.0, 114.2, 113.9, 110.5. 108.7, 102.5, 68.5, 55.4, 55.3, 31.9, 29.5, 29.3, 29.0, 25.9, 22.7, 14.1. MS (TOF- ESI): m/z: : Calcd: 1108.6312 $[M]^+$, Found: 1108.6331 $[M]^+$.

4.5. Conclusion

Bodipy dyes proved to be more than simple fluorophores, it was considered that, such straightforward functionalization and derivatization methodologies are likely to add to their impressive versatility. It appears that by fine tuning the reaction conditions, it should be possible to tether four different styryl groups to the Bodipy core. Needless to say, these novel and easily accessible chromophores are expected to make an impact as sensitizers for photodynamic therapy and dye sensitized solar cells, as structural units in dendritic light harvesters, and versatile building blocks in highly structured supramolecular entities. Setting aside reversible oxygen carrying function, it appears that the new generation of Bodipy dyes are poised to fully replace porphyrins as one of the prime building blocks in supramolecular chemistry.

CHAPTER 5

5. Energy Transfer in Tetrastyryl-Bodipy Based Dendritic Light Harvesters

This work is partially described in the following publication:

Kostereli, Z.; Ozdemir, T.; **Buyukcakir, O**. Akkaya, E.U. *Org. Lett*. **2012**, *14*, 3636-3639.

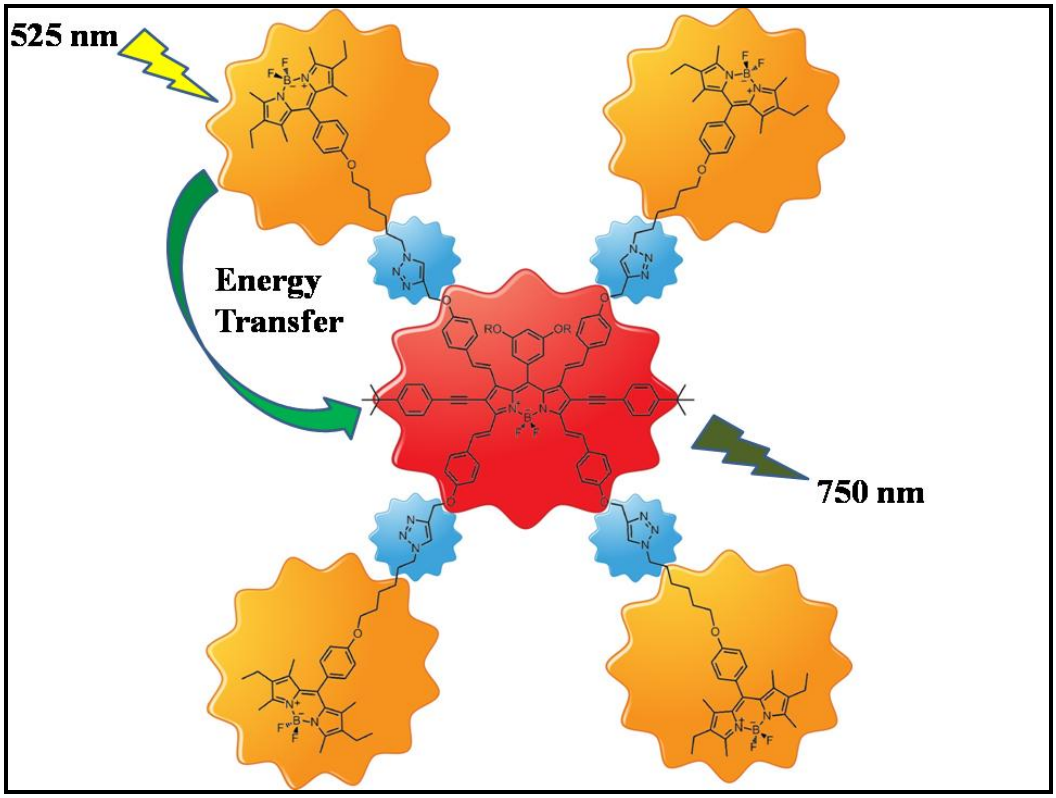

5.1. Objective

Versatile BODIPY dyes can be transformed into bright near-IR emitting fluorophores by quadruple-styryl substitutions. Light harvesting dendrimers were synthesized by a convergent synthesis methodology via "click chemistry" on versatile Boradiazaindacene (Bodipy) dyes. We demonstrated that by leaving clickable functionalities on the styryl moieties, an efficient synthesis of a light harvester is possible. Effective through-space energy transfer occurs from peripheral Bodipy and distryl-Bodipy units to a 1,3,5,7-Tetrastyryl functionalized near IR emissive Bodipy core. The resulting dendrimers are the first examples of tetrastyryl-Bodipy based light harvesting systems and highly promising candidates for design and synthesis of similar structures. In addition, we present clear spectral evidence showing that, in dendritic light harvesters, calculations commonly based on quantum yield or emission lifetime changes of the donor are bound to yield large overestimations of energy transfer efficiency.

5.3. Introduction

Efficient harvesting of solar radiation requires judiciously designed absorbers. Considering the fact that it would be difficult to have a single molecule with strong absorptions in the entire visible spectrum and near-IR (perfect black dye), it makes more sense to seek for multichromophoric dye ensembles. Different chromophoric units can be brought together either by covalent bonds or by non-covalent interactions. In either case, excitation energy transfer (EET) from the donor chromophores (shorter wavelength absorption) to the acceptor (longer wavelength absorbing core) module is expected. The efficiency of energy transfer from the antenna chromophores to the central core is very important. In such multichromophoric light harvesters, energy transfer can be either through space[135] or through bond[136]. Through space energy transfer is also possible between two or more free chromophoric units. This kind of energy transfer has been thoroughly studied and in fact, Förster (through space) energy transfer model is built on the interaction of such transition dipole coupled chromophoric pairs. Three important parameters

determine the efficiency of energy transfer: donor-acceptor distance, relative orientations of the transition dipoles and the spectral overlap between the relevant absorption and emission bands. In proteins, either utilizing endogenous fluorescence of tryptophan or using fluorescent labels, Förster model has been successful, but proteins are large and flexible enough for orientation of the dipoles to be averaged and typically, reference fluorophores are in the same microenvironment. This energy transfer model was later on applied to covalently linked multichromophoric light harvesters. In these energy transfer cassettes, energy funnels or dendritic light harvesters, energy transfer efficiency is calculated assuming that the original bimolecular Förster model system can be directly related to energy transfer process in a covalently linked multichromophoric system with short separation between the chromophores and many flexible linkers and/or side chains compared to simple reference chromophore modules. It has been recognized for some time that these values for energy transfer efficiency represent an upper limit and in most cases a significant overestimation.

5.3. Result and Discussion

It has been worked in the synthesis and characterization of light harvesting systems for some time by Akkaya and et.al.[123] In many other examples, BODIPY chromophores have been utilized either as energy donors or energy acceptors. In recent years, brightly emitting BODIPY dyes are in the focus of renewed interest with an eye towards to practical applications and new derivatization opportunities.[89] One particular derivatization which already proved to be highly fruitful is Knoevenagel condensation of acidic methyl groups found in methyl-substituted BODIPYs with selected aromatic aldehydes. Mono and di-styryl BODIPY compounds were reported in 2001[137] and 2006[132], respectively and in 2009, Akkaya research group reported[97] both tri and tetra-styryl BODIPY derivatives (also Chapter 4). Each styryl unit increases π- conjugation further, shifting the main absorption band ($S_0 \rightarrow S_1$ transition) to lower energy (longer wavelength region). By these simple sequences of reactions, absorption band of BODIPY dyes can be easily tuned in the

range of 500-900 nm. Relative ease of this modification alone, puts BODIPY derivatives in a very privileged place among organic chromophores.

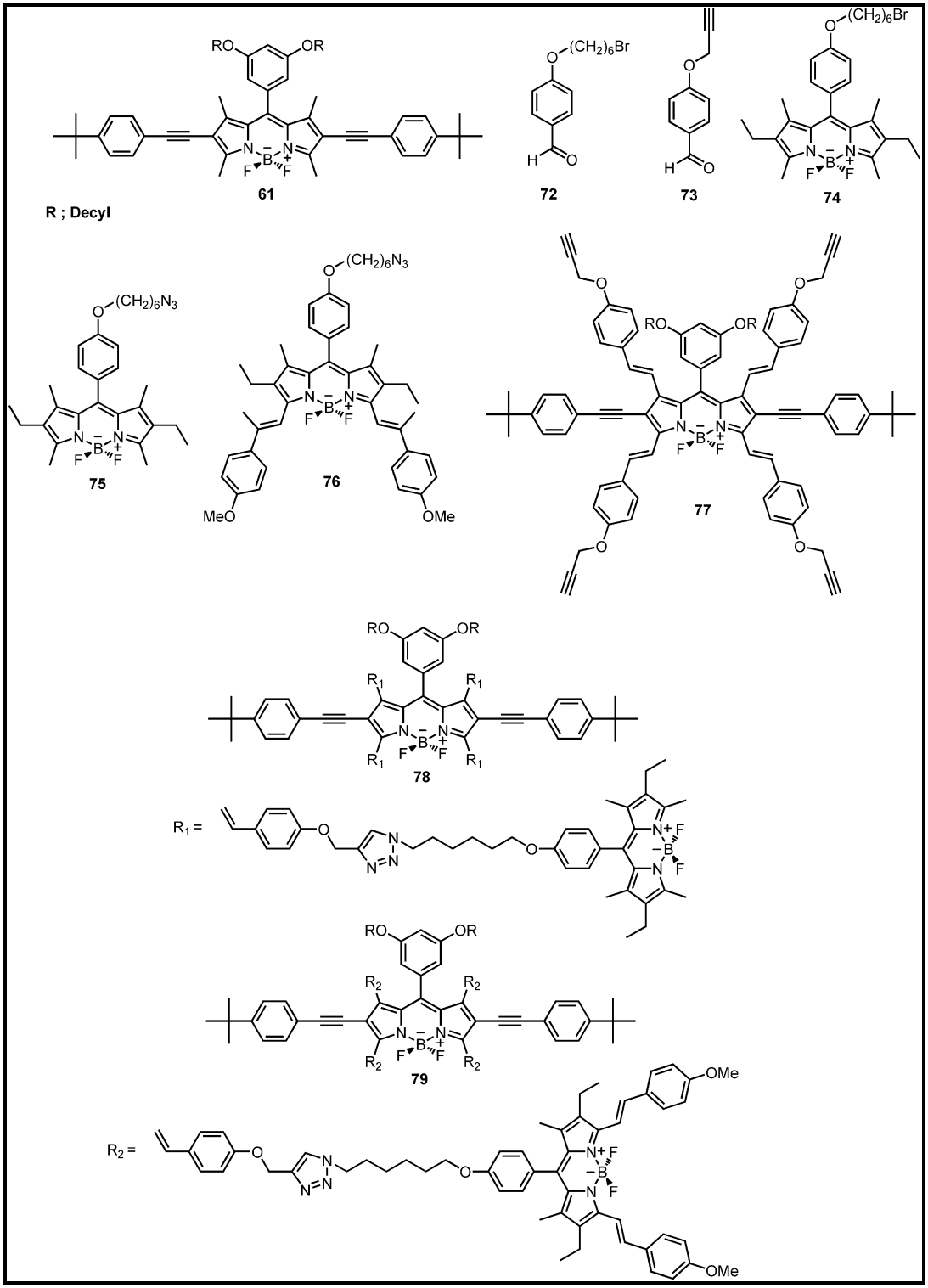

Figure 59. Structures of the modules used in the construction of tetrastyryl-Bodipy based light harvester and the target compounds **78** and **79**.

In order to investigate light harvesting properties of near-IR emitting tetra-styryl BODIPY dyes, we targeted modular harvesters **78** and **79**. The synthesis plan makes use of common intermediate **77**. Compound **77** is a tetrastyryl dye obtained by quadruple Knoevenagel condensation of a previously reported 2,6-disubstituted intermediate with 4-propynyloxybenzaldeyhde. The target compounds and precursors were depicted in Figure 59. The details of synthesis strategies were described in Experimental Details section.

Key intermediate compound **77** carries four clickable terminal alkyne groups. This design, conveniently allows modular attachment of essentially any azide functionalized chromophore. In the synthesis of compound **78**, it was reacted intermediate **77** and **75**. For compound **79**, modular units **76** and **77** were joined together by click chemistry.

Our light harvesting design involves attachment of four shorter wavelength antenna units and one central core. Absorbance spectra of compound **75**, **76**, **77**, **78** and **79** are shown in Figure 60.

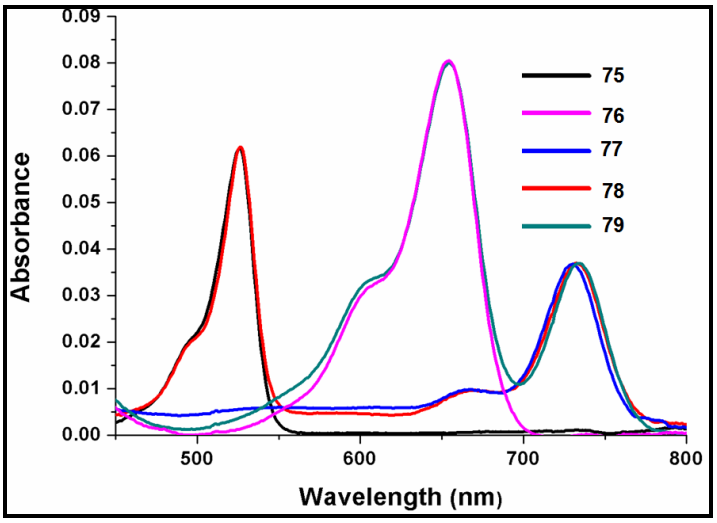

Figure 60. Absorbance spectra of compounds **75**, **76**, **77**, **78** and **79** at equal absorbances at 525 nm, for **75** and **78**, at 655 nm for **76** and **79**, at 730 nm for **77**, **78** and **79**. All in $CHCl_3$.

As expected, both light harvesters show two major absorption bands corresponding to two different chromophores. In compound **78**, absorption bands with peaks at 545

and 730 nm are apparent and in compound **79**, the two bands are centered around 652 and 732 nm. An experimental confirmation of energy transfer is readily obtained by comparing reference modules and the covalently assembled light harvesters. Figure 61 and 62 shows such comparisons. Emission spectra at equal concentrations of compounds **75** and **78** reveal a significant quenching of shorter wavelength BODIPY emission in compound **78**. Similar quenching of shorter wavelength emission is apparent in compound **79**, as well. This is no doubt and indicator of energy transfer efficiency. Another commonly employed demonstration of energy transfer is based on "enhanced core emission"[123] which is essentially obtained by exciting longer wavelength emitting modules at a common shorter wavelength used for exciting light harvesting system. As an example, **77**/**78** and **77**/**79** emissions excited at a shorter wavelength peak of **78** or **79**, respectively can be compared (Figures 61 and 62). It is clear, but also not surprising that emission from core is stronger in light harvester **78** and **79** compared to the core module **77**, when excited at 525 nm and 655 nm, respectively. Quantitative calculations of energy transfer can be based on the changes in lifetime or quantum yield.[4]

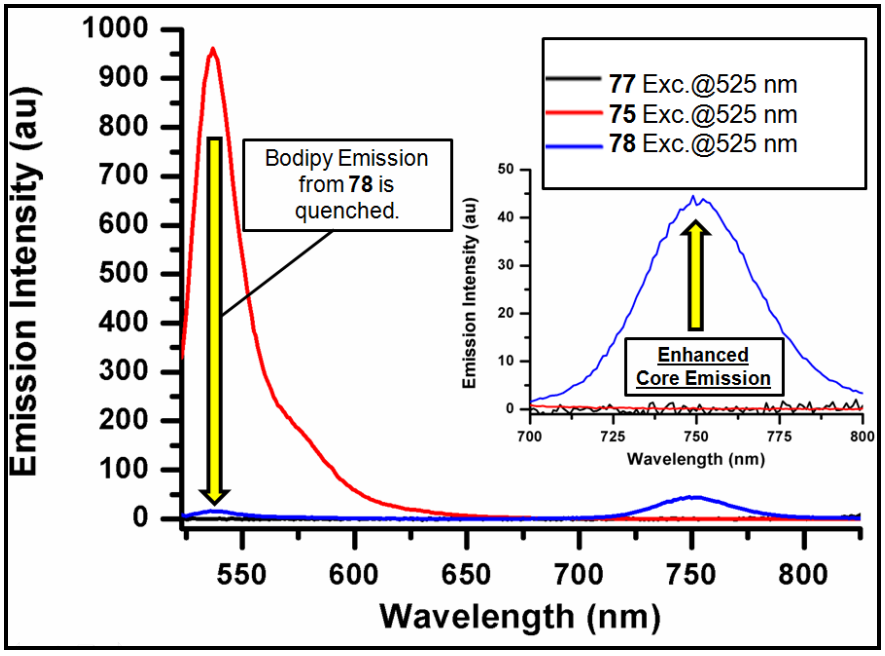

Figure 61. The emission spectra of **75**, **77**, and **78** at equal absorbances at 525 nm in $CHCl_3$. Inset: Energy transfer from peripheral Bodipy units **75** to tetrastyryl-Bodipy core **77** in light harvesting dendrimer **78.**

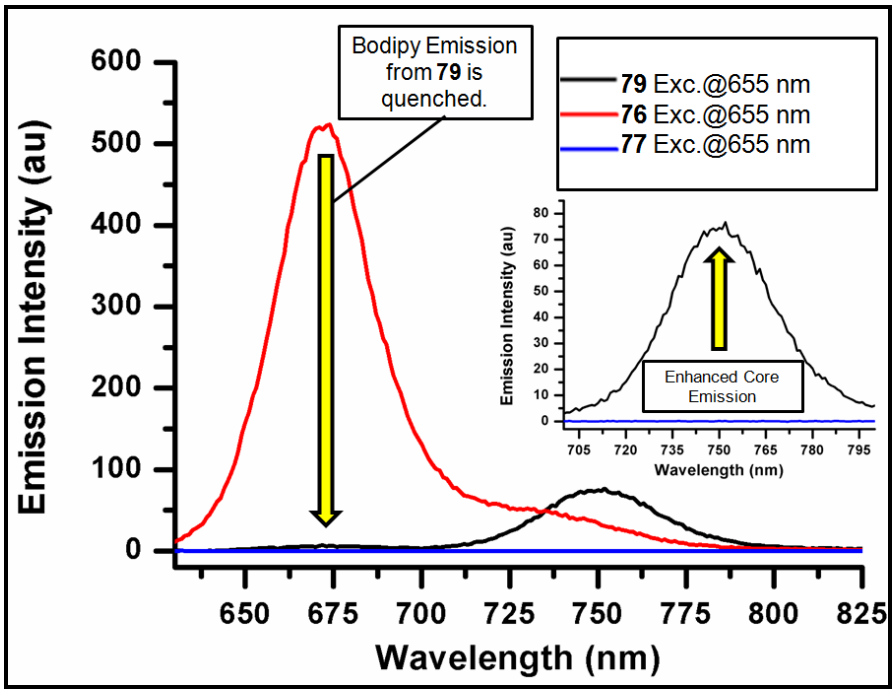

Figure 62. The emission spectra of **76**, **77**, and **79** at equal absorbances at 655 nm in $CHCl_3$. Inset: Energy transfer from distyryl-Bodipy units **75** to tetrastyryl-Bodipy core **77** in light harvesting dendrimer **79**.

This is again valid, only if bimolecular energy transfer arguments can be easily carried to larger and flexible unimolecular dendritic light harvesters. Spectral data and energy transfer rate/efficiencies are presented at Table 2 and Table 3, respectively. In light harvesters **78** and **79**, again, as expected shorter wavelength absorption is stronger with larger extinction coefficients over 300,000. Emission decay profiles from both compounds **78** and **79** are bi-exponential as expected since there is always residual emission from the shorter wavelength chromophores in addition to longer wavelength emission from the central core (Table 3). Based on the significantly reduced emission lifetimes of the donor moieties, we can calculate 90 and 92% energy transfer efficiency values for light harvesters **78** and **79**, respectively.

Table 2. Spectral data for Bodipy, distyryl-Bodipy and tetrastyryl-Bodipy dyes and light harvesting dendrimers.

Compound[a]	λ_{abs} (nm)	λ_{em} (nm)	Φ_f[b]	ε_{max}[c]
75	525	537	0.97[d]	76,000
76	655	672	0.67[e]	48,000
77	730	748	0.31[f]	143,000
78	525 733	750	0.089[d]	349,000 202,000
79	655 734	750	0.058[e]	396,000 186,000

[a] Data acquired in $CHCl_3$ in dilute solutions. [b] relative quantum yields. [c] unit: $cm^{-1}M^{-1}$. [d] Reference dye: rhodamine 6G in ethanol ($\Phi_f = 0.95$). [e] Reference dye: sulforhodamine 101 in ethanol ($\Phi_f = 0.90$). [f] Reference dye: tetrastyryl compound **63**.

Table 3. Energy Transfer rate and efficiencies of Light harvesting dendrimers **78** and **79.**

Compounds [a]	λ_{ems}[nm]	τ[ns] [b]	k_{en}(Förster) [s^{-1}]	Efficiency
78	537	0.13(40%)	$1.97x10^9$	90 %
		4.84(60%)	($1.39x10^8$)	(41%)
79	672	0.23(24%)	$2.05x10^9$	92 %
		4.10(76%)	($9.56x10^7$)	(30%)
75	537	5.02		
76	672	4.55		
77	748	3.41		

[a] Data acquired in $CHCl_3$ in dilute solutions. [b] Figures in parentheses refer to weight percentage of the contribution to emission decay.

Calculations based on quantum yields, also, result in comparable efficiency values. However, a simple inspection of excitation spectra suggests that these efficiency values are largely overestimated. Same methodology has been used in assessing energy transfer efficiencies in a large number of light harvesting molecules, energy

cascades and energy transfer cassettes.[138] Recently, in a dendritic light harvester designed for solar concentration, we have experimentally demonstrated that in such flexible light harvesting ensembles, Förster theory which was originally developed for bimolecular energy transfer is not applicable. Deviation between energy transfer efficiencies calculated by the application of Förster theory and calculations based on excitation spectra can be very large. One simple way of presenting energy transfer efficiency as a function of wavelength was proposed by Wittmershaus in 1998,[139] it is a comparison of absorption and excitation spectra, normalized at the peak wavelength of absorption of the putative energy acceptor.

In this way, the ratio of excitation to absorption values yields a plot of energy transfer efficiency as a function of excitation wavelength. Figure 63 and Figure 64 show two such operations done for the light harvesters **78** and **79**. From these ratios plotted as a function of wavelength, it is clear that in the region which corresponds to the absorption of energy donor (antenna chromophores) energy transfer efficiency is actually closer to 20-30%. This discrepancy, as mentioned previously is due to availability of additional vibrational and collisional non-radiative decay pathways in larger molecules incorporating a number of chromophores tethered with flexible linkers.

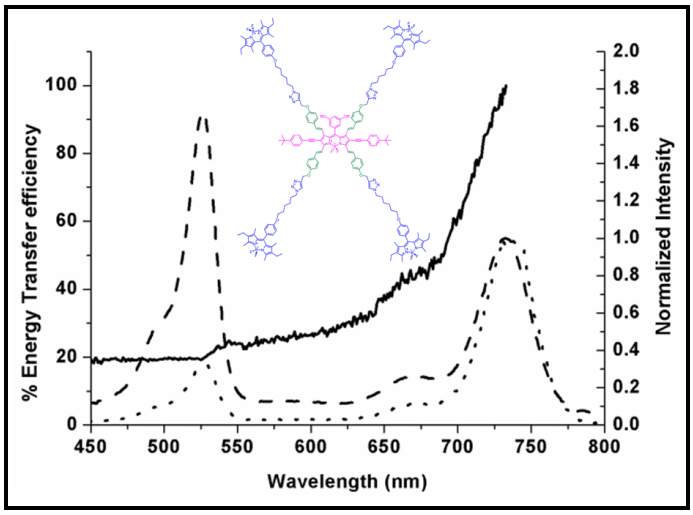

Figure 63. Percent energy transfer efficiency of **78** (solid line) as a function of wavelength of excitation. Excitation spectrum of **78** (dotted line) and absorption spectrum of **78** (dashed line), normalized at 735 nm.

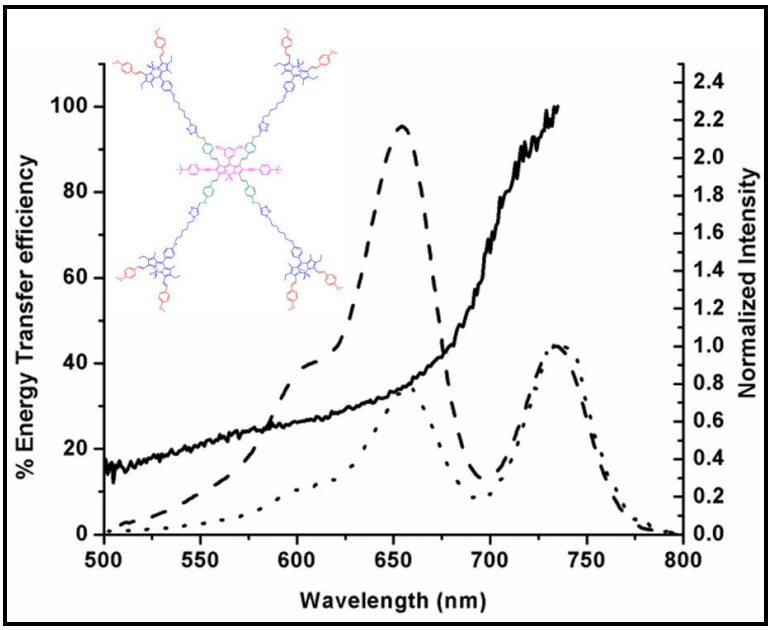

Figure 64. Percent energy transfer efficiency of **79** (solid line) as a function of wavelength of excitation. Excitation spectrum of **79** (dotted line) and absorption spectrum of **79** (dashed line), normalized at 735 nm.

5.4 Experimental Details

5.4.1. General Methods

^{1}H NMR and ^{13}C NMR spectra were recorded on Bruker DPX-400 (operating at 400 MHz for ^{1}H NMR and 100 MHz for ^{13}C NMR) in $CDCl_3$ with tetramethylsilane as internal standard. All spectra were recorded at 25^{0}C and coupling constants (*J values*) are given in Hz. Chemical shifts are given in parts per million (ppm). Absorption spectra were performed by using a Varian Cary-100 spectrophotometer. Fluorescence measurements were conducted on a Varian Eclipse spectrofluorometer. Mass spectra were recorded on Agilent Technologies 6530 Accurate-Mass Q-TOF LC/MS. MALDI mass spectra were recorded at the Izmir Institute of Technology, Izmir, Turkey and at the University of Sheffield, Mass Spectrometry Service Laboratory, Shieffield, U.K. Reactions were monitored by thin layer chromatography using Merck TLC Silica gel 60 F_{254}. Silica gel column chromatography was performed over Merck Silica gel 60 (particle size: 0.040-0.063 mm, 230-400 mesh ASTM). Compounds, **72**[140] and **73**[97] were synthesized according to literature.

Anhydrous tetrahydrofuran was obtained by refluxing over sodium/benzophenone prior to use. All other reagents and solvents were purchased from Aldrich and used without further purification.

5.4.2. Synthesis

Compound 74:

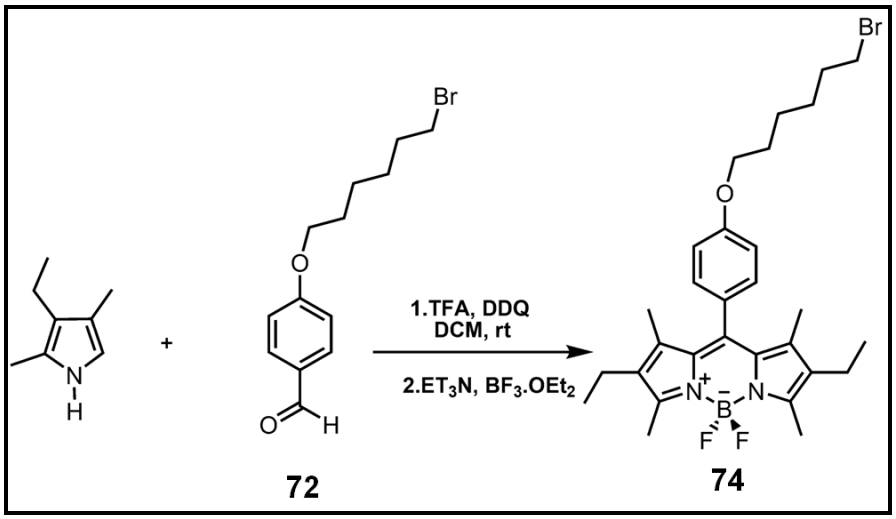

Argon gas was bubbled through 200ml CH_2Cl_2 for 30 min then 3-ethyl-2,4-dimethyl pyrrole (8.41 mmol, 1035 mg) and compound **72** (3.5 mmol, 1000 mg) were dissolved in it under argon atmosphere. 1-2 drop of TFA was added and the solution stirred at room temperature nearly 3-4 h and Argon is removed. At this point, a solution of DDQ (3.5 mmol, 794.5 mg) in 50 ml CH_2Cl_2 was added, stirring was continued for 30 min followed by the addition of 3 ml Et_3N and 3 ml $BF_3.OEt_2$. After stirring 30 min., the reaction mixture was washed three times with water and dried over Na_2SO_4. The solvent was evaporated and the residue was purified by column chromatography on silica gel using $CHCl_3$ as the eluant. Dark red solid (606.9 mg, 31%).

^{1}H NMR (400 MHz, $CDCl_3$): δ =1.0 (t, J= 7.52, 6H), 1.35 (s, 6H), 1.50-1.60 (m, 4H), 1.81-1.92 (m, 4H), 2.3 (q, J= 7.56, 4H), 2.55 (s, 6H), 3.59 (t, J= 6.64 Hz, 2H), 4.05 (t, J= 6.45 Hz, 2H), 7.0 (d, J= 8.56 Hz, 2H), 7.15 (d, J= 8. 56 Hz, 2H). ^{13}C NMR ($CDCl_3$, 100 MHz, δ ppm) 11.9, 12.5, 14.6, 17.1, 25.4, 26.7, 29.1, 32.5, 44.9, 67.9, 114.9, 127.8, 129.4, 130.1, 132.6, 138.4, 140.0, 153.5, 159.5.

Compound 75:

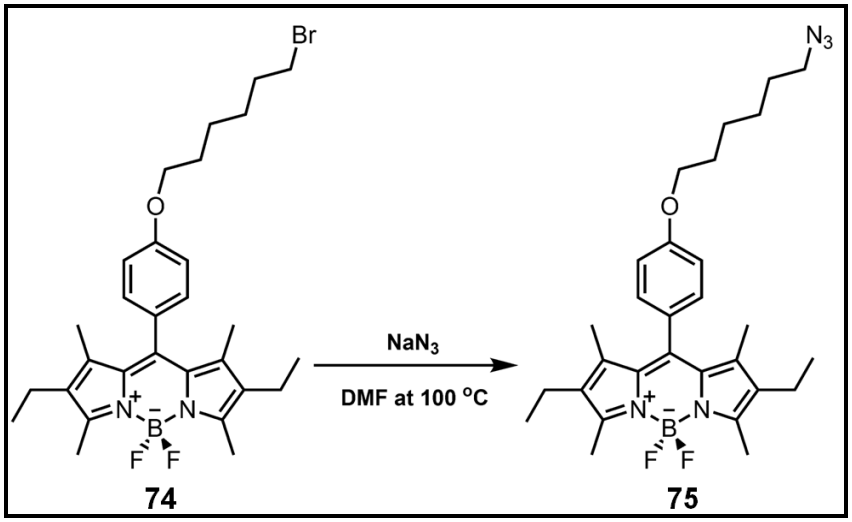

A mixture of compound **74** (1.43 mmol, 800 mg) and NaN_3 (3.576 mmol, 232 mg) in 20 ml DMSO was heated at 100 ^oC for 2h and controlled with TLC. When the reaction was completed, water (100 mL) was added to the residue and the product was extracted into the chloroform (3 x 100 mL). Organic phase dried over Na_2SO_4, evaporated and residue was used without further purification. Dark red solid (702.4 g, 97 %).

^1H NMR ($CDCl_3$, 400 MHz, δ ppm) δ =1.0 (t, J= 7.52 Hz, 6H), 1.35 (s, 6H), 1.50-1.60 (m, 4H), 1.62-1.71 (m, 2H), 1.80-1.91 (m, 2H), 2.3 (q, J= 7.56 Hz, 4H), 2.55 (s, 6H), 3.32 (t, *J*= 6.64 Hz, 2H), 4.05 (t, *J*= 6.45 Hz, 2H), 7.0 (d, *J*= 8.56 Hz, 2H), 7.15 (d, *J*= 8.56 Hz, 2H). ^{13}C NMR ($CDCl_3$, 100 MHz, δ ppm) 11.8, 12.5, 14.6, 17.1, 25.7, 26.6, 28.8, 29,1, 51.4, 67.9, 115.0, 127.8, 129.4, 131.2, 132.6, 138.4, 140.3, 153.5, 159.5 MS (TOF- ESI): m/z: : Calcd: 521.3137 $[M]^+$, Found: 520.30651$[M-H]^+$, Δ=1.6 ppm.

Compound 76:

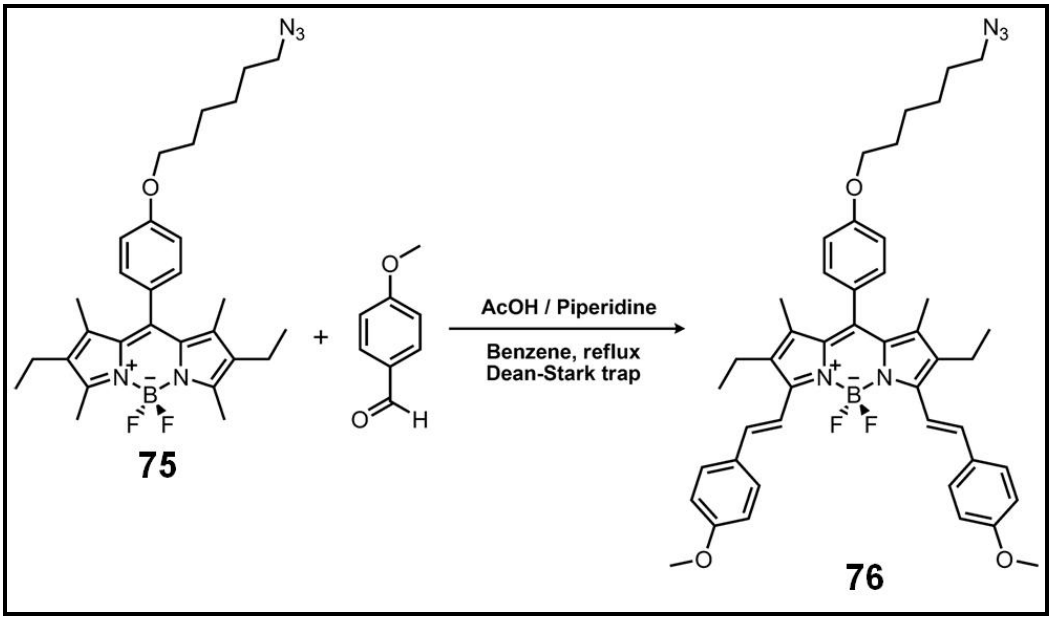

Compound **75** (0.384 mmol, 200 mg) and 4-Methoxybenzaldehyde (0.844 mmol, 115 mg) were added to a 100 mL round-bottomed flask containing 50 mL benzene and to this solution, piperidine (0.3 mL) and acetic acid (0.3 mL) were added. The mixture was heated under reflux by using a Dean Stark trap and it is monitored by TLC. When all the starting material had been consumed, the mixture was cooled to room temperature and solvent was evaporated. Water (100 mL) added to the residue and the product was extracted with the chloroform (3 x 100 mL). The organic phase dried over Na_2SO_4, evaporated The residue was poured into 2:1 EtOAc : Hexanes solution and dissolved by heating then it was cooled to 0 ^{0}C. Compound 7**6** precipitated at that temperature then it was filtered and obtained as pure product. Green solid (155.1 mg, 53%).

^{1}H NMR ($CDCl_3$, 400 MHz, δ ppm) 1.20 (t, J= 7.46 Hz, 6H), 1.40 (s, 6H), 1.50-1.60 (m, 4H), 1.65-1.75 (m, 2H), 1.85-1.95 (m, 2H), 2.65 (q, J= 7.62 Hz, 4H), 3.35 (t, *J*= 6.84 Hz, 2H), 3.89 (s, 6H), 4.10 (t, *J*= 6.40 Hz, 2H), 6.95 (d, *J*= 8.56 Hz, 2H), 7.05 (d, *J*= 8.44 Hz, 2H), 7.23 (d, *J*=8.44 Hz, 2H), 7.25 (d, *J*= 16.70 Hz, 2H), 7.62 (d, *J*= 8.60 Hz, 2H), 7.70 (d, *J*= 16.70 Hz, 2H). ^{13}C NMR ($CDCl_3$, 100 MHz, δ ppm) 11.70, 14.08, 18.40, 25.73, 26.58, 28.82, 29.16, 51.40, 55.39, 67.90, 114.22, 115.00, 118.24, 128.14, 128.76, 129.86, 130.35, 133.34, 133.48, 135.23, 138.15, 138.80, 150.31, 159.54, 160.15. MS (HRMS-ESI): m/z: : Calcd: 757.4 [M], Found: 757.5 $[M-H]^+$

Compound 77:

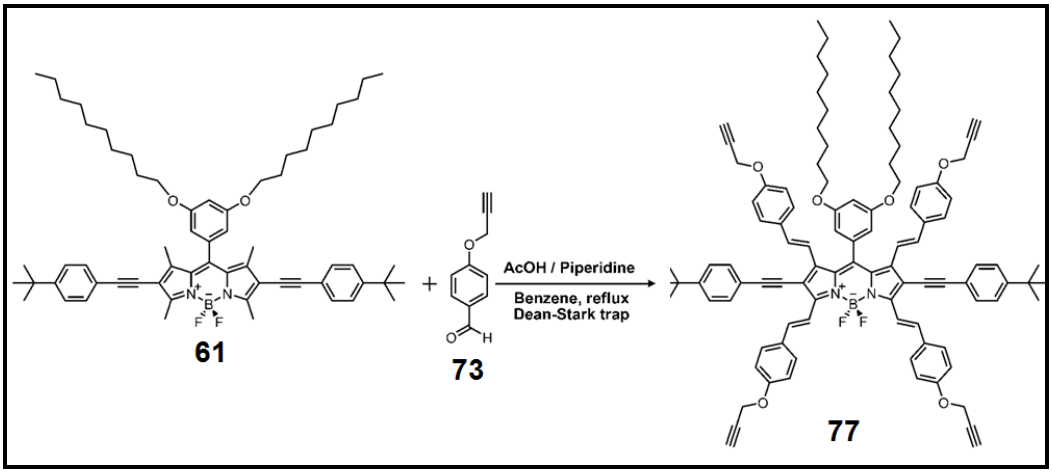

Compound **61** (0.42 mmol, 400 mg) and compound **73** (2.95 mmol, 472 mg) were added to a 100 mL round-bottomed flask containing 50 mL benzene and to this solution, piperidine (0.3 mL) and acetic acid (0.3 mL) were added. The mixture was heated under reflux by using a Dean Stark trap and it is monitored by TLC 3:2 Chloroform : Hexane. When all the starting material had been consumed, the mixture was cooled to room temperature and solvent was evaporated. Water (100 mL) added to the residue and the product was extracted into the chloroform (3 x 100 mL). Organic phase dried over Na_2SO_4, evaporated and residue was purified by silica gel column chromatography using 3:2 $CHCl_3$: Hexanes as the eluant. Dark green solid (416 mg, 65%).

^{1}H NMR (400 MHz, $CDCl_3$): δ = 0.88 (t; *J* = 6.8 Hz, 6H), 1.18-1.32 (m; 28H), 1.35 (s; 18H), 1.55-1.65 (m; 4H), 2.55 (t; *J* = 2.4 Hz, 1H), 2.60 (t; *J* = 2.4 Hz, 1H), 3.83 (t; *J* = 6.5 Hz, 4H), 4.70 (d; *J* = 2.4 Hz, 4H), 4.80 (d; *J* = 2.4 Hz, 4H), 6.10 (d; *J* = 16.2 Hz, 2H), 6.61 (d; *J* = 16.2 Hz, 2H), 6.72 (d; *J* = 2.2 Hz, 1H), 6.89 (d; *J* = 8.8 Hz, 4H), 7.02-7.10 (m; 8H), 7.42 (d; *J* = 8.7 Hz, 4H), 7.48 (d; *J* = 8.7 Hz, 4H), 7.70 (d; *J* = 8.8 Hz, 4H), 7.78 (d; *J* = 16.3 Hz, 2H), 7.82 (d; *J* = 17.0 Hz, 2H), 8.59 (d; *J* = 16.3 Hz, 2H). ^{13}C NMR (100 MHz, $CDCl_3$): δ =14.1, 22.7, 25.9, 29.0, 29.3, 29.6, 31.2, 31.9, 34.9, 55.8, 55.9, 68.7, 75.6, 75.9, 78.4, 78.5, 85.7, 98.9, 103.2, 108.3, 109.0, 114.9, 115.3, 117.4, 119.7, 120.7, 125.7, 128.0, 129.3, 130.5, 130.9, 131.2, 132.9, 133.7, 136.7, 137.6, 138.8, 142.1, 151.7, 153.4, 157.7, 158.6, 161.6. MS (HRMS-ESI): m/z: : Calcd: 1516.819 [M^+], Found: 1516.798 [M^+] , Δ=14 ppm

Compound 78:

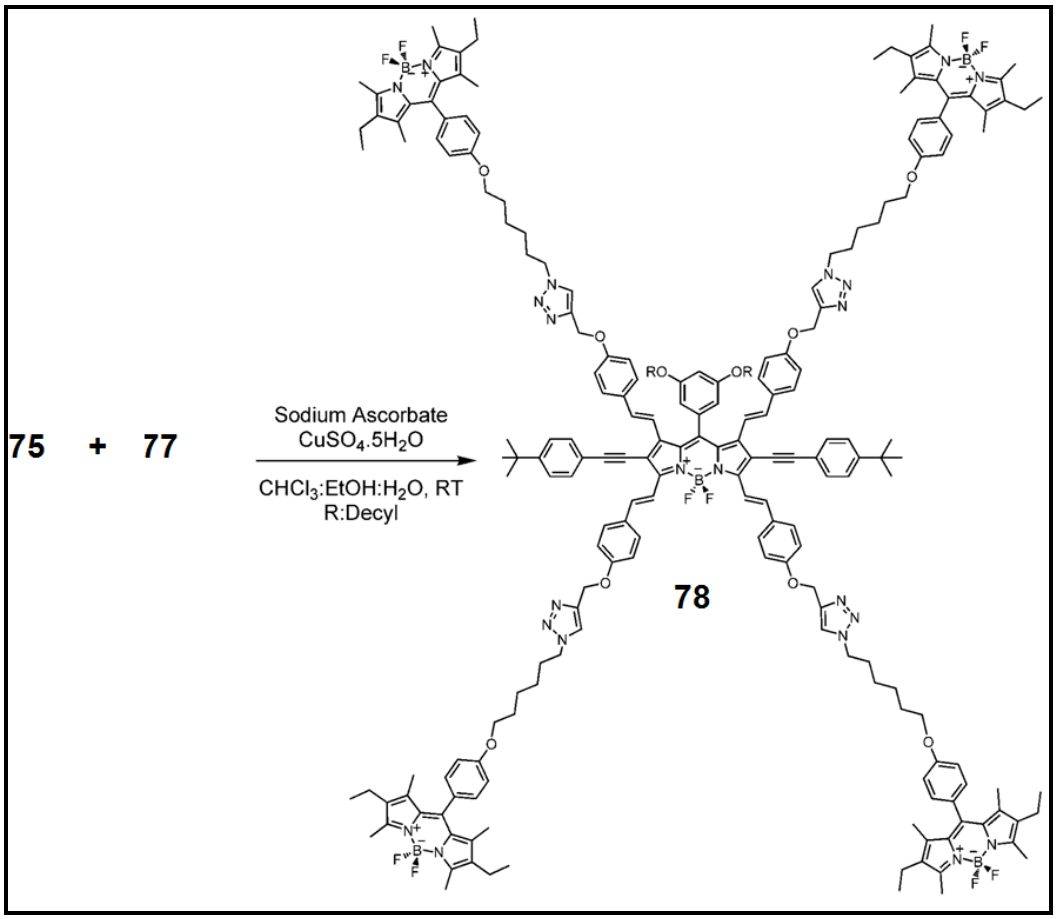

To the solution of the compound **75** (0.238 mmol, 124 mg) in a 12:1:1 mixture of $CHCl_3$, EtOH and water (14 ml); compound **77** (0.040 mmol, 60 mg), sodium ascorbate (0.0237 mmol, 4.7 mg), $CuSO_4$ (0.0118 mmol, 2.9 mg) and 3-4 drop Et_3N are added and it was stirred at room temperature for 24 h. Water (50 mL) was added to the residue and the product was extracted into the chloroform (3 x 50 mL). After evaporation of the solvents, the crude product was purified by column chromatography ($CHCl_3$). Black solid (122 mg, 85%).

^{1}H NMR ($CDCl_3$, 400 MHz, δ ppm) 0.75 (t, J= 6.76 Hz, 6H), 0.89 (t, *J*= 8.3 Hz, 24H), 1.05-1.20 (m, 28H), 1.24 (s, 18H), 1.26 (s, 24H), 1.36 (p, *J*= 8.39 Hz, 4H), 1.43-1.55 (m, 16H), 1.74 (p, *J*= 7.01 Hz, 8H), 1.92 (p, *J*= 7.34 Hz, 8H), 2.16-2.26 (m, 16H), 2.44 (s, 24H), 3.75 (t, *J*= 6.42 Hz, 4H), 3.91 (t, *J*= 6.24 Hz, 8H), 4.31 (t, *J*= 6.66 Hz, 8H), 5.14 (s, 4H), 5.22 (s, 4H), 6.00 (d, *J*= 16.20 Hz, 2H), 6.53 (s, 2H), 6.62 (s, 1H), 6.80 (d, *J*= 8.64 Hz, 4H), 6.89 (d, *J*= 8.52 Hz, 8H), 6.96 (d, *J*= 8.72 Hz, 4H), 6.99 (d, *J*= 8.64 Hz, 4H), 7.02-7.08 (m, 8H), 7.32 (d, *J*= 8.60 Hz, 4H), 7.37 (d, *J*=

8.48 Hz, 4H), 7.52 (s, 2H), 7.56 (s, 2H), 7.58 (d, *J*= 8.68 Hz, 4H), 7.69 (d, *J*= 16.12 Hz, 4H), 8.46 (d, *J*= 16.40, 2H). ($CDCl_3$, 100 MHz, δ ppm) 11.88, 12.48, 14.14, 14.21, 14.65, 17.08, 21.07, 22.69, 25.62, 25.66, 25.90, 26.36, 26.41, 28.97, 29.07, 29.12, 29.33, 29.58, 30.24, 30.28, 31.21, 31.90, 50.37, 60.40, 62.21, 62.25, 67.76, 68.66, 98.91, 114.81, 114.95, 115.29, 120.59, 122.44, 122.58, 125.77, 127.77, 127.83, 128.13, 129.32, 129.48, 130.49, 131.20, 132.62, 132.66, 136.66, 137.44, 138.39, 138.44, 138.68, 138.83, 140.31, 140.36, 142.09, 144.06, 153.43, 153.48, 158.43, 159.32, 159.43, 161.61. MS (MALDI): m/z: : Calcd: 3602.074 $[M]^+$, Found: 3711.572 $[M\text{-}Ag]^+$

Compound 79:

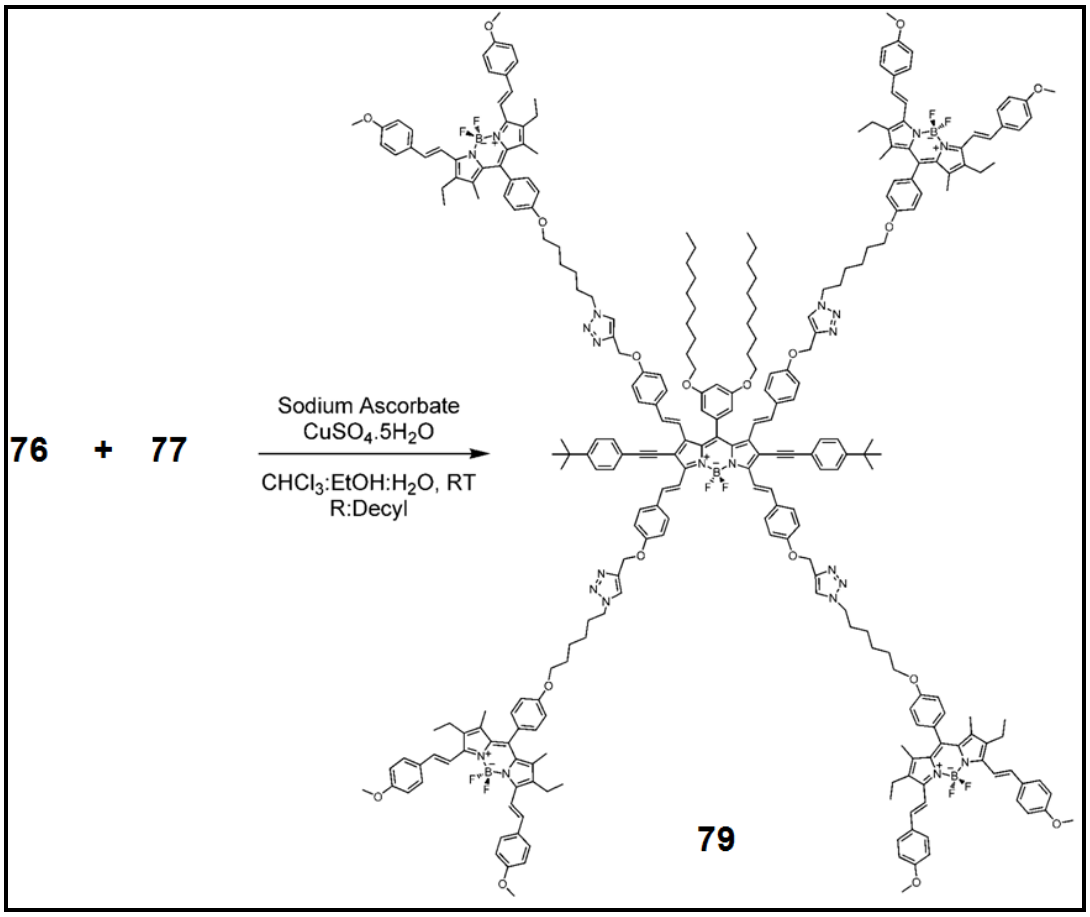

To the solution of the compound **76** (0.237 mmol, 335 mg) in a 12:1:1 mixture of $CHCl_3$, EtOH and water (14 ml); compound **77** (0.0396 mmol, 60 mg), sodium ascorbate (0.0237 mmol, 4.7 mg), $CuSO_4$ (0.0118 mmol, 2.9 mg) and 3-4 drop Et_3N

were added and it was stirred at room temperature for 24 h. Water (50 mL) was added to the residue and the product was extracted into the chloroform (3 x 50 mL). After evaporation of the solvents, the crude product was purified by column chromatography ($CHCl_3$). Black solid (144 mg, 80%).

^{1}H NMR ($CDCl_3$, 400 MHz, δ ppm) 0.90 (t, J= 6.90 Hz, 6H), 1.18 (t, *J*= 7.60 Hz, 24H), 1.19-1.30 (m, 28H), 1.37 (s, 18H), 1.40 (s, 24H), 1.41-1.50 (m, 4H), 1.52-1.69 (m, 16H), 1.79-1.90 (m, 8H), 1.95-2.07 (m, 8H), 2.55-2.65 (m, 16H), 3.86-3.90 (m, 28H), 4.09 (t, *J*= 6.20 Hz, 8H), 4.42 (t, *J*= 7.00 Hz, 8H), 5.25 (s, 4H), 5.32 (s, 4H), 6.11 (d, *J*= 16.13 Hz, 2H), 6.65 (d, *J*= 2.04 Hz, 2H), 6.75 (s, 1H), 6.92 (d, *J*= 8.56 Hz, 4H), 6.95 (d, *J*= 8.84 Hz, 16H), 7.01 (d, *J*= 8.50 Hz, 8H), 7.06 (d, *J*= 8.72 Hz, 4H), 7.10 (d, *J*= 8.00 Hz, 4H), 7.16-7.25 (m, 16H), 7.43 (d, *J*= 8.52 Hz, 4H), 7.48 (d, *J*= 8.52 Hz, 4H), 7.59 (d, *J*= 8.72 Hz, 16H), 7.63-7.74 (m, 16H), 7.78 (s, 2H), 7.83 (s, 2H), 8.58 (d, *J*= 16.13, 2H). ($CDCl_3$, 100 MHz, δ ppm) 11.74, 14.05, 14.16, 18.41, 22.71, 25.62, 25.69, 25.93, 26.32, 26.40, 28.99, 29.14, 29.34, 29.59, 30.22, 30.28, 31.22, 31.92, 34.93, 50.39, 55.43, 62.14, 62.21, 62.26, 67.78, 68.68, 85.74, 98.97, 108.28, 114.25, 114.82, 114.92, 114.99, 115.32, 118.13, 118.23, 119.52, 120.61, 122.49, 122.67, 122.76, 125.77, 128.05, 128.11, 128.16, 128.76, 129.34, 129.87, 130.39, 130.49, 133.22, 133.48, 133.81, 135.34, 138.20, 138.94, 142.13, 144.06, 150.31, 151.82, 153.38, 158.40, 159.17, 159.53, 160.25, 161.69. MS (MALDI): m/z: : Calcd: 4546.409 [M^+], Found: 4547.0 [M^+]

5.5. Conclusion

A thorough understanding of energy transfer process in large multichromophoric systems is quite important but before that is to be done, some persistent misunderstandings and mistakes in the literature have to be addressed and corrected. It was hope that a clarification of energy transfer efficiency issue will facilitate the design and synthesis of novel and unequivocally more efficient light harvesters and solar concentrators. It was considered that tetra-styryl BODIPY dyes or similarly tetra functionalized BODIPY dyes will continue to be at the core of these improved light harvesting assemblies.

CHAPTER 6

6. $[Cu(I)(dpp)_2]^+$ derivatives as candidates for sensitizers in Dye Sensitized Solar Cell

This work is partially described in the following publication:

Huang, J.; **Buyukcakir, O.**; Mara, M. W.; Coskun, A.; Dimitrijevic, N. M.; Barin, G.; Kokhan, O,; Stickrath, A. B., Ruppert, R., Tiede, D. M., Stoddart, J. F., Sauvage, J. P.; Chen, L. X. *Angew. Chem. Int. Ed.*, **2012**, *51*, 12711-12715.

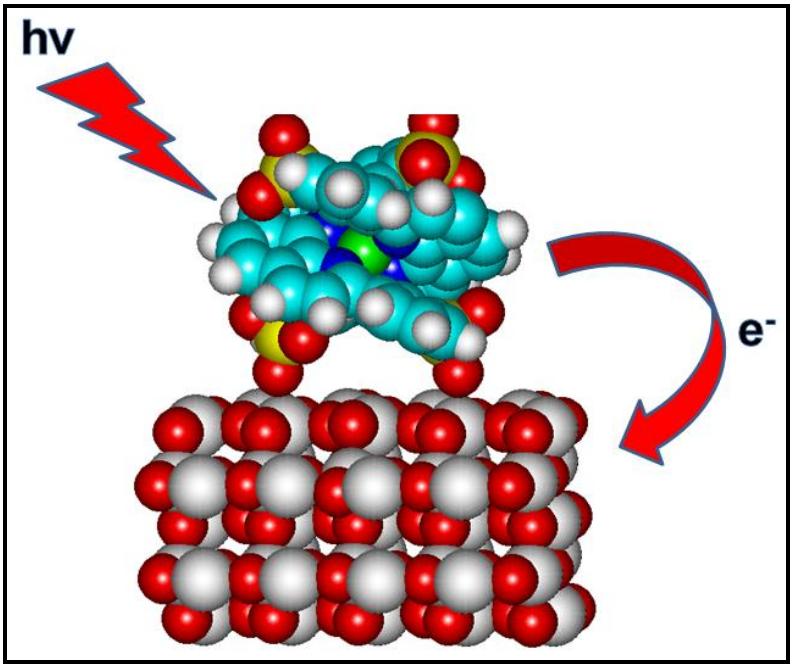

6.1. Objective

The need for the energy has been increasing dramatically. However, the fossil based energy sources exploit much faster depletion. Therefore, the exploration of new renewable energy sources have been attracted great attention in recent years. The solar energy conversion systems are the most promising systems especially solar cells. At this point, DSSC is the strongest candidate in these systems. DSSCs serve lower cost and simplicity in the manufacturing. However, the price to performance ration of DSSC is still high. Thus, there is a great effort to design novel DSSC systems with better performance. Ruthenium based DSSC systems have high light-to-electron energy conversion efficiency but their high cost inhibits the large scale production. At this point, the replacement of ruthenium with cheaper alternative such as Cu-diimine complexes plays a crucial role for the future of DSSC. Therefore, we investigated Cu(I) diimine complexes and their electron injection capability to TiO_2 nanoparticles. The results are very promising. This work potentially will generate significant impact for those working on solar energy conversion and DSSC.

6.2. Introduction

The photoinduced electron transfer (ET) from transition-metal complexes into semiconductor nanoparticles (NPs) plays crucial role in popular science such as photocatalysis, solar fuel generation, and dye sensitized solar cells (DSSCs).[141,142] Therefore, this energy transfer has been studied extensively in recent decades because of its relevance in these hot topics. Ruthenium based polpyridyl complex-sensitized TiO_2 NP electrodes are one of the most common systems in DSSCs and they can produces high light-to-electron energy conversion efficiency (11%).[143,144] However, these promising systems have high cost since the ruthenium is a rare earth metal. The low abundance of ruthenium leads to some limitation in large scale production of ruthenium dye based DSSCs. The usage of copper metal instead of using ruthenium has been studied. Polypyridiyl complexes of copper metal have been analyzed in literature.[145] Although these complexes show similar absorption spectra and photo physics as polypyridiyl ruthenium complexes, they cannot have similar

efficiencies and stabilities as ruthenium dye-based solar cells. It is a well known fact that there are many factors which affects the DSSCs device efficiency such as light harvesting, driving force for charge separation and recombination, excited-state lifetime. Therefore, it plays crucial role to understand how these factors can be optimized at molecular and electronic level.

6.3. Result and Discussion

There are two possible way to transfer an electron from the photo excited Cu^{I} polypyridyl complex to the TiO_2 NPs. First route is that electron transfer from ^{1}MLCT state with a higher energy and ET driving force but very short excited-state lifetime which is ca. 10 ps or shorter. Second way of electron transfer is from ^{3}MLCT state with a lower energy and ET driving force but much longer excited-state lifetime which is a few ns to a few hundred ns. However, the ^{1}MLCT state lifetime and so the intersystem crossing (ISC) rate can be effected from the coordination geometry of copper center and also solvent accessibility.[146,147] The coordination of copper center is very important because of the ^{1}MLCT states of CuI diimine complexes undergo a Jahn-Teller distortion. These distortion changes the lifetime efficiencies and the electron injection dynamics. These factors have not been analyzed to date and in this work we presented highly efficient electron injection from the exited state of $[Cu^{I}(dppS)_2]^{+}$ (dppS = 2,9-diphenyl-1,10-phenanthroline disulfonic acid disoddium salt) to TiO_2 nanoparticles. This injection was investigated by using multiple time-resolved spectroscopic methods. Electron paramagnetic resonance (EPR), optical transient absorption (TA), and X-ray transient absorption (XTA) spectroscopies were used to analyze the dynamics of charge separation and recombination with molecular structure (Figure 65).

Figure 66 shows the synthesis methodology of $[Cu(I)(dppS)_2]\cdot PF_6$. The synthesis sequence started with the functionalization of phenanthroline core. 2 and 9 di-phenyl substituted phenanthroline units were synthesized by using the procedure reported in the literature. [148]The sulphonation reaction was performed by using fuming sulfuric

acid (oleum) under ambient conditions. The sample preparation and experimental setup details was mentioned in experimental section.

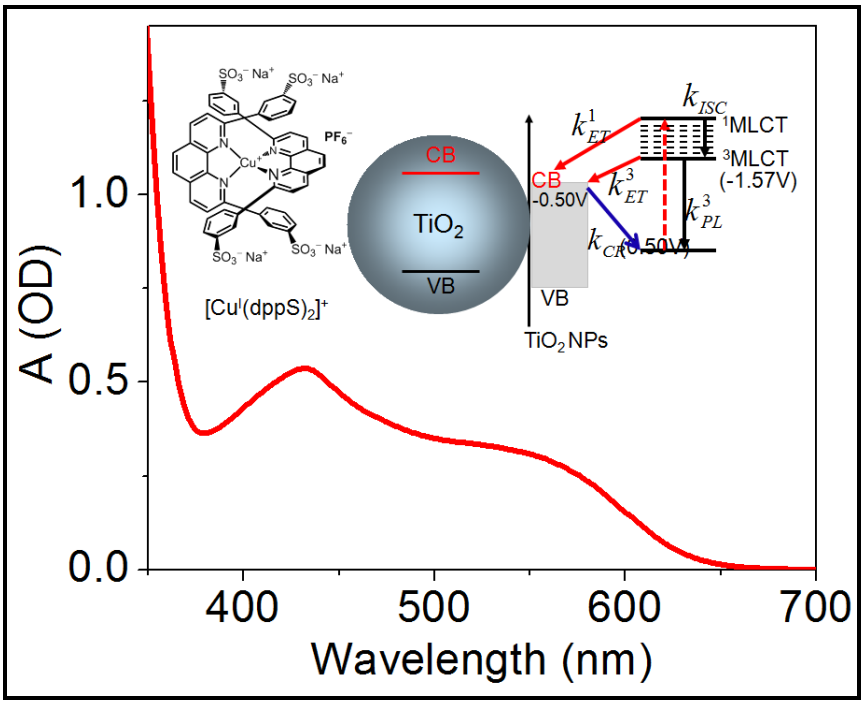

Figure 65. UV/Vis absorption spectrum of [Cu^{I}(dppS)$_2$]$^+$ in water; Inset: the molecular structure of [Cu^{I}(dppS)$_2$]$^+$ and the electron-injection and recombination model in the [Cu^{I}(dppS)$_2$]$^+$/TiO$_2$ hybrid.

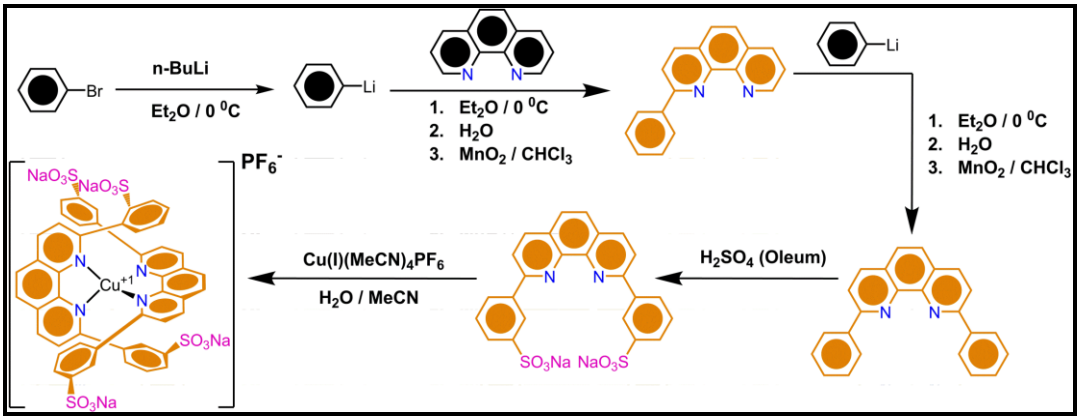

Figure 66. Synthesis of target complex [Cu(I)(dppS)$_2$]·PF$_6$.

The incorporation of fused aromatic rings to 2 and 9 positions of phenanthroline transform these units to an excellent tetrahedral enforcer ligands which can show

high affinity to Cu(I). Because of its electron deficient character, phenanthroline core cannot undergo electrophilic aromatic substitution reactions. Therefore, the sulfonation reaction on 2,9-diphenyl-1,10-phenanthroline gives only sulfonyl groups on the incorporated phenyl rings. It is a well-known fact that after the first sulfonation on pheny groups makes the phenyl ring deactivated to second sulphonation attack. Therefore, over sulphonation reactions are not possible. On the other hand, the orto position of phenyl ring not only electronically but also sterically do not allowed the sulphonation reaction on this side. Therefore, the sulpho groups can go to meta and para positions. Also, the meta position electronically more reactive than the para position so that meta substitution is more favored than para. As expected, the sulphonation reaction resulted with two positional isomer; meta-meta (m-m*) and meta-para (m-p). The distribution ratio of isomers could be easily determined from the pattern and integral of the proton NMR signals (Figure 67). The meta-meta (m-m*) is the major isomer (70%) and the other isomer is the meta-para (30%). There is also para-para (p-p*) isomers was formed but it can be neglected (<1%).

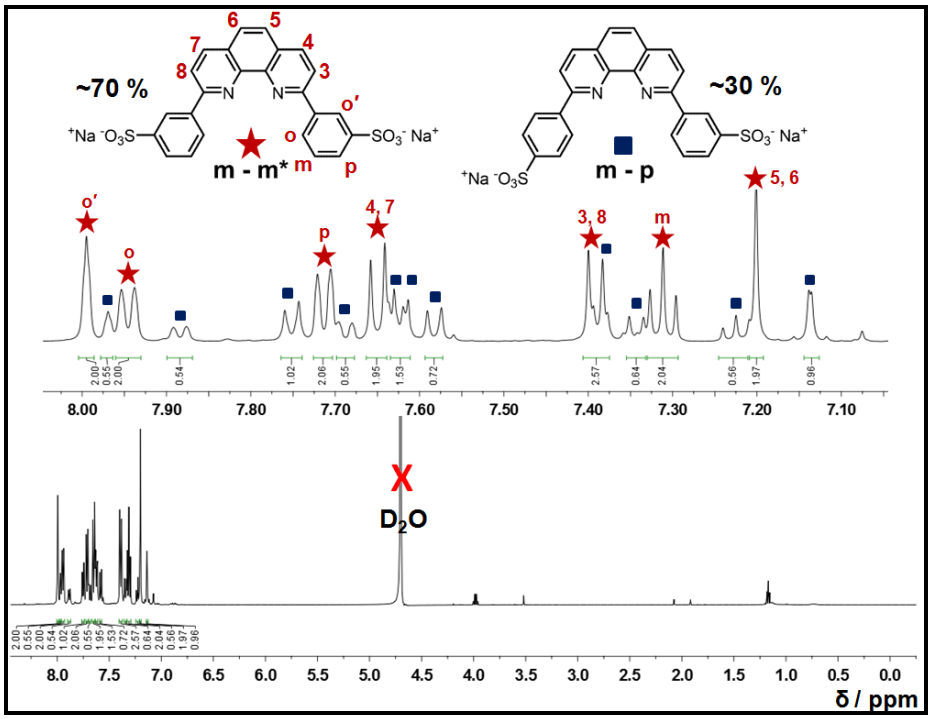

Figure 67. ^{1}H NMR spectrum of dppS ligand (mixture of isomers; m-m* (70%) and m-p (30%)) recorded at 298 K in D_2O.

Then, the copper complexation reaction of dppS ligand was performed under N_2 atmosphere. The water soluble dppS ligands were dissolved in pre-degassed H_2O. Simultaneously, the $[Cu(MeCN)_4]PF_6$ was dissolved in MeCN pre-purged with argon. Using the double-ended needle transfer technique, $[Cu(MeCN)_4]PF_6$ in MeCN solution was added under N_2 at room temperature to a stirred solution of dppS ligands in H_2O. Instantaneously, the color of reaction mixture turned dark red which is the indication of formation of $[Cu(I)(dppS)_2]\cdot PF_6$ complex. The proton NMR of copper complex of dppS ligand is very complex to analyze because of cross complexation of positional isomers (Figure 68).

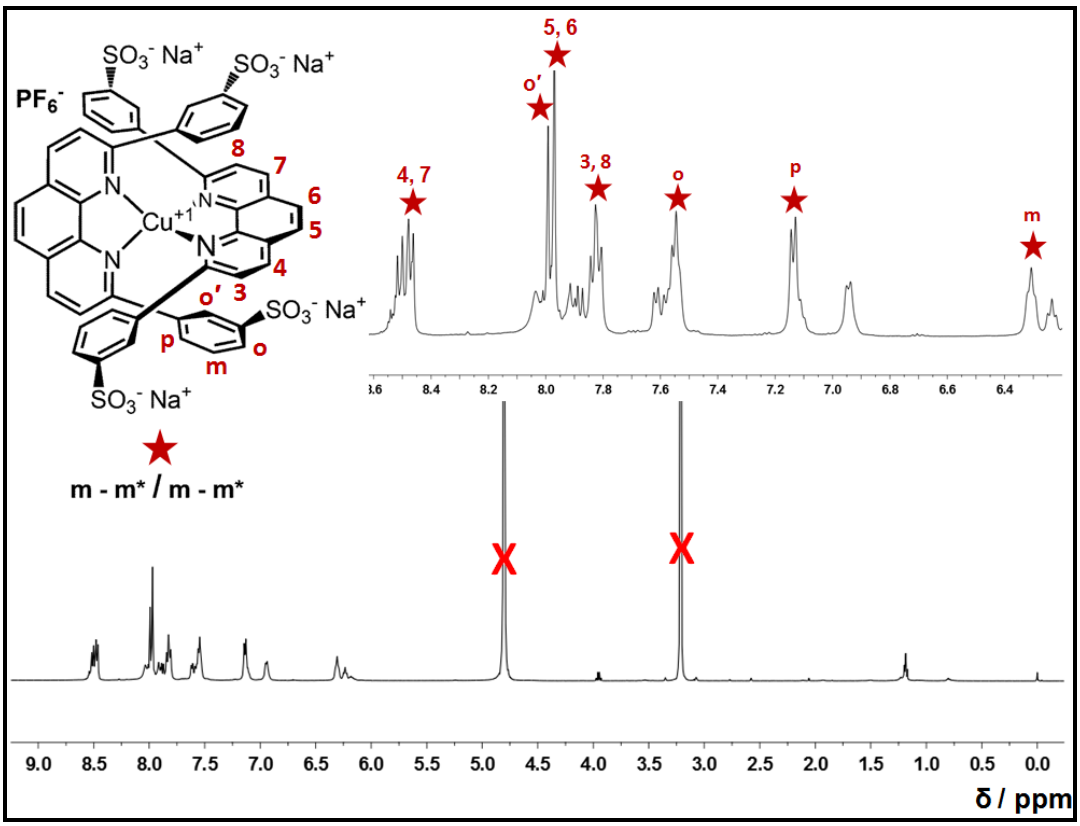

Figure 68. ^1H NMR spectrum of $[CuI(dppS)_2]^+\cdot PF_6^-$ complex recorded at 298 K in CD_3OD.

The sulfonated phenyl groups at 2, 9 positions of the phenanthroline ligands force the ground state of $[Cu^I(dppS)_2]^+$ to adopt a "flattened" pseudo-tetrahedral coordination geometry where the spin-orbit coupling is weakened resulting in an ISC rate

prolonged by two orders of magnitude compared to those of complexes with two phenanthroline ligand planes orthogonal with each other.[149] Moreover, the two sulfonated phenyl groups also block solvent access to the Cu centre to prevent the formation of an "exciplex", lowering the energy gap between the MLCT and the ground states and accelerating the ground state recovery.[150,151] Consequently, these structural factors result in a longer MLCT lifetime and a higher emission quantum yield. The sulfonate groups also serve as linkers to TiO_2 NP surfaces through electrostatic or covalent linkages.[152] The oxidation potential of the MLCT state was −1.57 V vs SCE. Compared with the conduction band (CB) edge of TiO_2 NPs (−0.5 V vs SCE),[153] the estimated upper limit of the Gibbs free energy change ΔG_{ET} for ET from the MLCT excited state of $[Cu^{I}(dppS)_2]^+$ to the CB of TiO_2 NPs is −1.07 V. The cyclic votammogram was depicted in Figure 69.

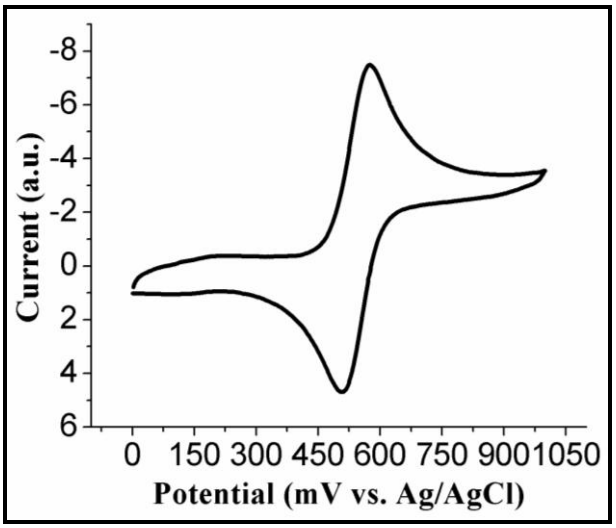

Figure 69. Cyclic Voltammogram of $[Cu^{I}(dppS)_2]\cdot PF_6$ in H_2O (0.1 M KCl) at 0.1 V/s scan rate.

Steady state EPR spectra of the $[Cu^{I}(dppS)_2]^+/TiO_2$ hybrid at 5 K were measured to verify the electron injection from the MLCT state of $[Cu^{I}(dppS)_2]^+$ to TiO_2 NPs (see the experimental section for details). A Xe lamp with a long pass filter (cut-off wavelength = 440 nm) was used to ensure selective excitation of $[Cu^{I}(dppS)_2]^+$ not TiO_2 NPs. As shown in Figure 70, the EPR spectrum of the $[Cu^{I}(dppS)_2]^+/TiO_2$ hybrid under the light illumination shows distinct features at 3341, 3388 G(gauss),

corresponding to $g_{\perp}$ =1.990 and $g_{\parallel}$ = 1.958, which agree well with the signals for Ti^{III} centers[154] and hence can be assigned to the electrons localized in the TiO_2 NP lattice. The remaining broad features ($g_{\perp}$ = 2.078, $g_{\parallel}$ = 2.397, and $A_{\parallel}$ = 120 G), are characteristic of a Cu^{II} ion in a tetragonally-distorted structure,[155] resulting from $[Cu^{II}(dppS)_2]^{2+}$ formed after the electron injection. The intensity of both Ti^{III} and Cu^{II} signals decreased after the lamp was turned off, indicating the recombination of injected electrons in the CB of TiO_2 with the oxidized $[Cu^{II}(dppS)_2]^{2+}$. The characteristic spectral features of charge separated state, although gradually faded, still remained visible several minutes after the Xe lamp was turned off, suggesting a super slow charge recombination at 5K. The results confirm the photoinduced ET from the ^{1,3}MLCT state of $[Cu^{I}(dppS)_2]^{+}$ to the CB of TiO_2 NPs and the subsequent recombination of the electron in the CB of TiO_2 with $[Cu^{II}(dppS)_2]^{2+}$ in dark.

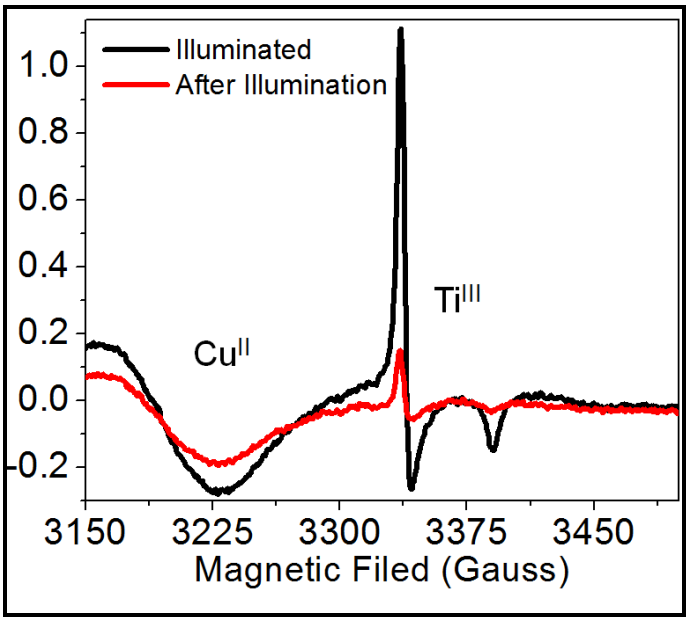

Figure 70. Electron paramagnetic resonance (EPR) spectrum of $[Cu^{I}(dppS)_2]^{+}/TiO_2$ hybrid at 5K.

Because the electron injection in presence of TiO_2 NPs is a new route for the ^{1,3}MLCT state of $[Cu^{I}(dppS)_2]^{+}$ injects the electron, the ^{1,3}MLCT state dynamics in the hybrid system were used to monitor the interfacial ET processes via the transient absorption (TA) under 415 nm excitation from a Ti:Sapphire laser system. Before

going further with TA experiment analysis, it is note worthy to observe the steady state absorption spectra of $[Cu^{I}(dppS)_2]^{+}/TiO_2$, $[Cu^{I}(dppS)_2]^{+}/Al_2O_3$, and $[Cu^{I}(dppS)_2]^{+}$ in water (Figure 71). We first measured TA spectra of a $[Cu^{I}(dppS)_2]^{+}/Al_2O_3$ hybrid as a reference for the MLCT state dynamics in the absence of the electron injection (Figure 73a). A broad positive feature in the entire spectral range is very similar with that of $[Cu^{I}(dppS)_2]^{+}$ in an aqueous solution (Figure 72), and hence can be assigned to the MLCT state absorption. At early delay times (<50 ps), the broad initial TA at 1 ps delay time grows in the 480–515 nm and 660–680 nm regions, respectively. The growth kinetics correlates well with the absorption decay in the 530–650 nm region bordered by the two isosbestic points at 518 and 657 nm, respectively, suggesting that the same dynamic process is associated with the spectral evolution in the three regions. The kinetic traces in the 480–515 and 660–680 nm regions (Figure 73c), fit by single-exponential rise and decay functions, both show a fast rise (13.7 ps) and a slow decay (>>3 ns) time constants, which correlate well with the two decay time constants of t_1=13.7 ps (25%) and t_2 >>3 ns (75%) in the 530–650 nm region fit by a bi-exponential decay function. The shorter time constant t_1=13.7 ps is consistent with the ISC time constant previously observed after the excited state flattening due to the Jahn-Teller distortion as the Cu centre changes from $3d^{10}$ to $3d^{9}$.[148, 149, 156]

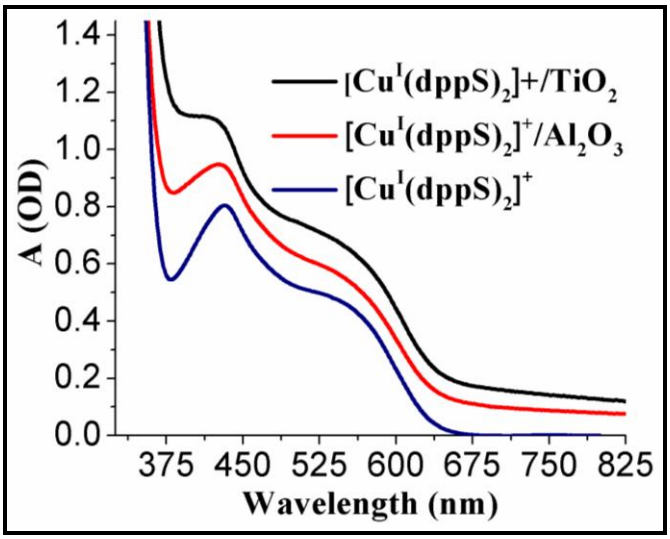

Figure 71. UV-vis Absorption spectra of $[Cu^{I}(dppS)_2]^{+}/TiO_2$, $[Cu^{I}(dppS)_2]^{+}/Al_2O_3$, and $[Cu^{I}(dppS)_2]^{+}$ in water.

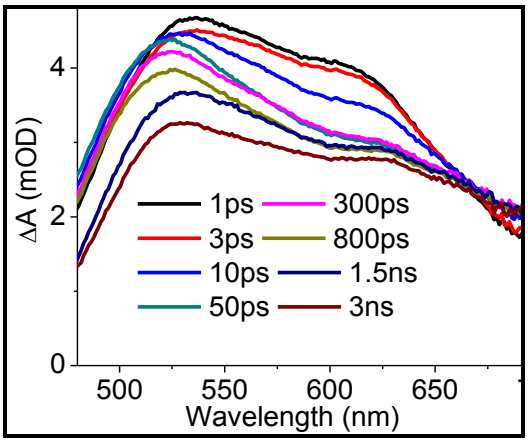

Figure 72. Femtosecond absorption spectra of $[Cu^{I}(dppS)_2]\cdot PF_6$ in H_2O.

The long decay time constant of >>3 ns is attributed to the ^{3}MLCT state decay, which is too long to be determined accurately in the femtosecond TA time window. It is noticeable that the kinetic trace in the 480–515 nm region after 50 ps decays slightly faster than that in 660–680 nm region. The origin of this difference is not clear. Nevertheless, the kinetics trace in longer time range measured subsequently by the nanosecond photolysis apparatus at three different probe wavelengths, 500nm, 570 nm and 700nm, respectively, agree well with each other (Figure 73e). Fitting the above kinetics by exponential decay functions yield a same decay time constant of 99.6 ns,which is consistent with the result from previous studies on $[Cu^{I}(dppS)_2]^+$ in solution.[157]

Compared to the reference TA spectra of $[Cu^{I}(dppS)_2]^+/Al_2O_3$ (Figure 73a), the TA spectra of $[Cu^{I}(dppS)_2]^+/TiO_2$ measured under the same conditions (Figure 73b) show a drastic change in spectral shape and much faster decay kinetics in the early time. A valley-like feature centred at 570 nm becomes more pronounced with the delay time *t* and results in a broad bleach band centred at 550 nm when $t > 1.5$ ns. This bleach feature, assigned as the ground state bleach, is sustained in the nanosecond TA spectra (inset of Figure 73f) and becomes more pronounced after the substantial decay of the MLCT state absorption signal from the MLCT state decays substantially due to the electron injection. All these facts suggest the ET from the excited $[Cu^{I}(dppS)_2]^+$ to TiO_2 NPs, which is consistent with the EPR measurement discussed earlier.

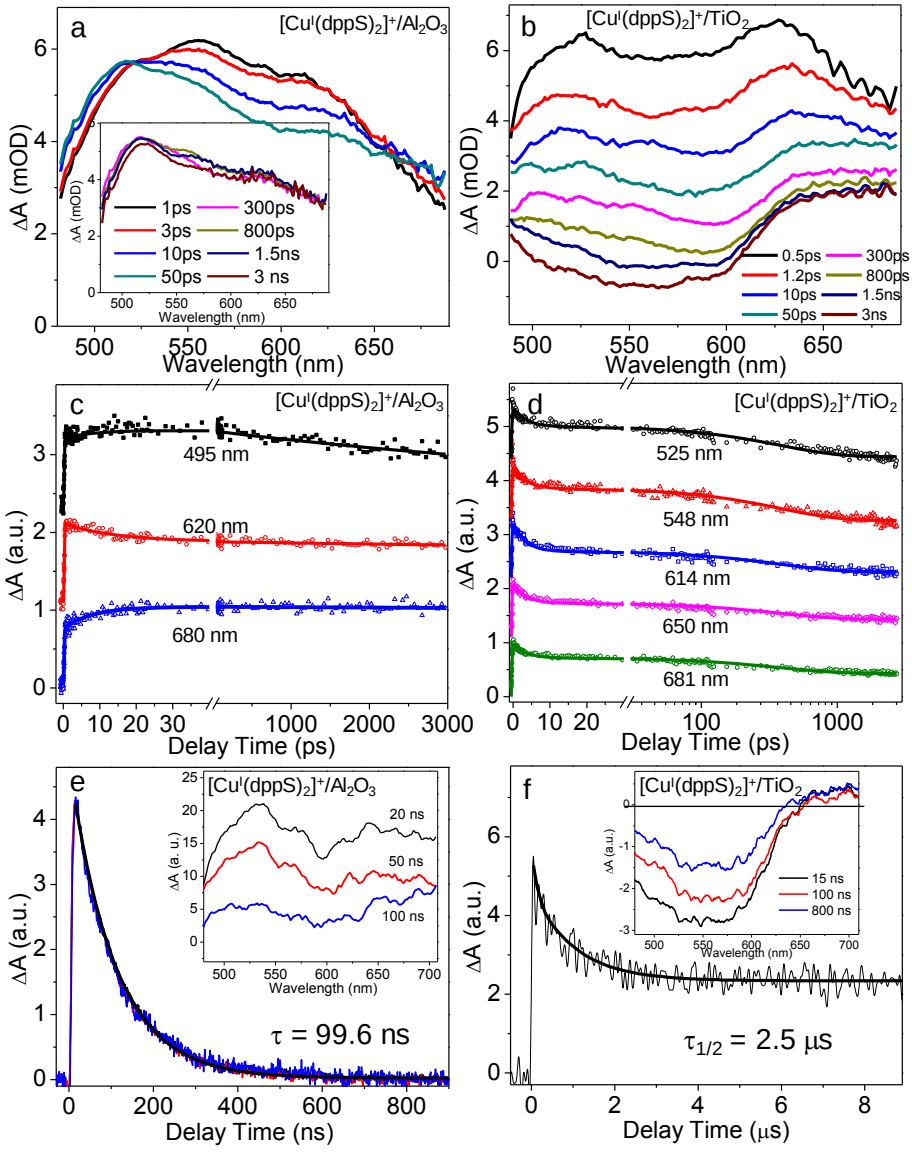

Figure 73. Femtosecond absorption spectra of $[Cu^{I}(dppS)_2]^+/Al_2O_3$ (a) and $[Cu^{I}(dppS)_2]^+/TiO_2$ hybrids (b). (c) Excited state decay kinetics of $[Cu^{I}(dppS)_2]^+/Al_2O_3$ at 495 nm (black filled square), 620 nm (red open dot), and 680 nm (blue open triangle). (d) The kinetic traces of $[Cu^{I}(dppS)_2]^+/TiO_2$ hybrids at probe wavelengths, 525, 548, 614, 650 and 681 nm. Nanosecond absorption kinetics of $[Cu^{I}(dppS)_2]^+/Al_2O_3$ at 500 nm (black), 570 nm (red), and 700 nm (blue) (e) and of $[Cu^{I}(dppS)_2]^+/TiO_2$ at 700 nm (f). Inset: nanosecond absorption spectra of $[Cu^{I}(dppS)_2]^+/Al_2O_3$ (e) and $[Cu^{I}(dppS)_2]\cdot PF_6/TiO_2$ (f). [Copyright © (2012) WILEY-VCH Verlag GmbH & Co. KGaA, Weinheim]

In principle, the ET and CR (charge recombination) rates can be measured by the TA signals of $[Cu^{II}(dppS)_2]^{2+}$, but such measurements prove to be difficult because of the

low extinction coefficient of $[Cu^{II}(dppS)_2]^{2+}$ absorption feature and its spectral overlap with those of the ground state bleach and excited state absorption. In order to circumvent this difficulty, the ET rate in this study was extracted quantitatively by global fitting the kinetics traces at different probe wavelengths. At probe wavelength λ, the TA singal (*S(λ, t)*) is given by the sum of the TA signals of the excited state absorption, the ground state bleach, and the oxidized state absorption of $[Cu^{I}(dppS)_2]^{+}$:

$$S(\lambda,t) = \varepsilon^1(\lambda)N^1(t) + \varepsilon^3(\lambda)N^3(t) - \varepsilon^0(\lambda)[N^1(t) + N^3(t) + N^+(t)] + \varepsilon^+(\lambda)N^+(t) \quad (1)$$

Where ($\varepsilon^1(\lambda)$, $N^1(t)$), ($\varepsilon^3(\lambda)$, $N^3(t)$), and ($\varepsilon^+(\lambda)$, $N^+(t)$) are the extinction coefficients and concentrations of singlet, triplet, and oxidized states of $[Cu^{I}(dppS)_2]^{+}$, respectively. Assuming that ET rate is much faster than ^{3}MLCT state intrinsic decay and charge recombination rate, we can use the following equations to express the concentrations of the above species:

$$N^1(t) = N_0 e^{-(k_{ET}^1 + k_{ISC})t}$$

$$N^3(t) = N_0 \frac{k_{ISC}}{k_{ET}^3 - k_{ISC} - k_{ET}^1}[e^{-(k_{ET}^1 + k_{ISC})t} - e^{-k_{ET}^3 t}]$$

$$N^+(t) = N_0[-\frac{k_{ET}^1}{k_{ET}^1 + k_{ISC}} e^{-(k_{ET}^1 + k_{ISC})t} - \frac{k_{ISC}}{k_{ET}^1 + k_{ISC}} e^{-k_{ET}^3 t}]$$

(2)Where k_{ET}^1 and k_{ET}^3 are rate constants for ET from singlet MLCT and triplet MLCT states, respectively. k_{ISC} is the intrinsic ISC rate constant determined by fitting the TA decay of the $[Cu^{I}(dppS)_2]^{+}$ MLCT excited state in the reference $[Cu^{I}(dppS)_2]^{+}/Al_2O_3$ hybrid. N^0 is the total excited state concentration at time 0. If multiple binding configurations exist, such as $[Cu^{I}(dppS)_2]^{+}$ binding with a single or double sulfonate linker(s), multiple sets of Equation (2) can appear in the TA signals fitting. According to this model, we can satisfactorily fit the kinetics at 525, 548, 614, 650, and 681 nm simultaneously by using the same rate constants while varying the extinction coefficients, as shown in Figure 73d. Restriction is given by the known extinction coefficients of ground state absorption at different wavelengths. The best fit values (listed in Table 4) for ET process are 0.4 ps (35%) and 10.1 ps (38%) for

ET from ^{1}MLCT state, and 1374 ps (27%) for ET from ^{3}MLCT. These results suggest an efficient ultrafast electron injection from ^{1}MLCT state to the TiO_2 NPs.

Table 4. Fitting Parameters for Excited State Kinetics of $[Cu^I(dppS)_2]\cdot PF_6$ in $[Cu^I(dppS)_2]\cdot PF_6/Al_2O_3$ and Charge Transfer and Recombination Kinetics of the $[Cu^I(dppS)_2]\cdot PF_6/TiO_2$ Hybrid.

	Laser	λ (nm)	τ_1 ps (A_1,%)	τ_2, ps (A_2,%)	τ_3, ps(A_3,%)
	fs	495	13.7± 0.5 (100)[r]	>> 3 ns	
	fs	620	13.7± 0.5 (25)	>> 3 ns (75)	
$[Cu^I(dppS)_2]\cdot PF_6/Al_2O_3$	fs	680	13.7± 0.5 (100)[r]	>> 3 ns	
	ns	500-700			99.6 ± 5.3 ns (100)
	fs	525-681	0.40 ± 0.02 (35)[S]	10.1 ± 0.4 (38)[S]	1374 ± 8 (27)[T]
$[Cu^I(dppS)_2]\cdot PF_6/TiO_2$	ns	700	0.27 ± 0.01 μs (44)	1.2 ± 0.1 □s (19)	>> 10 μs (37)

[r]The rising component in a multiple exponential fitting.
[S]The time constant for ET from singlet MLCT state.
[T]The time constant for ET from triplet MLCT state.

The CR dynamics of the $[Cu^I(dppS)_2]^+/TiO_2$ hybrid was also measured by the nanosecond TA setup. In the absence of the electron injection to TiO_2 NPs, the TA spectra of $[Cu^I(dppS)_2]^+/Al_2O_3$ (Figure 73e inset) are mostly due to the ^{3}MLCT state absorption. In contrast, the TA spectra of $[Cu^I(dppS)_2]^+/TiO_2$ (inset of Figure 73f) show a broad ground state bleach feature in the 480–620 nm region and an absorption at >620 nm, mainly due to the absorption features from both $[Cu^{II}(dppS)_2]^{2+}$ and CB electrons of the TiO_2 NPs as seen in the ground state $[Cu^{II}(dppS)_2]^{2+}$ (Figure 74) and other DSSC mimics, respectively.[158] Therefore, these absorption features can be used to monitor the CR process, i.e., back ET from CB of the TiO_2 NPs to $[Cu^{II}(dppS)_2]^{2+}$ which will cause the decay of these signals as shown in Figure 73f. The decay kinetics can be adequately fit by a three-exponential function with time consts of 270 ns (44%), 1.2 μs (19%), and >> 9 μs (37%),

corresponding to kinetics of the CR process that are several orders of magnitude slower than the ET process, suggesting efficient charge separation processes in this hybrid system.

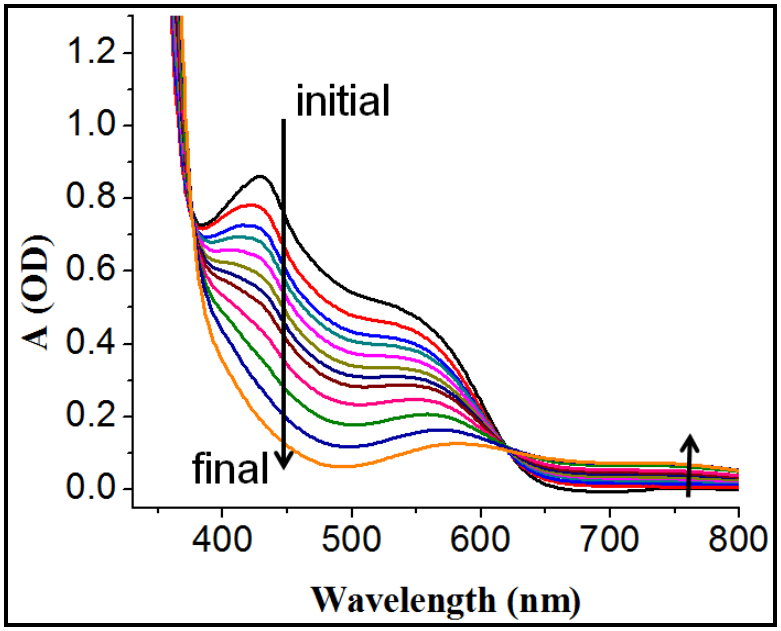

Figure 74. Absorption spectra of electrochemically (0.8V vs Ag/AgCl) generated $[Cu^{II}(dppS)_2]^{2+}$ in water.

The ET process in $[Cu^{I}(dppS)_2]^{+}/TiO_2$ can also be monitored by probing the oxidation state of Cu center using XTA at the Cu K-edge with and without the laser excitation (details described in experimental section). Figure 75 shows XANES (X-ray absorption near edge structure) spectra of $[Cu^{I}(dppS)_2]^{+}/TiO_2$ with the laser off and on, as well as the oxidized state after the electron injection to TiO_2 NPs. The oxidized state spectrum was obtained by subtracting the contribution of ~75% of the remaining ground state from the laser-on spectrum. The laser-on spectrum was taken at 9-ns delay time well after the electron injection, when only a negligible fraction (<<0.1%) of the MLCT state population remained according to the TA results. Therefore, the contribution of excited state to the XANES spectral changes caused by the laser pump pulse can be excluded. Three distinct changes are observed in the laser-on XANES spectrum compared to the laser-off spectrum: (i) a reduced shoulder feature at 8.979 keV, (ii) a reduced intensity at 8.987 keV, and (iii) an increase of the

intensity at 8.998 keV. These features are seen when $[Cu^{II}(dppS)_2]^{2+}$ is generated electrochemically or photochemically[149,151,159,160] and hence further confirm the ET to the TiO_2 NPs, consistent with the EPR and TA results. Compared to previously studied $[Cu^{I}(dmp)_2]^{+}$,[161,162] the shoulder feature in the XANES spectra of $[Cu^{I}(dppS)_2]^{+}$ at 8.979 keV, assigned as the 1s to $4p_z$ transition, has a higher intensity due to a flattened tetrahedral coordination geometry for the copper center in the ground state (Figure 75 inset),[161] where the spin-orbit coupling is significantly weakened and hence results in a much slower ISC process with a time constant of 13.7 ps, over a factor of 200 slower than the ISC process in the well-studied ruthenium based dye sensitizers.[162,163] Therefore, we have shown here a new example that the coordination symmetry of $[Cu^{I}(dppS)_2]^{+}$ effectively modulates its excited state properties, facilitating a direct electron injection pathway from the ^{1}MLCT state of $[Cu^{I}(dppS)_2]^{+}$ to TiO_2 NPs before its ISC generates the low energy ^{3}MLCT state. Without the steric hindrance of the two phenyl groups in the 2 and 9 positions of phenanthroline ligands, the two dppS ligands in the complex will be nearly orthogonal to each other resulting in a stronger spin-orbit coupling and hence much faster sub-ps ISC process.[151]

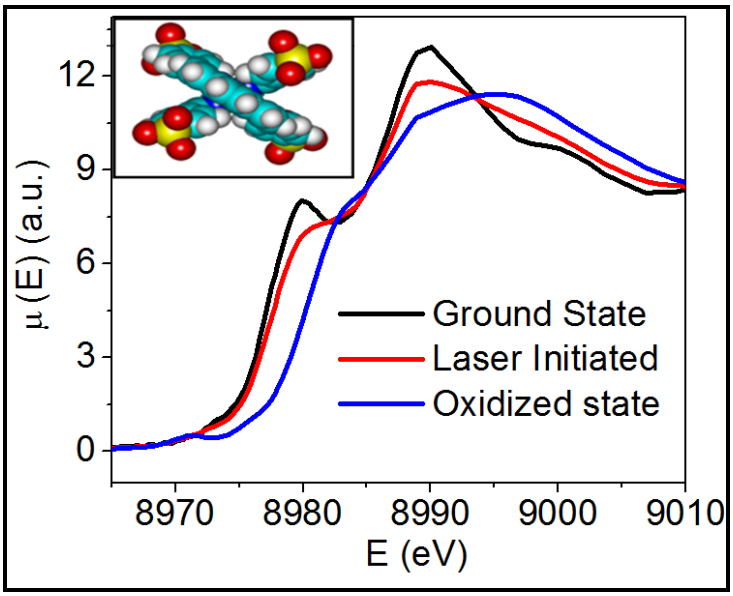

Figure 75. The XANES spectra of $[Cu^{I}(dppS)_2]^{+}$ in the $[Cu^{I}(dppS)_2]^{+}/TiO_2$ hybrid at the Cu K edge.

6.4. Experimental Details

6.4.1. General Methods

General . Starting materials and reagents were purchased from Aldrich or Fisher and used as received. 2,9-Diphenyl-1,10-phenanthroline was prepared following a procedure reported in the literature.[S1] All reactions were performed under an argon or nitrogen atmosphere and in dry solvents unless otherwise noted. Dry solvents were also purged with argon gas before using them. Analytical thin-layer chromatography (TLC) was performed on aluminum sheets, pre-coated with silica gel 60-F_{254} (Merck 5554). Flash chromatography was carried out using silica gel 60 (Silicycle) as the stationary phase. ^{1}H and ^{13}C NMR spectra were recorded on a Bruker Avance 500 MHz spectrometer at ambient temperature. Chemical shifts are reported in ppm relative to the signals corresponding to the residual non-deuterated solvents (D_2O: δ 4.79 ppm, CD_3OD: δ 3.31 ppm). High resolution electrospray ionization (HR ESI) mass spectra were measured on an Micromass Q-TOF Ultima mass spectrometer.

Electrochemical Measurement and Spectroelectrochemistry. Electrochemical measurements were performed using a CH Instruments Model 622 electrochemical workstation. All measurements were performed under an N_2 atmosphere in millipore H_2O containing 0.1 M KCl supporting electrolyte. Cyclic voltammetry measurements were performed using a 1.0 mm diameter glass carbon electrode, platinum wire counter electrode, and Ag/AgCl reference electrode. Spectroelectrochemistry was performed using a platinum mesh working electrode, a platinum wire counter electrode, and Ag/AgCl reference electrode in a 2-mm cell. The potential for bulk electrolysis is at +800 mV vs Ag/AgCl reference electrode.

Steady State UV-Vis Absorption and Emission Spectroscopy. Steady-state absorption spectra were obtained at room temperature on a Shimadzu UV-1601 spectrometer. For the suspension samples, the absorption spectra were collected on a Perkin Elmer Lamda 950 UV-VIS-NIR spectrometer equipped with a labsphere 150mm integrated sphere detector. During the measurement, 2mm curvette was

mounted at the entrance slit of the integrate sphere. Steady state luminescence spectra were collected on a PTI Instruments spectrofluorimeter equipped with a 75 W Xe arc lamp/monochromator excitation source, a R-928 PMT, and single photon counting electronics. This fluorimeter operates under the control of FeliX32 software from PTI.

The Excited State Oxidation Potential. Following standard practice, we have estimated the excitation energy of $[Cu^{I}(dppS)_2]\cdot PF_6$ to be 2.07 eV from the intersection of the emission and absorption spectra at 608 nm (Fig S3b). Combining this value with the ground-state oxidation potential of 0.50 V vs SCE (Fig. S3a), the excited-state oxidation potential of $[Cu^{I}(dppS)_2]\cdot PF_6$ was determined to be –1.57 V vs SCE.

Electron Paramagnetic Resonance (EPR) Measurement. The X-band (9.34 GHz) EPR measurements were carried out with a CW Bruker Elexsys E580 spectrometer (Bruker Biospin Corp.). A standard rectangular cavity was employed. The samples were transferred from liquid nitrogen to a pre-cooled microwave cavity at 5 K. The temperature was controlled with an Air Products temperature control system. The light-induced X-band EPR spectra were recorded at 5 K under continuous illumination with a 300 W Xe lamp (ILC). A 440 nm cutoff filter was used to remove photons from the UV spectral region, and a water filter (15 cm length) was used to remove the IR contribution. The samples were placed in 4 mm o.d. EPR tubes and then put in a N_2 box. The ~100 μL samples were bubbled briefly with Argon gas, followed by blowing of Argon gas over the top of the sample in the tube for 30 min. The EPR tubes were then septa capped. An initial EPR spectrum under room light was taken for each sample.

6.4.2. Synthesis

dppS Ligand:

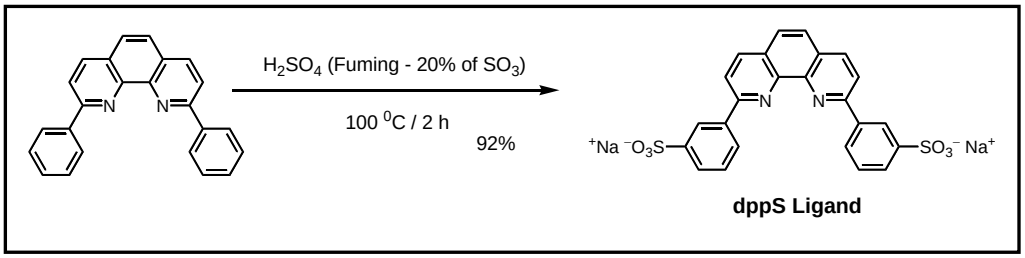

2,9-Diphenyl-1,10-phenanthroline (2.5 g, 7.52 mmol) was added to 25 mL of sulfuric acid (20% of SO_3) solution in 100 mL three-necked flask. The formed acid vapor was removed with a flow of argon. The mixture was heated up to 100 ^{0}C and stirred for 2 h. During the reaction, the color of the reaction mixture turned brown. Then, the temperature of solution was cooled to 0 ^{0}C and an aqueous solution of NaOH (20%) was added dropwise until the pH is basic. H_2O was removed under reduced pressure and the remaining solid was extracted four times with hot EtOH (4 x 50 mL). The solvent was evaporated under reduced pressure and the solid was dissolved in water (50 mL) and activated carbon (10 g) was added. The resulting mixture was stirred for 1 h at 80 ^{0}C. The filtration was performed using column chromatography [Abmerlite IR 120 (hydrogen form)]. After the column chromatography, the fractions were combined, the pH was adjusted to 9 and evaporated under reduced pressure to afford the corresponding dppS ligand which was re-precipitated (MeOH/H_2O) as a yellow pale solid (3.63g, 92%). The final product was isolated as a mixture of isomers — namely, meta-meta (m-m*), meta-para (m-p) and para-para (p-p*). The m-m* isomer was found to be the major one based on the ^{1}H NMR integrations. The *isomer* distribution in the sulfonation reaction is m-m* isomer (70%), m-p isomer (30%) and negligible amount of the p-p*. *m-m* Isomer*: ^{1}H NMR (500 MHz, D_2O) δ = 7.99 (s, 2H), 7.95 (d, *J* = 7.8 Hz, 2H), 7.71 (d, *J* = 7.8 Hz, 2H), 7.65 (d, *J* = 8.3 Hz, 2H), 7.39 (d, *J* = 8.3 Hz, 2H), 7.31 (t, *J* = 7.7 Hz, 2H), 7.20 (s, 2H). ^{13}C NMR (125 MHz, D_2O) δ = 153.6, 143.1, 142.6, 137.9, 137.7, 130.1, 129.5, 127.6, 126.3, 126.2, 123.8, 119.9. *m-p Isomer*: ^{1}H NMR (500 MHz, D_2O) δ = 7.97 (s, 1H), 7.88 (d, *J* = 7.7 Hz, 1H), 7.75 (d, *J* = 8.3 Hz, 2H), 7.69 (d, *J* = 7.9 Hz, 1H), 7.64 – 7.61 (m, 3H), 7.58 (d, *J* = 8.3 Hz, 1H), 7.39 (d, *J* = 8.4 Hz, 1H), 7.34 (d, *J* = 8.3 Hz, 1H), 7.22 (t, *J* = 7.9 Hz,

1H), 7.14 (d, *J* = 1.5 Hz, 2H). Mixture of Isomers: ^{13}C NMR (125 MHz, D_2O) δ = 153.6, 153.5, 153.4, 143.1, 143.0, 142.6, 142.6, 142.5, 140.1, 137.9, 137.8, 137.7, 137.6, 130.1, 130.0, 129.5, 129.4, 127.7, 127.6, 127.5, 127.4, 126.3, 126.2, 126.1, 126.0, 125.7, 125.6, 123.8, 123.7, 120.4, 119.9, 119.7. ESI-HRMS calcd for *m/z* = 513.0196 [*M* – Na]$^-$, found *m/z* = 513.0193.

$[Cu^{I}(dppS)_2]\cdot PF_6$:

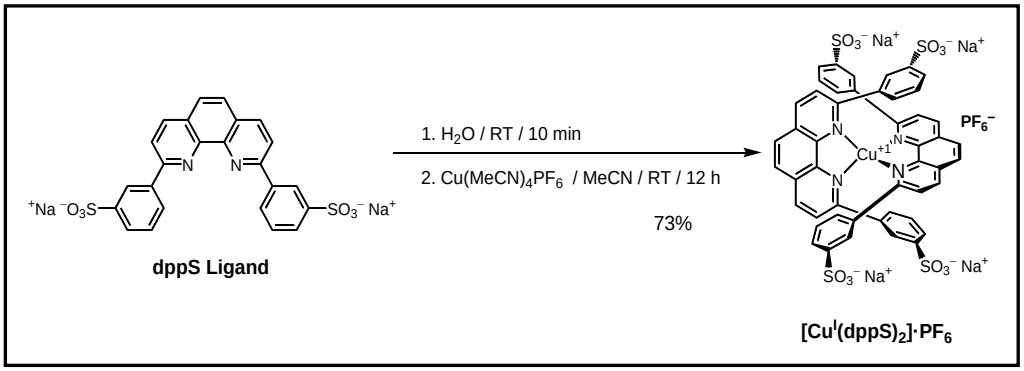

The dppS ligand (107 mg, 0.20 mmol) was dissolved in degassed H_2O (10 mL) and stirred for 10 min under N_2 atmosphere. $[Cu(MeCN)_4]PF_6$ (37.3 mg, 0.10 mmol) was dissolved in degassed MeCN (5 mL) and stirred under N_2 until a clear solution was observed. Using a cannula transfer technique, $Cu(MeCN)_4]PF_6$ solution was transferred under N_2 at room temperature to a stirred solution of dppS ligand in H_2O. Upon addition of copper(I), the color of reaction mixture turned dark red, indicating the formation of the $[Cu^{I}(dppS)_2]\cdot PF_6$ complex. The reaction mixture was stirred for additional 12 h at room temperature under N_2 atmosphere and then concentrated under reduced pressure. The remaining dark red solid was dissolved in a minimum amount of MeOH and filtered. The filtrate was evaporated under reduced pressure to yield $[Cu^{I}(dppS)_2]\cdot PF_6$ complex (94 mg, 73%) as a dark red solid. . *The ^{1}H NMR is listed for the major m-m* / m-m* isomer:* ^{1}H NMR (500 MHz, CD_3OD) δ = 8.47 (d, *J* = 8.2 Hz, 4H), 7.99 (s, 4H), 7.97 (s, 4H), 7.82 (d, *J* = 10.3 Hz, 4H), 7.55 (d, *J* = 7.0 Hz, 4H), 7.14 (d, *J* = 7.5 Hz, 4H), 6.31 (br s, 4H). Mixture of isomers: ^{13}C NMR (125 MHz, CD_3OD) δ = 156.93, 156.88, 156.84, 156.80, 156.77, 156.71, 156.67, 156.64, 145.33, 145.27, 144.92, 140.76, 140.65, 140.55, 139.69, 139.64, 139.49, 139.44, 139.33, 139.26, 139.18, 139.09, 131.02, 130.91, 130.89, 130.76, 130.30, 130.28, 130.24, 129.35, 129.30, 129.27, 128.24, 128.16, 128.05, 127.96, 127.93,

127.87, 127.83, 127.32, 127.22, 126.95, 126.08, 126.05, 125.95, 125.87, 125.81, 125.79. ESI-HRMS calcd for *m/z* = 1134.9468 $[M - PF_6]^+$, found *m/z* = 1134.9486.

$[Cu^I(dppS)_2]\cdot PF_6/Al_2O_3$ and $[Cu^I(dppS)_2]\cdot PF_6/TiO_2$ Hybrids: Al_2O_3 (5 nm in diameter) and TiO_2 (5-10 nm diameter) nanoparticles (NPs) were purchased from Skyspring Nanomaterials, Inc.. To remove the small amount of large NPs (diameter > 10 nm), NPs were dispersed in millipore H_2O and were left untouched for 30 mins. The NPs in the suspension were collected and dried in air for future use. A $[Cu^I(dppS)_2]\cdot PF_6$ sensitized NP suspension was prepared by mixing NPs with $[Cu^I(dppS)_2]\cdot PF_6$ in aqueous solution. Briefly, NPs were gradually added to a 1 mM $[Cu^I(dppS)_2]\cdot PF_6$ aqueous solution (30 mL) with stirring. The pH value of the suspension was adjusted to 4.5. The suspension was left to stand until the NPs adsorbed with or without $[Cu^I(dppS)_2]\cdot PF_6$ settled to the bottom of the container, leaving the unattached $[Cu^I(dppS)_2]\cdot PF_6$ in the top liquid layer. This procedure was repeated several times until the top layer was colorless, indicating that all $[Cu^I(dppS)_2]\cdot PF_6$ in the solution was attached to NPs.

6.5. Conclusion

In summary, a highly efficient and ultrafast interfacial electron injection from the ^{1}MLCT state of surface bound $[Cu^I(dppS)_2]^+$ to TiO_2 NPs has been observed in EPR and XTA studies with the charge separation and recombination dynamics correlated with the ground and excited state structures. The studies confirmed the formation of $[Cu^{II}(dppS)_2]^{2+}$, resulting from an efficient charge transfer process in $[Cu^I(dppS)_2]^+/TiO_2$ where electrons are injected into TiO_2 NPs. The flattened tetrahedral geometry of the ground state $[Cu^I(dppS)_2]^+$ in the hybrid system as detected by the XTA effectively prolongs the ISC time to enable ET from the ^{1}MLCT state. Further studies in tuning the HOMO-LUMO levels of these complexes by structural constraints will be conducted in the future. This research not only demonstrates the structural control necessary for effective ET processes, but also shows the potential of using low cost copper complexes for the dye sensitized solar cells in the future.

CHAPTER 7

7. Autonomous Shuttling in a Cucurbit[7]uril-Bodipy Pseudorotaxane

This work is partially described in the following publication:

Buyukcakir, O.; Yasar, F.T.; Bozdemir, O.A.; Icli, B.; Akkaya, E.U. *Org. Lett*. **2013**, *15*, 1012-1015.

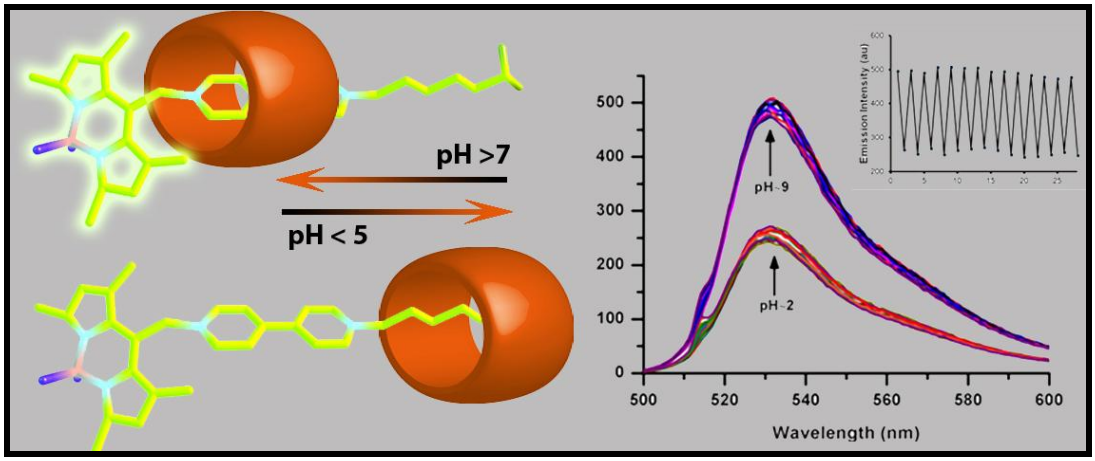

7.1. Objective

In this study, we present a bipyridinium dication substituted boradiazaindacene (BODIPY) with a terminal carboxylic acid function provides two alternative stations for cucurbit[7]uril. Changing pH from basic to acidic results in shuttling of the cucurbituril from one station to the other. In addition, this shuttling is accompanied by a change in the emissive properties of the BODIPY dye, which is only observed in the presence of cucurbituril. This system yields a clear demonstration of shuttling in aqueous solution as a result of the protonation/deprotonation equilibrium of the carboxylic acid group incorporated into the pseudorotaxane structure. More striking, is a demonstration of autonomous switching in an oscillating pH system. it is also worthy to say this work is the first demonstration truly an autonomous system in molecular switch/machine systems.

7.2. Introduction

Interlocked molecules with multiple metastable states are of great interest becauser of their potential applications in molecular device manufacturing.[164] Switching between these metastable states can be achieved via acid-base chemistry,[165] electrochemical[166] and/or photochemical[167] means. Such switchable systems are referred to as molecular machines,[168] and recent years witnessed a remarkable progress and increasing elegance in their design. There are also studies where some autonomous characters are built-in to these systems.[169] The basic requirement for molecular machines is simple, a relatively rigid “axle”, and a mobile “wheel” unit which can be stationed at two or more different locations along the axle, through non-covalent interactions.

The very well documented process of shuttling in these systems almost always requires some sort of an external stimulus. We were motivated to offer an alternative and potentially autonomous mechanism by coupling the shuttling process to an oscillating chemical reaction. Oscillating reactions[170] represent an interesting class of dynamic self-assembly. The archetypical Belousov-

Zhabotinski reaction[171] behave very well in closed systems, with large number of identifiable concentration peaks and troughs before the oscillations dampen. Unfortunately, we could not make use of Ce(III)-Ce(IV) couple. Metallo-catenanes/rotaxanes looked promising, but there has to be a match between the oscillation frequency and the switching rate between the two states.[172] In most cases, switching back to the original states is much slower than what seemed appropriate. We then focused on aqueous systems and thus pH oscillations.[173] We envisioned a situation where pH of a solution would be altered in a cyclic manner, switching the rotaxane between two metastable states. Thus, as long as the oscillation is sustained, the molecular machine would switch autonomously between these states.

There are only a few systems where pH oscillates in a controlled manner. Thiosulfate-sulfite-iodate is one of them, which displays high amplitude but irregular oscillations in batch systems.[174] In continuously stirred tank reactor (CSTR), oscillations are well behaved and essentially permanent, provided a steady supply of reactants and constant rate of removal for the products. Nevertheless, the batch system offered solid potential for a proof of principle study.

7.3. Result and Discussion

To demonstrate the proof of principle operation of such an autonomous system, it was set out to synthesize our target molecule shown in Figure 76. The wheel component is Cucurbit[7]uril (CB7). Cucurbiturils are an interesting class of molecules with excellent host properties.[175] There are exciting examples of molecular switches and machines built using these host species.[176] CB7 seems more relevant with regards to molecular machine design, since they can form very stable complexes with a number of aromatic amines and quaternized pyridinium and viologen species.[177]

The axle component of the pseudorotaxane system is a Bodipy derivative (Figure 76). Bodipy is a remarkable fluorophore with an amazing degree of versatility.[89]

Previous work established by Akkaya group with the bipyridyl derivatives of BODIPY has shown[178] that when complexed to Zn(II), bipyridyl LUMO energy level changes, allowing an oxidative or reverse PET (Photoinduced Electron Transfer) from the excited BODIPY unit, decreasing the intensity of emission. Later on, a systematic study of the relative frontier orbital energy levels of BODIPY and the *meso* substituents by Nagano[179] proved earlier suggestion of Akkaya and et.al.

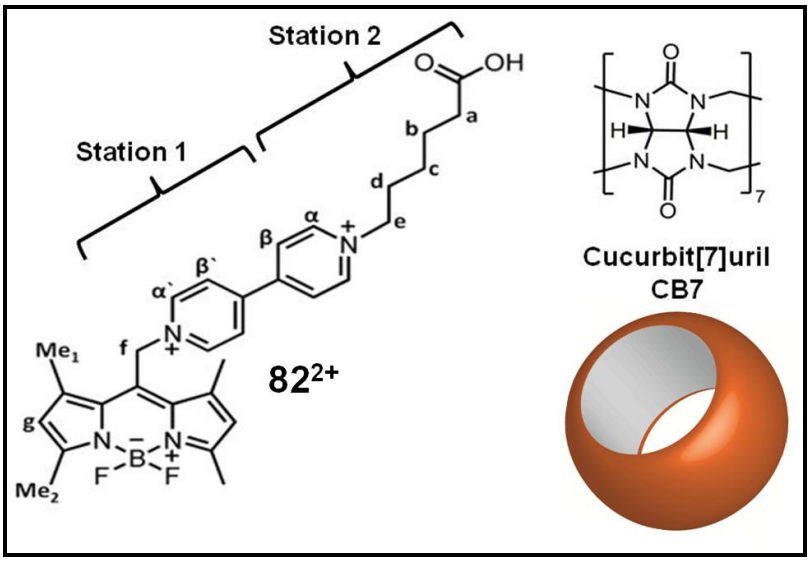

Figure 76. Structure of the fluorogenic "axle unit" with two potential stations for CB7.

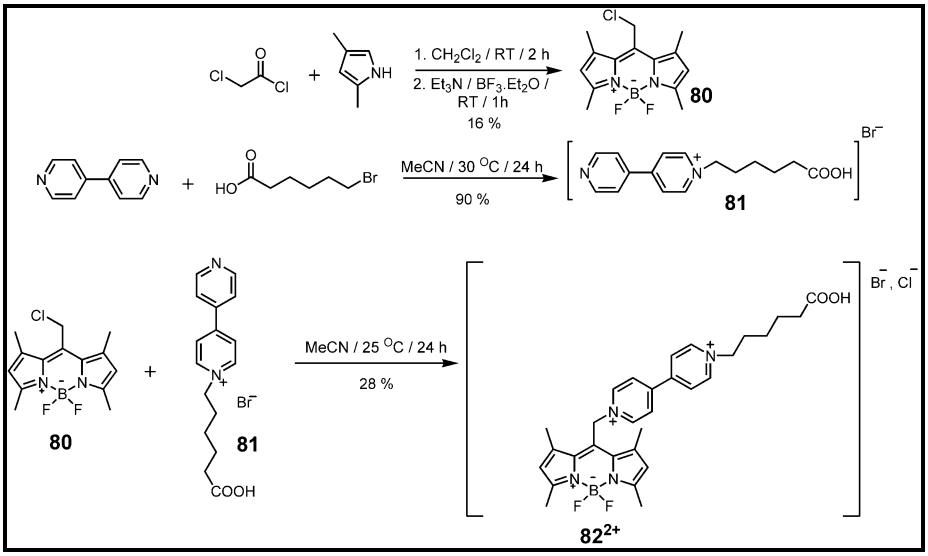

Figure 77. Total reaction scheme

Thus, we expect that any interaction reducing the charge density on pyridinium moiety would increase the emission intensity as a result of decreased reverse (oxidative) PET. The rest of our design was built on the results obtained by Kaifer.[180] Carboxylic acid functionality linked to a bipyridinium dication moiety with pentamethylene spacers were shown to offer two binding sites for CB7. It was shown by NMR studies that at neutral pH, CB7 prefers bipyridinium dication station, whereas under acidic conditions (when carboxylate group is protonated) carboxylic terminus becomes the preferred station. With these considerations in this design, a carboxypentyl group was incorporated as the second station. The BODIPY unit is the fluorescent reporter of the position of the wheel on the molecular axle, it is also a stopper, so at least from one end, CB7-**82**$^{2+}$ complex is stoppered.

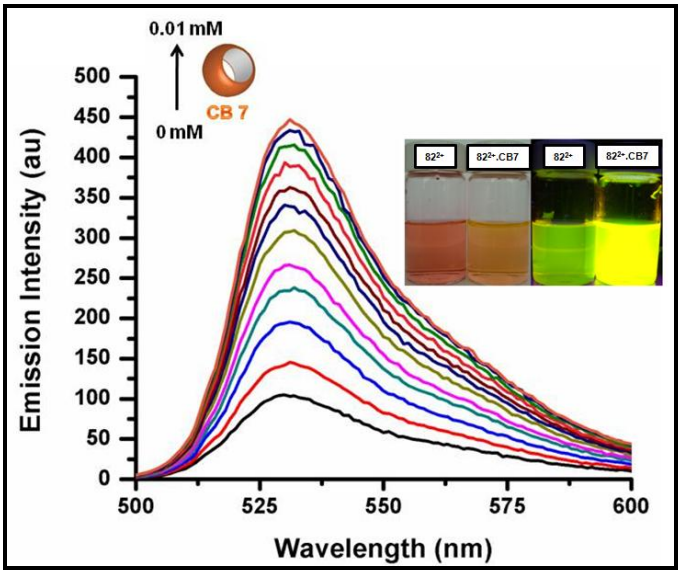

Figure 78. Emission spectra of compound **82**$^{2+}$ (0.01 mM, in 0.1M NaCl 2% MeCN in D_2O) in the presence of increasing CB7 concentrations (0, 0.1, 0.2, 0.3, 0.4, 0.5 0.6, 0.7, 0.8, 0.9, 1.0, 1.1 x 10^{-5}M). The inset show the appereance of solutions under ambient light (left) and under a hand-held 360 nm UV lamp (right).

The synthesis was accomplished starting from 8-chloromethyl-bodipy derivative and the preparation details of all the new compounds are seen Figure 77 and described in Experimental Details section. The target Bodipy derivative has a reduced quantum yield as expected, reverse PET process competes effectively with the radiative

deexcitation. The emission spectra of **82**$^{2+}$ in the presence of increasing concentrations of CB7 are highly instructive (Figure 78). In the presence of CB7 at 10 µM (1.0 eq.), there is more than a fourfold increase in the emission intensity.

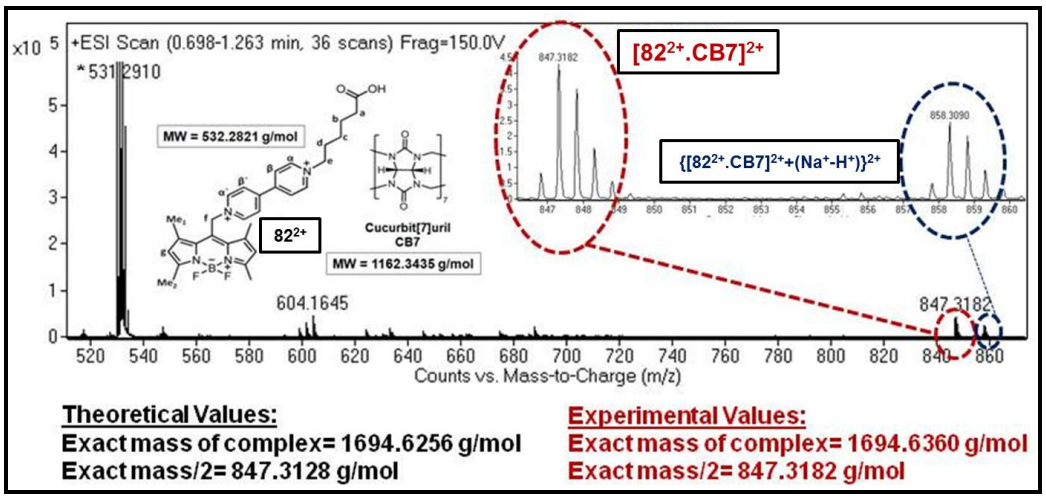

Figure 79. MASS spectrum of complex **82**$^{2+}$·CB7

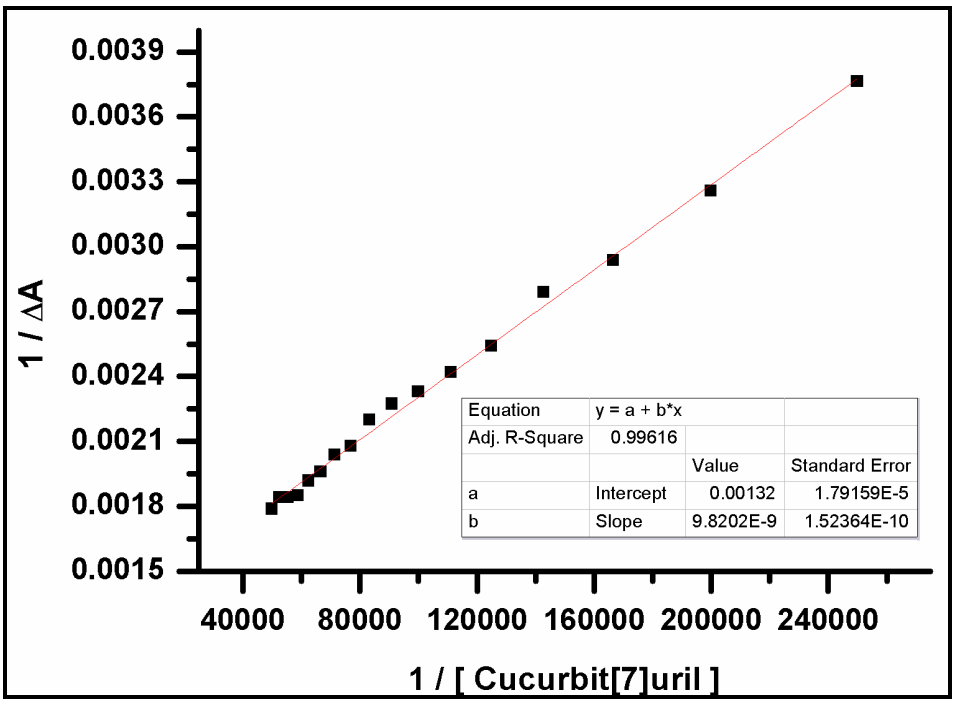

Figure 80. Benesi-Hildebrand analysis of compound **82**$^{2+}$ at different CB7 concentrations.

Equation: $y = a + bx$, $K = a/b = 1.34 \times 10^5\ M^{-1}$

The formation of inclusion complex between viologen dication and CB7 is also monitored by using mass spectrometry which clearly shows the complexation (Figure 79). The complexation affinity was analyzed by the Benesi-Hildebrand treatment of the titration curve of **82**$^{2+}$ by CB7 (Figure 80), the host-guest binding constant was obtained (K = 1.34 x 10^5 M^{-1}) and the result was in agrrement in literature.

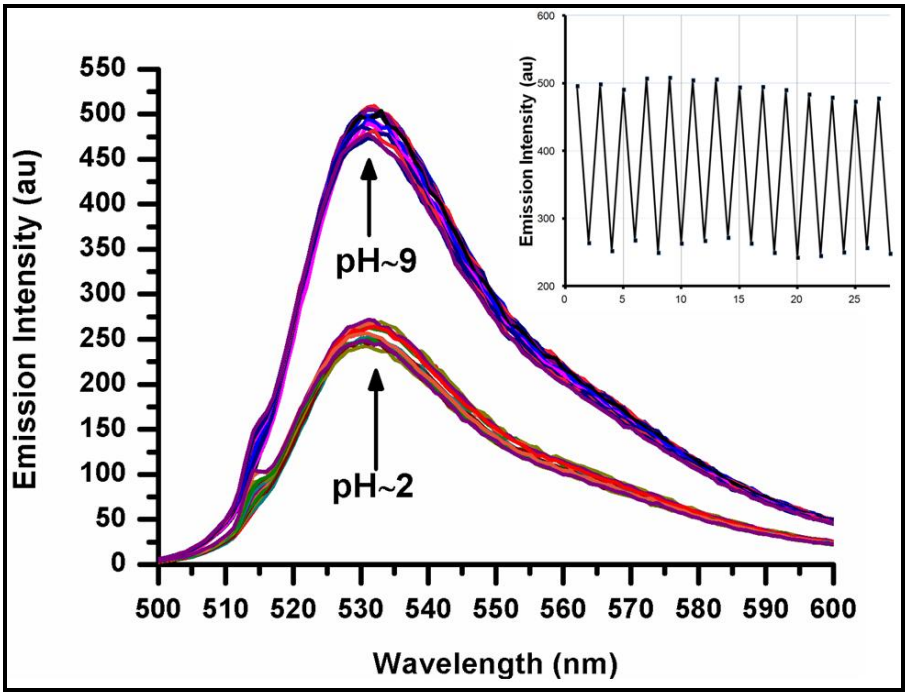

Figure 81. Emission spectra of solution compound **82**$^{2+}$ (0.01 mM, in 0.1M NaCl 2% MeCN in D_2O) in the presence of 1.0 eq. CB7 cycled between pH~2 and pH~9. The inset shows emission versus pH~2 to pH~9 cycle recorded at 531 nm.

Figure 81 shows the pH directed reversible oscillations in emission spectra with the inclusion complex of **82**$^{2+}$ and CB7 as monitored by switching pH between pH~2 and pH~9. As expected, the emission intensity is higher at neutral/alkaline pH, because when the CB7 moiety encapsulates bipyridinium dication (station 1), ion-dipole interactions partially neutralize the positive charge on the bipyridinium, slowing down reverse PET and allowing radiative transition to be the dominant mode of relaxation of the excited state. Thus, the spectra clearly show the switching of CB7 from one station to the other when pH is changed

from 9.0 to 2. It has to be pointed out that in the absence of CB7, emission spectrum of **82**$^{2+}$ in aqueous medium shows (Figure 82) essentially no dependence on pH in the range of interest (pH 2 to 9).

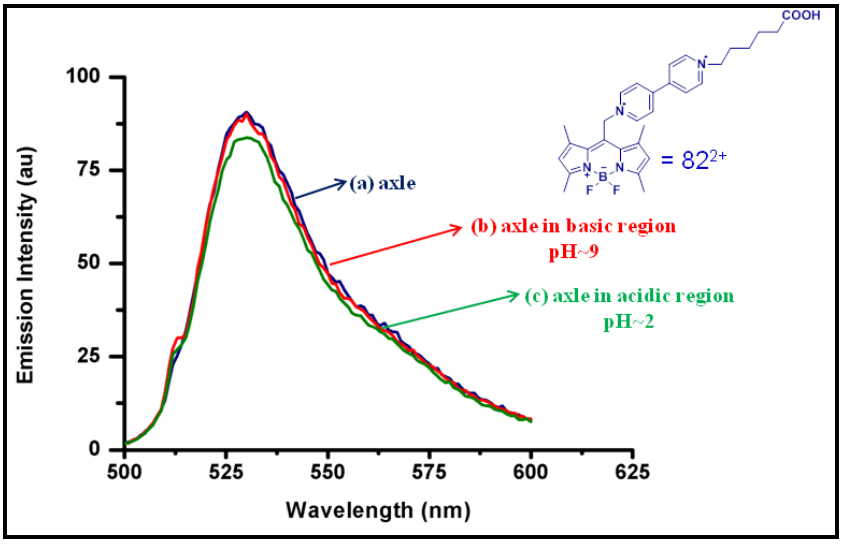

Figure 82. Emission spectra of (a) **82**$^{2+}$ (0.01 mM, in 0.1M NaCl 2% MeCN in D_2O) (b) in basic region (pH~9) (c) in acidic region (pH~2).

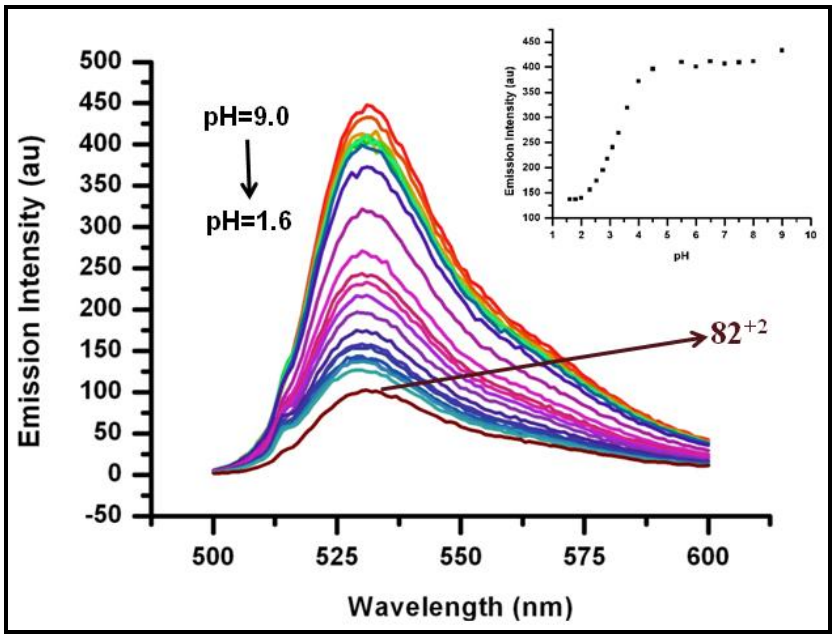

Figure 83. Emission spectra of compound **82**$^{2+}$ (0.01 mM, in 0.1M NaCl 2% MeCN in D_2O) in the presence of 1.0 eq. CB7 with decreasing pH (9.0, 8.0, 7.5, 7.0, 6.5, 6.0, 5.5, 4.5, 4.0, 3.6, 3.3, 3.1, 2.9, 2.7, 2.5, 2.3, 2.0, 1.8, 1.6). Inset shows emission of **82**$^{2+}$ complex as a function of pH recorded at 531nm.

To investigate the emission intensity variation as a function of pH (Figure 83), 1:1 complex (the pseudorotaxane) was titrated in the pH range 9 to 1.6. When the pK_a value of the carboxylic acid function is considered, the inflection point of the titration curve at pH 5 is in agreement with the literature data.[181] Interestingly, the emission intensity of the complex is still higher than $\mathbf{82}^{2+}$.

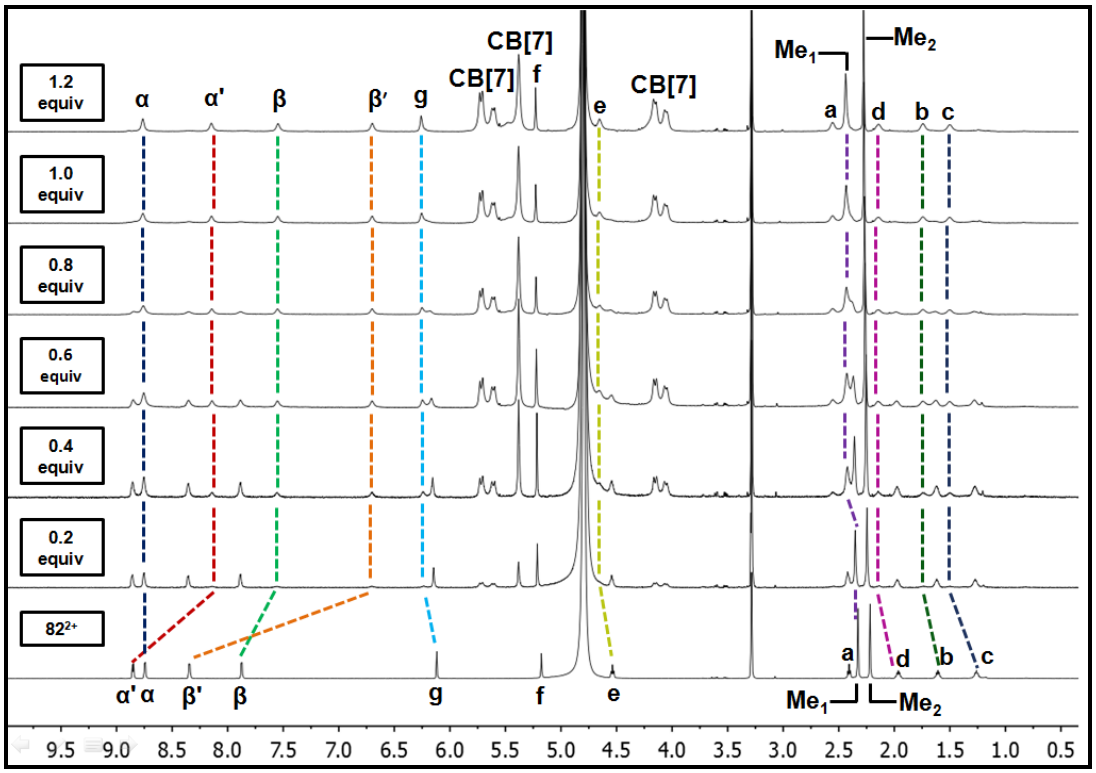

Figure 84. ^{1}H NMR spectra (400 MHz, 0.1 M NaCl in D_2O: CD_3OD; 70:30 at 25 ^oC) of $\mathbf{82}^{2+}$ (3.0 mM) in slightly basic media pH ~8 with increasing concentrations of CB7 (0-1.2 eq).

The interaction between $\mathbf{82}^{2+}$ and CB7 was also studied by ^{1}H-NMR spectroscopy. Figure 84 shows the titration experiment of $\mathbf{82}^{2+}$ (3 mM) with CB7 in 0.1 M NaCl / D_2O : CD_3OD (80 : 20) solution (pD~8). As previously reported by Kaifer and Kim[182,181] , the addition of 1.0 eq. CB7 resulted in an upfield shift of β and β' protons of viologen unit, by ~0.4 and ~1.6 ppm, respectively. Although the α proton, as expected, shows minor shift in the peak position (<0.1 ppm), the observed upfield shift for α' is 0.7 ppm. This reveals that in basic

media, the Bodipy side of the viologen guest is pushed more into the cavity of CB7 which explains the unexpected large upfield displacement of the α' protons and also the different upfield shifts of β and β' protons. These shifts were also clearly monitored by using 2D-COSY experiments of **82**$^{2+}$ in absence (Figure 85) and presence (Figure 86) of 1.2 equivalent CB7 in same conditions.

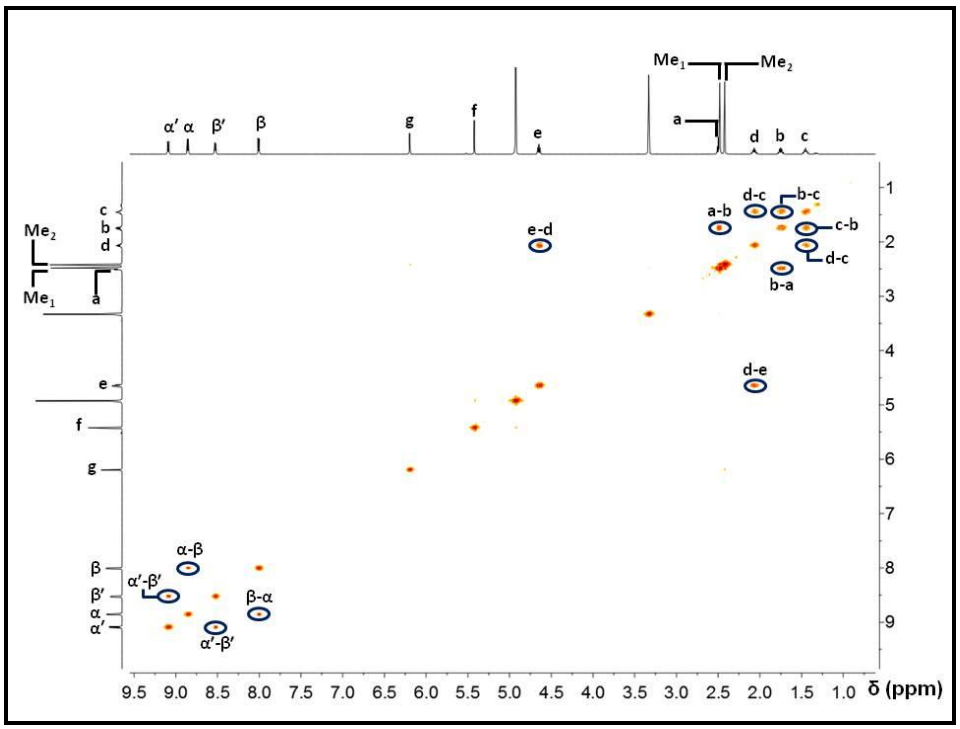

Figure 85. 2D-COSY NMR spectrum of **82**$^{2+}$ recorded at 298K in CD_3OD.

Because of this asymmetric arrangement within the pseudorotaxane, Me_1 and g protons interact with the carbonyl oxygens of CB7 portals and undergo a downfield shift. This interaction is also predominant in aliphatic region, especially e and d protons undergo a downfield shift. However, the more remote protons of the axle (a and b) are only slightly affected from the deshielding zone of the host and show a minor shift in peak positions. Furthermore, this asymmetrical intrusion of viologen unit of the axle gives rise to splitting of CB7 protons. The formation of inclusion complex between the guest (**82**$^{2+}$) and host (CB7) molecules was also confirmed by 2D-NOESY NMR spectroscopy. (Figure 87)

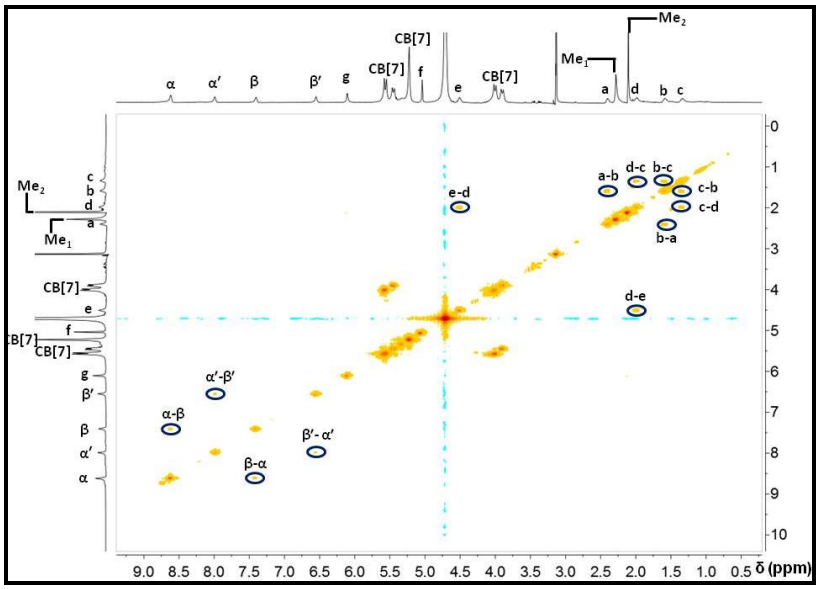

Figure 86. 2D COSY NMR spectrum of **82**$^{2+}$ in presence of 1.2 eq CB7 in basic media pH~8 recorded at 298K in CD_3OD : D_2O (30 : 70).

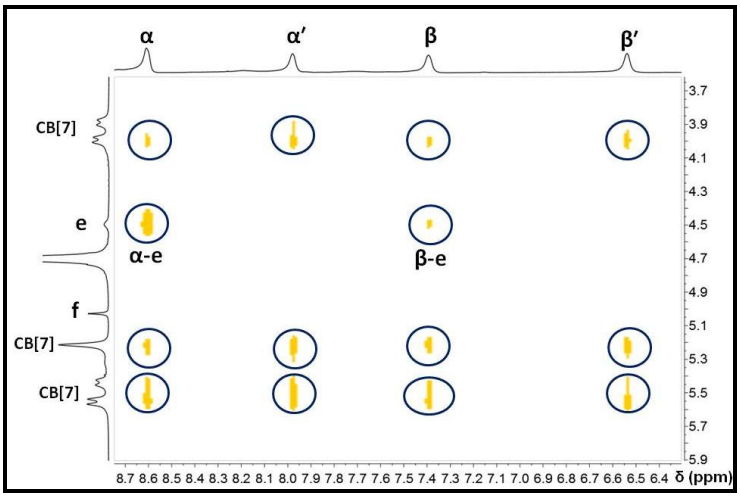

Figure 87. 2D NOESY NMR spectrum of **82**$^{2+}$ in presence of 1.2 eq CB7 in basic media pH~8 recorded at 298K in CD_3OD : D_2O (30 : 70).

In acidic media, concomitant to the reduction in emission intensity (suggesting a move away from the pyridinium cation immediately adjacent to the bodipy unit). 2D-NMR date shows revealing changes. Methylene hydrogens show off-diagonal (cross peaks) with CB7 protons, a feature which does not show up in neutral/basic medium. Thus, it is apparent that CB7 does not dissociate from the Bodipy axle, yet it moves in the predicted direction (Figure 88).

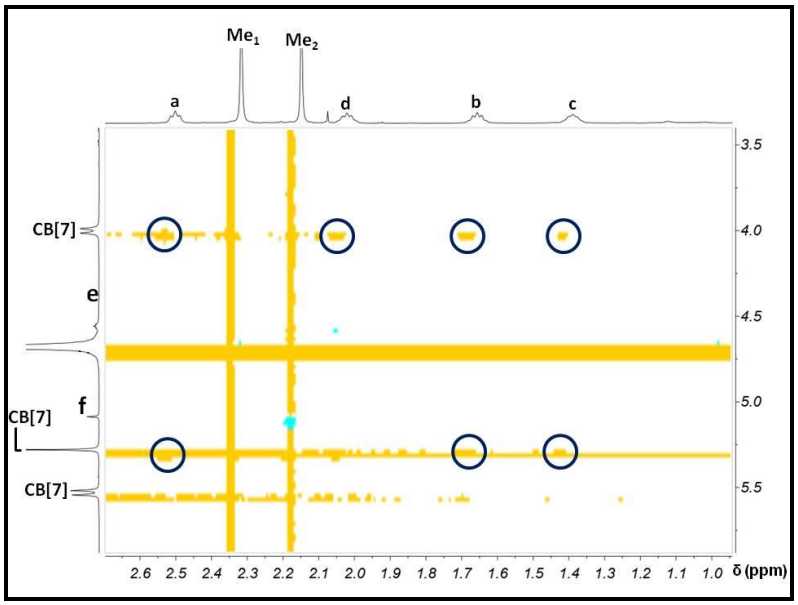

Figure 88. 2D NOESY NMR spectrum of **82**$^{2+}$ in presence of 1.4 eq CB7 in acidic media (pH~3) recorded at 298K in CD_3OD : D_2O (30 : 70).

Once we established pH-mediated shuttling in aqueous solutions, we designed an experiment to realize similar shuttling in solution, but this time autonomously. In closed-batch systems, pH oscillations for solutions containing thiosulfate (17.5 mM), sulphite (24.4 mM) and iodate (10mM) ions are well documented. The change in pH is erratic. We observed a small decrease in pH by 0.1 units, then a sharp drop of 3(unit) pH units to nearly pH 2.4, and then oscillations die out, pH reaching a constant value. To couple this oscillation to shuttling of the pseudorotaxane, we carried out following experiments: in a fresh solution of the reagents, we added CB7 (0.012 mM) and 0.01 mM **82**$^{2+}$. Oscillations were started by the addition of H_2SO_4 (5.5 mM). The switching was followed simultaneously by fluorescence spectroscopy and pH-meter: the first an 8% increase in the emission intensity, was observed, and at 360 seconds into the progression of the reaction, within a few seconds, a relatively fast drop (-84%) in the emission intensity was observed. The emission changes were reproducible, and juxtaposed very well with the changes in pH (Figure 89). In separate control experiments without CB7, no change in the emission was observed, eliminating any possibility of chemical processes altering the Bodipy emission. The batch pH oscillations are

highly irregular and only sustained for just one or at most two cycles, nevertheless our results clearly serve as a proof of principle for autonomous switching in a pseudorotaxane through coupling to an oscillating reaction.

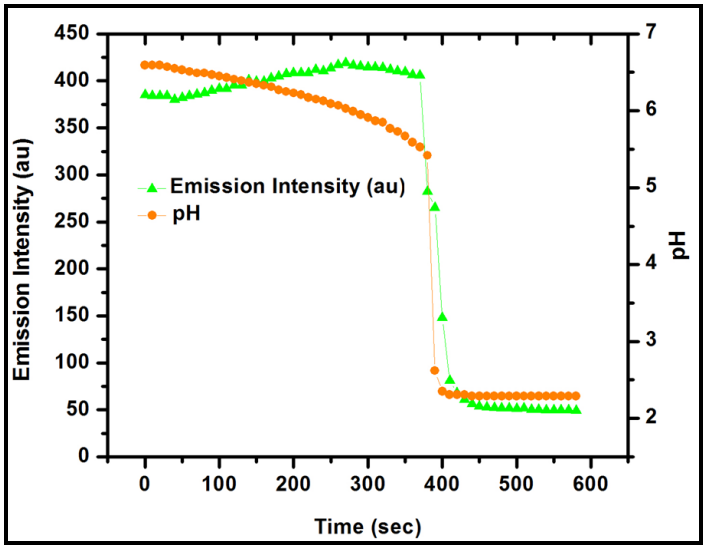

Figure 89. The plot of emission intensity and pH versus time obtained during the pH oscillation reaction.

The absorbance change of **82**$^{2+}$ with the increasing concentration of CB7 was depicted in Figure 90.

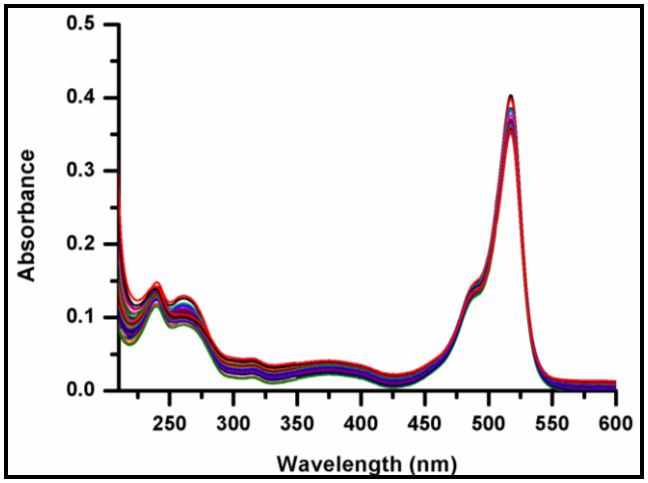

Figure 90. Absorbance spectra of compound **82**$^{2+}$ (0.01 mM, in 0.1M NaCl 2% MeCN in D_2O) in the presence of increasing CB7 concentrations (0, 0.1, 0.2, 0.3, 0.4, 0.5 0.6, 0.7, 0.8, 0.9, 1.0, 1.1 x 10^{-5}M).

7.4. Experimental Details

7.4.1. General Methods

Solvents used in synthesis were reagent grade. CH_2Cl_2, MeCN and Et_3N were used without further purification. Starting materials and reagents were purchased from Aldrich, Fluka, or Acros and used as received. Compound **80** was prepared following a procedure reported in the literature.[182] All reactions were performed under an argon or nitrogen atmosphere and in dry solvents unless otherwise noted. Dry solvents were also purged with argon gas before using them. Analytical thin-layer chromatography (TLC) was performed on aluminum sheets, precoated with silica gel 60-F_{254} (Merck 5554). ^1H and ^{13}C NMR spectra were recorded on a Bruker DPX-400 (operating at 400 MHz for ^1H NMR and 100 MHz for ^{13}C NMR) at ambient temperature. Chemical shifts are reported in ppm relative to the signals corresponding to the residual non-deuterated solvents (D_2O: δ 4.79 ppm, CD_3OD: δ 3.31 ppm, $CDCl_3$: δ 7.26 ppm, DMSO-d_6: δ 2.50 ppm). All spectra were recorded at 25°C and coupling constants (*J values*) are given in Hz. Splitting patterns are designated as singlet (*s*), doublet (*d*), triplet (*t*) and multiplet (*m*). Mass spectra were measured on an Agilent Technologies 6530 Accurate-Mass Q-TOF LC/MS spectrometer.

7.4.2. Synthesis

Compound 80[182]:

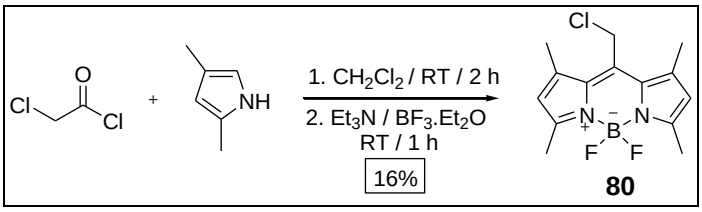

To a 500 mL round-bottomed flask containing 250 mL argon-degassed CH_2Cl_2 were added 2,4-dimethyl-3-ethyl pyrrole (11.4 mmol, 1.5 g) and chloroacetyl chloride (5.7 mmol, 0.64 g) and the resulting mixture was stirred for 2 hours at room temperature. 8 mL of Et_3N and 10 mL of $BF_3.OEt_2$ were successively added and after 30 min, the reaction mixture was washed three times with water and carefully dried over anhydrous Na_2SO_4. The solvent was evaporated under reduced pressure to give the

crude product. Then, it was purified by using column chromatography (3:1 Toluene:Hexane) to give red solid (0.32 g, 16%). ^{1}H NMR (400 MHz, $CDCl_3$) δ = 6.03 (s, 2H), 4.71 (s, 2H), 2.47 (s, 6H), 2.46 (s, 6H). ^{13}C NMR (100 MHz, $CDCl_3$) δ = 156.63, 141.13, 135.92, 131.36, 129.04, 128.23, 122.30, 122.28, 37.17, 15.56, 14.72.

Compound 81:

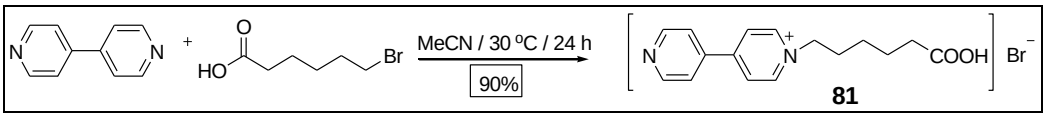

4, 4'- Bipyridine (15.39 mmol, 2.4 g), 6-Bromohexanoic acid (15.13 mmol, 1 g) and KI (5.13 mmol, 852 mg) were dissolved in pre-degassed MeCN (20 mL). The reaction mixture was stirred overnight at 30 °C. Cloudy solution was evaporated to 5 mL and the resulting suspension was added to 200 mL of diethyl ether to give the crude solid. Filtration and washing with 50 mL of diethyl ether yielded the product as pale yellow solids (1.2 g, 90%). ^{1}H NMR (400 MHz, D_2O) δ = 8.87 (d, *J* = 6.4 Hz, 2H), 8.69 (d, *J* = 5.2 Hz, 2H), 8.30 (d, *J* = 6.4 Hz, 2H), 7.92 (d, *J* = 5.7 Hz, 2H), 4.56 (t, *J* = 7.3 Hz, 2H), 2.2 2 (t, *J* = 7.3 Hz, 2H), 1.96 (p, *J* = 7.5 Hz, 2H), 1.52 (p, *J* = 7.4 Hz, 2H), 1.36 – 1.09 (m, 2H). ^{13}C NMR (100 MHz, D_2O) δ = 179.62 , 152.97 , 148.14 , 144.81 , 144.59 , 126.17 , 123.26 , 61.39 , 34.11 , 30.11 , 24.65 , 23.78 . MS (TOF- ESI): m/z: : (M = **81**) Calcd: 271.14410 $[M-Br]^+$, Found: 271.1441 0$[M-Br]^+$.

Compound 82:

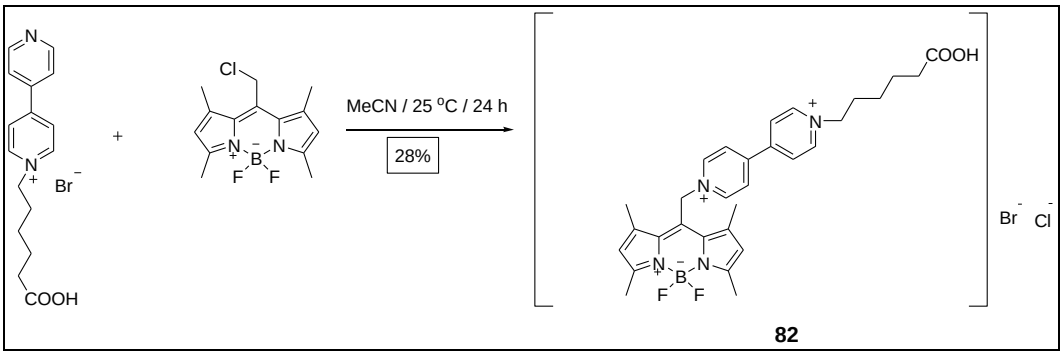

Compound **80** (0.33 mmol, 100 mg), compound **81** (0.67 mmol, 183 mg) and catalytic amount of KI were added to a 100 mL round-bottomed flask containing 30

mL pre-degassed MeCN. The reaction mixture was heated at 45 ^{o}C under argon atmosphere for overnight. The resulting red suspension was evaporated under reduced pressure until 5 mL of solvent remained in the round-bottomed flask. Then, this concentrated suspension was added to 200 mL of cold diethyl ether to give dark red solids. The filtrated solids were washed with diethyl ether extensively. The crude product was purified by alumina gel column chromatography (5:95 MeOH:$CHCl_3$) to give dark red solids (0.06 g, 28%).^{1}H NMR (400 MHz, CD_3OD) δ = 9.09 (d, *J* = 6.9 Hz, 2H), 8.86 (d, *J* = 6.3 Hz, 2H), 8.53 (d, *J* = 6.9 Hz, 2H), 8.01 (d, *J* = 6.3 Hz, 2H), 6.20 (s, 2H), 5.42 (s, 2H), 4.65 (t, *J* = 7.6 Hz, 2H), 2.50 (t, *J* = 7.3 Hz, 2H), 2.48 (s, 6H), 2.42 (s, 6H), 2.07 (p, *J* = 7.7 Hz, 2H), 1.75 (p, *J* = 7.4 Hz, 2H), 1.56 – 1.39 (m, 2H). ^{13}C NMR (100 MHz, CD_3OD) δ = 174.29 , 157.61 , 155.14 , 151.84 , 146.49 , 143.62 , 143.41 , 135.71 , 133.76 , 127.13 , 123.55 , 123.27 , 62.39 , 58.85 , 34.32 , 31.96 , 26.51 , 25.29 , 15.79 , 14.66 . MS (TOF- ESI): m/z: : (M = $\mathbf{82^{2+}}$) Calcd: 531.2732 $[M-H]^-$, Found: 531.2735 $[M-H]^-$; Δ = 5.6 ppm.

7.5. Conclusion

This is the first demonstration of a molecular shuttle system in which the "mobile" component moving from one station to the other in a truly autonomous fashion. The coupling of pH oscillation to the shuttling process is clear, during which free energy of the oscillatory reactions is exploited. This kind of chemical coupling of an energetically favorable reaction (or set of reactions with complex kinetics) to molecular motion is reminiscent of many biological analogs and therefore highly exciting. This work is a proof of principle study and shows solid compelling evidence that oscillating reactions may provide such autonomy to molecular machines.

CHAPTER 8

8. CONCLUSION

There is no doubt that the investigation of new designs responding to today`s problems is the main concern of today science and scientist. At this point, supramolecular chemistry is one of the field which drives the today`s technology and science. So far, it has played a very important role in the design of new technological designs and product developments. To feeds this productivity, there is a strong demand to propose new approaches.

In this thesis, I have presented some novel and rational approaches in the construction of different supramolecular architectures. These proposed approaches include four main titles; ion sensing, light harvesting, energy conversion and self-assembled systems in five different chapters.

In the first chapter, we have designed two dosimetric probes to detect fluoride sensing not only in solution but also in polymethylmethaacraylate (PMMA) matrix. These reaction based probes have been designed to give selective chemical reaction with fluoride. These reactions lead an influence in the triggering of photophysical process, in these probes namely PET and ICT. Therefore, it is obvious that in the presence of fluoride anions, an emission or visible color change could be followed by reproducibly. The probes showed impressive selectivity to fluoride anion. Furthermore, they served high sensitivity even in micro molar concentration of fluoride. By doping these probes into PMMA matrix, we were able to show that these probes can be used in practical applications in which one can easily perform fluoride detection analysis by using a dipstick for fluoride anion.

In the second chapter, we have reported a novel approach to synthesize new fluorescent Bodipy based fluorophores. By optimizing the reaction conditions, we were able to synthesize near-IR emissive dyes bearing four stryl derivatives on Bodipy skeleton. This straightforward functionalization modality made a significant contribution to versatility of Bodipy dyes. These new generation will be used in the targeting of medically and environmentally important anions and cations as an indicator, in photodynamic therapy, in dendritic light harvesters, and in highly complex supramolecular architectures as versatile building blocks.

In another study (Chapter 5), we presented two dendritic light harvesters in which tetra-stryl Bodipy dyes centered at the core of dendrimers and short wavelength Bodipy dyes located at the periphery. Furthermore, on the basis of spectral evidence, we observed that the direct application of Forster theory in energy transfer leads to large overestimation in the calculation of energy transfer efficiency. Therefore, an elucidation in the calculation of energy transfer efficiency will make possible to fabricate more efficient light harvesting systems and solar concentrators.

In Chapter 6, we designed a Cu (I)-diimine complex as a photosensitizer used in DSSC. The surface bound Cu(I) complex showed highly efficient electron injection from the excited state (^{1}MLCT) to TiO_2 nanoparticles and this injection has been followed by using EPR, TA and XTA analysis. The dynamic of charge separation and recombination were correlated with the ground and excited state structure of complex. This is the first demonstration of effective electron transfer from a singlet MLCT state of surface bound transition metal based photosensitizes into TiO_2. It was proved that Cu(I) diimine with capability of ultrafast electron injection to TiO_2 nanoparticles could be a strong candidate for replacing Ru(II) included complexes at a much lower cost. This study potentially will generate significant impact for the scientist working on DSSC.

In the final part, we reported a cucubituril[7]uril-Bodipy based pseudorotaxane which shuttles autonomously. It provides a fresh approach in initiating and controlling molecular shuttling. In this study, we have proposed to utilize oscillations

in pH to move the components of a pseudorotaxane in relation to each other. This is the first demonstration of a molecular shuttle system in which the mobile component CB7 is moving from one station to the other in a truly autonomous fashion. This shuttling were monitored by following the emision of the Bodipy working as an axle. Although batch oscillation systems are highly irregular and sustain very limited number of cycles, we constructed a batch system to establish pH oscillation. We observed just only one cycle. However the results serve as a proof of principle for autonomous shuttling in a pseudorotaxane driven by pH oscillating reaction.

CHAPTER 9

9. REFERENCES

[1] C. J. Pedersen, "Macrocyclic polyethers for complexing metals," *Aldrichchimica Acta,* vol. 4, no. 1, pp.1-4, 1971.

[2] D. J. Cram, "The design of moecular hosts, guests, and their complexes (Nobel Lecture)," *Angewandte Chemie-International Edition in English,* vol. 27, no. 8, pp. 1009-1020, 1988.

[3] J. M. Lehn, "Supramolecular chemistry - scope and perspectives molecules, supermolecules, and molecular devices," *Angewandte Chemie-International Edition in English,* vol. 27, no. 1, pp. 89-112, 1988.

[4] B. Valeur, "Molecular fluorescence: principles and applications," Wiley-VCH: Weinheim, 2002.

[5] D. L. Andrews, "Encyclopedia of applied spectroscopy," Wiley-VCH: Weinheim, 2009.

[6] J. R. Lakowicz, "Principles of fluorescence spectroscopy," Plenum Press: New York, 1999.

[7] A. Sharma and S. G. Schulman, "Introduction to fluorescence spectroscopy," Wiley Interscience:Canada, 1999.

[8] A. Jablonski, "Uber den mechanism des photolumineszenz von farbstoffphosphoren," *Zeitschrify für Physik A Hadrons and Nuclei,* vol. 94, no. 1, pp. 38-46, 1935.

[9] J. Franck, and E. G. Dymond, "Elementary processes of photochemical reactions," *Transactions of the Faraday Society,* vol. 21, no. February, pp. 536-542, 1926.

[10] E. Condon, "A theory of ıntensity distribution in band systems," *Physical Review,* vol. 28, no. 6, pp. 1182-1201, 1926.

[11] J. B. Pawley, "Handbook of biological confocal microscopy," Springer Science & Business Media, New York, 2006.

[12] http://www.piercenet.com/browse.cfm?fldID=4DD9D52E-5056-8A76-4E6E-E217FAD0D86B

[13] O. Shimomura, F. H. Johnson, and Y. Saiga, "Extraction, purification and properties of aequorin, a bioluminescent protein from the luminous hydromedusan, *aequorea*," *Journal of Cellular and Comparative Physiology*, vol. 59, no. 3, pp. 223-239, 1962.

[14] M. Chalfie, Y. Tu, G. Euskirchen, W.W. Ward and D.C. Prasher, "Green fluorescent protein as a marker for gene-expression," *Science*, vol. 263, no. 5148, pp. 802-805, 1994.

[15] R. Heim, A. B. Cubitt, and R. Y. Tsien, "Improved green fluorescence," *Nature*, vol. 373, no. 6516, pp. 663-664, 1995.

[16] M. Yang, E. Baranov, A.R. Moossa, S. Penman and R.M. Hoffman, "Visualizing gene expression by whole-body fluorescence imaging," *Proceedings of the National Academy of Sciences*, vol. 97, no. 22, pp. 12278-12282, 2000.

[17] S. Cabantous, T. C. Terwilliger, and G. S. Waldo, "Protein tagging and detection with engineered self-assembling fragments of green fluorescent protein," *Nature Biotechnology*, vol. 23, no. 1, pp. 102-107, 2005.

[18] J. Lippincott-Schwartz, E. Snapp, and A. Kenworthy, "Studying protein dynamics in living cells," *Nature Reviews Molecular Cell Biology*, vol. 2, no. 6, pp. 444-456, 2001.

[19] C. J. Li, R. Heim, P. Lu, Y. M. Pu, R. Y. Tsien and D. C. Chang, "Dynamic redistribution of calmodulin in HeLa cells during cell division as revealed by a GFP-calmodulin fusion protein technique," *Journal of Cell Science*, vol. 112, no. 10, pp. 1567-1577, 1999.

[20] A. S. Belmont, "Visualizing chromosome dynamics with GFP," *Trends in Cell Biology*, vol. 11, no. 6, pp. 250-257, 2001.

[21] A. I. Ekimov and A. A. Onushchenko, "Quantum size effect in three-dimensional microscopic semiconductor crystals," *Journal of Experimental and Theoretical Physics Letters*, vol. 34, no. 6, pp.345-349, 1981.

[22] J. Li, and J.-J. Zhu, "Quantum dots for fluorescent biosensing and bio-imaging applications," *Analyst*, vol. 138, no. 9, pp. 2506-2515, 2013.

[23] F. Pinaud, X. Michalet, L.A. Bentolila, J.M. Tsay, S. Doose, J.J. Li, G. Iyer and S. Weiss, "Advances in fluorescence imaging with quantum dot bio-probes," *Biomaterials*, vol. 27, no. 9, pp. 1679-1687, 2006.

[24] H. Mattoussi, G. Palui, and H. B. Na, "Luminescent quantum dots as platforms for probing in vitro and in vivo biological processes," *Advanced Drug Delivery Reviews*, vol. 64, no. 2, pp. 138-166, 2012.

[25] R. N. Dsouza, U. Pischel, and W. M. Nau, "Fluorescent dyes and their supramolecular host/guest complexes with macrocycles in aqueous solution," *Chemical Reviews*, vol. 111, no. 12, pp. 7941-7980, 2011.

[26] M. S. T. Gonçalves, "Fluorescent labeling of biomolecules with organic probes," *Chemical Reviews*, vol. 109, no. 1, pp. 190-212, 2008.

[27] V. Balzani and F. Scandola, "Supramolecular photochemistry" EllisHorwood: Chichester, 1991.

[28] I. Ravikumar, P. Lakshminarayanan, B. Nisar Ahamed and P. Ghosh, "Chemical sensing of ions and its clinical applications," *Asian Journal of Experimental Sciences*, vol. 22, no. 2, pp. 103-111, 2008.

[29] E. V. Anslyn, "Supramolecular analytical chemistry," *The Journal of Organic Chemistry*, vol. 72, no. 3, pp. 687-699, 2007.

[30] L. Basabe-Desmonts, D. N. Reinhoudt, and M. Crego-Calama, "Design of fluorescent materials for chemical sensing," *Chemical Society Reviews*, vol. 36, no. 6, pp. 993-1017, 2007.

[31] A P. de Silva, H.Q.N. Gunaratne, T. Gunnlaugsson, A .J. M. Huxley, C. P. McCoy, J. T. Rademacher and T. E. Rice, "Signaling recognition events with fluorescent sensors and switches," *Chemical Reviews*, vol. 97, no. 5, pp. 1515-1566, 1997.

[32] B. Valeur, and I. Leray, "Design principles of fluorescent molecular sensors for cation recognition," *Coordination Chemistry Reviews*, vol. 205, pp. 3-40, 2000.

[33] K. Kaur, R. Saini, A. Kumar, V. Luxami, N. Kaur, P. Singh and S. Kumar, "Chemodosimeters: An approach for detection and estimation of biologically and medically relevant metal ions, anions and thiols," *Coordination Chemistry Reviews*, vol. 256, no. 17-18, pp. 1992-2028, 2012.

[34] A. P. de Silva, T. S. Moody, and G. D. Wright, “Fluorescent PET (Photoinduced Electron Transfer) sensors as potent analytical tools,” *Analyst*, vol. 134, no. 12, pp. 2385-2393, 2009.

[35] V. Bojinov and N. Georgiev, “Molecular sensors and molecular logic gates, ” *Journal of the University of chemical Technology and Metallorgy*, vol. 46, no. 1, pp. 3-26, 2011.

[36] A. P. de Silva, and S. A. de Silva, “Fluorescent signalling crown ethers; 'switching on' of fluorescence by alkali metal ion recognition and binding in situ,” *Journal of the Chemical Society, Chemical Communications*, no. 23, pp. 1709-1710, 1986.

[37] E. U. Akkaya, M. E. Huston, and A. W. Czarnik, “Chelation-enhanced fluorescence of anthrylazamacrocycle conjugate probes in aqueous solution,” *Journal of the American Chemical Society*, vol. 112, no. 9, pp. 3590-3593, 1990.

[38] R. E. Gawley, H. Mao, M. M. Haque, J. B. Thorne and J. S. Pharr, “Visible fluorescence chemosensor for saxitoxin,” *The Journal of Organic Chemistry*, vol. 72, no. 6, pp. 2187-2191, 2007.

[39] K. Golchini, M. Mackovicbasic, S.A. Gharib, D. Masilamani, M.E. Lucas and I. Kurtz, “Synthesis and characterızation of a new fluorescent-probe for measuring potassium,” *American Journal of Physiology*, vol. 258, no. 2, pp. F438-F443, 1990.

[40] A. P. De Silva, H. Q. N. Gunaratne, and K. Sandanayake, “A new benzo-annelated cryptand and a derivative with alkali cation-sensitıve fluorescence,” *Tetrahedron Letters*, vol. 31, no. 36, pp. 5193-5196, 1990.

[41] M. E. Huston, K. W. Haider, and A. W. Czarnik, “Chelation enhanced fluorescence in 9,10-bis[[(2-(dimethylamino)ethyl)methylamino]methyl]-anthracene,” *Journal of the American Chemical Society*, vol. 110, no. 13, pp. 4460-4462, 1988.

[42] G. K. Walkup, S. C. Burdette, S. J. Lippard and R. Y. Tsien, “A new cell-permeable fluorescent probe for Zn^{2+},” *Journal of the American Chemical Society*, vol. 122, no. 23, pp. 5644-5645, 2000.

[43] B. Turfan, and E. U. Akkaya, “Modulation of boradiazaindacene emission by cation-mediated oxidative PET,” *Organic Letters*, vol. 4, no. 17, pp. 2857-2859, 2002.

[44] E. Deniz, G.C. Isbasar, O. A. Bozdemir, L. T. Yildirim, A. Siemiarczuk and E.U. Akkaya, “Bidirectional switching of near IR emitting boradiazaindacene fluorophores,” *Organic Letters*, vol. 10, no. 16, pp. 3401-3403, 2008.

[45] A. I. Bush, W.H. Pettingell, G. Multhaup, M. D. Paradis, J. P. Vonsattel, J. F. Gusella, K. Beyreuther, C .L. Masters and R. E. Tanzi, “Rapid induction of alzheimer a-beta amyloid formation by zinc,” *Science*, vol. 265, no. 5177, pp. 1464-1467, 1994.

[46] D. T. Quang, and J. S. Kim, “Fluoro- and chromogenic chemodosimeters for heavy metal ion detection in solution and biospecimens,” *Chemical Reviews*, vol. 110, no. 10, pp. 6280-6301, 2010.

[47] J. Du, M. Hu, J. Fan and X. Peng,, “Fluorescent chemodosimeters using "mild" chemical events for the detection of small anions and cations in biological and environmental media,” *Chemical Society Reviews*, vol. 41, no. 12, pp. 4511-4535, 2012.

[48] H. N. Kim, W. X. Ren, J. S. Kim and J. Yoon, “Fluorescent and colorimetric sensors for detection of lead, cadmium, and mercury ions,” *Chemical Society Reviews*, vol. 41, no. 8, pp. 3210-3244, 2012.

[49] Z. Xu, J. Yoon, and D. R. Spring, “Fluorescent chemosensors for Zn^{2+},” *Chemical Society Reviews*, vol. 39, no. 6, pp. 1996-2006, 2010.

[50] E. Kawabata, K. Kikuchi, Y. Urano, H. Kojima, A. Odani and T. Nagano, “Design and synthesis of zinc-Selective chelators for extracellular applications,” *Journal of the American Chemical Society*, vol. 127, no. 3, pp. 818-819, 2004.

[51] H. Koutaka, J.-I. Kosuge, N. Fukasaku,T. Hirano, K. Kikuchi, Y. Urano, H. Kojima and T. Nagano, “A novel fluorescent probe for zinc ion based on boron dipyromethane (Bodipy) chromophore” *Chemical and Pharmaceutical Bulletin*, vol. 52, no. 6, pp. 700-703, 2004.

[52] O. A. Bozdemir, R. Guliyev, O. Buyukcakir, S. Selcuk, S. Kolemen, G. Gulseren, T. Nalbantoglu, H. Boyaci and E. U. Akkaya, "Selective manipulation of ICT and PET processes in styryl-Bodipy derivatives: Applications in molecular logic and fluorescence sensing of metal ions," *Journal of the American Chemical Society,* vol. 132, no. 23, pp. 8029-8036, 2010.

[53] H. Lu, Q. Wang, Z. Li, G. Lai, J. Jiang and Z. Shen,, "A specific chemodosimeter for fluoride ion based on a pyrene derivative with trimethylsilylethynyl groups," *Organic & Biomolecular Chemistry,* vol. 9, no. 12, pp. 4558-4562, 2011.

[54] Z. Ekmekci, M. D. Yilmaz, and E. U. Akkaya, "A monostyryl-boradiazaindacene (BODIPY) derivative as colorimetric and fluorescent probe for cyanide ions," *Organic Letters,* vol. 10, no. 3, pp. 461-464, 2008.

[55] Y. C. Cheng, and G. R. Fleming, "Dynamics of light harvesting in photosynthesis," *Annual Review of Physical Chemistry,* Annual Review of Physical Chemistry, pp. 241-262, 2009.

[56] S. Lin, E. Katilius, R.P. Ilagan, G.N. Gibson, H.A. Frank and N.W. Woodbury, "Mechanism of carotenoid singlet excited state energy transfer in modified bacterial reaction centers," *The Journal of Physical Chemistry B,* vol. 110, no. 31, pp. 15556-15563, 2006.

[57] J. Fan, M. Hu, P. Zhan and X. Peng, "Energy transfer cassettes based on organic fluorophores: construction and applications in ratiometric sensing," *Chemical Society Reviews,* vol. 42, no. 1, pp. 29-43, 2013.

[58] X. Zheng, J. Garcia, and A. A. Stuchebrukhov, "Theoretical study of excitation energy transfer in DNA photolyase," *The Journal of Physical Chemistry B,* vol. 112, no. 29, pp. 8724-8729, 2008.

[59] T. Forster, "Zwischenmolekulare energiewanderung und fluoreszenz," *Annals Physics,* vol. 6, pp. 55, 1948.

[60] M. D. Yilmaz, O. A. Bozdemir, and E. U. Akkaya, "Light harvesting and efficient energy transfer in a boron-dipyrrin (BODIPY) functionalized perylenediimide derivative," *Organic Letters,* vol. 8, no. 13, pp. 2871-2873, 2006.

[61] J. M. Serin, D. W. Brousmiche, and J. M. J. Fréchet, "A FRET-based ultraviolet to near-infrared frequency converter," *Journal of the American Chemical Society,* vol. 124, no. 40, pp. 11848-11849, 2002.

[62] N. J. Turro, "*Modern Molecular Photochemsitry,*" University Science Books, Sausalito, **1991**

[63] W. Y. Lin, L. Yuan, Z. M. Cao, Y. M. Feng and J. Z. Song, "Through-bond energy transfer cassettes with minimal spectral overlap between the donor emission and acceptor absorption: Coumarin-Rhodamine dyads with large pseudo-stokes shifts and emission shifts," *Angewandte Chemie-International Edition,* vol. 49, no. 2, pp. 375-379, 2010.

[64] C. W. Wan, A. Burghart, J. Chen, F. Bergstrom, L. B.-A. Johansson, M. F. Wolford, T. G. Kim, M. R. Topp, R. M. Hochstrasser and K. Burgess, "Anthracene-BODIPY cassettes: syntheses and energy transfer," *Chemistry-a European Journal,* vol. 9, no. 18, pp. 4430-4441, 2003.

[65] A. Nantalaksakul, D. R. Reddy, C .J. Bardeen and S. Thayumanavan, "Light harvesting dendrimers," *Photosynthesis Research,* vol. 87, no. 1, pp. 133-150, 2006.

[66] P. D. Frischmann, K. Mahata, and F. Wurthner, "Powering the future of molecular artificial photosynthesis with light-harvesting metallosupramolecular dye assemblies," *Chemical Society Reviews,* vol. 42, no. 4, pp. 1847-1870, 2013.

[67] O. A. Bozdemir, M. D. Yilmaz, O. Buyukcakir, A. Siemiarczuk, M. Tutas, and E.U. Akkaya, "Convergent synthesis and light harvesting properties of dendritic boradiazaindacene (BODIPY) appended perylenediimide dyes," *New Journal of Chemistry,* vol. 34, no. 1, pp. 151-155, 2010.

[68] A. Haefele, G. Ulrich, P. Retailleau and R. Ziessel, "Synthesis of multi-branched dipyrromethene dyes with soluble diethynylphenyl links," *Tetrahedron Letters,* vol. 49, no. 23, pp. 3716-3721, 2008.

[69] M. Gratzel, "Photoelectrochemical cells," *Nature,* vol. 414, no. 6861, pp. 338-344, 2001.

[70] B. O'Regan, and M. Gratzel, "A low-cost, high-efficiency solar cell based on dye-sensitized colloidal TiO_2 films," *Nature,* vol. 353, no. 6346, pp. 737-740, 1991.

[71] A. Hagfeldt, G. Boschloo, L. Sun, L. Kloo and H. Pettersson, "Dye-sensitized solar cells," *Chemical Reviews,* vol. 110, no. 11, pp. 6595-6663, 2010.

[72] Y. Ooyama, and Y. Harima, "Molecular designs and syntheses of organic dyes for dye-sensitized solar cells," *European Journal of Organic Chemistry,* vol. 2009, no. 18, pp. 2903-2934, 2009.

[73] S. Ardo, and G. J. Meyer, "Photodriven heterogeneous charge transfer with transition-metal compounds anchored to TiO2 semiconductor surfaces," *Chemical Society Reviews,* vol. 38, no. 1, pp. 115-164, 2009.

[74] M. K. Nazeeruddin, A. Kay, I. Rodicio, R. Humphry-Baker, E. Mueller, P. Liska, N. Vlachopoulos and M. Graetzel, "Conversion of light to electricity by cis-X_2bis(2,2'-bipyridyl-4,4'-dicarboxylate)ruthenium(II) charge-transfer sensitizers (X = Cl-, Br-, I-, CN-, and SCN-) on nanocrystalline titanium dioxide electrodes," *Journal of the American Chemical Society,* vol. 115, no. 14, pp. 6382-6390, 1993.

[75] M. K. Nazeeruddin, P. Pechy, and M. Gratzel, "Efficient panchromatic sensitization of nanocrystalline TiO_2 films by a black dye based on a trithiocyanato-ruthenium complex," *Chemical Communications,* vol. 0, no. 18, pp. 1705-1706, 1997.

[76] F. Gao, Y. Wang, D. Shi, J. Zhang, M. Wang, X. Jing, R. Humphry-Baker, P. Wang, S. M. Zakeeruddin and M. Grätzel, "Enhance the optical absorptivity of nanocrystalline TiO_2 film with high molar extinction coefficient ruthenium sensitizers for high performance dye-sensitized solar cells," *Journal of the American Chemical Society,* vol. 130, no. 32, pp. 10720-10728, 2008.

[77] F. Gao, Y. Wang, J. Zhang, D. Shi, M. Wang, R. Humphry-Baker, P. Wang, S.M. Zakeeruddin and M. Gratzel,, "A new heteroleptic ruthenium sensitizer enhances the absorptivity of mesoporous titania film for a high efficiency dye-sensitized solar cell," *Chemical Communications,* vol. 0, no. 23, pp. 2635-2637, 2008.

[78] J. Faiz, A. I. Philippopoulos, A. G. Kontos, P. Falaras and Z. Pikramenou, "Functional supramolecular ruthenium cyclodextrin dyes for nanocrystalline solar cells," *Advanced Functional Materials,* vol. 17, no. 1, pp. 54-58, 2007.

[79] A. Islam, H. Sugihara, K. Hara, L.P. Singh, R. Katoh, M. Yanagida, Y. Takahashi, S. Murata, H. Arakawa and G. Fujihashi, "Dye sensitization of nanocrystalline titanium dioxide with square planar platinum(II) diimine dithiolate complexes," *Inorganic Chemistry,* vol. 40, no. 21, pp. 5371-5380, 2001.

[80] S. Altobello, R. Argazzi, S. Caramori, C. Contado, S. Da Fré, P. Rubino, C. Choné, G. Larramona and C.A. Bignozzi, "Sensitization of Nanocrystalline TiO2 with Black Absorbers Based on Os and Ru Polypyridine Complexes," *Journal of the American Chemical Society,* vol. 127, no. 44, pp. 15342-15343, 2005.

[81] S. Ferrere, and B. A. Gregg, "Photosensitization of TiO_2 by [FeII(2,2'-bipyridine-4,4'-dicarboxylic acid)2(CN)2]: band selective electron injection from ultra-short-lived excited states," *Journal of the American Chemical Society,* vol. 120, no. 4, pp. 843-844, 1998.

[82] S. Sakaki, T. Kuroki, and T. Hamada, "Synthesis of a new copper(I) complex, [Cu(tmdcbpy)2]+ (tmdcbpy = 4,4[prime or minute],6,6[prime or minute]-tetramethyl-2,2[prime or minute]-bipyridine-5,5[prime or minute]-dicarboxylic acid), and its application to solar cells," *Journal of the Chemical Society, Dalton Transactions,* vol. 0, no. 6, pp. 840-842, 2002.

[83] T. Bessho, E. C. Constable, M. Graetzel, A. Hernandez Redondo, C. E. Housecroft, W. Kylberg, M. K. Nazeeruddin, M. Neuburger and S. Schaffner, "An element of surprise-efficient copper-functionalized dye-sensitized solar cells," *Chemical Communications,* vol. 0, no. 32, pp. 3717-3719, 2008.

[84] J. M. Rehm, G. L. McLendon, Y. Nagasawa, K. Yoshihara, J. Moser and M. Grätzel, "Femtosecond electron-transfer dynamics at a sensitizing dye−semiconductor (TiO_2) interface," *The Journal of Physical Chemistry,* vol. 100, no. 23, pp. 9577-9578, 1996.

[85] K. Hara, T. Sato, R. Katoh, A. Furube, Y. Ohga, A. Shinpo, S. Suga, K. Sayama, H. Sugihara and H. Arakawa, "Molecular design of coumarin dyes

for efficient dye-sensitized solar cells," *The Journal of Physical Chemistry B,* vol. 107, no. 2, pp. 597-606, 2002.

[86] G. Zhou, N. Pschirer, J. C. Schöneboom, F. Eickemeyer, M. Baumgarten and K. Müllen, "Ladder-type pentaphenylene dyes for dye-sensitized solar cells," *Chemistry of Materials,* vol. 20, no. 5, pp. 1808-1815, 2008.

[87] A. Treibs, and F.-H. Kreuzer, "Difluorboryl-Komplexe von Di- und Tripyrrylmethenen," *Justus Liebigs Annalen der Chemie,* vol. 718, no. 1, pp. 208-223, 1968.

[88] G. Ulrich, R. Ziessel, and A. Harriman, "The chemistry of fluorescent Bodipy dyes: versatility unsurpassed," *Angewandte Chemie International Edition,* vol. 47, no. 7, pp. 1184-1201, 2008.

[89] A. Loudet, and K. Burgess, "BODIPY dyes and their derivatives: syntheses and spectroscopic properties," *Chemical Reviews,* vol. 107, no. 11, pp. 4891-4932, 2007.

[90] J. H. Boyer, A. M. Haag, G. Sathyamoorthi, M.-L. Soong, K. Thangaraj and T. G. Pavlopoulos, "Pyrromethene–BF_2 complexes as laser dyes: 2," *Heteroatom Chemistry,* vol. 4, no. 1, pp. 39-49, 1993.

[91] M. Shah, K. Thangaraj, M.-L. Soong, L. T. Wolford, J. H. Boyer, I. R. Politzer and T. G. Pavlopoulos, "Pyrromethene–BF_2 complexes as laser dyes," *Heteroatom Chemistry,* vol. 1, no. 5, pp. 389-399, 1990.

[92] T. Yogo, Y. Urano, Y. Ishitsuka, F. Maniwa and T. Nagano, "Highly efficient and photostable photosensitizer based on BODIPY chromophore," *Journal of the American Chemical Society,* vol. 127, no. 35, pp. 12162-12163, 2005.

[93] C.-W. Wan, A. Burghart, J. Chen, F. Bergström, L. B. Å. Johansson, M.F. Wolford, T. G. Kim, M. R. Topp, R. M. Hochstrasser and K. Burgess, "Anthracene–BODIPY cassettes: Syntheses and energy transfer," *Chemistry – A European Journal,* vol. 9, no. 18, pp. 4430-4441, 2003.

[94] C. Goze, G. Ulrich, L. J. Mallon, B. D. Allen, A. Harriman and R. Ziessel, "Synthesis and photophysical properties of borondipyrromethene dyes bearing aryl substituents at the boron center," *Journal of the American Chemical Society,* vol. 128, no. 31, pp. 10231-10239, 2006.

[95] C. Goze, G. Ulrich, and R. Ziessel, “Unusual fluorescent monomeric and dimeric dialkynyl dipyrromethene−borane complexes,” *Organic Letters,* vol. 8, no. 20, pp. 4445-4448, 2006.

[96] C. Goze, G. Ulrich, and R. Ziessel, “Tetrahedral boron chemistry for the preparation of highly efficient “cascatelle” devices,” *The Journal of Organic Chemistry,* vol. 72, no. 2, pp. 313-322, 2006.

[97] O. Buyukcakir, O. A. Bozdemir, S. Kolemen, S. Erbas and E.U. Akkaya, “Tetrastyryl-Bodipy dyes: Convenient synthesis and characterization of elusive near IR fluorophores,” *Organic Letters,* vol. 11, no. 20, pp. 4644-4647, 2009.

[98] W. W. Qin, T. Rohand, M. Baruah, A. Stefan, M. Van der Auweraer, W. Dehaen and N. Boens, “Solvent-dependent photophysical properties of borondipyrromethene dyes in solution,” *Chemical Physics Letters,* vol. 420, no. 4-6, pp. 562-568, 2006.

[99] T. Rohand, M. Baruah, W. Qin, N. Boens and W. Dehaen, “Functionalisation of fluorescent BODIPY dyes by nucleophilic substitution,” *Chemical Communications,* vol. 0, no. 3, pp. 266-268, 2006.

[100] M. Baruah, W. Qin, R. A. L. Vallée, D. Beljonne, T. Rohand, W. Dehaen and N. Boens, “A highly potassium-selective ratiometric fluorescent indicator based on BODIPY azacrown ether excitable with visible light,” *Organic Letters,* vol. 7, no. 20, pp. 4377-4380, 2005.

[101] R. P. Feynman, “There`s plenty of room at the bottom,” Engineering and Science, vol. 23, no. 5, pp. 22-36, 1960.

[102] K. Kinbara, and T. Aida, “Toward intelligent molecular machines: Directed motions of biological and artificial molecules and assemblies,” *Chemical Reviews,* vol. 105, no. 4, pp. 1377-1400, 2005.

[103] V. Balzani, A. Credi, B. Ferrer, S. Silvi and M. Venturi, "Artificial molecular motors and machines: Design principles and prototype systems," *Molecular Machines,* Topics in Current Chemistry T. R. Kelly, ed., pp. 1-27, Berlin: Springer-Verlag Berlin, 2005.

[104] A. Coskun, M. Banaszak, R. D. Astumian, J. F. Stoddart and B. A. Grzybowski, "Great expectations: can artificial molecular machines deliver on their promise?," *Chemical Society Reviews,* vol. 41, no. 1, pp. 19-30, 2012.

[105] P. R. Ashton, R. Ballardini, V. Balzani, I. Baxter, A. Credi, M. C. T. Fyfe, M. T. Gandolfi, M. Gómez-López, M. V. Martínez-Díaz, A. Piersanti, N. Spencer, J. F. Stoddart, M. Venturi, A. J. P. White and D. J. Williams, "Acid−base controllable molecular shuttles," *Journal of the American Chemical Society,* vol. 120, no. 46, pp. 11932-11942, 1998.

[106] P. R. Ashton, R. Ballardini, V. Balzani, A. Credi, K. R. Dress, E. Ishow, C. J. Kleverlaan, O. Kocian, J.A. Preece, N. Spencer, J.F. Stoddart, M. Venturi and S. Wenger, "A photochemically driven molecular-level abacus," *Chemistry – A European Journal,* vol. 6, no. 19, pp. 3558-3574, 2000.

[107] F. P. Schmidtchen, and M. Berger, "Artificial organic host molecules for anions," *Chemical Reviews,* vol. 97, no. 5, pp. 1609-1646, 1997.

[108] R. Martinez-Manez, and F. Sancenon, "Chemodosimeters and 3D inorganic functionalised hosts for the fluoro-chromogenic sensing of anions," *Coordination Chemistry Reviews,* vol. 250, no. 23-24, pp. 3081-3093, 2006.

[109] R. Martínez-Máñez, and F. Sancenón, "Fluorogenic and Chromogenic Chemosensors and Reagents for Anions," *Chemical Reviews,* vol. 103, no. 11, pp. 4419-4476, 2003.

[110] Y.-C. Lin, and C.-T. Chen, "Acridinium salt-based fluoride and acetate chromofluorescent probes: Molecular insights into anion selectivity switching," *Organic Letters,* vol. 11, no. 21, pp. 4858-4861, 2009.

[111] S. V. Bhosale, S. V. Bhosale, M.B. Kalyankar and S. J. Langford, "A core-substituted naphthalene diimide fluoride sensor," *Organic Letters,* vol. 11, no. 23, pp. 5418-5421, 2009.

[112] T. W. Hudnall, and F. P. Gabbaï, "Ammonium Boranes for the selective complexation of cyanide or fluoride ions in water," *Journal of the American Chemical Society,* vol. 129, no. 39, pp. 11978-11986, 2007.

[113] S. Y. Kim, and J.-I. Hong, "Chromogenic and fluorescent chemodosimeter for detection of fluoride in aqueous solution," *Organic Letters,* vol. 9, no. 16, pp. 3109-3112, 2007.

[114] A. Coskun, E. Deniz, and E. U. Akkaya, "Effective PET and ICT switching of boradiazaindacene emission: A unimolecular, emission-mode, molecular half-subtractor with reconfigurable logic gates," *Organic Letters*, vol. 7, no. 23, pp. 5187-5189, 2005.

[115] D. P. Kennedy, C. M. Kormos, and S. C. Burdette, "FerriBRIGHT: A rationally designed fluorescent probe for redox active metals," *Journal of the American Chemical Society*, vol. 131, no. 24, pp. 8578-8586, 2009.

[116] A. P. de Silva, H. Q. N. Gunaratne, T. Gunnlaugsson, A. J. M. Huxley, C. P. McCoy, J. T. Rademacher and T. E. Rice, "Signaling recognition events with fluorescent sensors and switches," *Chemical Reviews*, vol. 97, no. 5, pp. 1515-1566, 1997.

[117] E. Deniz, G. C. Isbasar, O. A. Bozdemir, L. T. Yildirim, A. Siemiarczuk, and E.U. Akkaya, "Bidirectional switching of near IR emitting boradiazaindacene fluorophores," *Organic Letters*, vol. 10, no. 16, pp. 3401-3403, 2008.

[118] I. K. Sebhat, Y. L. Tan, D. A. Widdowson, R. Wilhelm, A. J. P. White and D. J. Williams, "Directed lithiation in arenetricarbonylchromium(0) complexes: Assessment of some directing group specificities and of electrophilic quench efficacies," *Tetrahedron*, vol. 56, no. 33, pp. 6121-6134, 2000.

[119] A. Treibs, and F.-H. Kreuzer, "Difluorboryl-Komplexe von Di- und Tripyrrylmethenen," *Justus Liebigs Annalen der Chemie*, vol. 718, no. 1, pp. 208-223, 1968

[120] L. Li, J. Han, B. Nguyen and K. Burgess, "Syntheses and spectral properties of functionalized, water-soluble BODIPY derivatives," *The Journal of Organic Chemistry*, vol. 73, no. 5, pp. 1963-1970, 2008.

[121] S. Goeb, and R. Ziessel, "Convenient Synthesis of Green Diisoindolodithienylpyrromethene−Dialkynyl Borane Dyes," *Organic Letters*, vol. 9, no. 5, pp. 737-740, 2007.

[122] S. P. Diring, F. Puntoriero, F. Nastasi, S. Campagna and R. Ziessel, "Star-shaped multichromophoric arrays from Bodipy dyes grafted on truxene core," *Journal of the American Chemical Society*, vol. 131, no. 17, pp. 6108-6110, 2009.

[123] M. D. Yilmaz, O. A. Bozdemir, and E. U. Akkaya, "Light harvesting and efficient energy transfer in a boron-dipyrrin (BODIPY) functionalized perylenediimide derivative," *Organic Letters,* vol. 8, no. 13, pp. 2871-2873, 2006.

[124] S. Erten-Ela, M. D. Yilmaz, B. Icli, Y. Dede, S. Icli and E.U. Akkaya, "A panchromatic boradiazaindacene (BODIPY) sensitizer for dye-sensitized solar cells," *Organic Letters,* vol. 10, no. 15, pp. 3299-3302, 2008.

[125] A. Gorman, J. Killoran, C. O'Shea, T. Kenna, W .M. Gallagher and D. F. O'Shea, "In vitro demonstration of the heavy-atom effect for photodynamic therapy," *Journal of the American Chemical Society,* vol. 126, no. 34, pp. 10619-10631, 2004.

[126] T. N. Singh-Rachford, A. Haefele, R. Ziessel and F. N. Castellano, "Boron dipyrromethene chromophores: next generation triplet acceptors/annihilators for low power upconversion schemes," *Journal of the American Chemical Society,* vol. 130, no. 48, pp. 16164-16165, 2008.

[127] F. Camerel, L. Bonardi, M. Schmutz, R. Ziessel., "Highly luminescent gels and mesogens based on elaborated borondipyrromethenes," *Journal of the American Chemical Society,* vol. 128, no. 14, pp. 4548-4549, 2006.

[128] Ö. A. Bozdemir, O. Büyükcakir, and E. U. Akkaya, "Novel molecular building blocks based on the boradiazaindacene chromophore: applications in fluorescent metallosupramolecular coordination polymers," *Chemistry – A European Journal,* vol. 15, no. 15, pp. 3830-3838, 2009.

[129] M. Yuan, Y. Li, J. Li, C. Li, X. Liu, J. Lv, J. Xu, H. Liu, S. Wang and D. Zhu, "A colorimetric and fluorometric dual-modal assay for mercury ion by a molecule," *Organic Letters,* vol. 9, no. 12, pp. 2313-2316, 2007.

[130] S. Ozlem, and E. U. Akkaya, "Thinking outside the silicon box: Molecular AND logic As an additional layer of selectivity in singlet oxygen generation for photodynamic therapy," *Journal of the American Chemical Society,* vol. 131, no. 1, pp. 48-49, 2008.

[131] A. Harriman, L.J. Mallon, S. Goeb, G. Ulrich and R. Ziessel, "Electronic energy transfer to the S_2 level of the acceptor in functionalised boron

dipyrromethene dyes," *Chemistry – A European Journal,* vol. 15, no. 18, pp. 4553-4564, 2009.

[132] Z. Dost, S. Atilgan, and E. U. Akkaya, "Distyryl-boradiazaindacenes: facile synthesis of novel near IR emitting fluorophores," *Tetrahedron,* vol. 62, no. 36, pp. 8484-8488, 2006.

[133] E. Lager, J. Liu, A. l. Aguilar-Aguilar, B. Z. Tang and E. Peña-Cabrera, "Novel meso-polyarylamine-BODIPY hybrids: Synthesis and study of their optical properties," *The Journal of Organic Chemistry,* vol. 74, no. 5, pp. 2053-2058, 2009.

[134] S. L. Niu, G. Ulrich, R. Ziessel, A. Kiss, P.-Y. Renard and A. Romieu, "Water-Soluble BODIPY Derivatives," *Organic Letters,* vol. 11, no. 10, pp. 2049-2052, 2009.

[135] T. Förster, "Experimentelle und theoretische untersuchung des zwischenmolecularen uebergangs von electronenanregungsenergie," *Z. Naturforsch,* vol. 4a, pp. 321, 1949.

[136] D. L. Dexter, "A theory of sensitized luminescence in solids," *Journal of Chemical Physics,* vol. 21, no. 5, pp. 836-851,1953.

[137] A. Coskun, and E. U. Akkaya, "Difluorobora-s-diazaindacene dyes as highly selective dosimetric reagents for fluoride anions," *Tetrahedron Letters,* vol. 45, no. 25, pp. 4947-4949, 2004.

[138] C. J. Hawker, and J. M. J. Frechet, "Preparation of polymers with controlled molecular architecture. A new convergent approach to dendritic macromolecules," *Journal of the American Chemical Society,* vol. 112, no. 21, pp. 7638-7647, 1990.

[139] D. V. Roberts, B. P. Wittmershaus, Y.-Z. Zhang, S. Sharon and M. P. Klinosky, "Efficient excitation energy transfer among multiple dyes in polystyrene microspheres," *Journal of Luminescence,* vol. 79, no. 4, pp. 225-231, 1998.

[140] S. Atilgan, T. Ozdemir, and E. U. Akkaya, "Selective Hg(II) sensing with improved stokes shift by coupling the internal charge transfer process to

excitation energy transfer," *Organic Letters,* vol. 12, no. 21, pp. 4792-4795, 2010.

[141] A. Hagfeldt, and M. Graetzel, "Light-induced redox reactions in nanocrystalline systems," *Chemical Reviews,* vol. 95, no. 1, pp. 49-68, 1995.

[142] P. V. Kamat, "Photochemistry on nonreactive and reactive (semiconductor) surfaces," *Chemical Reviews,* vol. 93, no. 1, pp. 267-300, 1993.

[143] K. Sayama, H. Sugihara, and H. Arakawa, "Photoelectrochemical properties of a porous Nb_2O_5 electrode sensitized by a ruthenium dye," *Chemistry of Materials,* vol. 10, no. 12, pp. 3825-3832, 1998.

[144] J. B. Asbury, E. Hao, Y. Wang, H. N. Ghosh and T. Lian, "Ultrafast electron transfer dynamics from molecular adsorbates to semiconductor nanocrystalline thin films," *The Journal of Physical Chemistry B,* vol. 105, no. 20, pp. 4545-4557, 2001.

[145] A. Yella, H. W. Lee, H. N. Tsao, C. Y. Yi, A. K. Chandiran, M .K. Nazeeruddin, E. W. G. Diau, C. Y. Yeh, S. M. Zakeeruddin and M. Gratzel, "Porphyrin-sensitized solar cells with cobalt (II/III)-based redox electrolyte exceed 12 percent efficiency," *Science,* vol. 334, no. 6056, pp. 629-634, 2011.

[146] Z. A. Siddique, Y. Yamamoto, T. Ohno and K. Nozaki, "Structure-dependent photophysical properties of singlet and triplet metal-to-ligand charge transfer states in copper(I) bis(diimine) compounds," *Inorganic Chemistry,* vol. 42, no. 20, pp. 6366-6378, 2003.

[147] G. B. Shaw, C. D. Grant, H. Shirota, E. W. Castner, G. J. Meyer and L. X. Chen, "Ultrafast structural rearrangements in the mlct excited state for copper(I) bis-phenanthrolines in solution," *Journal of the American Chemical Society,* vol. 129, no. 7, pp. 2147-2160, 2007.

[148] P. Yang, Y. Yang, C. Zhang, X.-J. Yang, H.-M. Hu, Y. Gao and B. Wu, "Synthesis, structure, and catalytic ethylene oligomerization of nickel(II) and cobalt(II) complexes with symmetrical and unsymmetrical 2,9-diaryl-1,10-phenanthroline ligands," *Inorganica Chimica Acta,* vol. 362, no. 1, pp. 89-96, 2009.

[149] J. V. Lockard, S. Kabehie, J. I. Zink, G. Smolentsev, A. Soldatov and L. X. Chen, "Influence of ligand substitution on excited state structural dynamics in cu(I) bisphenanthroline complexes†," *The Journal of Physical Chemistry B,* vol. 114, no. 45, pp. 14521-14527, 2010.

[150] D. R. McMillin, J. R. Kirchhoff, and K. V. Goodwin, "Exciplex quenching of photo-excitd copper complexes," *Coordination Chemistry Reviews,* vol. 64, no. 0, pp. 83-92, 1985.

[151] E. M. Kober, J. V. Caspar, R. S. Lumpkin and T .J. Meyer., "Application of the energy gap law to excited-state decay of osmium(II)-polypyridine complexes: calculation of relative nonradiative decay rates from emission spectral profiles," *The Journal of Physical Chemistry,* vol. 90, no. 16, pp. 3722-3734, 1986.

[152] C. Bauer, P. Jacques, and A. Kalt, "Investigation of the interaction between a sulfonated azo dye (AO7) and a TiO_2 surface," *Chemical Physics Letters,* vol. 307, no. 5–6, pp. 397-406, 1999.

[153] E. Palomares, J. N. Clifford, S. A. Haque, T. Lutz and J. R. Durrant, "Control of charge recombination dynamics in dye sensitized solar cells by the use of conformally deposited metal oxide blocking layers," *Journal of the American Chemical Society,* vol. 125, no. 2, pp. 475-482, 2002.

[154] D. C. Hurum, A. G. Agrios, K. A. Gray, T. Rajh and M .C. Thurnauer, "Explaining the enhanced photocatalytic activity of degussa P25 mixed-phase TiO_2 using EPR," *The Journal of Physical Chemistry B,* vol. 107, no. 19, pp. 4545-4549, 2003.

[155] M. Geoffroy, M. Wermeille, C. O. Buchecker, J.-P. Sauvage and G. Bernardinelli, "Copper(I) and copper(II) complexes of entwined or interlocked phenanthroline type ligands: ESR and crystallographic investigations," *Inorganica Chimica Acta,* vol. 167, no. 2, pp. 157-164, 1990.

[156] M. Iwamura, S. Takeuchi, and T. Tahara, "Real-time observation of the photoinduced structural change of bis(2,9-dimethyl-1,10-phenanthroline)copper(I) by femtosecond fluorescence spectroscopy: A realistic potential curve of the jahn−teller distortion," *Journal of the American Chemical Society,* vol. 129, no. 16, pp. 5248-5256, 2007.

[157] C. O. Dietrich-Buchecker, P. A. Marnot, J.-P. Sauvage, J. R. Kirchhoff and D. R. McMillin, "Bis(2,9-diphenyl-1,10-phenanthroline)copper(I): a copper complex with a long-lived charge-transfer excited state," *Journal of the Chemical Society, Chemical Communications*, vol. 0, no. 9, pp. 513-515, 1983.

[158] A. Safrany, R. Gao, and J. Rabani, "Optical properties and reactions of radiation ınduced TiO_2 electrons in aqueous colloid solutions," *The Journal of Physical Chemistry B*, vol. 104, no. 24, pp. 5848-5853, 2000.

[159] L. X. Chen, G. Jennings, T. Liu, D .J. Gosztola, J. P. Hessler, D. V. Scaltrito and G. J. Meyer, "Rapid excited-state structural reorganization captured by pulsed X-rays," *Journal of the American Chemical Society*, vol. 124, no. 36, pp. 10861-10867, 2002.

[160] L. X. Chen, G. B. Shaw, I. Novozhilova, T. Liu, G. Jennings, K. Attenkofer, G. J . Meyer and P. Coppens, "MLCT state structure and dynamics of a copper(I) diimine complex characterized by pump−probe X-ray and laser spectroscopies and DFT calculations," *Journal of the American Chemical Society*, vol. 125, no. 23, pp. 7022-7034, 2003.

[161] L. S. Kau, D. J. Spira-Solomon, J. E. Penner-Hahn, K. O. Hodgson and E. I. Solomon, "X-ray absorption edge determination of the oxidation state and coordination number of copper. Application to the type 3 site in Rhus vernicifera laccase and its reaction with oxygen," *Journal of the American Chemical Society*, vol. 109, no. 21, pp. 6433-6442, 1987.

[162] A. C. Bhasikuttan, M. Suzuki, S. Nakashima and T. Okada,, "Ultrafast fluorescence detection in Tris(2,2'-bipyridine)ruthenium(II) complex in solution: relaxation dynamics involving higher excited states," *Journal of the American Chemical Society*, vol. 124, no. 28, pp. 8398-8405, 2002.

[163] O. Bräm, F. Messina, A.M. El-Zohry, A. Cannizzo and M. Chergui, "Polychromatic femtosecond fluorescence studies of metal–polypyridine complexes in solution," *Chemical Physics*, vol. 393, no. 1, pp. 51-57, 2012.

[164] A. R. Pease, J. O. Jeppesen, J. F. Stoddart, Y. Luo, C. P. Collier and J. R. Heath, "Switching devices based on interlocked molecules," *Accounts of Chemical Research*, vol. 34, no. 6, pp. 433-444, 2001.

[165] S. J. Vella, J. Tiburcio, and S. J. Loeb, "Optically sensed, molecular shuttles driven by acid-base chemistry," *Chemical Communications,* vol. 0, no. 45, pp. 4752-4754, 2007.

[166] W.-Q. Deng, A. H. Flood, J. F. Stoddart and W. A. Goddard, "An electrochemical color-switchable RGB dye: tristable [2]catenane," *Journal of the American Chemical Society,* vol. 127, no. 46, pp. 15994-15995, 2005.

[167] S. Saha, and J. F. Stoddart, "Photo-driven molecular devices," *Chemical Society Reviews,* vol. 36, no. 1, pp. 77-92, 2007.

[168] H.-Y. Gong, B. M. Rambo, E. Karnas, V. M. Lynch, K. M. Keller and J. L. Sessler, "Environmentally responsive threading, dethreading, and fixation of anion-induced pseudorotaxanes," *Journal of the American Chemical Society,* vol. 133, no. 5, pp. 1526-1533, 2011.

[169] V. Balzani, M. Clemente-Leon, A. Credi, B. Ferrer, M. Venturi, A. H. Flood and J. F. Stoddart, "Autonomous artificial nanomotor powered by sunlight," *Proceedings of the National Academy of Sciences of the United States of America,* vol. 103, no. 5, pp. 1178-1183, 2006.

[170] R. M. Noyes, "Some models of chemical oscillators," *Journal of Chemical Education,* vol. 66, no. 3, pp. 190, 1989.

[171] A. N. Zaikin and A. M. Zhabotinsky, "Concentration wave propogation in two-dimensional liquid-phase self-oscillating system," *Nature(London),* vol. *225*, pp. 535, 1970.

[172] J.-M. Kern, L. Raehm, J.-P. Sauvage, B. Divisia-Blohorn and P.-L. Vidal, "Controlled molecular motions in copper-complexed rotaxanes: An XAS study," *Inorganic Chemistry,* vol. 39, no. 7, pp. 1555-1560, 2000.

[173] I. Matzusaki, J. H. Woodson and H. A. Liebhafsky, "pH and templated pulses during the periodic decomposition of hydrogen perioxide" *Bulletin of the Chemical Society of Japan, vol. 43, no. 10, pp. 3317, 1970.*

[174] G. Rabai, and M. T. Beck, "High-amplitude hydrogen ion concentration oscillation in the iodate-thiosulfate-sulfite system under closed conditions," *The Journal of Physical Chemistry,* vol. 92, no. 17, pp. 4831-4835, 1988.

[175] J. W. Lee, S. Samal, N. Selvapalam, H.-J. Kim and K. Kim, "Cucurbituril homologues and derivatives: New opportunities in supramolecular chemistry," *Accounts of Chemical Research,* vol. 36, no. 8, pp. 621-630, 2003.

[176] V. Ramalingam, and A. R. Urbach, "Cucurbit[8]uril rotaxanes," *Organic Letters,* vol. 13, no. 18, pp. 4898-4901, 2011.

[177] M. Freitag, L. Gundlach, P. Piotrowiak and E. Galoppini, "Fluorescence enhancement of di-p-tolyl viologen by complexation in cucurbit[7]uril," *Journal of the American Chemical Society,* vol. 134, no. 7, pp. 3358-3366, 2012.

[178] B. Turfan, and E. U. Akkaya, "Modulation of boradiazaindacene emission by cation-mediated oxidative PET," *Organic Letters,* vol. 4, no. 17, pp. 2857-2859, 2002.

[179] T. Ueno, Y. Urano, H. Kojima and T. Nagano, "Mechanism-Based Molecular Design of Highly Selective Fluorescence Probes for Nitrative Stress," *Journal of the American Chemical Society,* vol. 128, no. 33, pp. 10640-10641, 2006.

[180] V. Sindelar, S. Silvi, and A. E. Kaifer, "Switching a molecular shuttle on and off: simple, pH-controlled pseudorotaxanes based on cucurbit[7]uril," *Chemical Communications,* vol. 0, no. 20, pp. 2185-2187, 2006.

[181] H. J. Kim, W. S. Jeon, Y. H. Ko and K. Kim, "Inclusion of methylviologen in cucurbit 7 uril," *Proceedings of the National Academy of Sciences of the United States of America,* vol. 99, no. 8, pp. 5007-5011, 2002.

[182] L. Zeng, E.W. Miller, A. Pralle, E. Y. Isacoff and C. J. Chang, "A selective turn-on fluorescent sensor for imaging copper in living cells," *Journal of the American Chemical Society,* vol. 128, no. 1, pp. 10-11, 2005.

10. APPENDIX

^{1}H-NMR, ^{13}C-NMR and Mass Spectra of Compounds

10.1. Reaction Based Sensing of Fluoride Ions (CHAPTER 3)

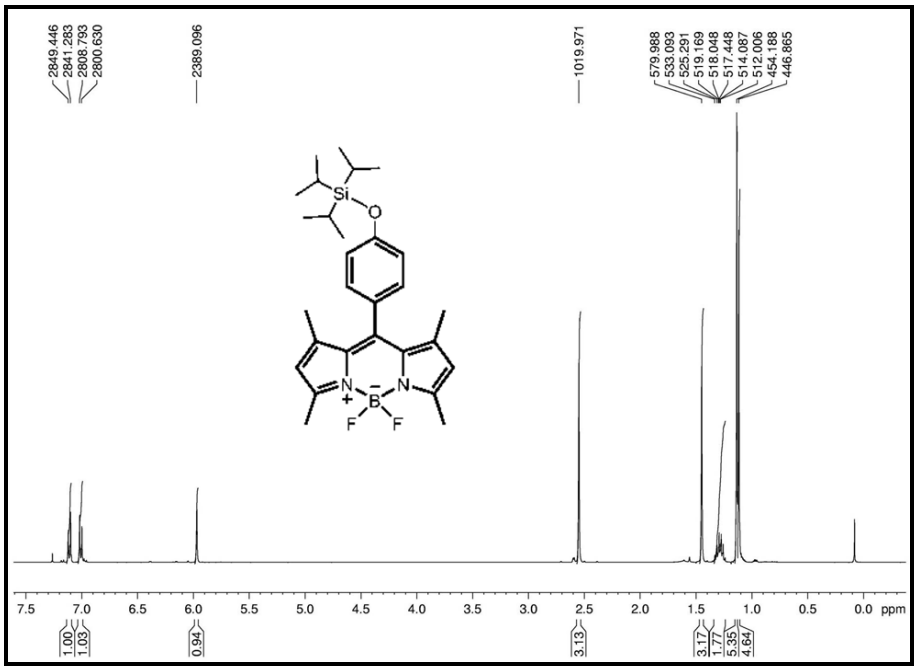

Figure A1. ^{1}H NMR spectrum of **55** (400 MHz, $CDCl_3$).

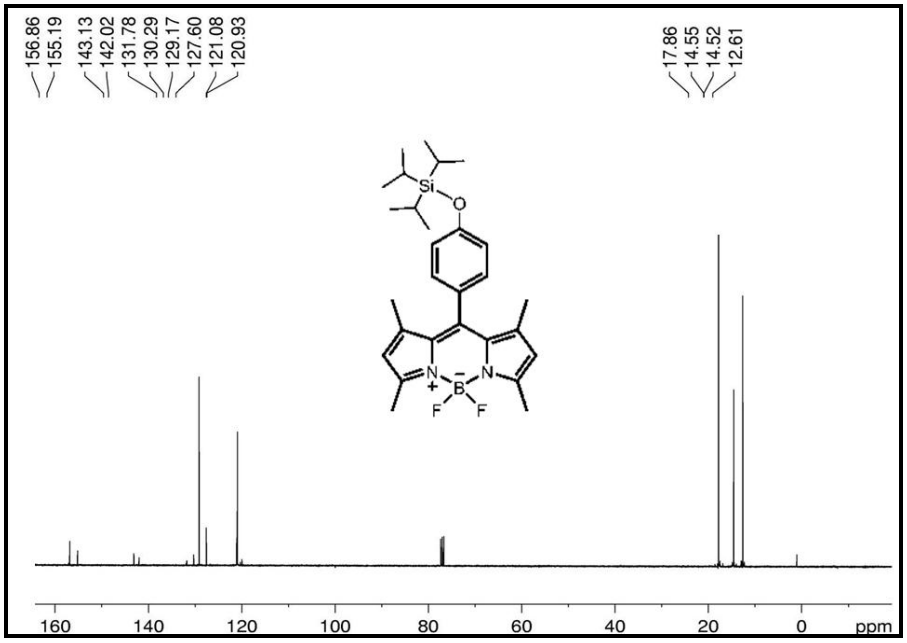

Figure A2. ^{13}C NMR spectrum of **55** (100 MHz, $CDCl_3$).

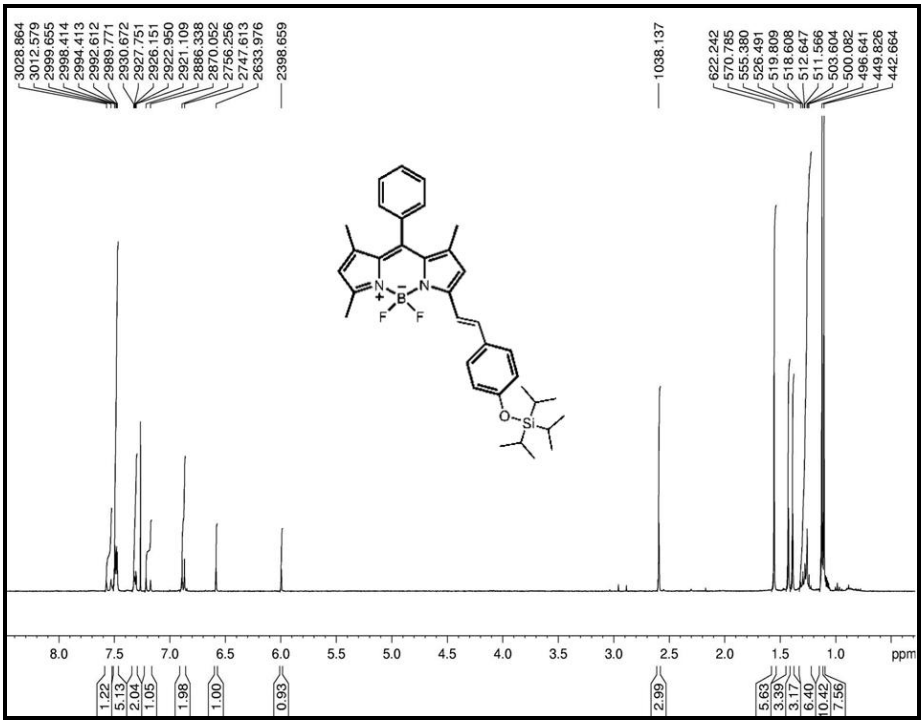

Figure A3. ^{1}H NMR spectrum of **56** (400 MHz, $CDCl_3$).

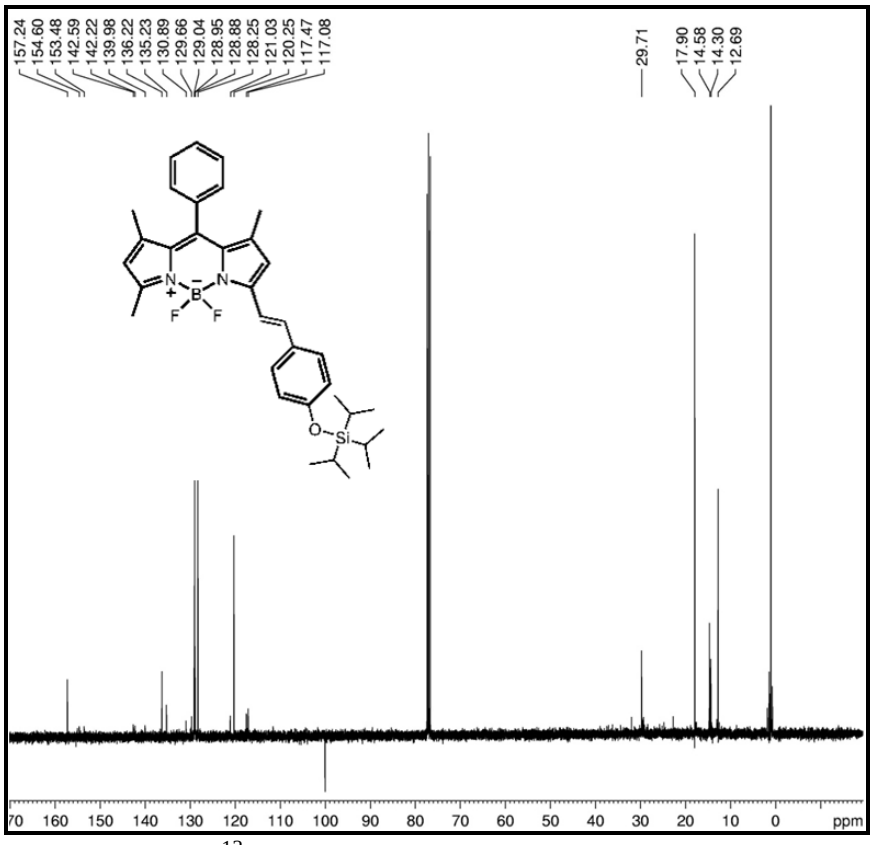

Figure A4. ^{13}C NMR spectrum of **56** (100 MHz, $CDCl_3$).

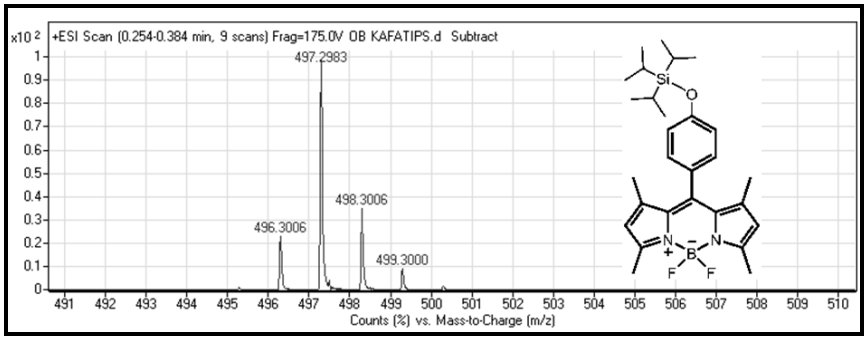

Figure A5. HR-Mass spectrum of (**55**)

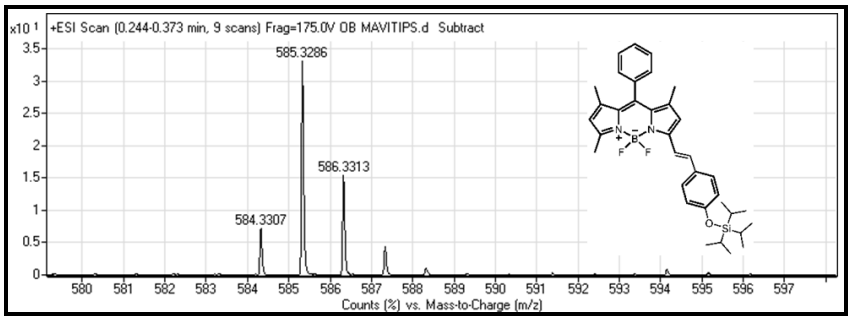

Figure A6. HR-Mass spectrum of (**56**)

10.2. Convenient Synthesis of Near IR Emitting Tetrastyryl-Bodipy Dyes (CHAPTER 4)

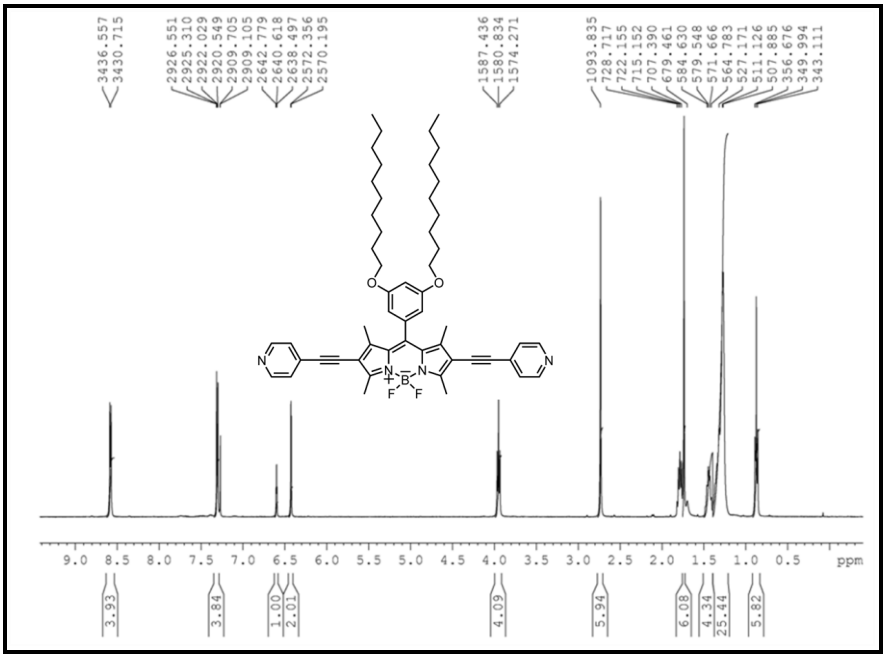

Figure A7. ^{1}H NMR spectrum of **60** (400 MHz, $CDCl_3$).

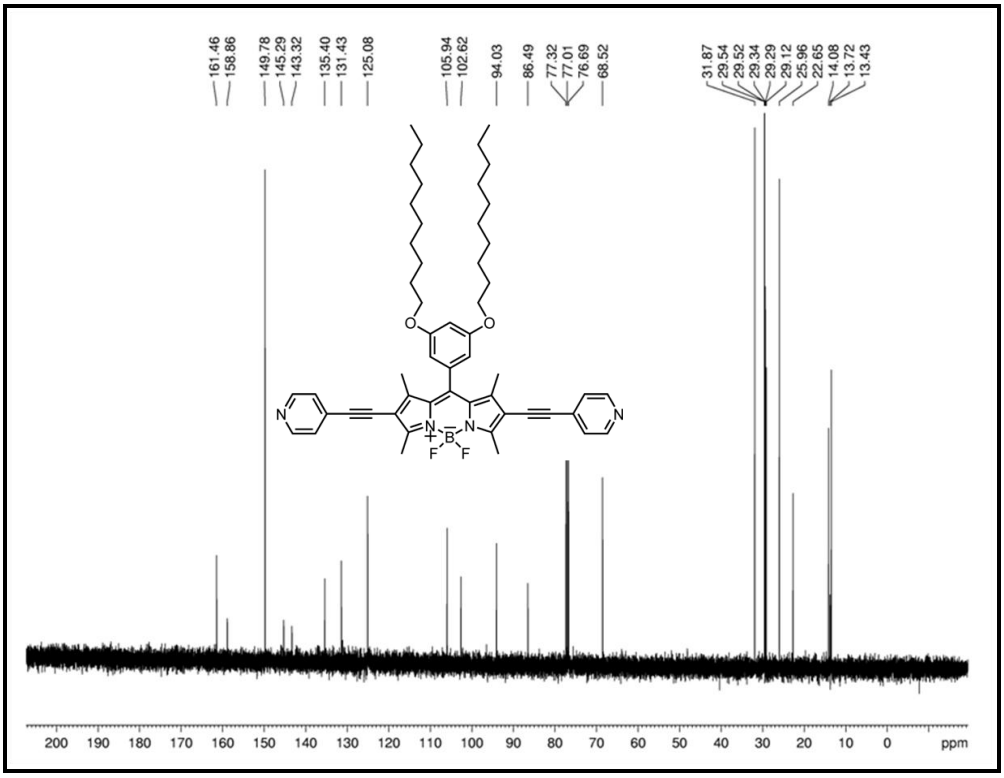

Figure A8. ^{13}C NMR spectrum of **60** (100 MHz, $CDCl_3$).

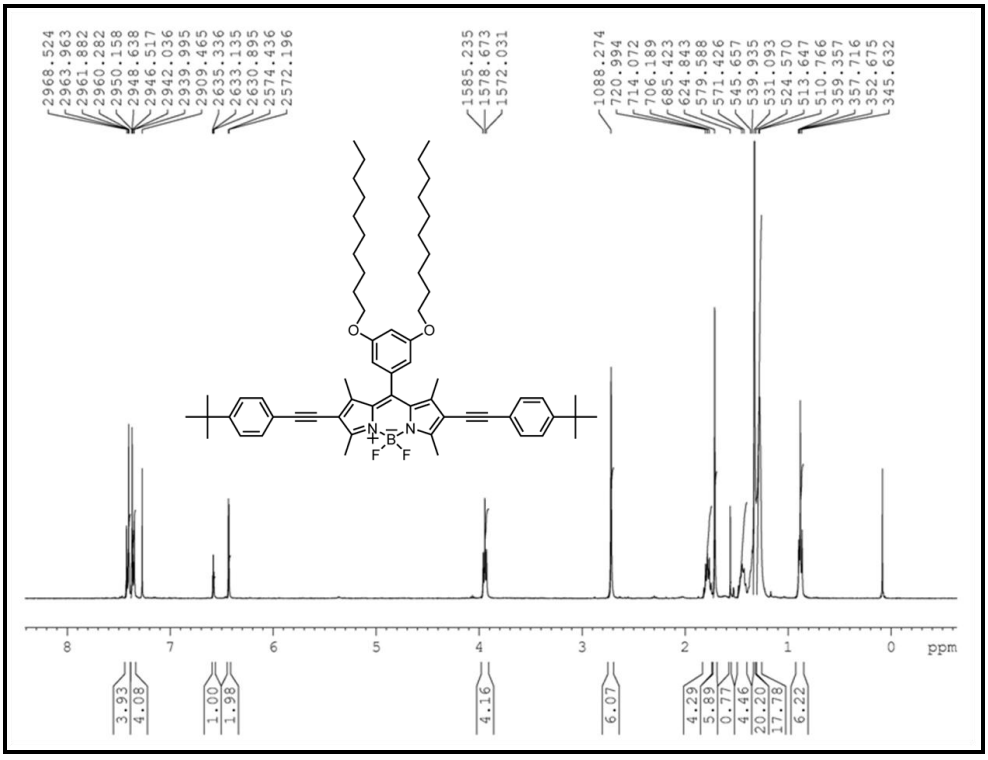

Figure A9. ^{1}H NMR spectrum of **61** (400 MHz, $CDCl_3$).

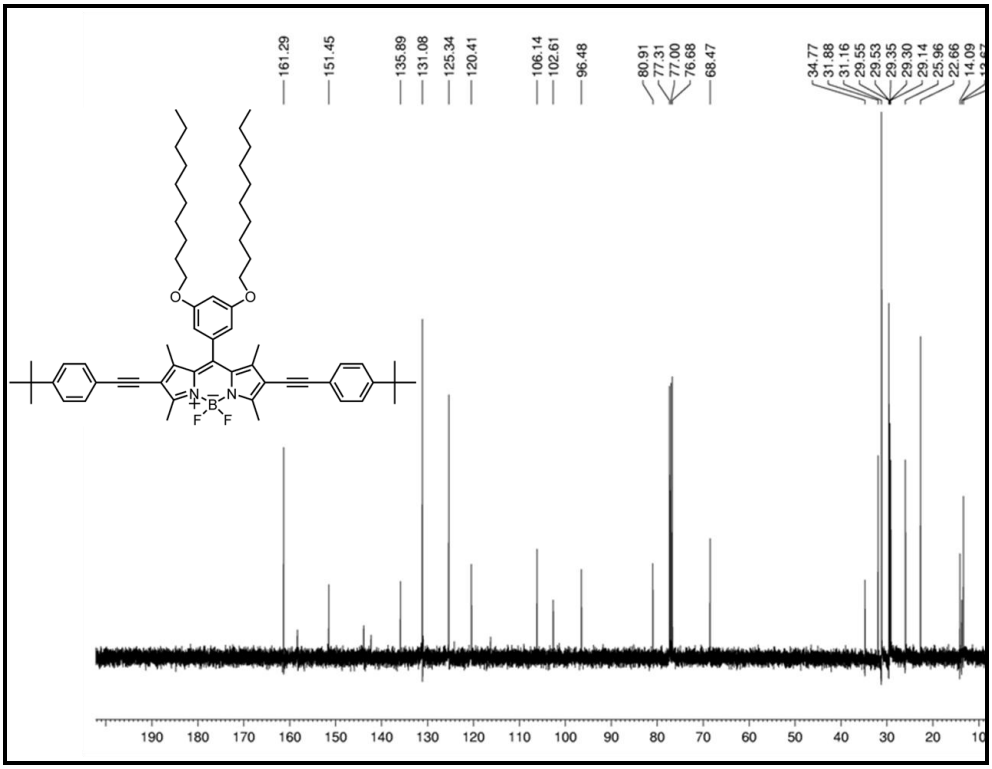

Figure A10. ^{13}C NMR spectrum of **61** (100 MHz, $CDCl_3$).

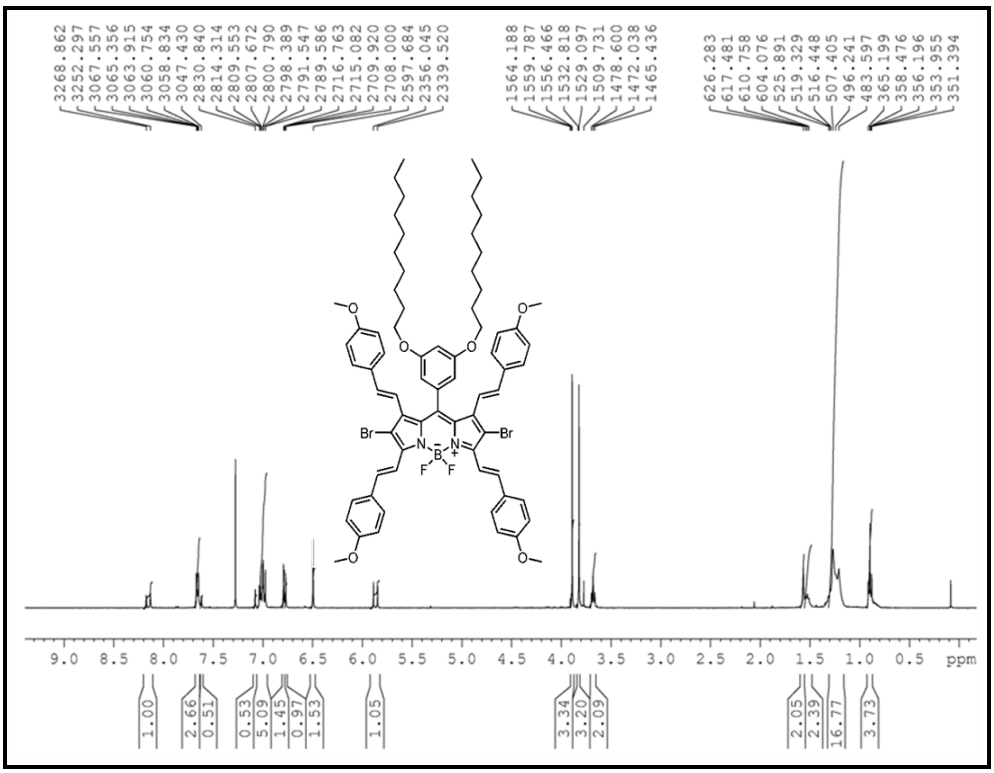

Figure A11. ^{1}H NMR spectrum of **62** (400 MHz, $CDCl_3$).

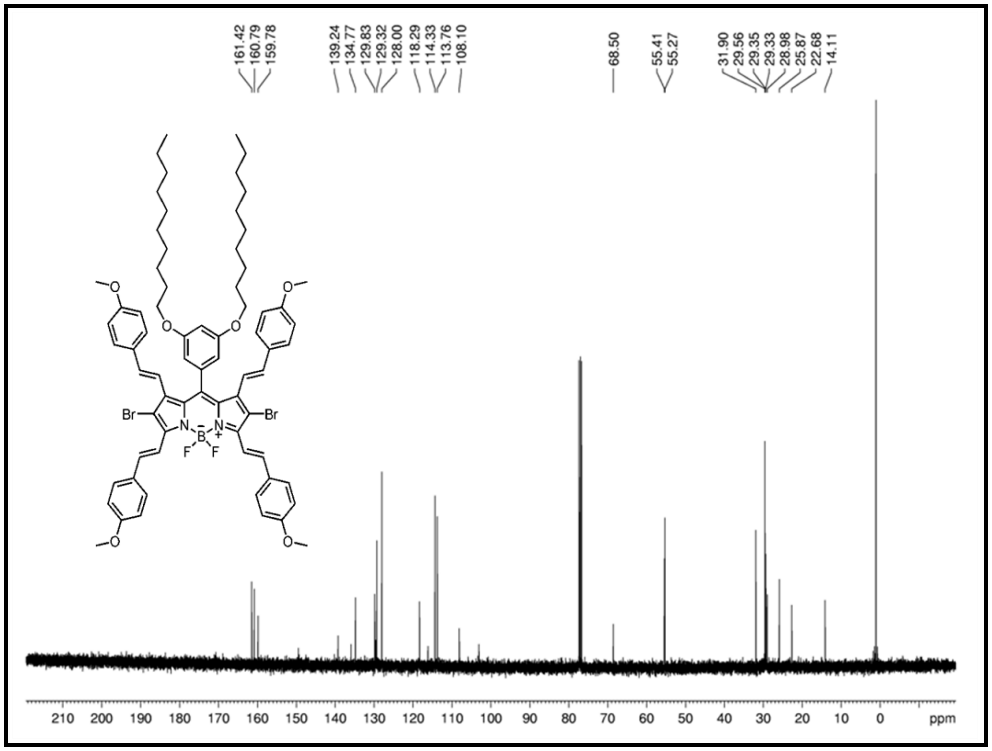

Figure A12. ^{13}C NMR spectrum of **62** (100 MHz, $CDCl_3$).

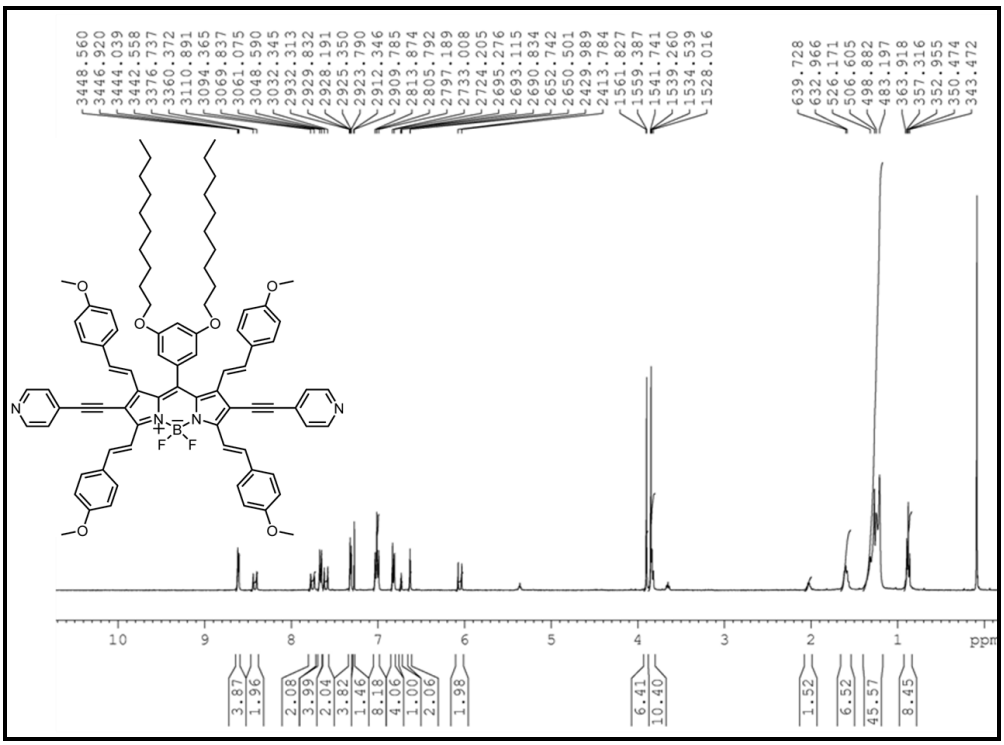

Figure A13. ^{1}H NMR spectrum of **63** (400 MHz, $CDCl_3$).

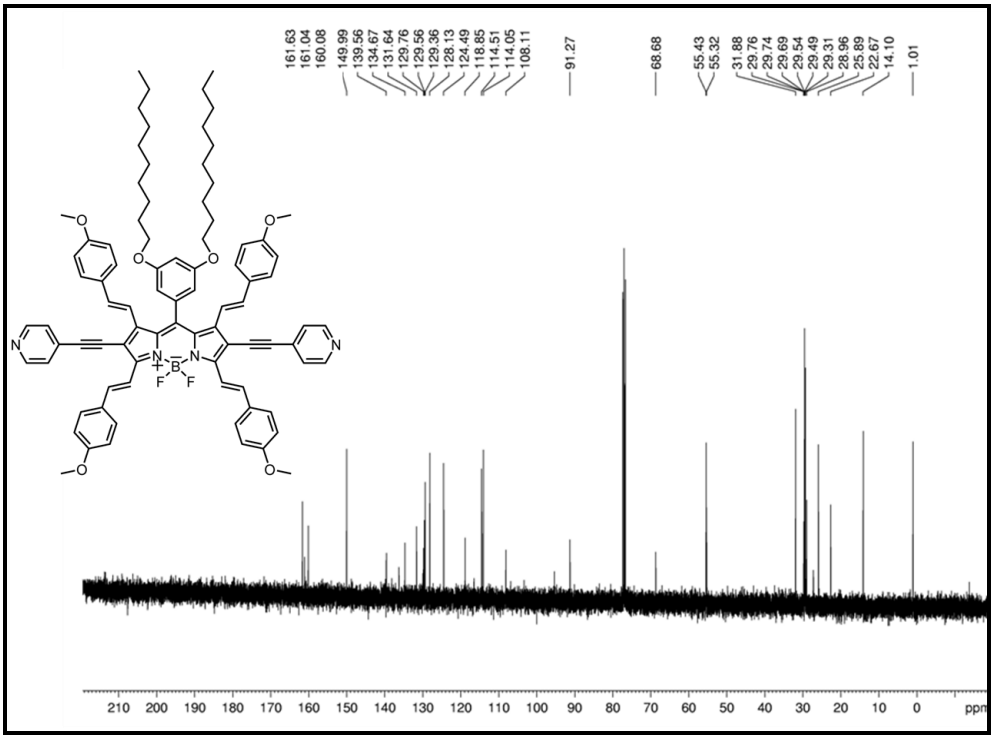

Figure A14. ^{13}C NMR spectrum of **63** (100 MHz, $CDCl_3$).

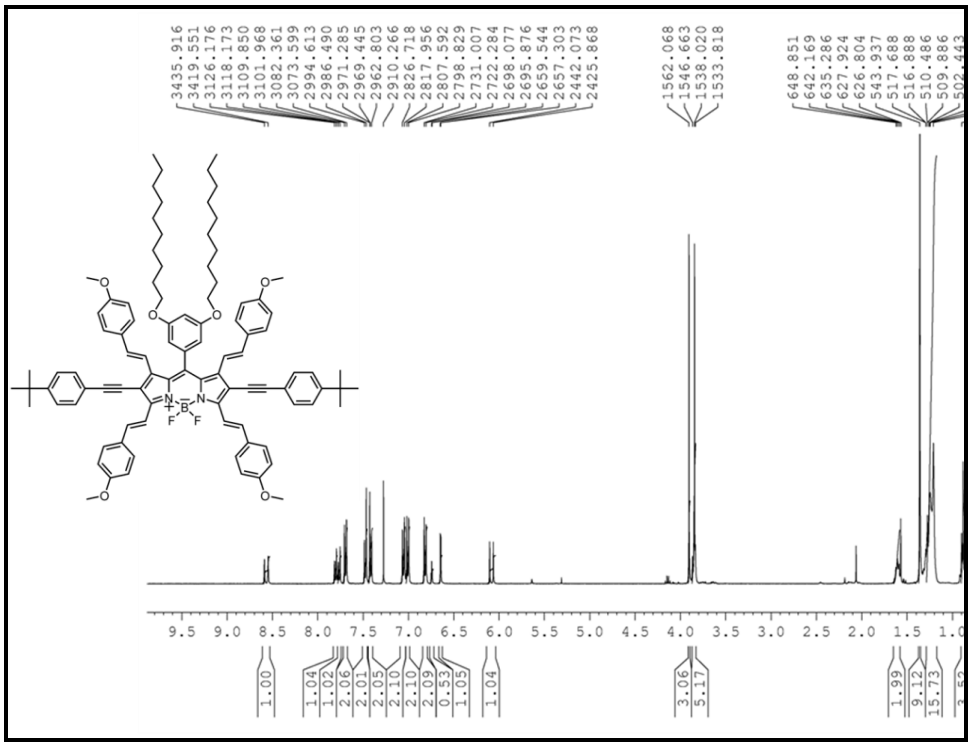

Figure A15. ^{1}H NMR spectrum of **64** (400 MHz, $CDCl_3$).

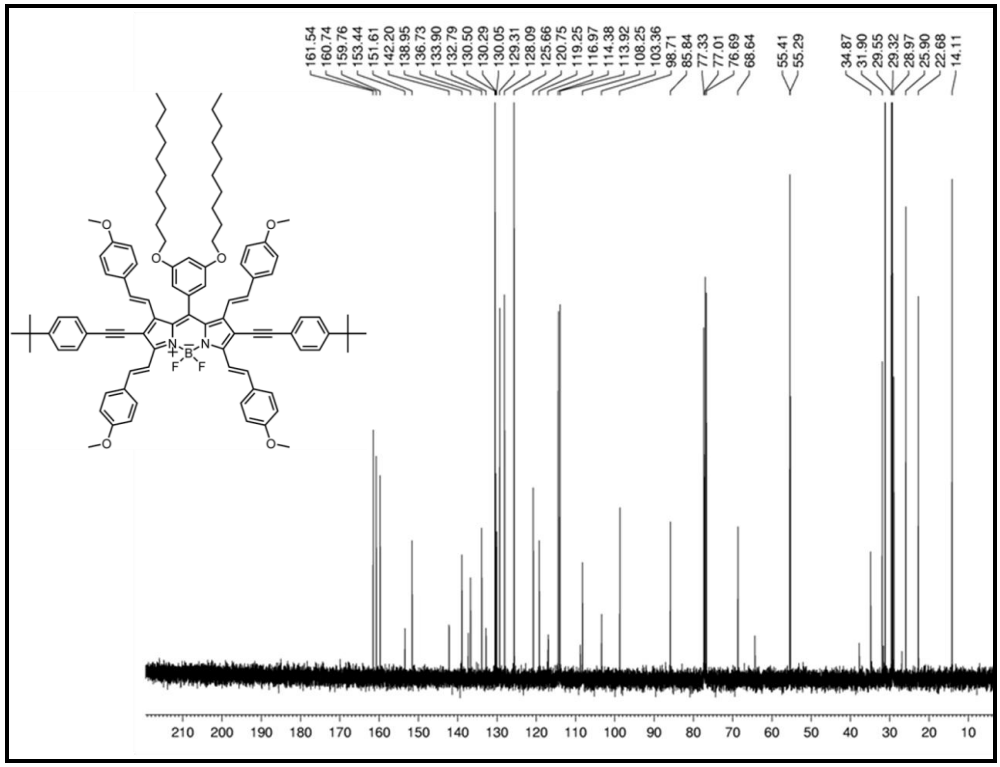

Figure A16. ^{13}C NMR spectrum of **64** (100 MHz, $CDCl_3$).

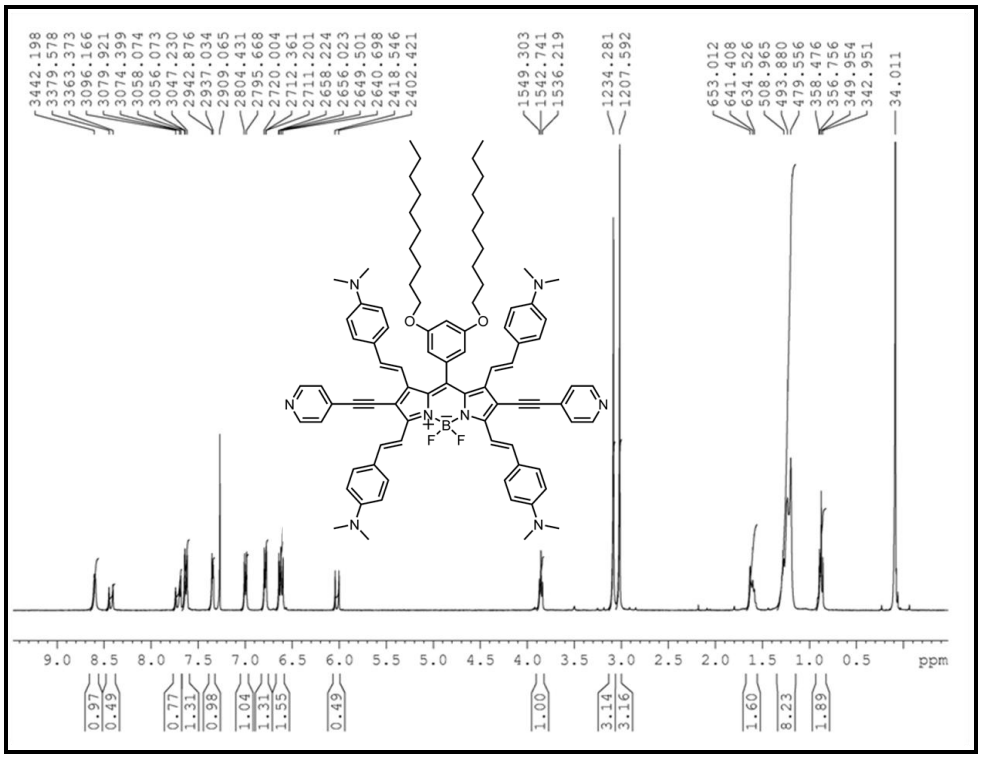

Figure A17. ^{1}H NMR spectrum of **65** (400 MHz, $CDCl_3$).

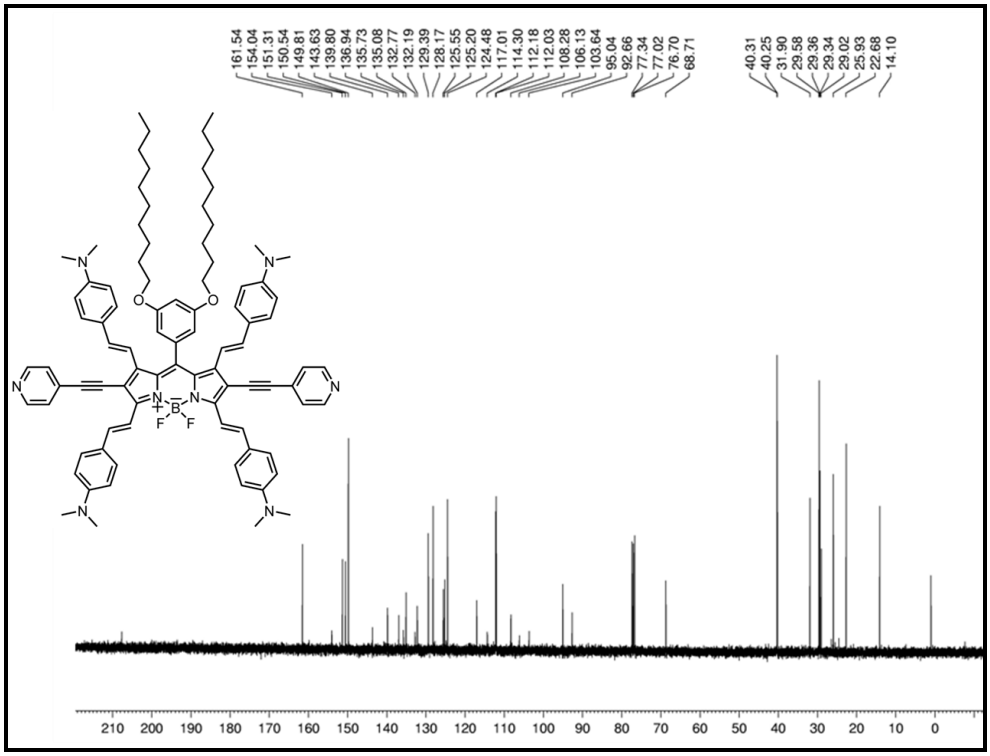

Figure A18. ^{13}C NMR spectrum of **65** (100 MHz, $CDCl_3$).

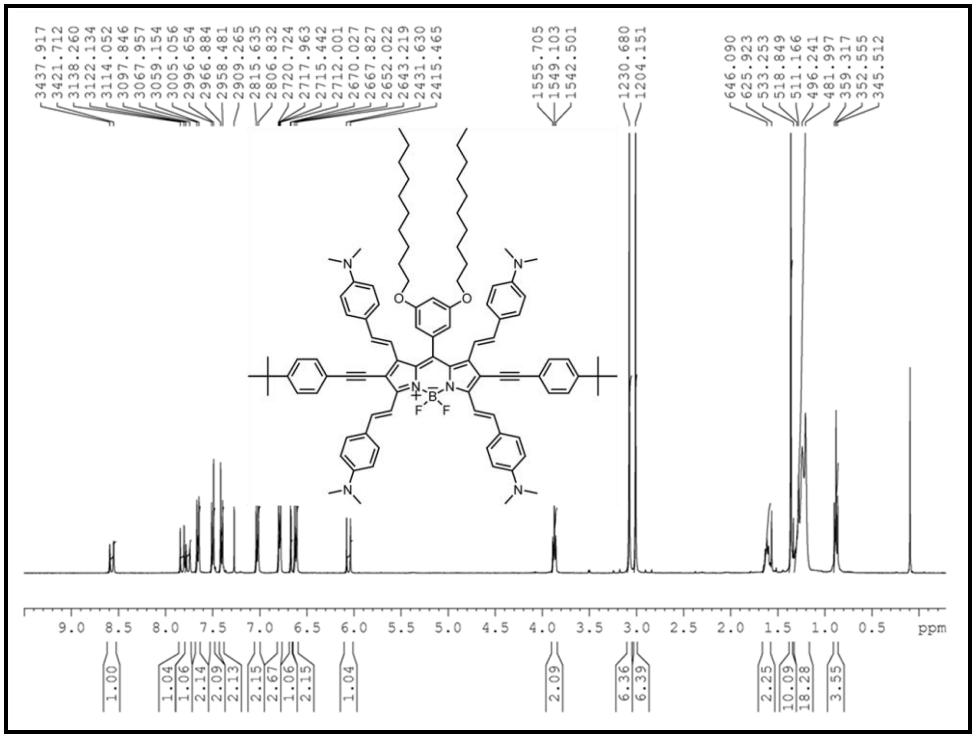

Figure A19. ^{1}H NMR spectrum of **66** (400 MHz, $CDCl_3$).

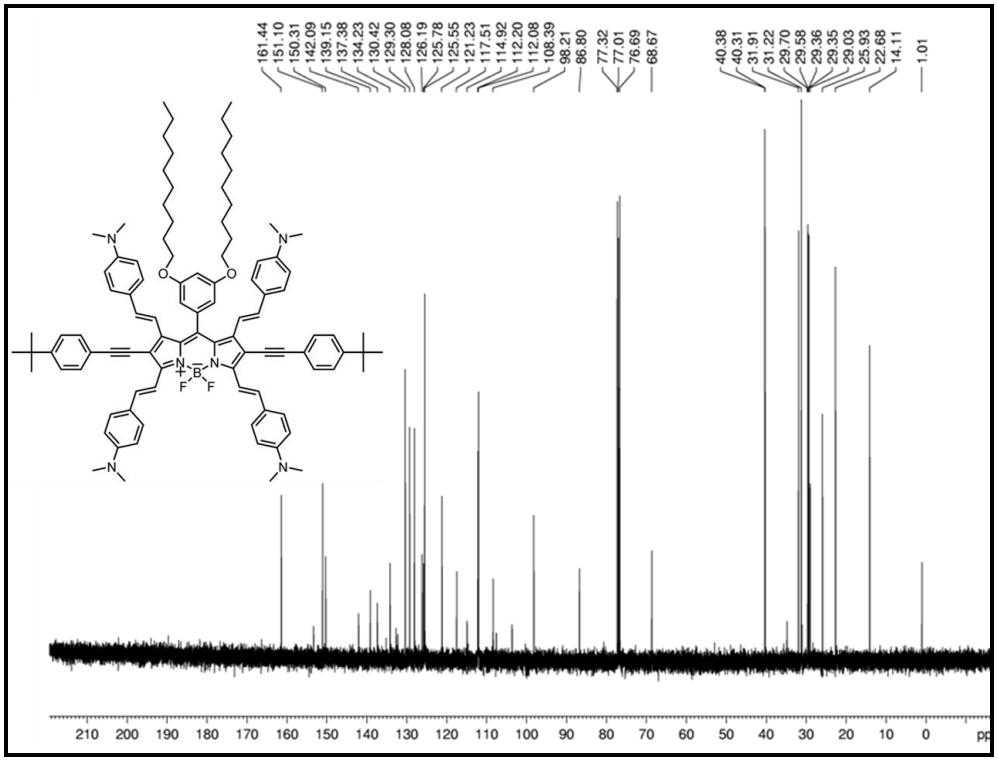

Figure A20. ^{13}C NMR spectrum of **66** (100 MHz, $CDCl_3$).

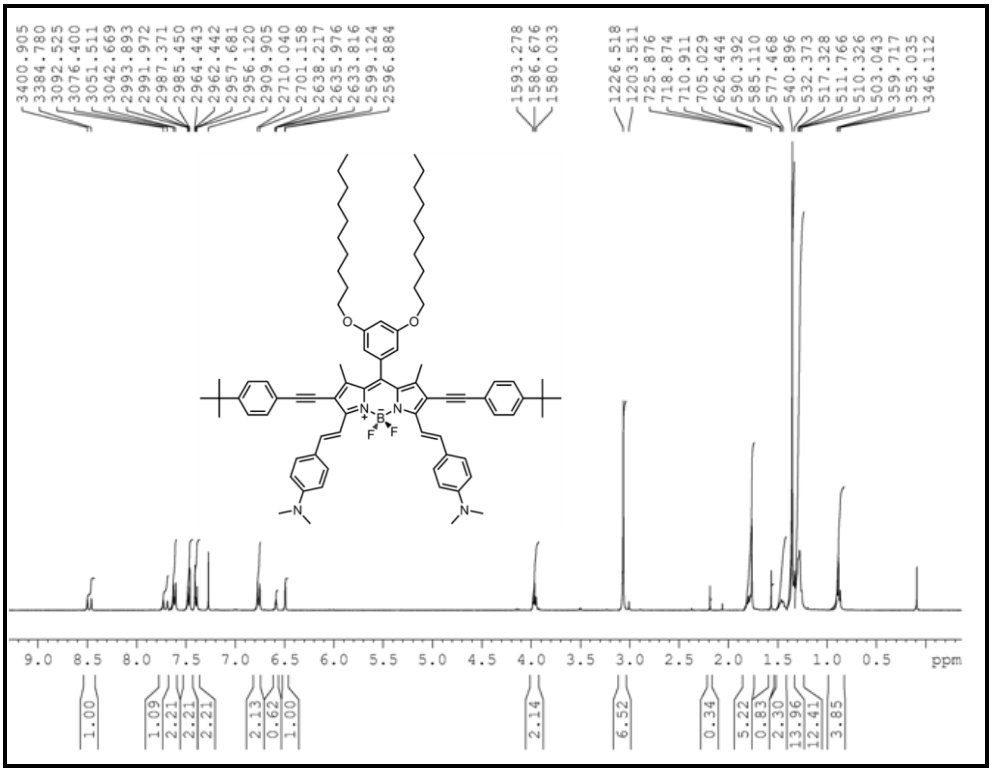

Figure A21. ^{1}H NMR spectrum of **67** (400 MHz, $CDCl_3$).

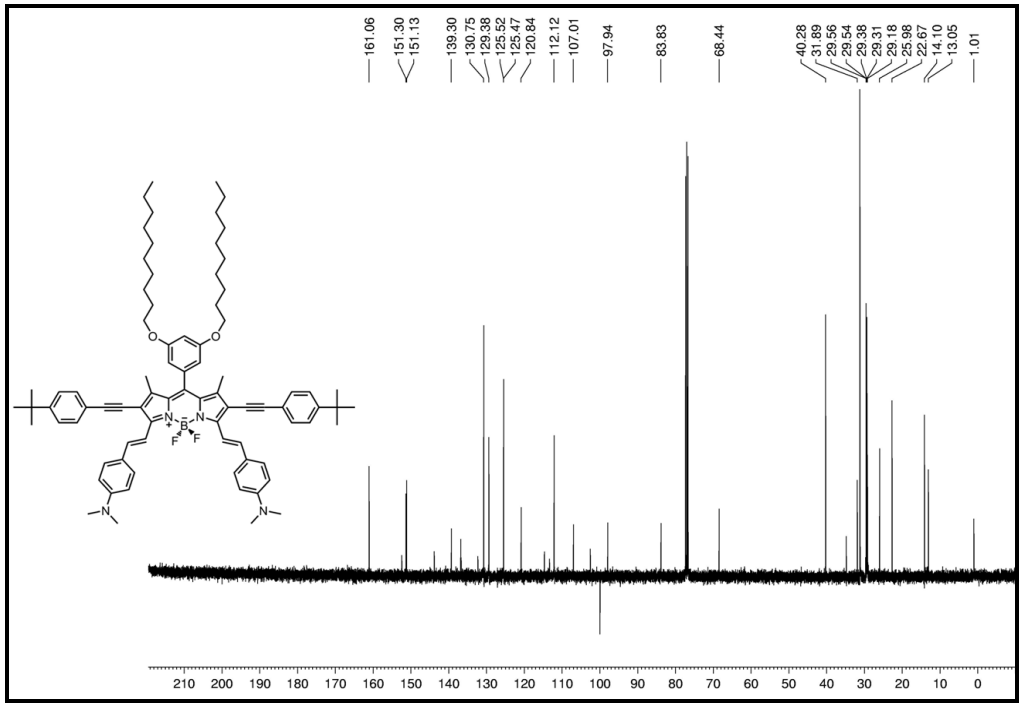

Figure A22. ^{13}C NMR spectrum of **67** (100 MHz, $CDCl_3$).

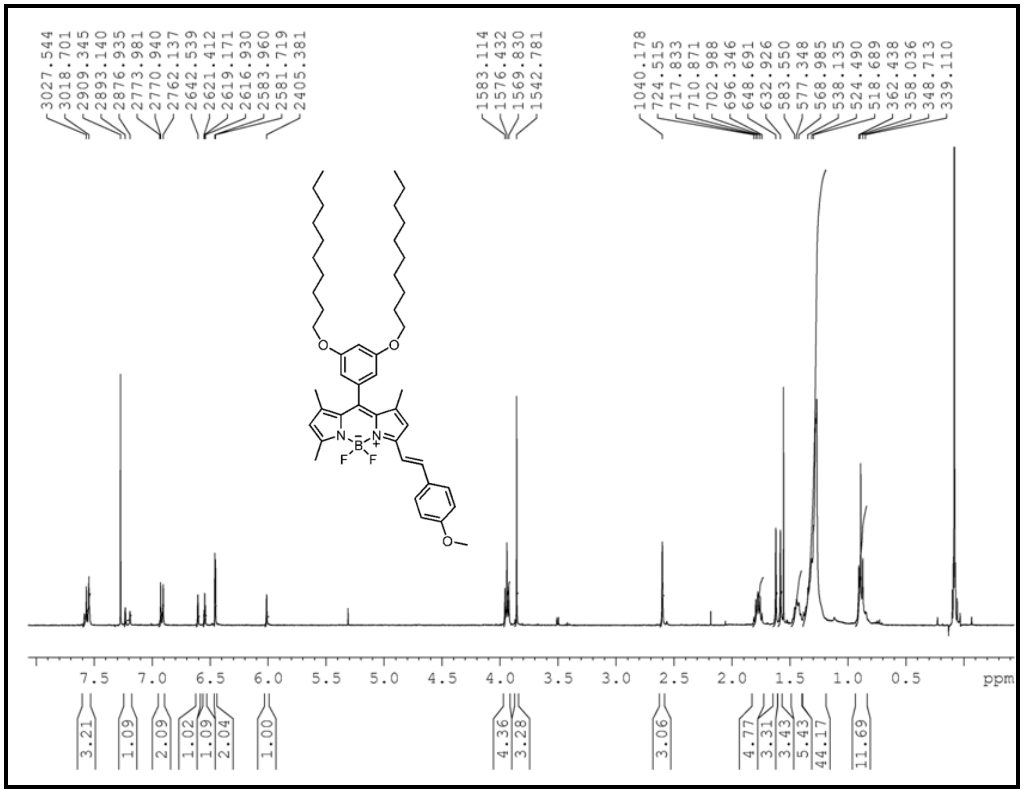

Figure A23. ^{1}H NMR spectrum of **68** (400 MHz, $CDCl_3$).

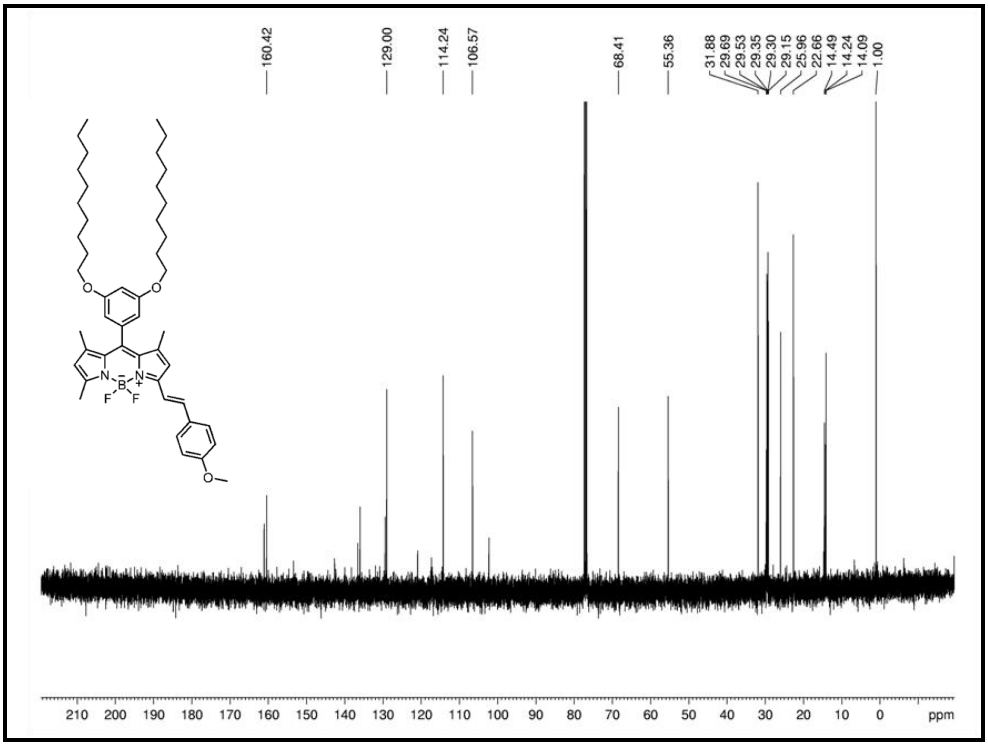

Figure A24. ^{13}C NMR spectrum of **68** (100 MHz, $CDCl_3$).

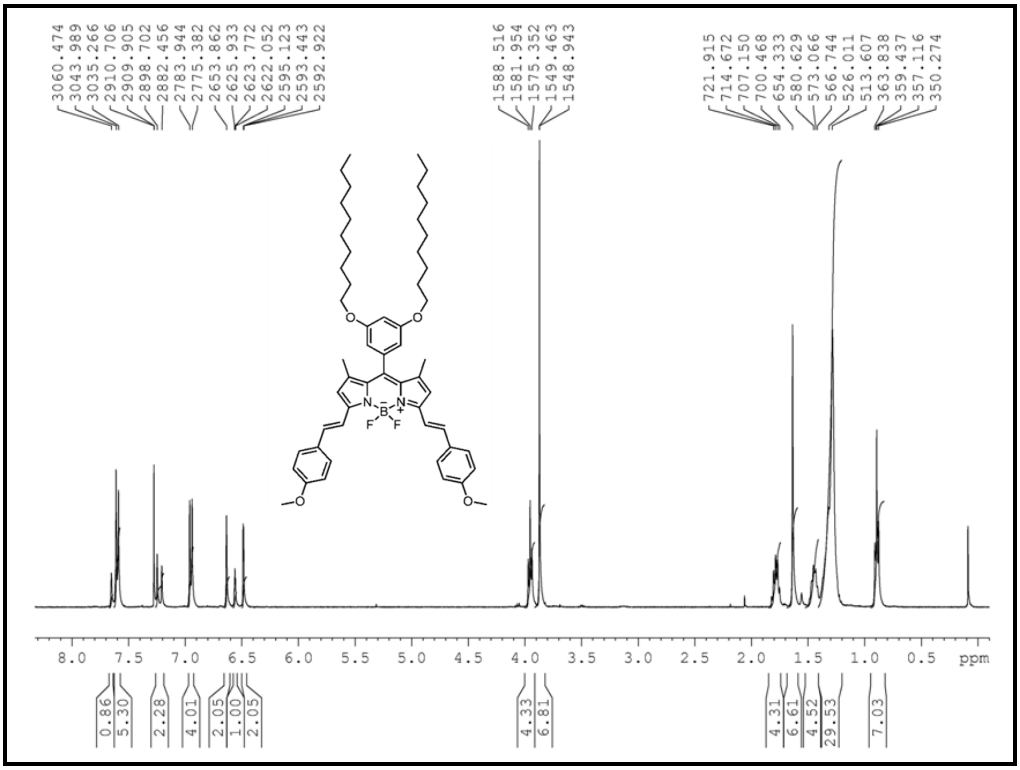

Figure A25. ^{1}H NMR spectrum of **69** (400 MHz, $CDCl_3$).

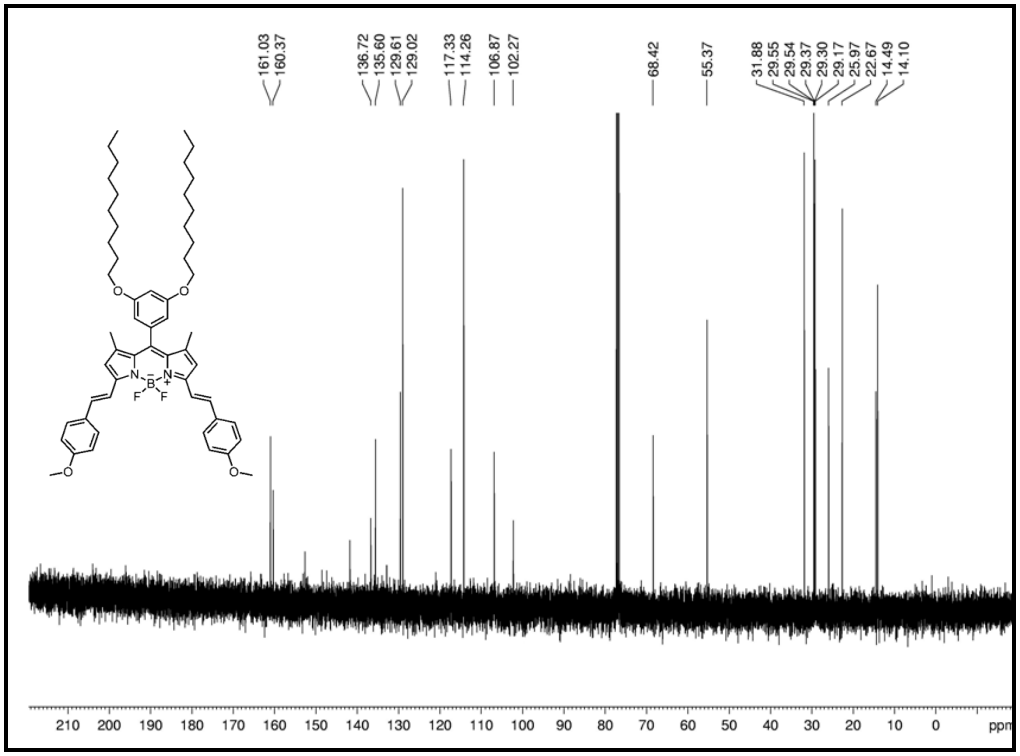

Figure A26. ^{13}C NMR spectrum of **69** (100 MHz, $CDCl_3$).

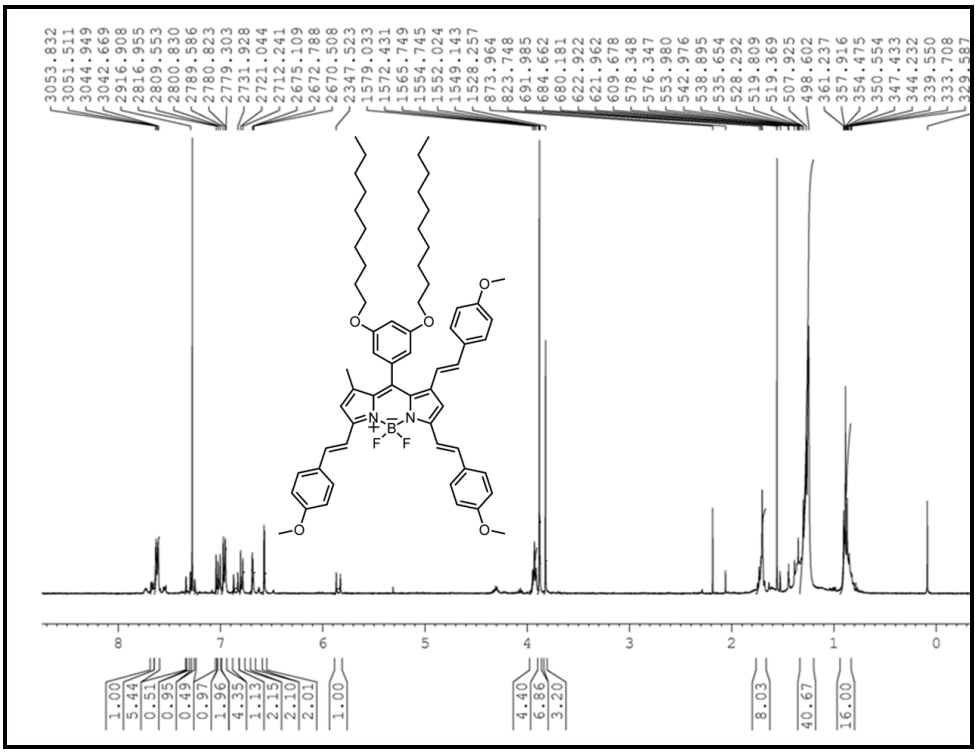

Figure A27. ^{1}H NMR spectrum of **70** (400 MHz, $CDCl_3$).

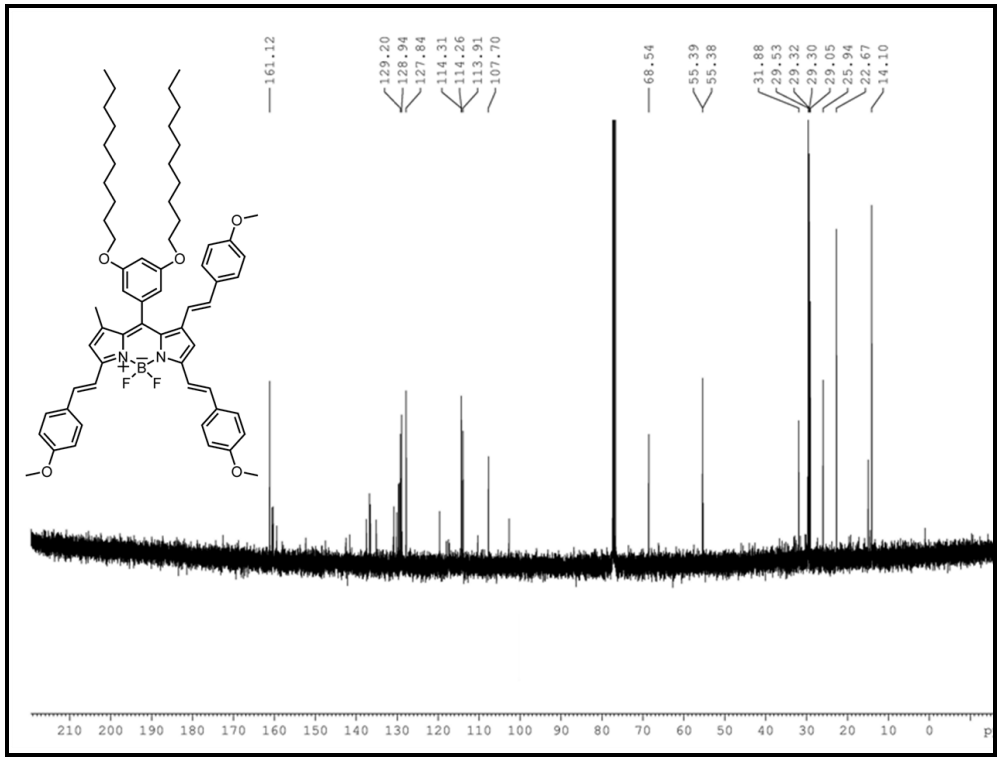

Figure A28. ^{13}C NMR spectrum of **70** (100 MHz, $CDCl_3$).

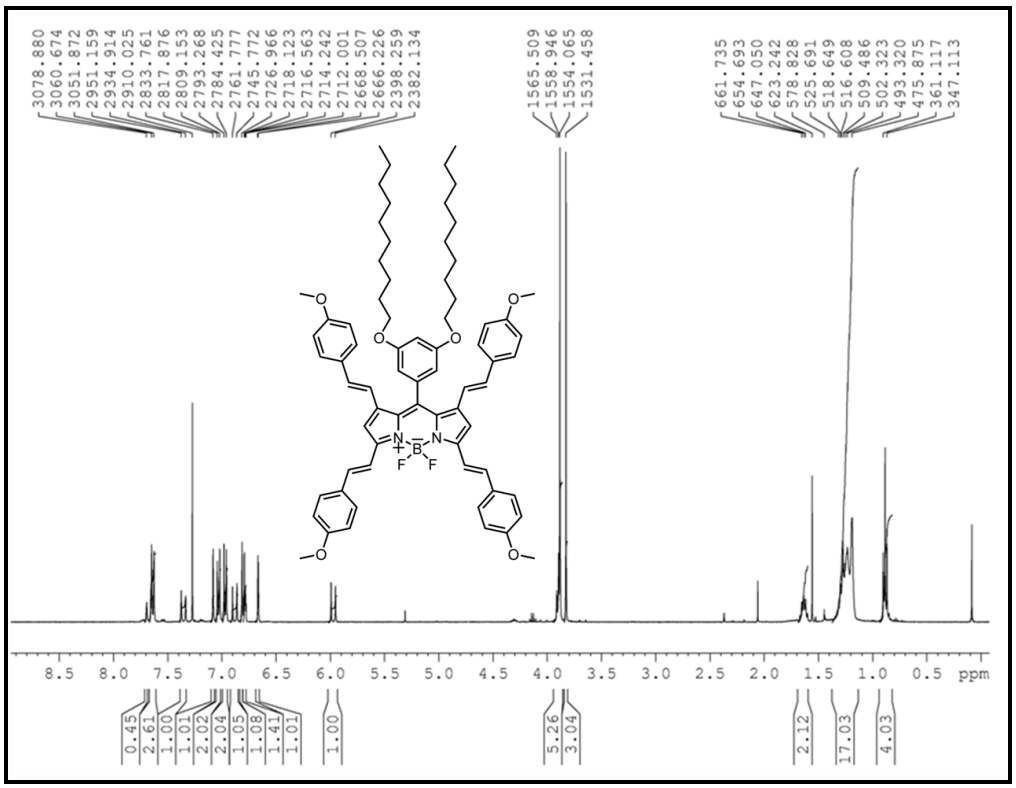

Figure A29. ^{1}H NMR spectrum of **71** (400 MHz, $CDCl_3$).

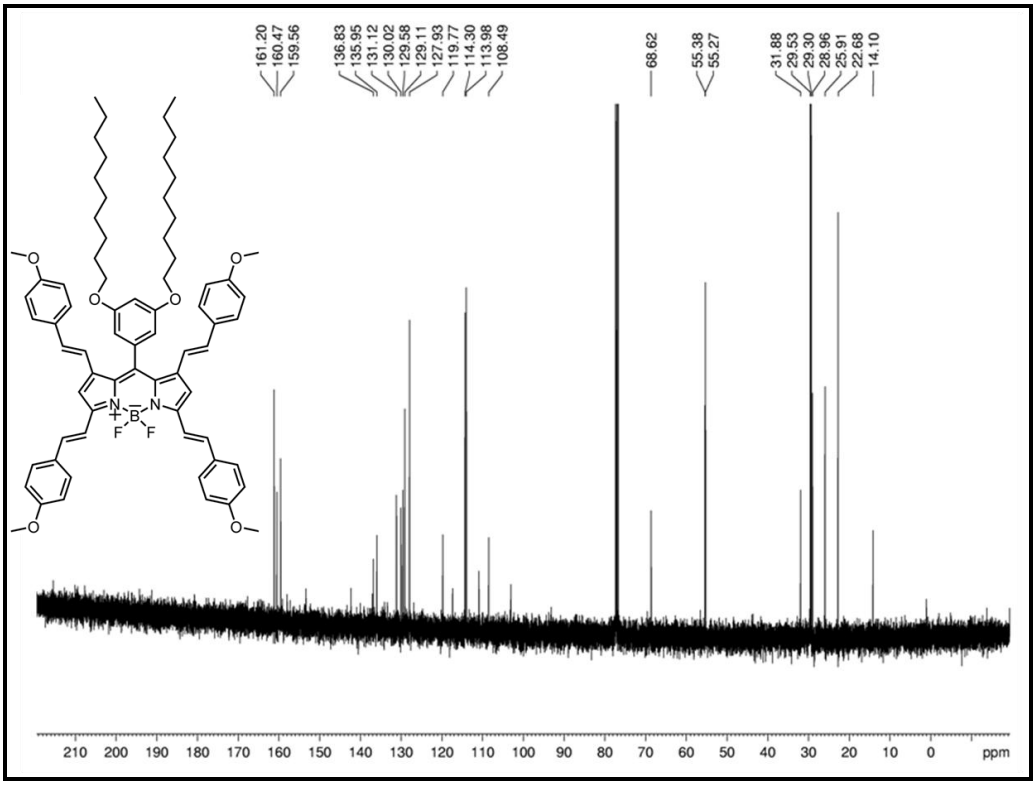

Figure A30. ^{13}C NMR spectrum of **71** (100 MHz, $CDCl_3$).

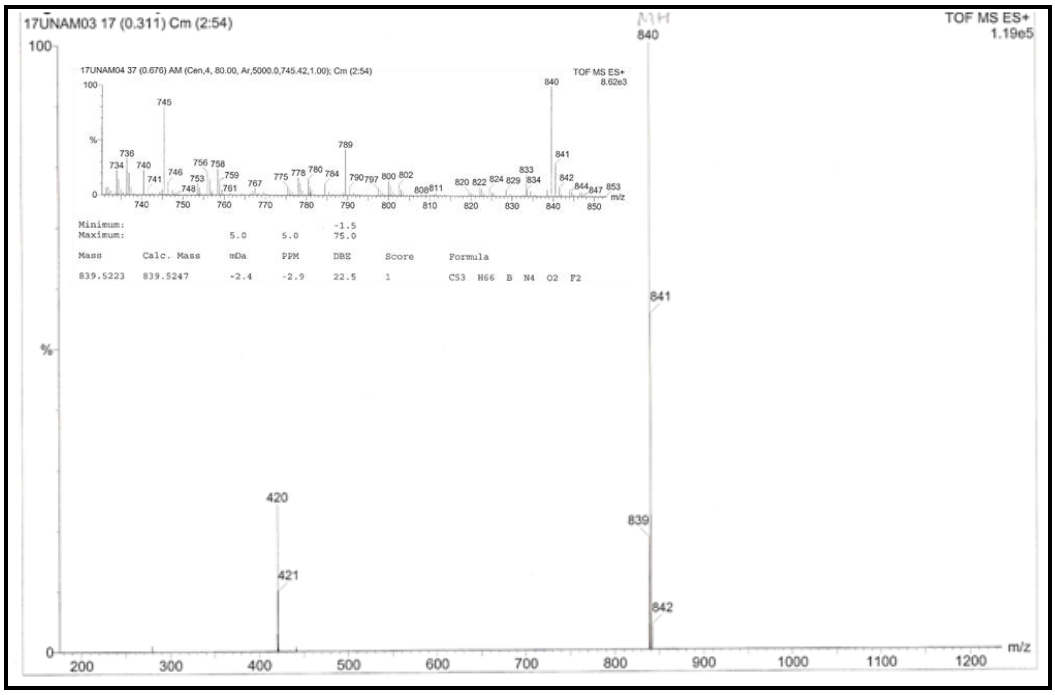

Figure A31. Mass Spectrum of **60**

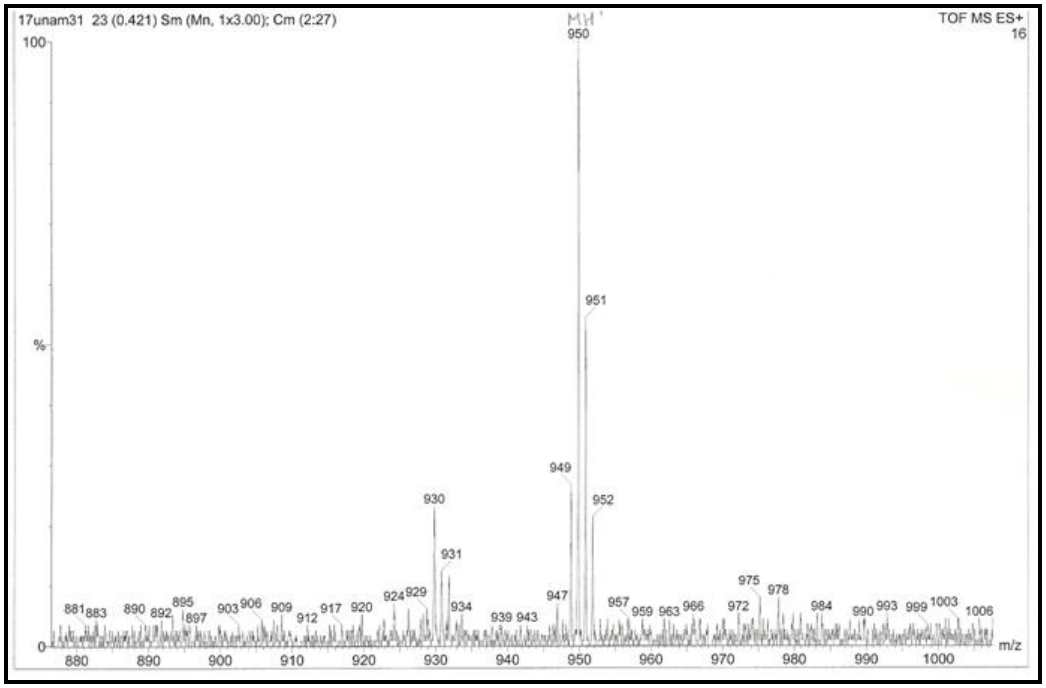

Figure A32. Mass Spectrum of **61**

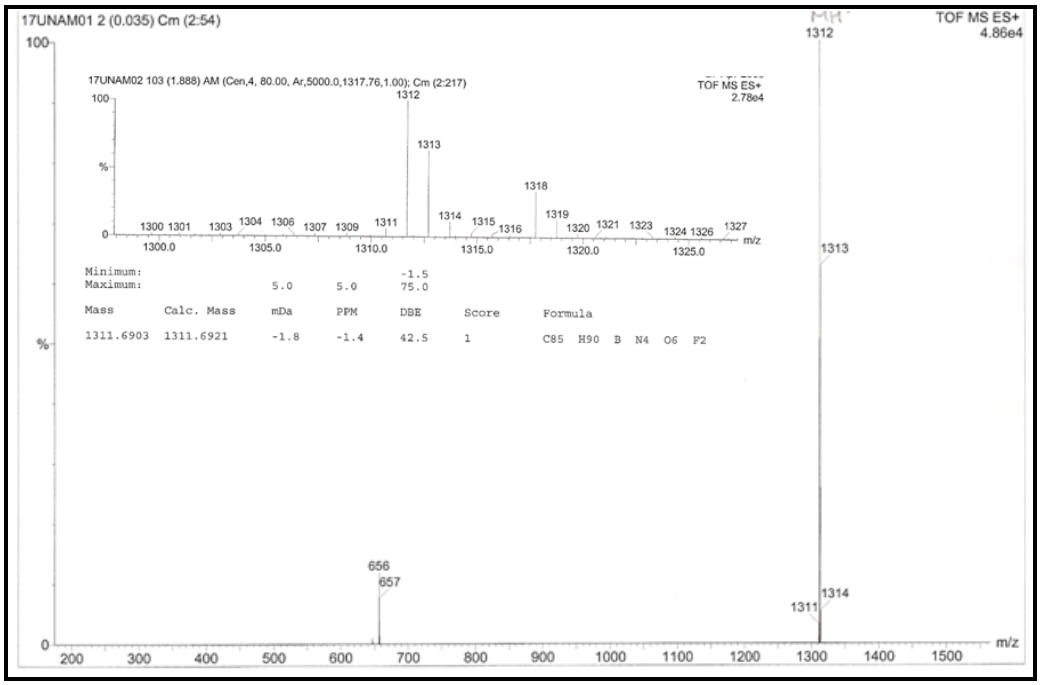

Figure A33. Mass Spectrum of **63**

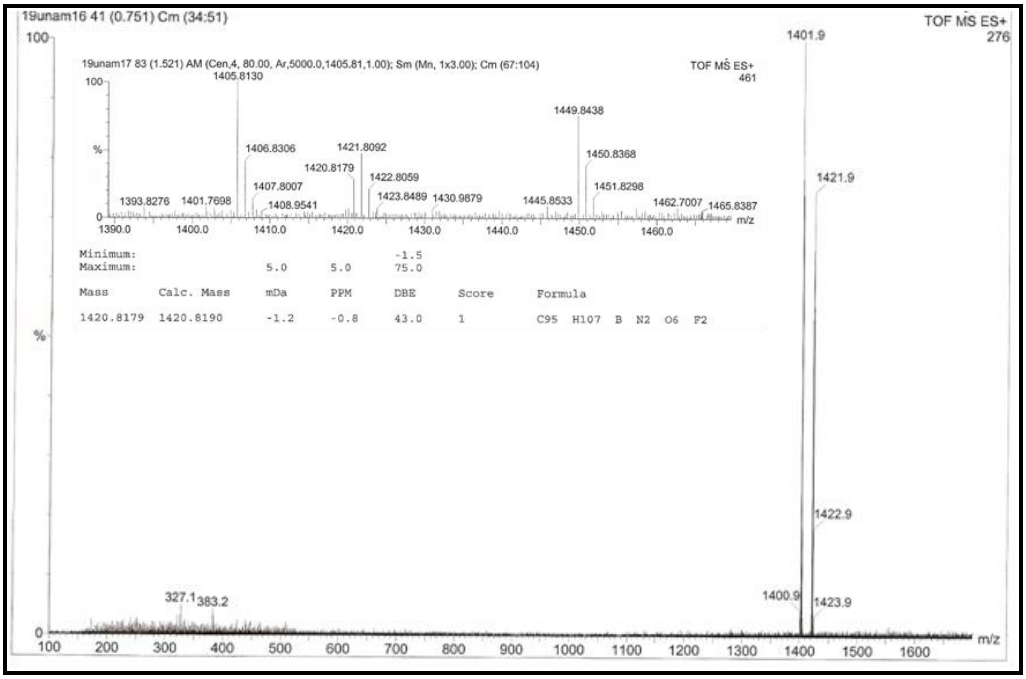

Figure A34. Mass Spectrum of **64**

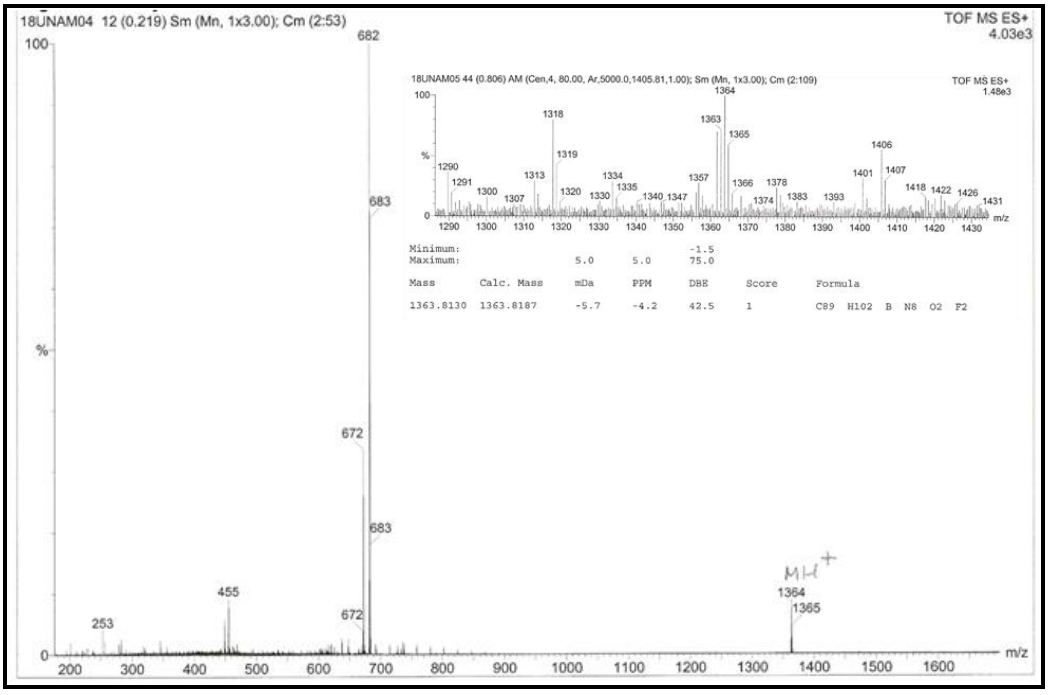

Figure A35. Mass Spectrum of **65**

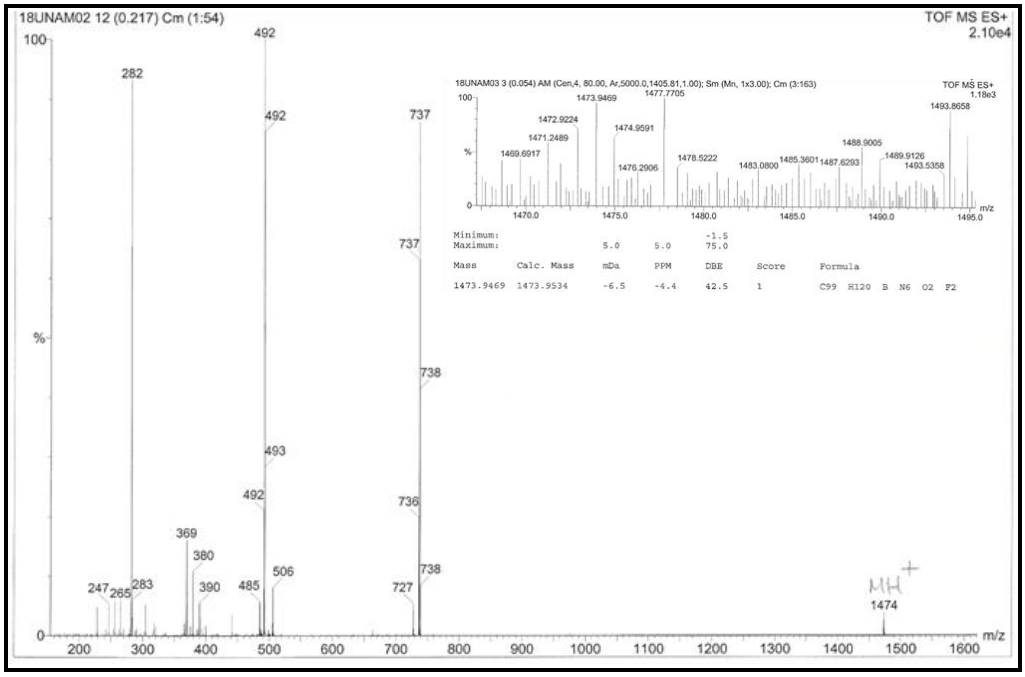

Figure A36. Mass Spectrum of **66**

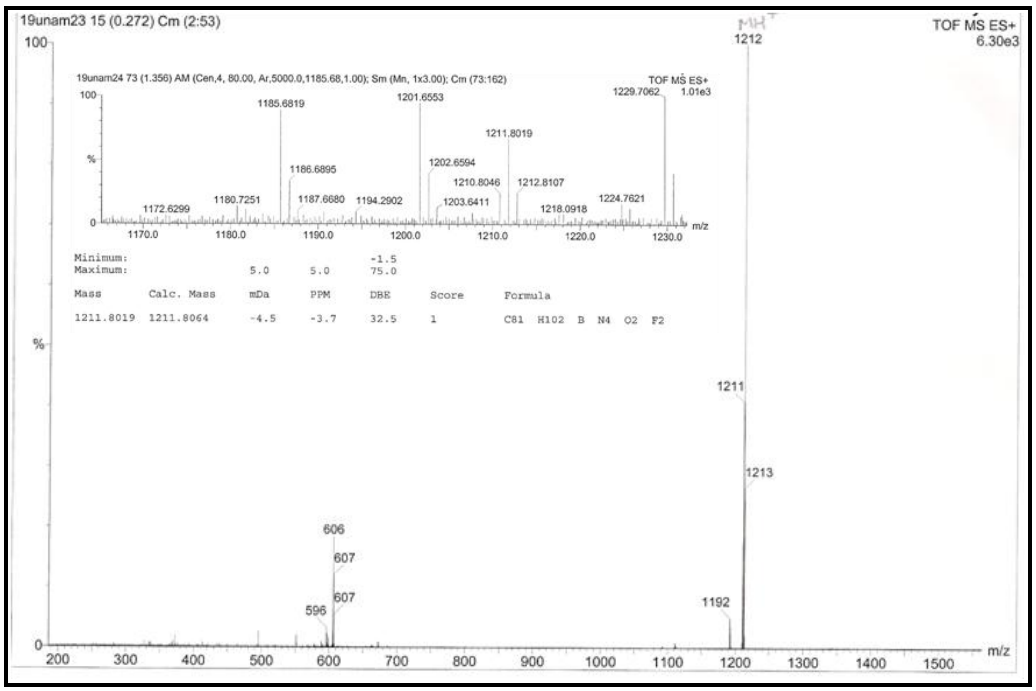

Figure A37. Mass Spectrum of **67**

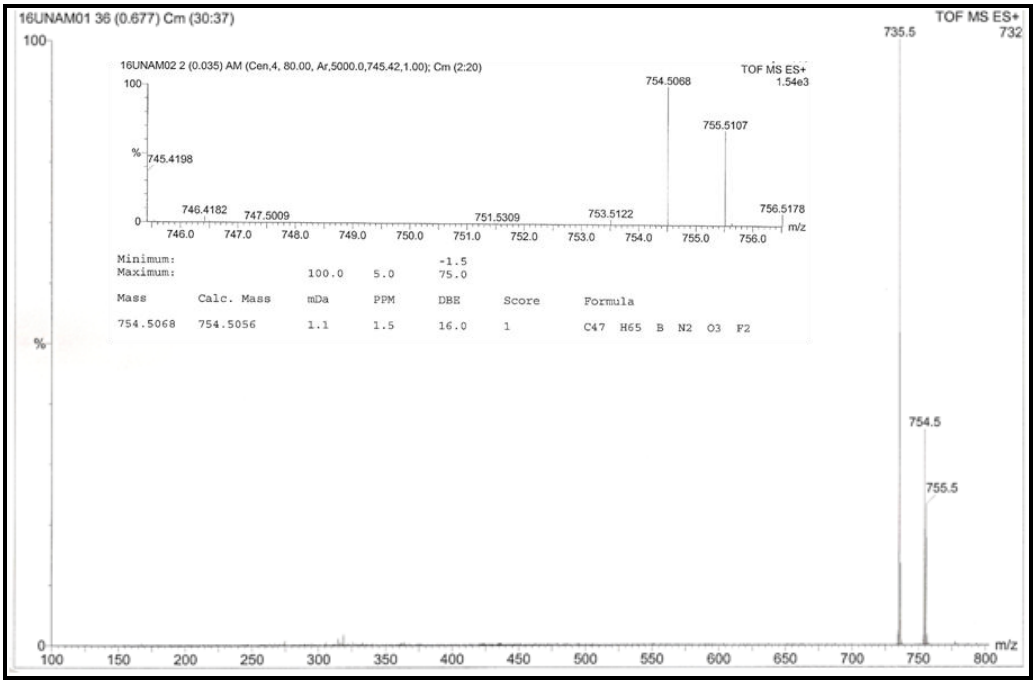

Figure A38. Mass Spectrum of **68**

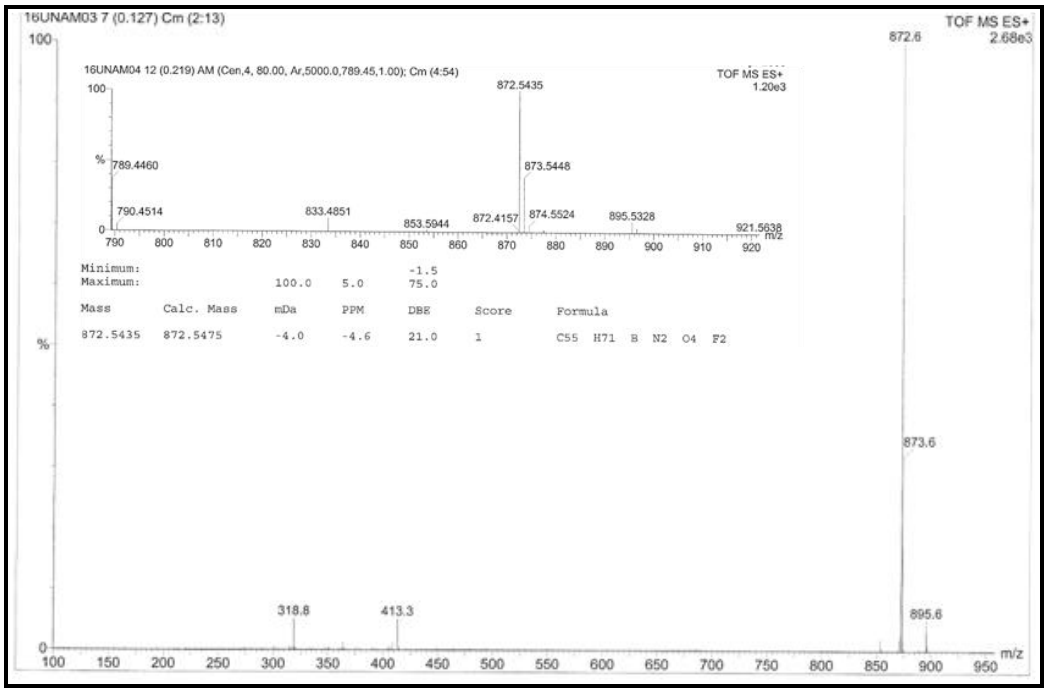

Figure A39. Mass Spectrum of **69**

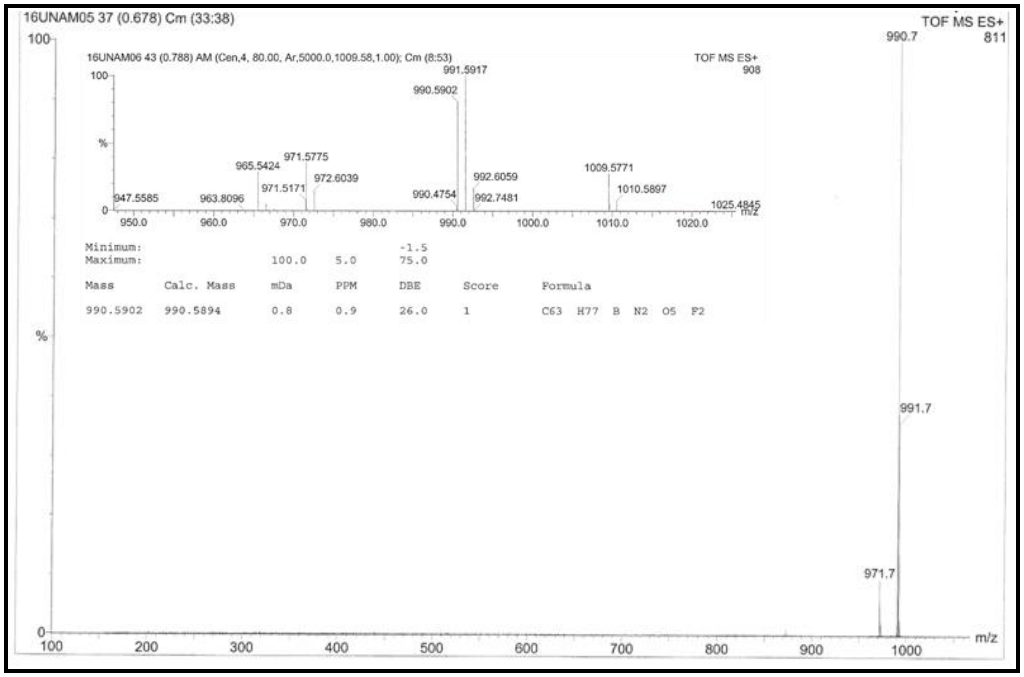

Figure A40. Mass Spectrum of **70**

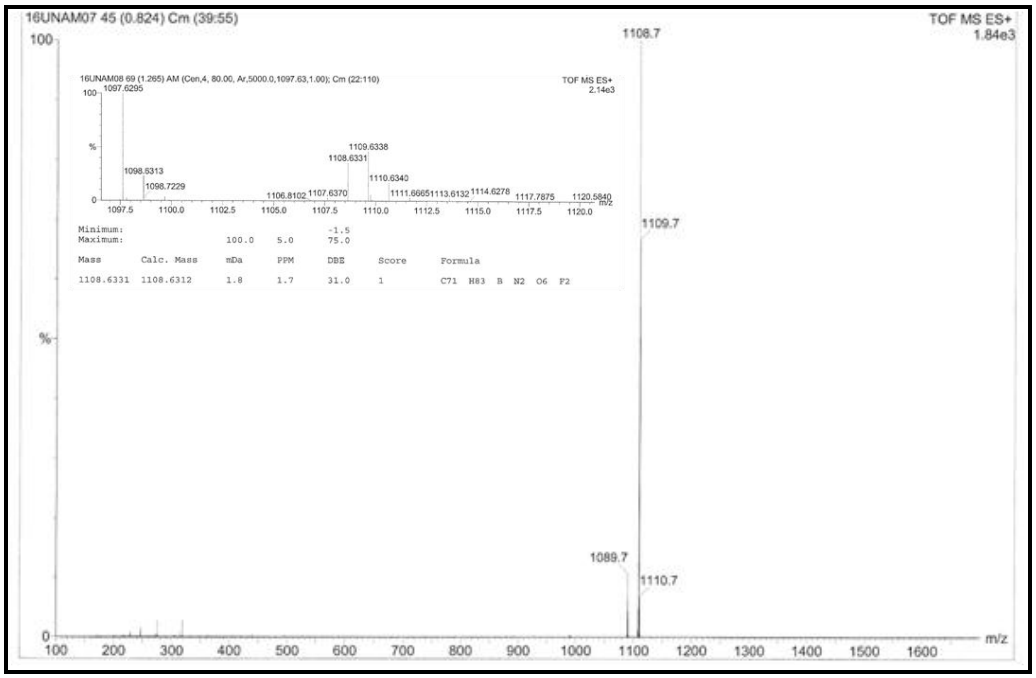

Figure A41. Mass Spectrum of **71**

10.3. Energy Transfer in Tetrastyryl-Bodipy Based Dendritic Light Harvesters (CHAPTER 5)

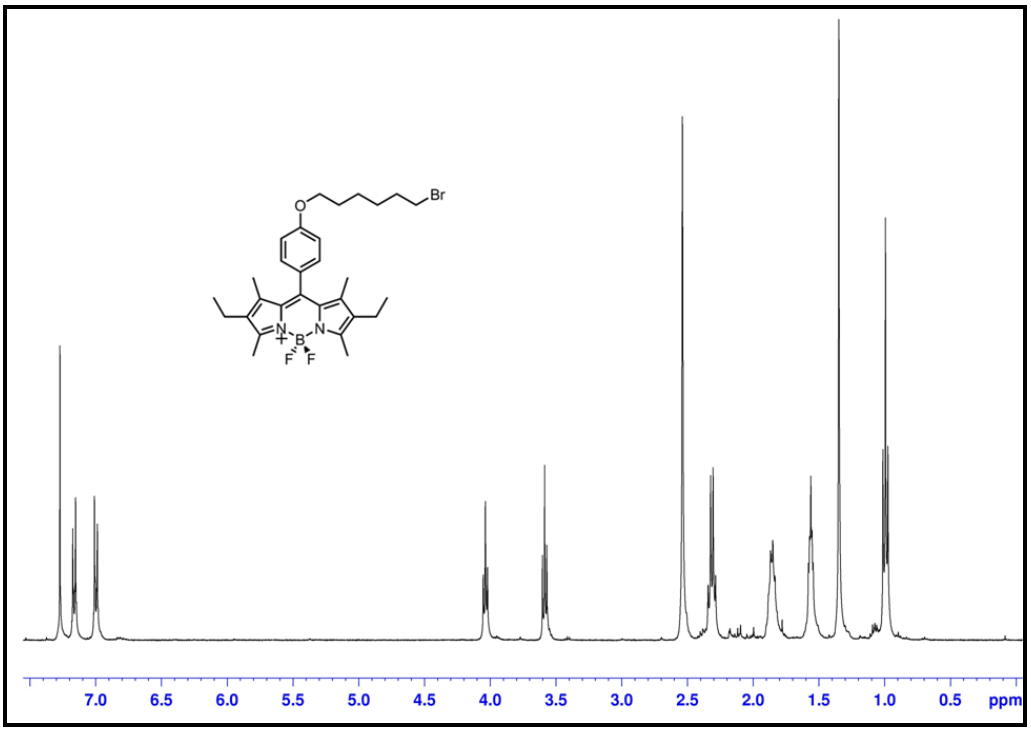

Figure A42. ^{1}H NMR spectrum of **74** (400 MHz, $CDCl_3$).

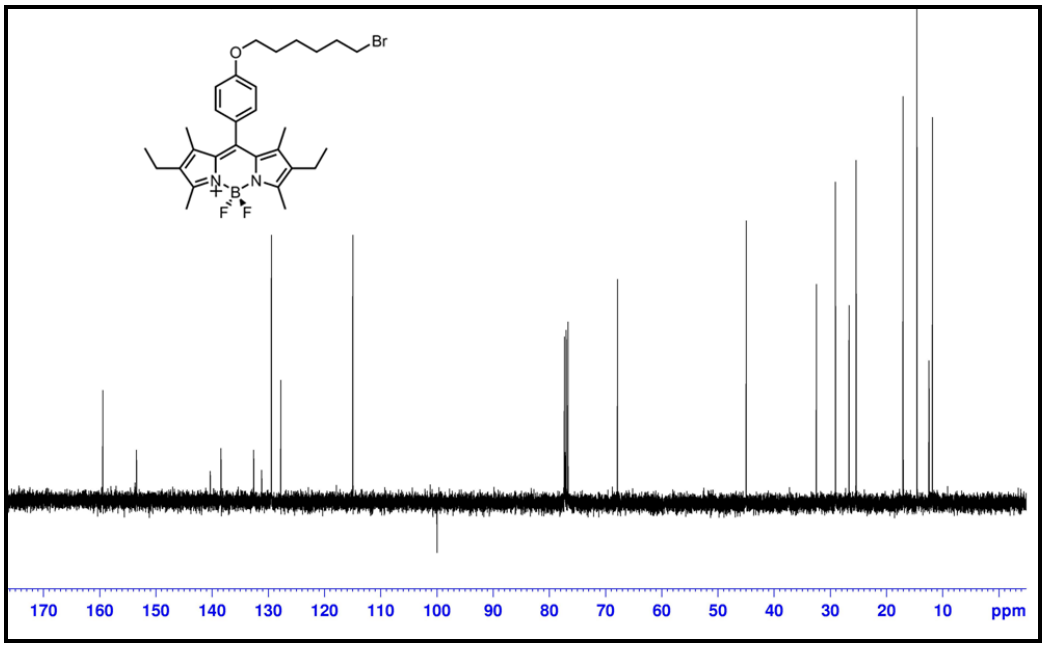

Figure A43. ^{13}C NMR spectrum of **74** (100 MHz, $CDCl_3$).

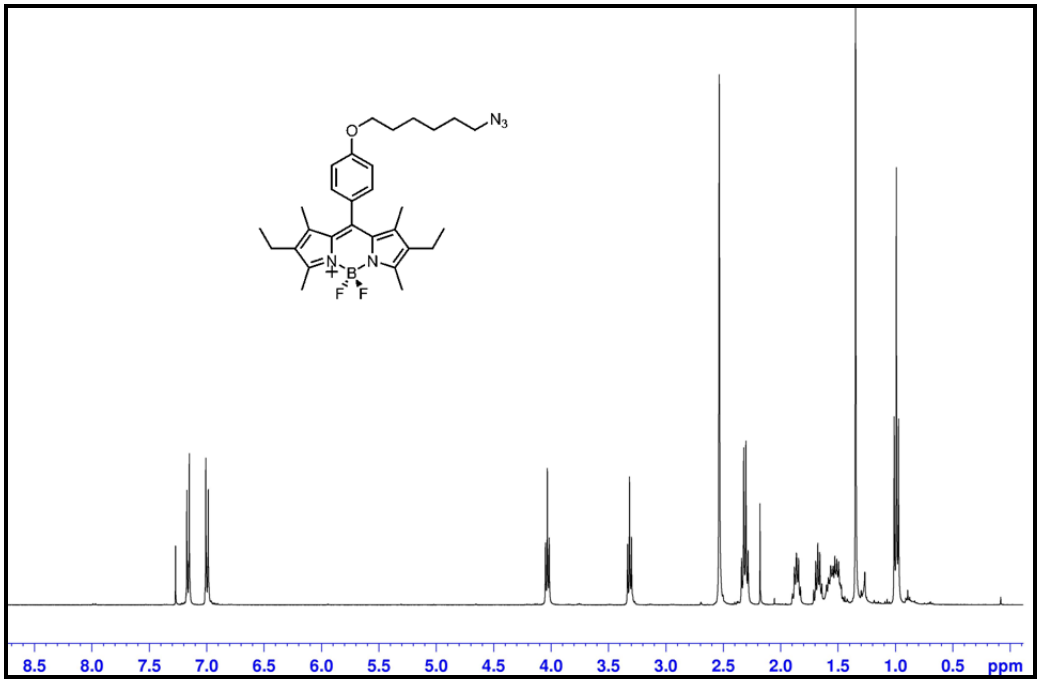

Figure A44. ^{1}H NMR spectrum of **75** (400 MHz, $CDCl_3$).

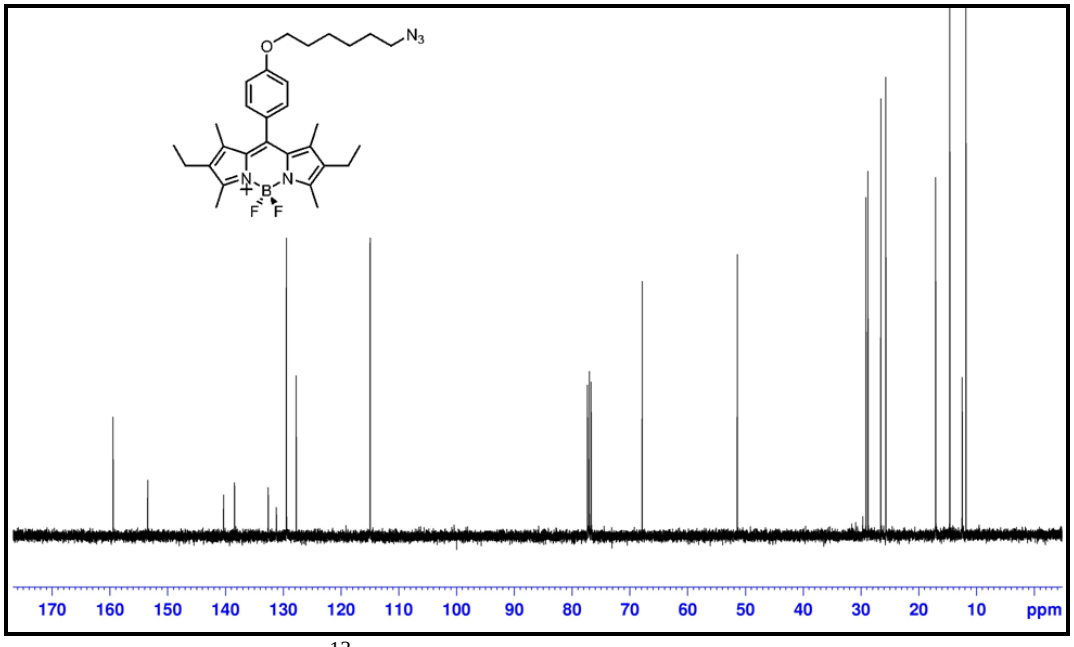

Figure A45. ^{13}C NMR spectrum of **75** (100 MHz, $CDCl_3$).

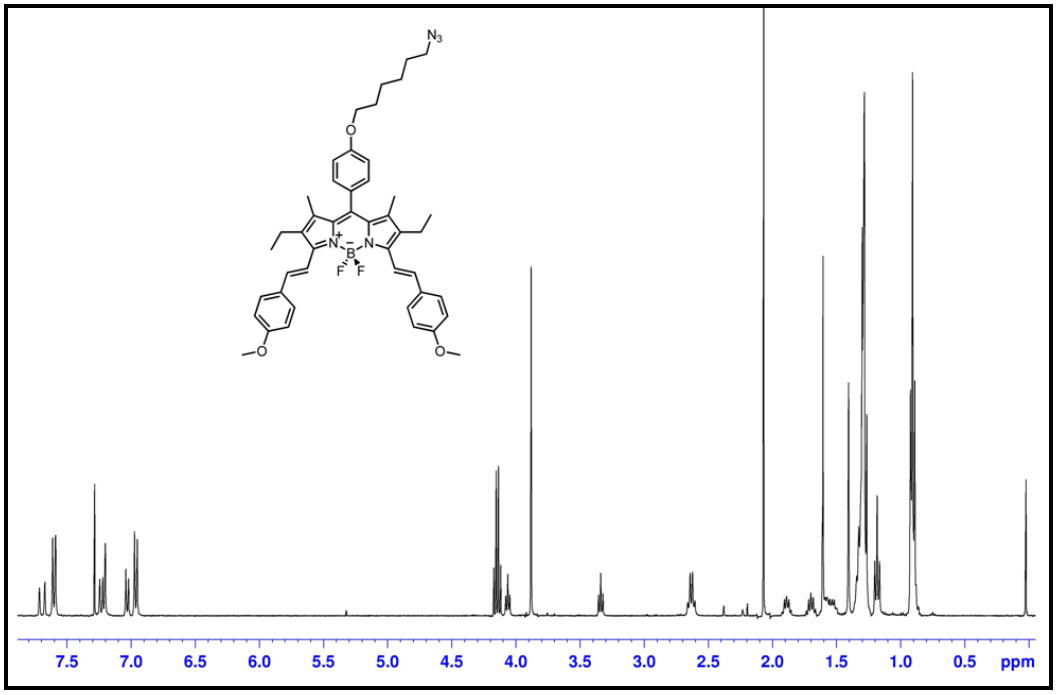

Figure A46. ^{1}H NMR spectrum of **76** (400 MHz, $CDCl_3$).

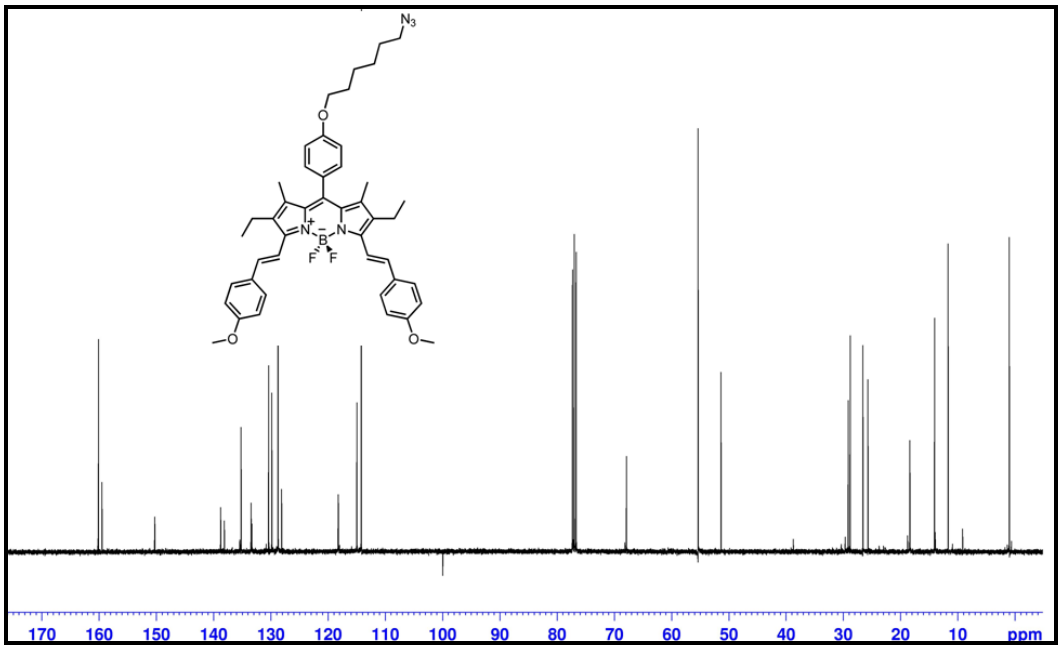

Figure A47. ^{13}C NMR spectrum of **76** (100 MHz, $CDCl_3$).

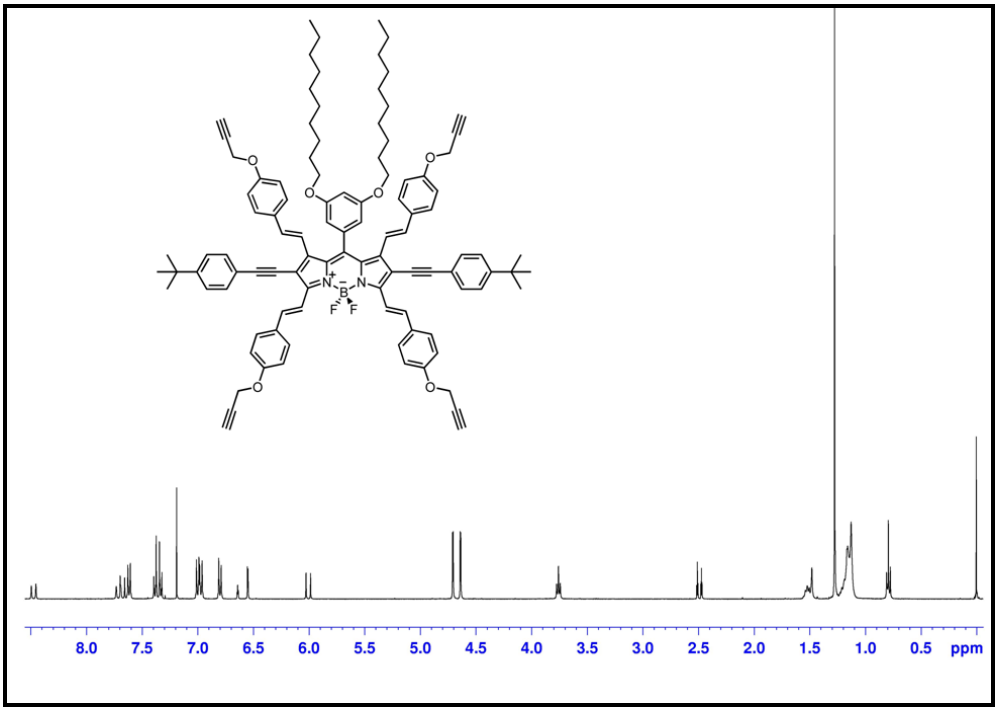

Figure A48. ^{1}H NMR spectrum of **77** (400 MHz, $CDCl_3$).

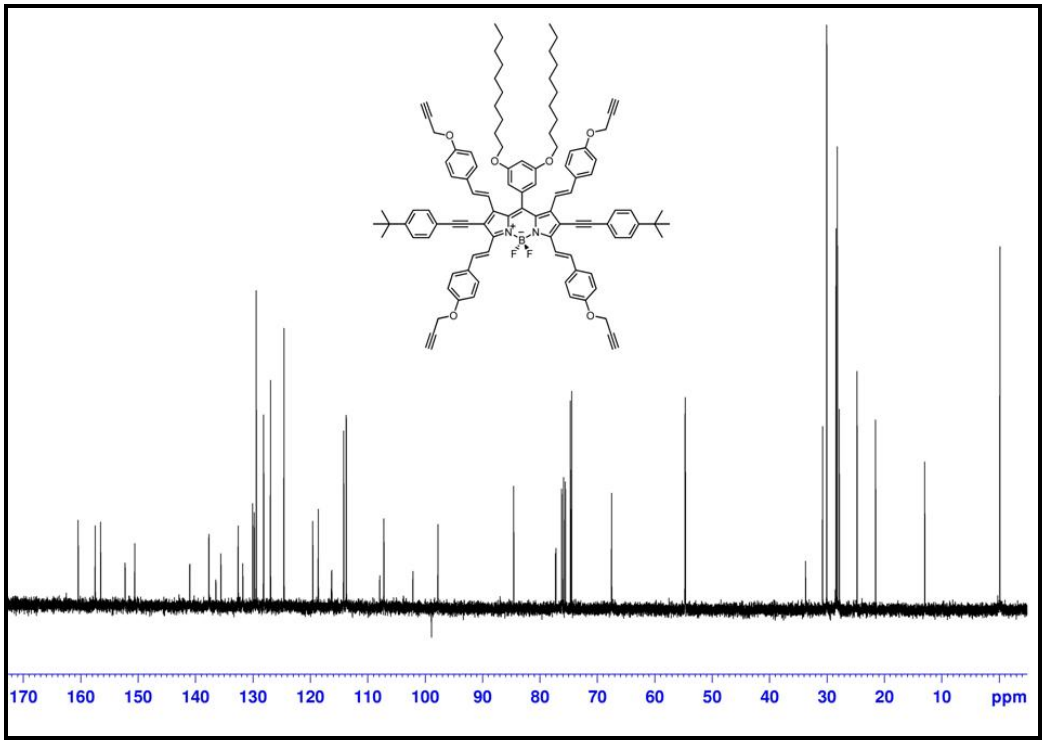

Figure A49. ^{13}C NMR spectrum of **77** (100 MHz, $CDCl_3$).

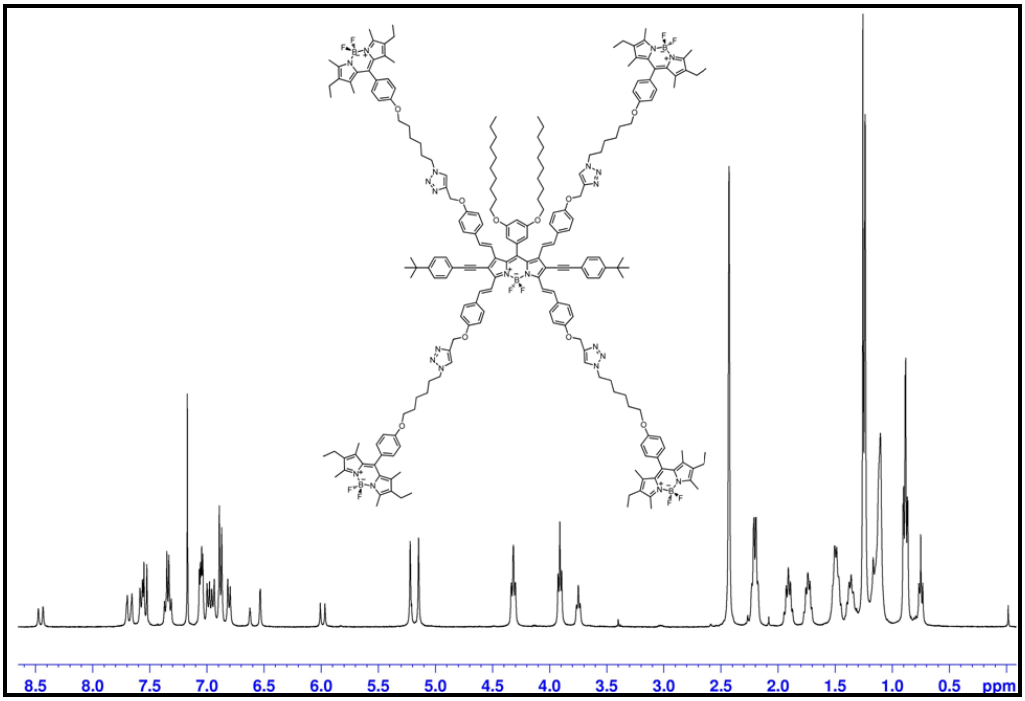

Figure A50. ^{1}H NMR spectrum of **78** (400 MHz, $CDCl_3$).

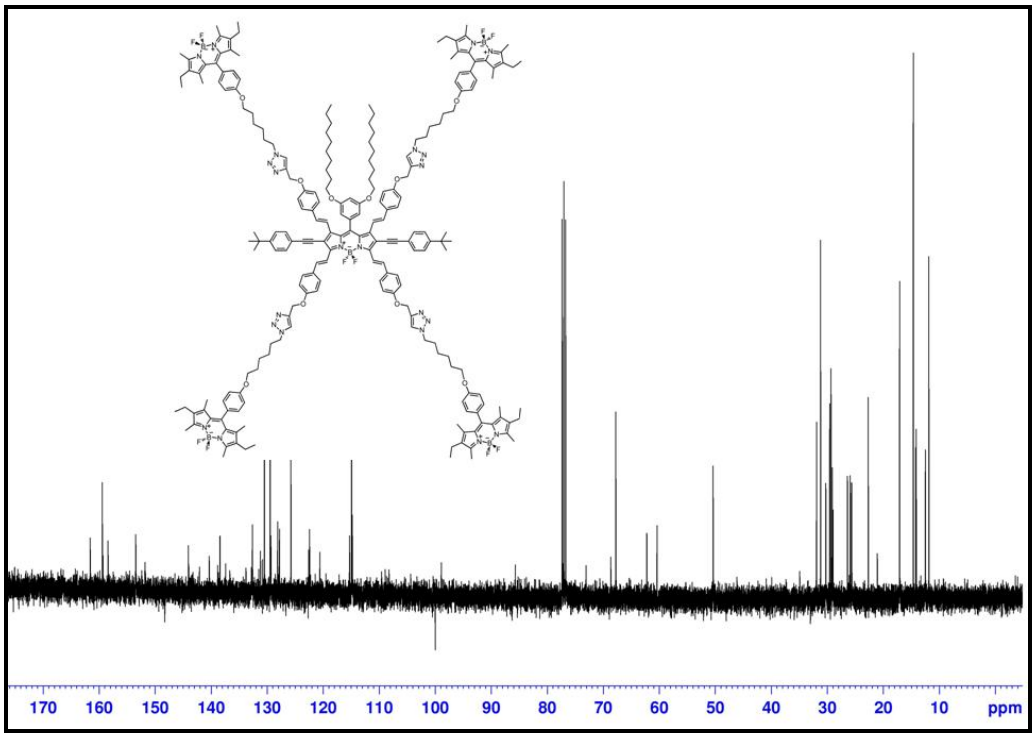

Figure A51. ^{13}C NMR spectrum of **78** (100 MHz, $CDCl_3$).

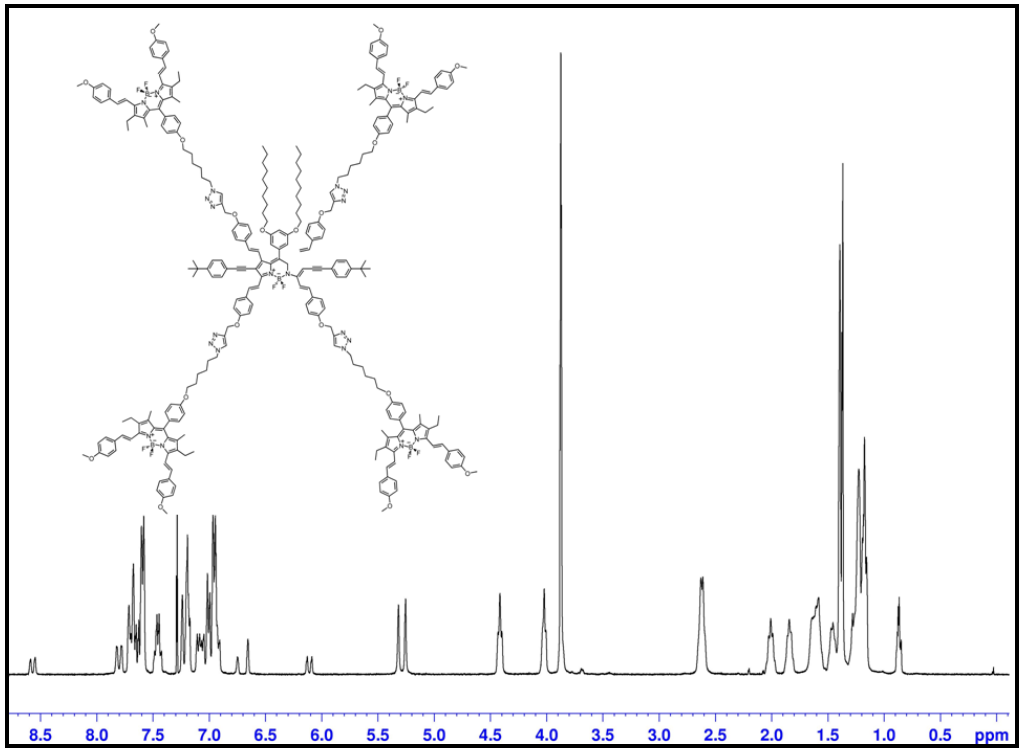

Figure A52. ^{1}H NMR spectrum of **79** (400 MHz, $CDCl_3$).

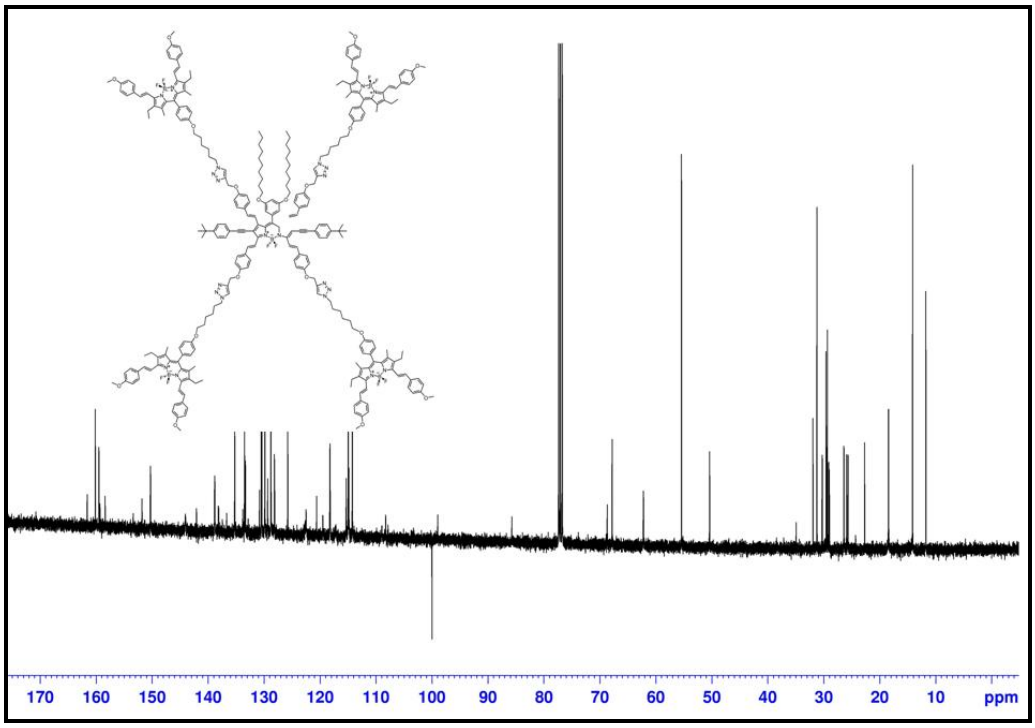

Figure A53. ^{13}C NMR spectrum of **79** (100 MHz, $CDCl_3$).

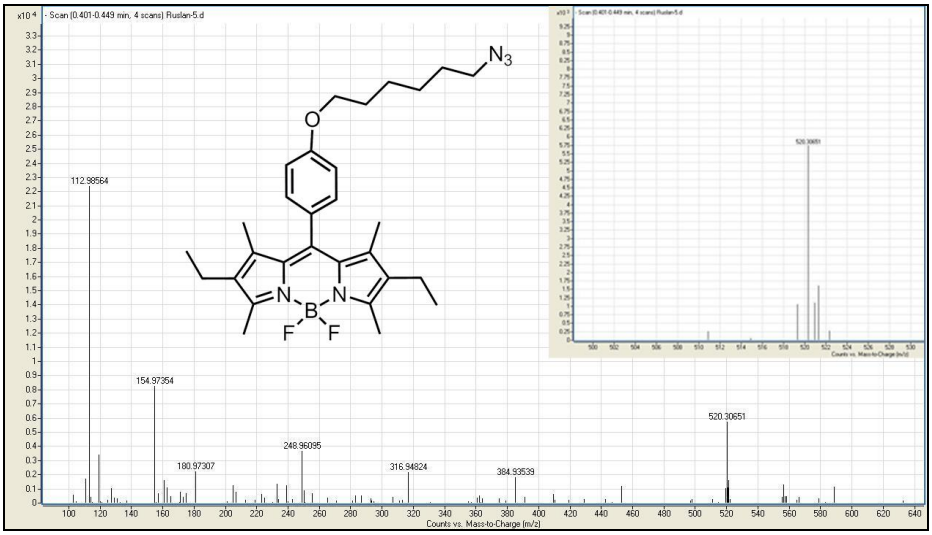

Figure A54. Mass Spectrum of **75**

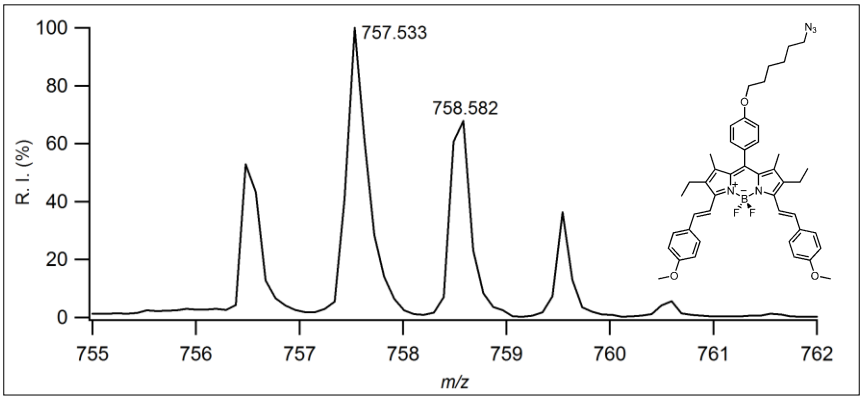

Figure A55. Mass Spectrum of **76**

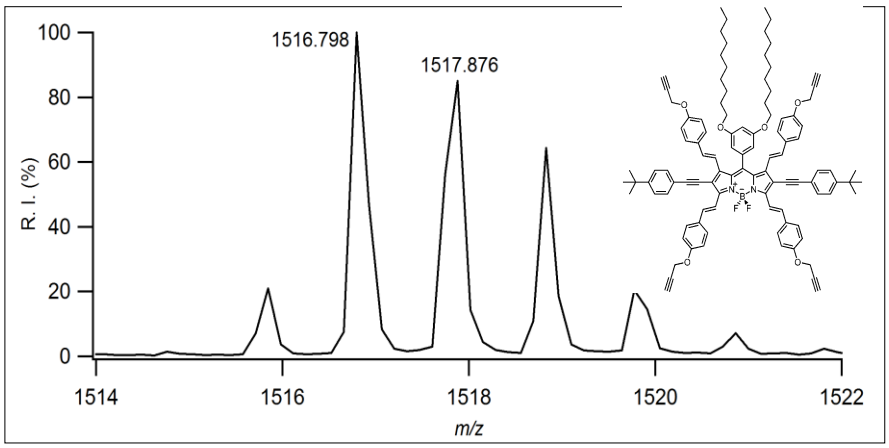

Figure A56. Mass Spectrum of **77**

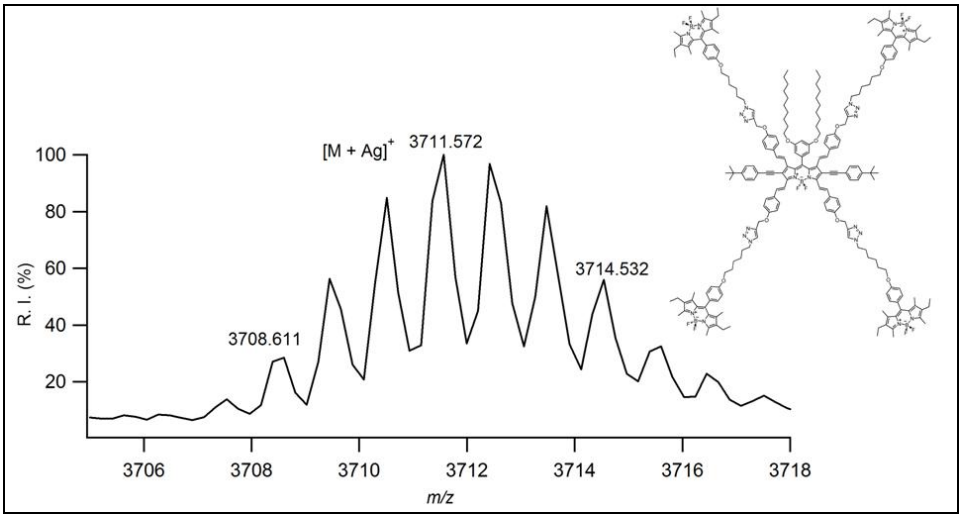

Figure A57. Mass Spectrum of **78**

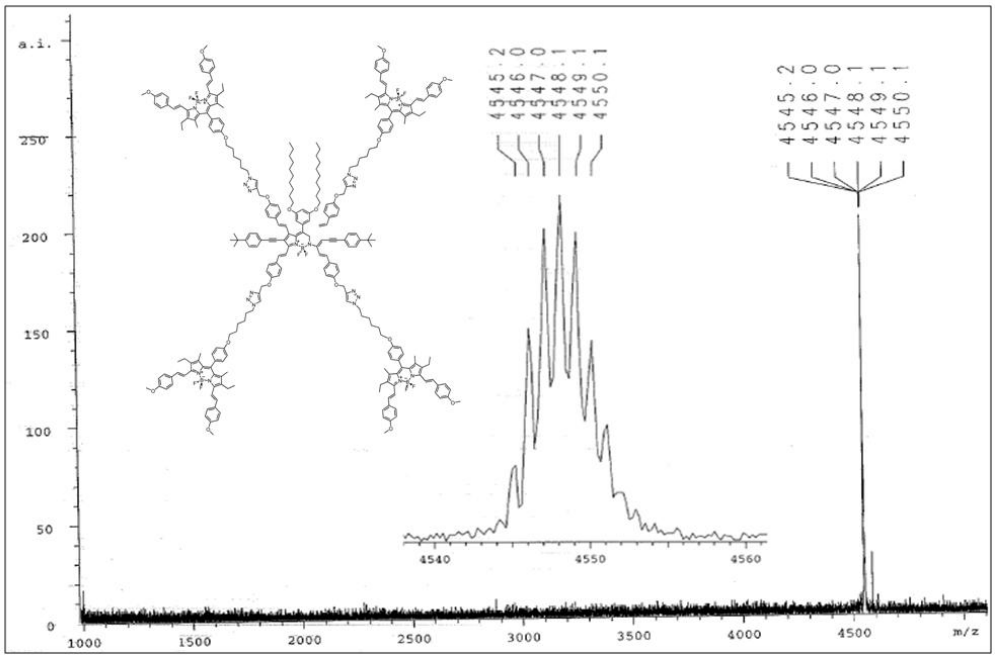

Figure A58. Mass Spectrum of **79**

10.4. Autonomous Shuttling in a Cucurbit[7]uril-Bodipy Pseudorotaxane (CHAPTER 7)

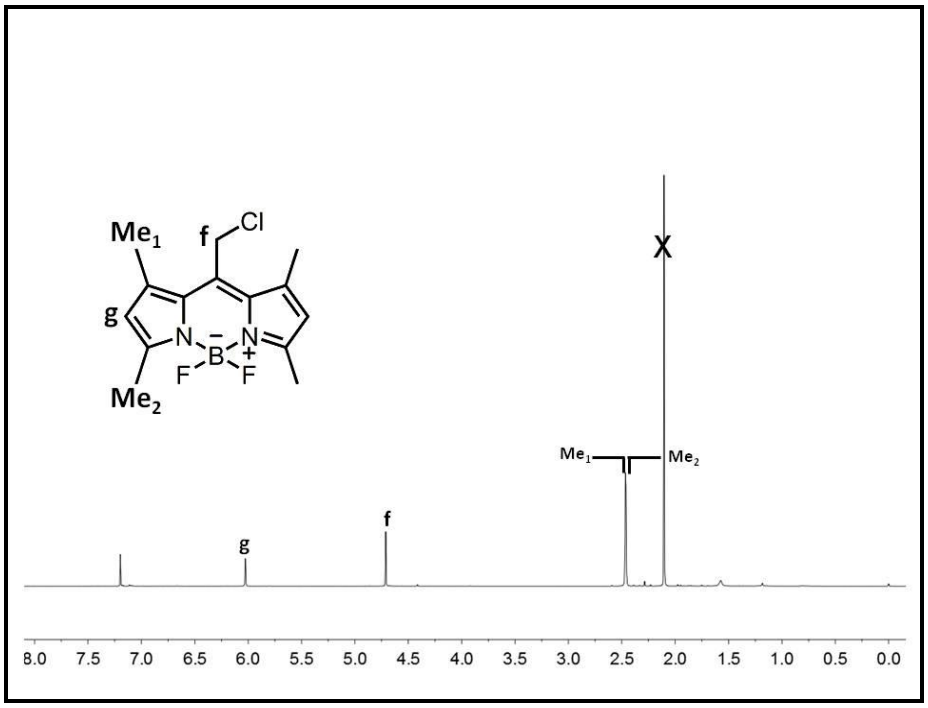

Figure A59. 1H NMR spectrum of **80** (400 MHz, $CDCl_3$).

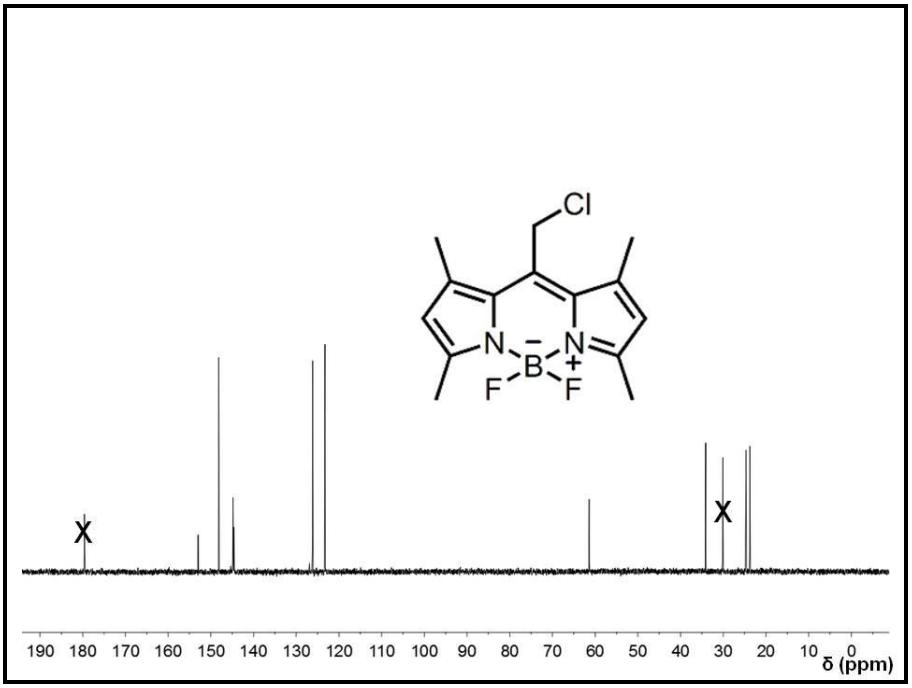

Figure A60. ^{13}C NMR spectrum of **80** (100 MHz, $CDCl_3$).

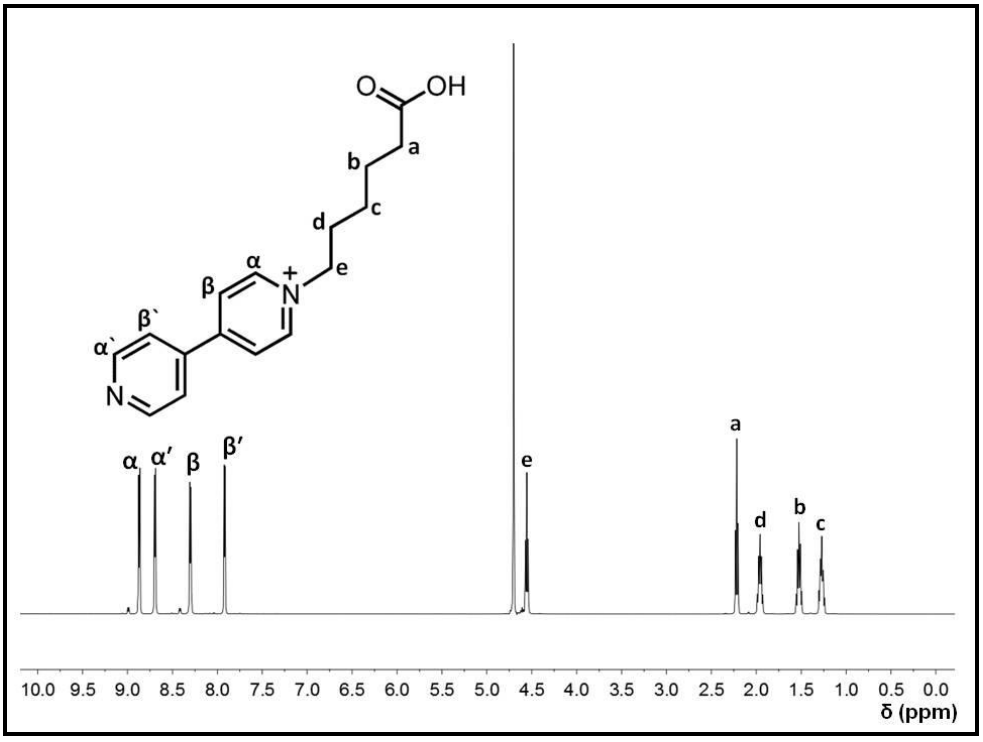

Figure A61. 1H NMR spectrum of **81** (400 MHz, $CDCl_3$).

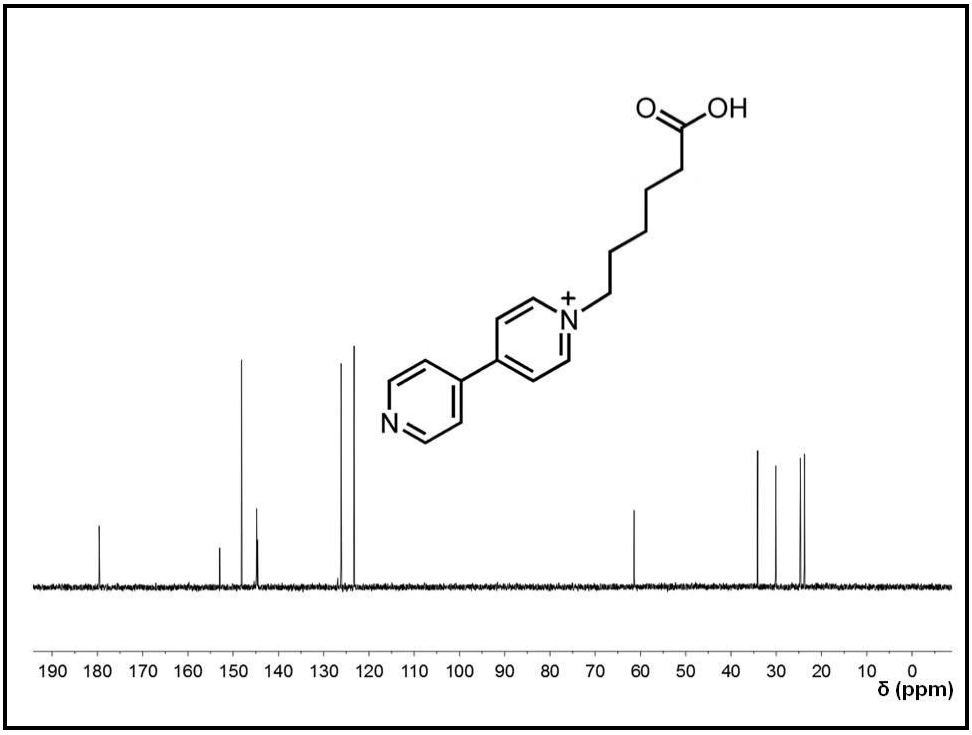

Figure A62. ^{13}C NMR spectrum of **81** (100 MHz, $CDCl_3$).

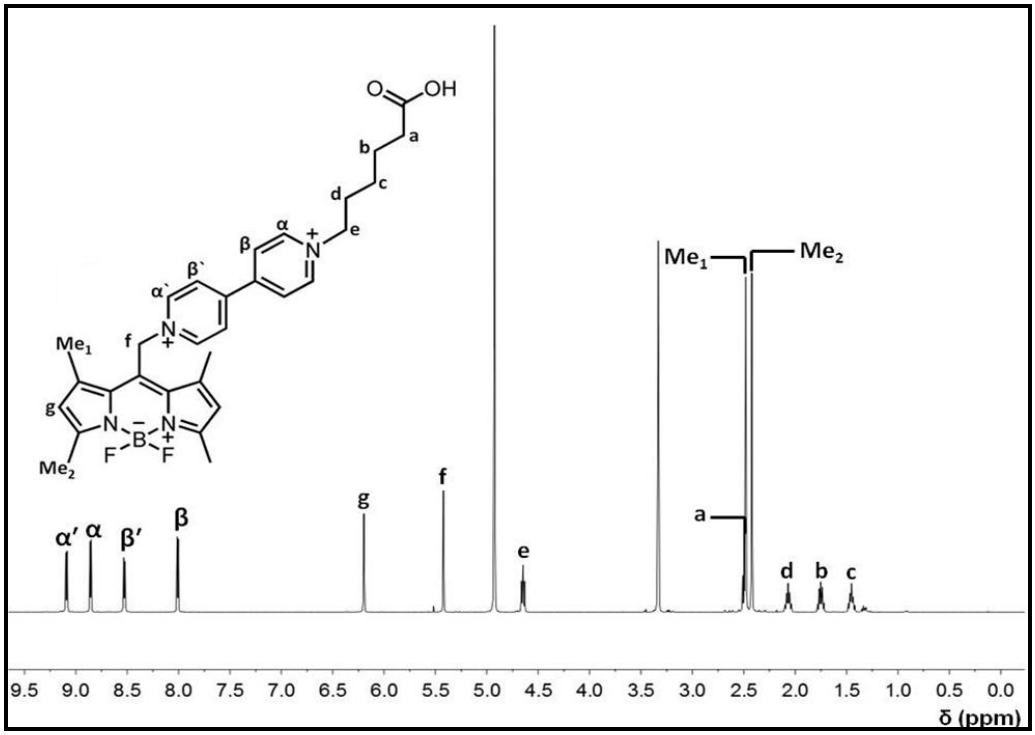

Figure A63. 1H NMR spectrum of **82** (400 MHz, $CDCl_3$).

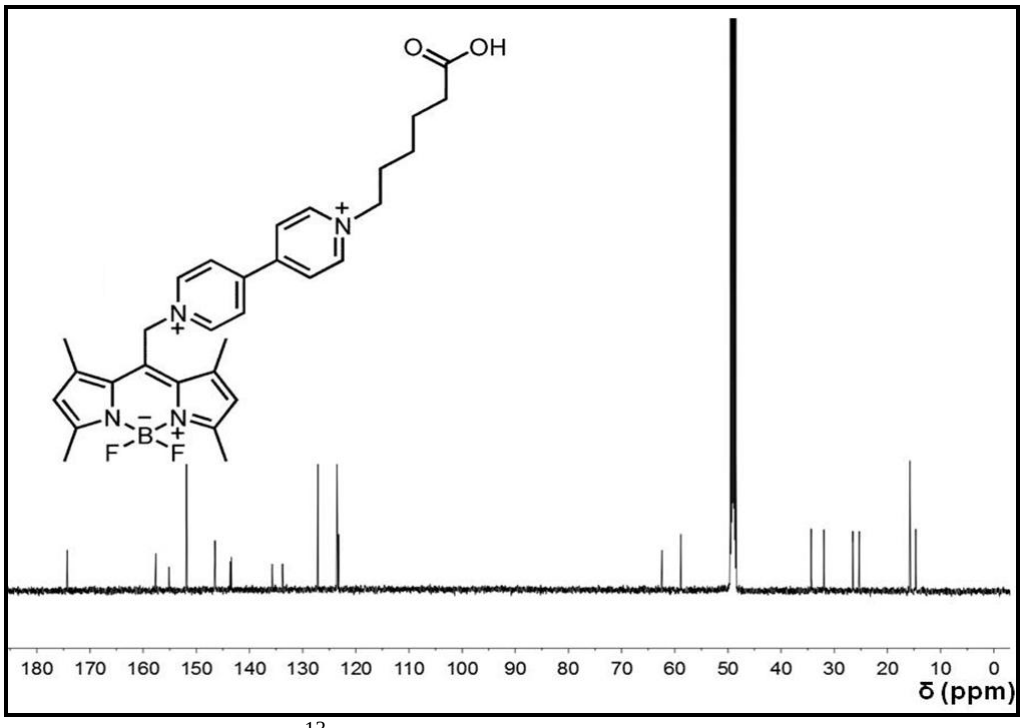

Figure A64. ^{13}C NMR spectrum of **82** (100 MHz, $CDCl_3$).

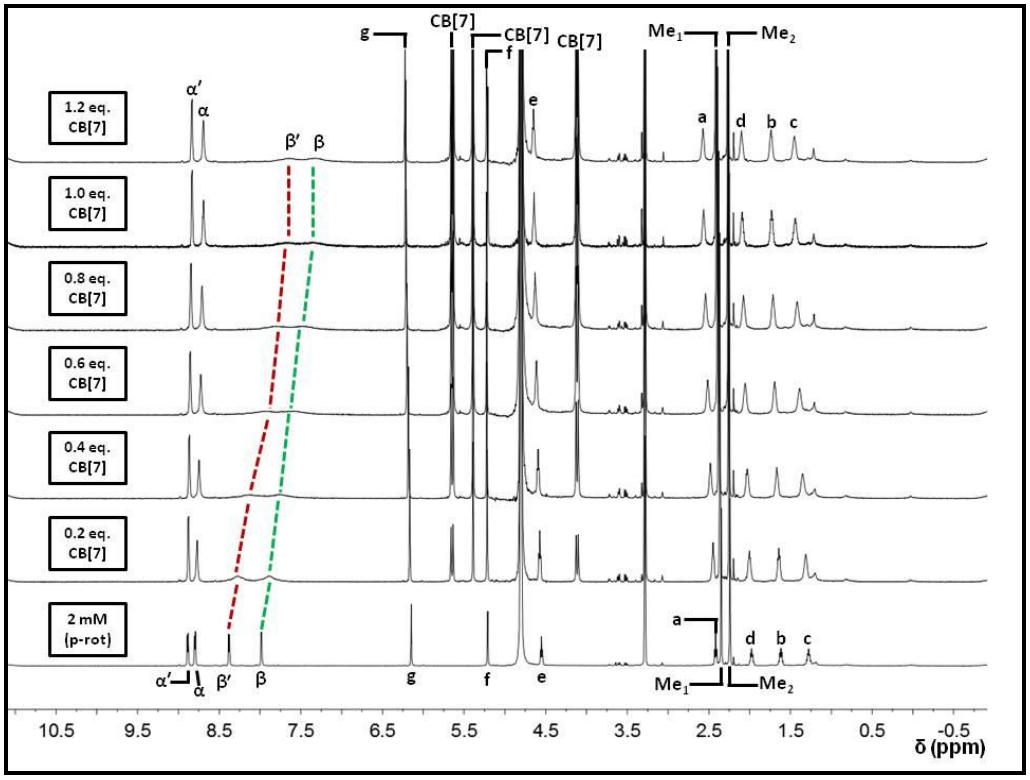

Figure A65. ^{1}H NMR spectra (400 MHz, 0.1 M NaCl in D_2O: CD_3OD; 70:30 at 25 ^{o}C) of **82**$^{2+}$ (3.0 mM) in slightly basic media pH ~3 with increasing concentrations of CB7 (0-1.2 eq).

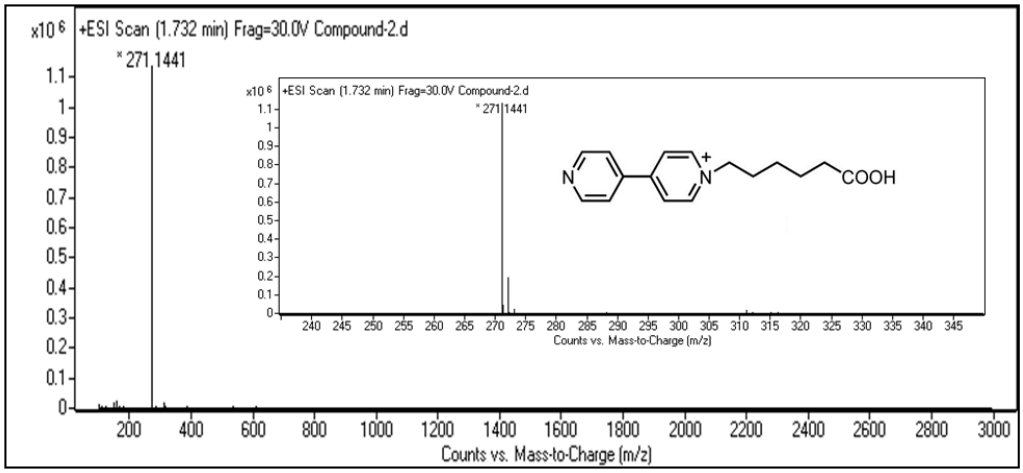

Figure A66. Mass Spectrum of **81**

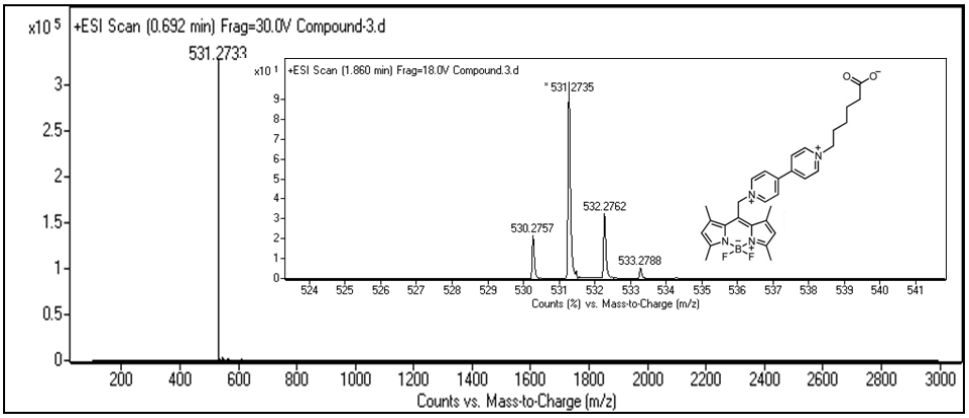

Figure A67. Mass Spectrum of **82**